Catalytic Transformation of Alcohols for the Production of Hydrogen, Fuels and Specialty Chemicals Using Pincer-Ruthenium and Pincer-Nickel Complexes

A Dissertation

Submitted in Partial Fulfillment for the Degree of

Doctor of Philosophy

by

Vinay Arora
(Roll No: 186122045)

Thesis Supervisor: Dr. Akshai Kumar A. S.

Department of Chemistry
Indian Institute of Technology Guwahati
Guwahati – 781039, Assam, INDIA

October 2024

Dedicated

To

My Family and Friends

"Success is not an accident. It is the result of your attitude and your attitude is a choice."

Shiv Khera

Acknowledgments

This thesis has come to existence because of many people's assistance, encouragement and inspiration. I would like to sincerely thank everyone from Indian Institute of Technology Guwahati, India who has been directly or indirectly involved in shaping up this thesis. I express my sincere gratitude to everyone who helped me along the way with my research and made it possible for me to submit my thesis.

- To begin with, I would like to especially thank my supervisor and mentor **Dr. Akshai Kumar A. S.** for giving me this wonderful opportunity to do my thesis work under his supervision. I sincerely thank him for making me part of his vision towards sustainable organometallic chemistry and its applications. Thanks for helping me out whenever I was stuck and always guiding me towards a better path. I would also like to express my gratitude to his family, Anupama Ma'am and Abhiram for their support in this journey.
    - I would like to extend my sincere thanks to Late Dr. Hemanth K. Srivastava and Dr. Farhan Ahmad Pasha for helping me out in DFT calculations.
    - I am also grateful to my collaborator Dr. Rajkumar P. Thummer for his guidance during my research.
    - I would like to acknowledge the assistance of my doctoral committee chairman Prof. Biplab Mondal and the doctoral committee members Prof. Chandan K. Jana and Prof. Chandan Mukherjee.
    - I gratefully acknowledge the help provided by Dr. Raksh Vir Jasra, Dr. Sunil Dhole and Mr. Tushar Wagh in my research work.
    - I would like thank Dr. Babulal Das and Dr. Venkatesha R. Hathwar for their help in X-ray crystallography.
    - I sincerely thank my lab mates Dr. Kanu Das, Dr. Khadimul Islam, Dr. Moumita Dutta, Dr. Lakshay, Dr. Harsh, Mr. Pran Gobinda Nandi, Ms. Himani Narjinari, Ms. Eileen Yasmin, Ms. Akshara Bisarya, Ms. Niharika Tanwar, Mr. Vikas, Mr. Bedabara Nag, Mr. Soumen Maity, Mr. Pabitra Maity, Mr. Babu V., Ms. Susmita Das, Mr. Amir, Ms. Arunima, Ms. Gargi Mandal, Mr. Rounak Ranjit, Mr. Lalit Pandey, Ms. Tanima Pal, Ms. Aditi, Mr. Kailas Mahipal M, Mr.

Dheeraj, Mr. Sudhanva for their valuable help and support during my research work.

- I want to acknowledge Department of Chemistry, Centre for Nanotechnology IIT Guwahati and Central Instruments Facilities (CIF, NECBH, IIT Guwahati) for giving me the opportunity to use the instrument facilities during my thesis work.

- I am highly grateful to MHRD and IIT Guwahati for providing me with the doctoral fellowship during my PhD tenure. I also express my gratitude to ISRO and MEITY for the same.

- Words would less to express my deepest regards to my department seniors Dr. M. Adil Afroz, Dr. Maimur Hossain, Dr. Debasis Barman, Dr. Prasenjit Sarkar, Dr. Biswajit Nayak, Dr. Debojit Bhattacherjee, Dr. Rupa Adanki, Dr. Pinaki Bhushan De, Dr. Sonbidya, Mr. Shubhojit, Mr. Partha Pratim Das, Dr. Megha Balha, Dr. Nimisha, Ms. Oindrila, Dr. Chandrakanta, Dr. Tapas Pal, Dr. Suvendu, Dr. Ananya, Dr. Angana, Dr. Arpita Shome, Dr. Dibgyangana, Dr. Swapna, Dr. Monika, Dr. Nasim Akhtar, Dr. Sandeep, Dr. Gobinda, Dr. Rabindra, Dr. Munendra, Dr. Santa Mondal, Dr. Araghni, Dr. Bitan, Dr. Avijit, Dr. Chiranjib and Dr. Vinod for their suggestions and encouragement in research during my entire PhD program.

- I want to thank the Assam State Disaster Management Authority (ASDMA) and IIT Guwahati (CRT) during the lockdown & unlocking of COVID-19 pandemic situation for helping in maintaining the research work unhampered.

- I want to like to thank Academic Section, Student Affairs, IISI section and R&D Section of IIT Guwahati.

- A special thanks to all the security guards, mess workers, staff of food court, hostel canteen (especially Anna), juice centre and others for helping me during this journey.

- My heartiest thanks to Doctors and staffs of IIT Guwahati hospital for their care during my illness.

- I would also like to express my sincere thanks to student gymkhana club's members who helped me during my journey.
- I am deeply indebted to the operators of various instruments in the department and CIF, for their support in my research.
- Thank to my dearest friends Suraj Pandey, Sandeep, Priyanka Adhikari, Sourav Mondal, Supriyo Halder, Tirupati, Indraneel, Samir, Tanumouy, Debjyoti, Altaf, Chan, Sagnik, Mrinmoy, Monu, Masud, Rahul, Jitendra, Aritra, Priyam, Purnodas, Raj, Rabu, Sanjib, Shnakhadeep, Bapan, Madhurjya, Bikoshita, Suravi, Beetu, Rinki, Sabina, Riya, Priyanka Sarkar, Manideepa, Trisha, Yashdeep, Nilotpal, Ameer, Nikita, Sukanya, Somnath, Pallab for their support, valuable suggestions and mentally support during my Ph.D period. Thanks for making this journey fun.
- Also, can't forget my dear friends Mayank, Pranay, Nirmal, Sachin, Harshika, Manpreet, Neha, Neeru, Nitika, Shruti, Meenakshi, Bablu, Ravinder. Thank you for everything.
- I want to express my deepest regards to my juniors in the department, Pallav, Rupkumar, Abhay, Amlan, Angela, Anisha, Sayani, Riya Ghosh, Sujoy, Surya, Sawmya, Niku, Ashish, Tapsi, Debika, Siddarth, Nitu, Kritarth, Nandini, Mayukh, Suryaveer, Ashwini and many others who helped me in this journey.
- A special thanks to my friends not from my department, whom I met and interacted during this journey. Thanks to Atal, Amritanshu, Arin, Rohit, Aryan, Prakhar, Ankit, Dhruv, Tiwari, Ravi, Kritika, Vatsal, Aman, Jay, Harsh, Shlok, Aman Gupta and many more. I also want to thank my undergrad juniors whom I interacted during my TA duty, Aditya, Keshav, Ayush, Astik, Sinha, Dyuti, Kshitij, Kunal, Rishabh, Kartik, Hardik, Harshit, Ritik, Arpita, Ravi and others.
- This journey would not have been possible without my Ph.D. batchmates, seniors and juniors who helped directly or indirectly during my research.
- A special thanks to Ruma for the support and guidance during my journey.

- I would also like to express the profound gratitude from my deep heart to my beloved parents and siblings for their unconditional love and continuous support, both emotionally and mentally.

Indian Institute of Technology Guwahati

Department of Chemistry

Declaration

I do hereby declare that the research work embodied in this thesis entitled "***Catalytic Transformation of Alcohols for the Production of Hydrogen, Fuels and Specialty Chemicals Using Pincer-Ruthenium and Pincer-Nickel Complexes***" has been carried out by me in the Department of Chemistry, Indian Institute of Technology Guwahati, Assam-781039, India, under the supervision of **Dr. Akshai Kumar A. S.** for the award of the degree of doctor of philosophy and it has not been submitted elsewhere for the award of any degree or diploma.

In keeping with the general practice of reporting scientific observation, due acknowledgments have been made wherever the work described is based on the findings of other investigators.

Guwahati

October, 2024

Vinay Arora

Roll No– 186122045
Department of Chemistry
IIT Guwahati, Guwahati
Assam, INDIA-781039

भारतीय प्रौद्योगिकी संस्थान गुवाहाटी
Indian Institute of Technology Guwahati

Dr. Akshai Kumar Alape Seetharam
Associate Professor, Department of Chemistry, Guwahati – 781039, Assam, INDIA
Tel: +91-3612583479 (O), Mobile: +91-8133036890, Fax: +91-3612582349
Email: akshaikumar@iitg.ac.in, akshaikumara@gmail.com

@iit-g
Centre for Nanotechnology

CERTIFICATE

I hereby certify that the entire work embodied in the thesis entitled "***Catalytic Transformation of Alcohols for the Production of Hydrogen, Fuels and Specialty Chemicals Using Pincer-Ruthenium and Pincer-Nickel Complexes***" is the result of investigations carried out by **Mr. Vinay Arora** (Roll No: 186122045) at the Department of Chemistry, Indian Institute of Technology Guwahati, India under my guidance and the same has not been submitted elsewhere for the award of any degree or diploma.

17/10/2024

Guwahati

October 17, 2024

Dr. Akshai Kumar A. S.

Supervisor

Abbreviation

T	Temperature	IR	Infrared
°C	Degree Celsius	*m/z*	Mass to charge ratio
δ	Chemical shifts	*e.g.*	For example
K	Kelvin	equiv.	Equivalent
g	Grams	*ca.*	Around
mg	Milligram	*i.e.*	Namely
mmol	Millimole	vs.	Versus
μM	Micromole	*via*	Through
mL	Milliliter	Me	Methyl
ppm	Parts per million	Et	Ethyl
r.t.	Room temperature	^{i}Pr	*iso*-Propyl
h	Hours	^{t}Bu	*tert*-Butyl
EPR	Electron Paramagnetic Resonance	Cy	Cyclohexyl
MS	Mass spectrometry	Ar	Aromatic
HRMS	High-resolution mass spectrometry	Ph	Phenyl
Hz	Hertz	py	Pyridine
MHz	Megahertz	THF	Tetrahydrofuran
NMR	Nuclear Magnetic Resonance	RDS	Rate determining step
J	Spin – spin coupling constant	TON	Turnover number
s	Singlet	DFT	Density functional theory
d	Doublet	TS	Transition state
dd	Doublet of Doublet	RDTS	Rate determining transition state
ddd	Doublet of Doublet of Doublet	TOF	Turnover frequency
t	Triplet	TO/h	Turnover per hour
q	Quartet	DME	Dimethoxyethane
m	Multiplate	Bim	*Bis*(benzimidazole)
bs	Broad singlet	SCXRD	Single crystal X-ray diffraction
ORTEP	Oak Ridge Thermal Ellipsoid Plot	EWG	Electron withdrawing group
CCDC	Cambridge Crystallographic Data Center	KIE	Kinetic isotope effect
LOHC	Liquid Organic Hydrogen Carrier	NHC	*N*-heterocyclic carbene
FA	Formic Acid		
LA	Lactic acid		

Abstract

The contents of the present thesis entitled ***"Catalytic Transformation of Alcohols for the Production of Hydrogen, Fuels and Specialty Chemicals Using Pincer-Ruthenium and Pincer-Nickel Complexes"*** have been divided into four chapters based on the results achieved from the experimental work carried out during the entire course of the PhD research program.

Chapter I provides a concise overview of the literature regarding pincer-metal complexes and organic transformations facilitated by them. The transformation of alcohols and their tandem reactions using transition metal complexes is also discussed. The chapter concludes by outlining and defining the scope of the current thesis.

Chapter II describes the synthesis of pincer-ruthenium complexes based on *bis*(imino)pyridine ligands of the type (^{R2}NNN)$RuCl_2(CH_3CN)$. These complexes, in addition to their analogous phosphine and carbonyl complexes were studied for the reforming of methanol in presence of water and base. Among the complexes screened, (^{Cy2}NNN)$RuCl_2(PPh_3)$ (0.2 mol%) gave the best yield of formic acid (81%) and hydrogen (81%) with 100% selectivity for a 2:1 mixture of methanol and water at 100 °C. Further, for a 3:1 mixture of methanol and water, 84% H_2 with 81% formic acid at 95% selectivity were obtained at 0.8 mol% catalyst loading. The kinetic isotope effect studies resulted in an average value of 1.96, when CH_3OH was replaced with CD_3OD in the reaction. A combined kinetic and DFT (*vide infra*) analysis indicated that the methanol C–H bond activation occurs as a part of the mechanism and is not a part of the RDS, while the O-H bond activation is the RDS and contributes majorly to the observed average k_H/k_D value of 1.96. These results are well complimented by the DFT studies, which point towards the involvement of σ-bond metathesis leading to the generation of first hydrogen molecule as the rate determining step for the both the cycles *i.e* till formic acid and till CO_2. The cycle leading to the formation of formic acid is kinetically more favored by 4.54 kcal/mol as compared to the CO_2 formation cycle. The homogeneity of the reaction is proved by the kinetic studies, where rate of the reaction is first-order relative to both catalyst and methanol. The current reaction has also been extended towards to the generation of D_2, which has been further employed for the deuteration of unsaturated compounds such as styrene, stilbene and medicinally important quinolines.

Chapter III investigates the catalytic aqueous–phase reforming of ethanol employing a series of NNN pincer–ruthenium complexes based on *bis*(imino)pyridine and 2,6–*bis*(benzimidazole-2-yl) ligands. These ruthenium complexes have been studied for H_2 production from ethanol

in water in the presence of base at 120 °C. Among the complexes considered, the best results were obtained using (^{Cy2}NNN)$RuCl_2(PPh_3)$, which gave a yield of up to 70% of H_2 and 73% of acetic acid from a mixture of ethanol and water in a 2:1 ratio in the presence of 1.5 equivalents of KO^{t}Bu at 0.2 mol % of catalyst loading. Labelling studies provide key evidence for the involvement of C–H activation in the catalytic ethanol reforming reaction with an average KIE of 5.23. Kinetic studies have been performed which indicate the first order rate dependence on concentration of both pincer-ruthenium catalyst and ethanol, which also validates the homogeneity of the reaction. The HRMS and NMR studies provide conclusive evidence for the release of PPh_3 and generation of (^{Cy2}NNN)RuCl(H) species which plays a key role in catalytic aqueous ethanol reforming reaction. The Ru–H species involved in the catalytic cycle has also been detected as its phosphine adduct by NMR studies. The computational studies are in agreement with the control experiments, and it indicates that the σ-bond metathesis step resulting in the release of first molecule of H_2, is the rate–determining step (RDS).

Chapter IV deals with the synthesis of a series of novel NNN pincer-Ni(II) complexes based on *bis*(imino)pyridine ligands ((^{R2}NNN)$NiCl_2(CH_3CN)$; R = ^{i}Pr, ^{t}Bu, Cy, Ph and *p*-F-C_6H_4). These complexes have been well characterized and effectively used for the catalytic *β*– alkylation of various secondary alcohols with primary alcohols, achieving high yields and remarkable turnover numbers. Among all the complexes studied, very high TONs (up to 18400) have been observed for the reaction of benzyl alcohol with 1-(4-trifluoromethyl)phenyl)ethane-1-ol in the presence of 0.005 mol% of (^{Ph2}NNN)$NiCl_2(CH_3CN)$ and 5 mol% NaO^{t}Bu at 140 °C after 24 h. The kinetic studies point towards the aldol condensation being the rate determining step, with the overall reaction showing zero-order dependence of rate on the catalyst concentration and first-order dependence of rate on the concentration of base and substrates. The control experiments and HRMS studies are in accordance with the proposed mechanism which point towards the involvement of hydrogenolysis/alcoholysis pathway in the product formation step.

The current thesis describes the synthesis of novel pincer-ruthenium and pincer-nickel complexes based on *bis*(imino)pyridine ligands. These novel pincer-ligated ruthenium complexes along with the earlier reported pincer-Ru(II) complexes have been employed for the reforming of alcohols to generate hydrogen and industrially valuable chemicals. Further, the transformation of alcohols to higher alcohols *via* pincer-Ni(II) catalyzed *β*– alkylation of secondary alcohols with primary alcohols has been demonstrated.

Contents

Chapter I

Introduction to Pincer-Metal Complexes and their Application in Generation of Hydrogen and Specialty Chemicals from Alcohols

1.1 Organometallic complexes

Organometallic complexes play a pivotal role in catalyzing plethora of organic reactions which are otherwise hard to complete.[1] An organometallic compound contains at least one metal-carbon bond/ metal-hydrogen/phosphorus bond in its moiety.[1] William Zeise synthesized one of the first organometallic compounds in 1827, which was Pt(II) based system named as *Zeise's salt* $K[(\eta\text{-}C_2H_4)PtCl_3]$.[2] Some of the early organometallic compounds that have been utilized on a large scale include tetraethyllead and Grignard reagent. In 1899, Victor Grignard reported the synthesis of Grignard reagent (RMgX) starting from magnesium and organic halides (RX; R = alkyl and X = halogen), which probably has been the most widely used organometallic reagent during the past century.[3] Over the past few decades, numerous organometallic complexes have been extensively applied towards industrial applications for the manufacturing of value-added chemicals.[1] In 1963, Ziegler[4] and Natta[5] were awarded the Nobel Prize for their discovery of catalytic system based on early transition metals such as Ti, Zr or Hf along with organoaluminium compounds and their application towards the polymerization of α-olefins with high regio- and stereo-selectivity. Later, in 2001 W. S Knowles, R. Noyori and Karl Barry Sharpless received the Nobel Prize in chemistry for their work based on transition metal catalyzed asymmetric hydrogenation.[6] This was followed by another Nobel Prize in 2005, which was awarded to Rober H. Grubbs, Yves Chauvin and, Richard R. Schrock for their breakthrough research in metal catalyzed alkene metathesis.[7] In 2010, Richard F. Heck, Ei-ichi Negishi and, Akira Suzuki won the Nobel Prize for palladium catalyzed cross-coupling reactions.[8]

The transition metals have incomplete *d*-orbitals, and therefore have a tendency to bind to various ligands to achieve stability. In organometallic complexes, ligands donate electrons to the metal centre and help them in achieving the stable 18-electron configuration.[1] Based on the number of donor sites present on the ligands, they can be classified as monodentate, bidentate, tridentate and so on. In the context of organometallic catalysis, multiple factors contribute towards the efficiency of a catalyst such as its thermal stability, number of vacant sites present of metal centre and its oxidattion state. Typically, multidentate ligand systems provide greater stability as compared to monodentate ones, but lesser catalytic activity.[1] Therefore, systematic tuning from monodentate system to polydentate is essential to obtain a balance between stability and catalytic efficiency of organometallic complexes. However, it has been observed that tridentate pincer ligands form complexes with optimal reactivity and stability.[9]

1.2 Pincer complexes

The initial organometallic complexes containing tridentate ligands adopting a meridional geometry were demonstrated in the late 1970s by Moulton and Shaw,[10] and the term "pincer" was coined by van Koten in 1989.[11, 12] The term "pincer" initially referred to tridentate ligands with a central anionic carbon and two flanking donor units having meridional geometry on binding to the metal center.[12] Since then, the definition of pincer has greatly broadened and now it generally refers to any three-coordinate ligand bound to metal centre in a meridional fashion. The formation of two five-membered metallocyclic rings occurs upon complexation of the pincer ligand to the metal centre.[13] The general depiction of a typical pincer-metal complex is shown in Figure 1.10, and among the three donor atoms , two (Y) are *trans* to each other and a central donor atom (Z) is *cis* to both.[13]

Figure 1.10. Schematic representation of a pincer metal complex showing variable parameters.[13]

The synthesis of first pincer complex was reported by Moulton and Shaw in 1976, in which the treatment of *bis*phosphine ligand (^{t}Bu4PCP) with metal salts resulted in C-H activation of the central carbon of the ligand.[10] For close to five decades now, the pincer chemistry has made steady progress and in the past 15 years, pincer based metal complexes have gained significance in the field of homogeneous catalysis owing to their high thermal stability and versatility, arising from the rigidity of the pincer framework.[9, 14-18] Pincer-metal complexes find wide applications in plethora of catalytic reactions, which have also been extended to heterogeneous versions.[19] The chemistry of pincer-metal complexes based on Ir,[18, 20] Pd,[21] Ru,[22] Fe,[23] Ni,[17] Co[14, 24] and Mn[23, 24] have been covered in several review articles.

1.3 Catalytic applications of pincer-metal complexes

In the last two decades, pincer-ligated metal complexes have been highly employed for a variety of organic reactions having both industrial and social applications. They exhibit excellent activity towards numerous reactions such as alkane dehydrogenation,[15] C-C/C-N

cross coupling reaction,[17, 25] hydrogenation of carbon dioxide,[26, 27] nitrile,[26, 27] olefins[26, 27] and alkynes[26, 27] and dehydrogenation of alcohols.[28, 29] In the context of current thesis, the transformation of alcohols leading to hydrogen and value-added chemicals employing homogeneous systems (mainly pincer-metal complexes) has been discussed.

1.3.1 Dehydrogenation of alcohols and their tandem reactions

Alcohols are abundant and significant feedstock for organic synthesis. They are cheap, have low toxicity, and readily available.[30] They are present in a great number of renewable feedstocks (eg. lignocellulosic biomass and carbohydrates)[31] and apart from that they can be readily synthesized *via* reliable methods.[30] While for the dehydrogenation of alcohols with high hydrogen content, the generation of H_2 is the target,[29] for higher alcohols (with low H_2 wt%), dehydrogenation of alcohols leads to reactive carbonyl species[32] and their further functionalization represents a convenient strategy for the clean synthesis of fine chemicals such as esters, higher alcohols, carboxylic acids, amines, imines and others.[33]

The dehydrogenation of alcohol resulting in extrusion of hydrogen atoms in the form of molecular hydrogen has a high energy barrier and therefore a catalyst is required to accelerate the rate of this reaction.[34] For example, the sequential conversion of methanol to formaldehyde and further to CO has a rate determining barrier of 94.5 kJ/mol.[34] An alternate route with a lower barrier can only be encountered in the presence of a catalyst.

1.3.1.1 Acceptorless dehydrogenation of alcohols

The first report based on pincer-ruthenium catalyzed acceptorless dehydrogenation of alcohols was published in 2004 by Milstein and co-workers,[35] where they introduced electron-rich and bulky ruthenium PNP complex **1.12**. They were able to obtain up to 91% yield of corresponding ketones starting from secondary alcohols in the presence of 0.4 mol% **1.12** and sodium isopropoxide (1 equivalent relative to **1.12**) in dioxane at 100 °C after 70 h.[35] Following the pioneering work by Milstein, several homogeneous complexes were described for catalytic acceptorless dehydrogenation of alcohols, with major reports being reported with pincer-Ru complexes (Figure 1.11).[36] In 2017, Sun designed the PNN-ruthenium complex **1.13** (Figure 1.11), which was able to effectively catalyze the dehydrogenation of secondary alcohols to ketones under low catalyst loading (0.0125–0.025 mol%) and 1 equivalent of KO^{t}Bu, resulting in very high TONs (up to 8000) and 100% conversion.[37] Later, Yu and co-workers reported the acceptorless dehydrogenation of secondary alcohols employing a NNC pincer Ru(II) hydride

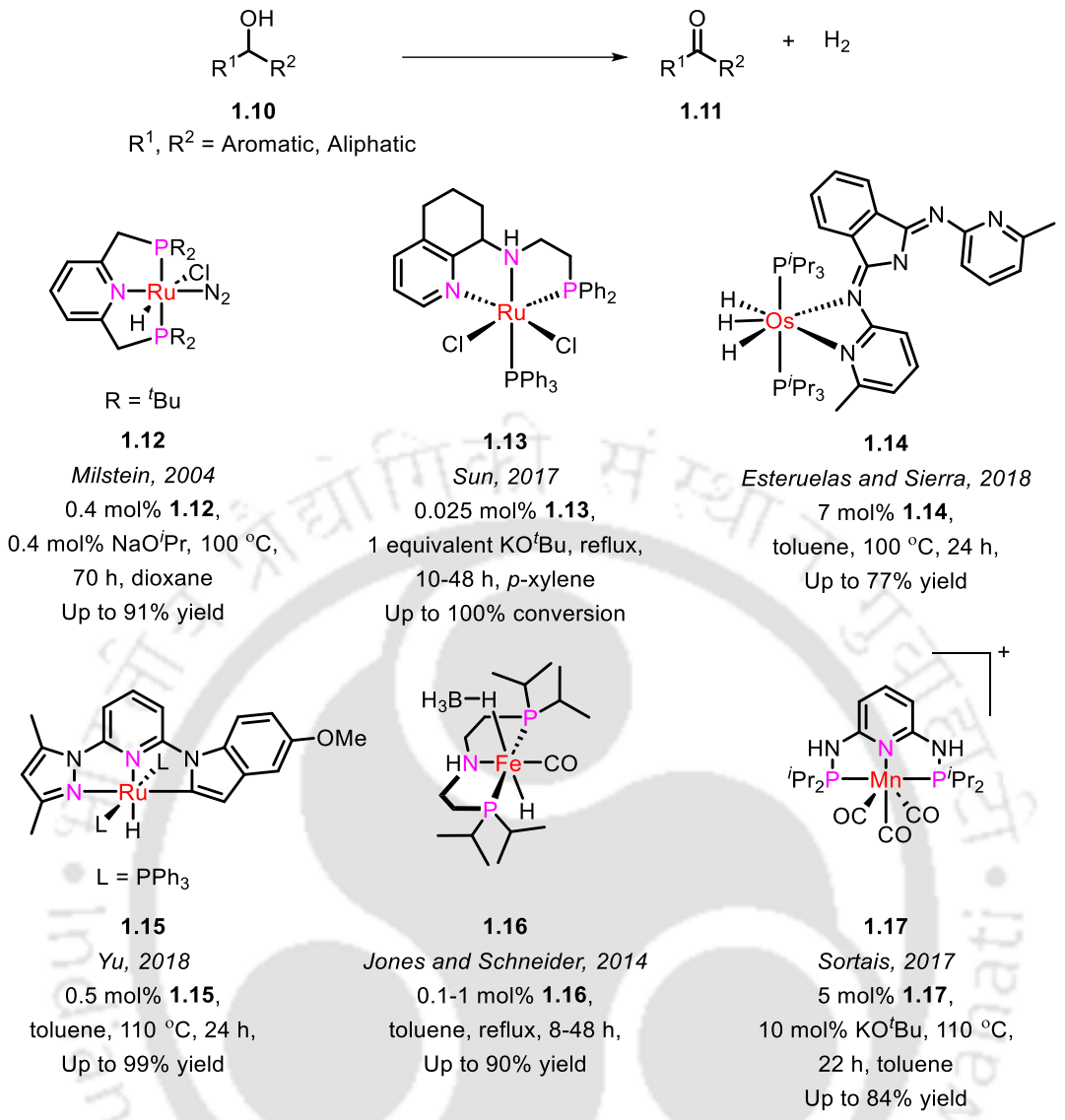

Figure 1.11. Homogeneous catalysts including pincer-based metal complexes reported for the acceptorless dehydrogenation of alcohols to ketones.[36]

complex (**1.15**) (Figure 1.11) at 0.5 mol% catalyst loading without any base additive.[38] The complex **1.15** exhibited vast substrate scope and up to 99% yields of the corresponding ketone was obtained in the presence of 0.5 mol% **1.15** in toluene as solvent at 110 °C after 24 h.

Since the initial studies on alcohol dehydrogenation reaction were reported with noble metals, the catalysts with earth-abundant metals such as manganese,[24] iron,[39] cobalt[24] and nickel[17] have recently been described for the dehydrogenation of alcohols.[32] In 2014, Jones and Schneider reported the catalytic acceptorless dehydrogenation of alcohols using well-defined iron-complex chelated aliphatic PNP pincer ligand **1.16** based on metal-ligand cooperativity mechanism.[40] This was the first report based on homogeneous iron-based system and in

presence of low catalyst loading (0.1–1 mol%), secondary alcohols underwent transformation to corresponding ketones. In the presence of 1 mol% of **1.16** and toluene as solvent, up to 94% yield of the desired product was observed after 12 h under reflux conditions.[40] Recently, Sortais and co-workers utilized the air stable PN_3P Mn carbonyl complex **1.17** for the dehydrogenation of secondary alcohols to ketones, where they observed very low TON (up to 18) and the reaction was completely reversible (Figure 1.11).[41] In the presence of 5 mol% **1.17** and 10 mol% KO^{t}Bu, 84% yield of acetophenone was obtained after 22 h at 110 °C.

A large library of pincer-metal catalyzed acceptorless dehydrogenation reactions of alcohols have been reported and well-reviewed in the past.[32, 36b] In this section, selected examples of pincer-metal complexes comprising of noble and earth-abundant metals have been discussed. The acceptorless dehydrogenation of alcohols to corresponding aldehyde and ketones is a green process, as it is atom economical and eliminates the use of toxic oxidants.[36b] These valuable aldehydes and ketones can be subsequently used as building blocks for the production of various value-added chemicals[28, 42] which is discussed in the sections below.

1.3.1.2 *N*-Alkylation of alcohols

In the past few decades, the hydrogen borrowing strategy or hydrogen auto-transfer method has been successfully described to afford new C-X bonds starting from alcohols, producing water as sole by-product.[42] The selective *N*-alkylation of primary amines using alcohols *via* hydrogen borrowing strategy is recognized as an effective strategy to access secondary amines.[43] This strategy of shuttling hydrogen between substrates without the need of external hydrogen, provides a practical approach towards the synthesis of valuable organic frameworks in chemical industries.[43] Along with the hydrogen, this process generates more reactive aldehyde/ketone from alcohol, which undergoes condensation with electron-rich coupling partners such as amines or carbonyl compounds to afford C-N and C-C double bonds, which are further reduced with the evolved hydrogen in the presence of catalyst (Scheme 1.10).[44]

The *N*-alkylation of amines was initially demonstrated by Watanabe[45] and Grigg[46], and since then tremendous progress has been made in this field mainly using precious metal catalysts (Figure 1.12) based on Ru[22, 42, 43] and Ir.[20, 33, 42, 43] In the context of pincer complexes mediated *N*-alkylation reactions, Kundu and co-workers demonstrated the catalytic activity of pincer ruthenium complex **1.20** (Figure 1.12) towards the alkylation of aniline with benzyl alcohol under inert atmosphere.[47] The use of 0.2 mol% **1.20** along with 25 mol% KO^{t}Bu in the presence

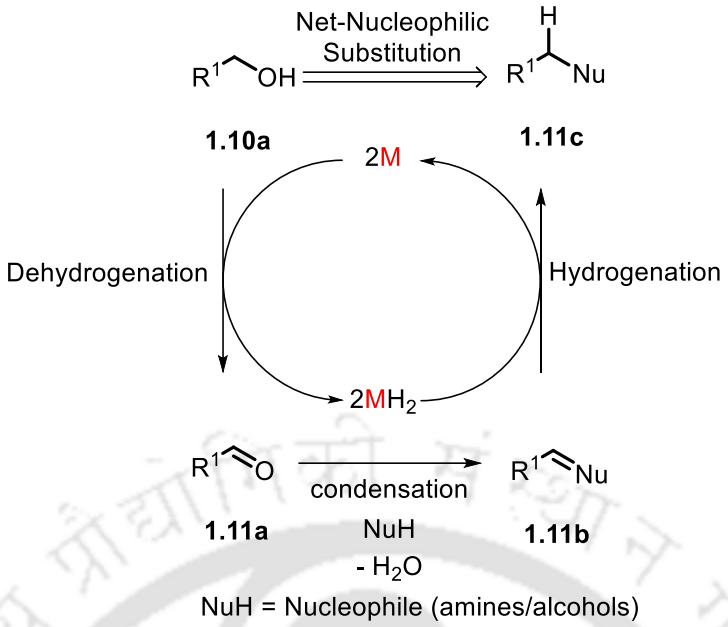

Scheme 1.10. General scheme for hydrogen borrowing methodology.

of dioxane as solvent, resulted in 98% conversion of benzyl alcohol after 12 h at 110 °C. This protocol was further extended to the *N*-methylation of several amines using methanol as methylating agent, where up to 86% yield of the desired product was obtained.[47] Later in 2019, Kumar and co-workers employed NNN pincer ligated ruthenium complex **1.21** (Figure 1.12) for the alkylation of amines with alcohols under inert conditions.[48] The reaction was carried out in the presence of sodium, which generated sodium-alkoxide *in-situ* thereby making the process atom-economical. *N*-Benzylaniline was synthesized with 57% yield (TON 2850) at 140 °C in 20 h under solvent-free conditions employing 0.02 mol% of **1.21** and 0.75 equivalents of sodium. The authors reported very high TONs (up to 29000) for the alkylation of aniline with cyclohexyl methanol, when 0.002 mol% of catalyst loading was used. The work was also extended to *N*-methylation of anilines and excellent turnovers (12000 TONs) were obtained under similar conditions with 1 equivalent of sodium.[48]

The use of environmentally benign, less-toxic, cheap and earth-abundant 3*d* transition metals instead of precious metals towards the *N*-alkylation of alcohols poses a significant challenge and is one of the emerging areas of present research.[44, 49, 50] Recently, base metal mediated alkylation of alcohols with amines employing Ni,[17] Co,[14] Mn,[24] Fe[39] and Cr[51] has been reported where the authors have obtained comparable yields under similar conditions as used in case of precious metals (Figure 1.12).[49] In 2020, Kempe reported the first chromium catalyzed amination of alcohols, which was able to effectively catalyze alkylation of several amines with

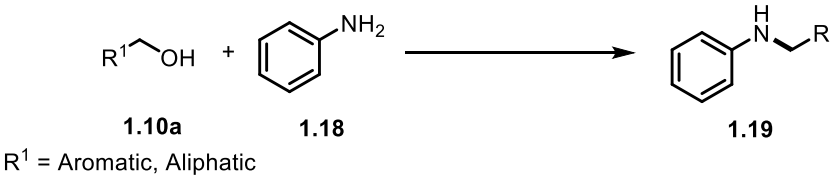

1.10a **1.18** **1.19**

R^1 = Aromatic, Aliphatic

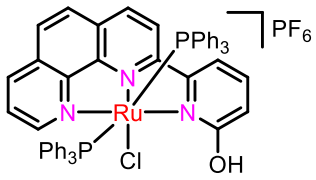

1.20
Kundu, 2018
0.2 mol% **1.20**,
25 mol% KO^{t}Bu, 110 °C,
16 h, dioxane
Up to 95% yield

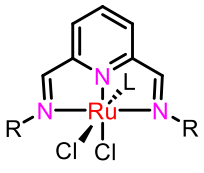

L = PPh_3
R = ^{t}Bu

1.21
Kumar, 2019
0.02 mol% **1.21**,
0.75-1 equivalent Na,
140 °C,
20-48 h, neat
Up to 80% yield

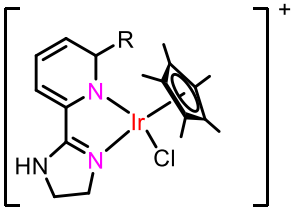

R = OMe

1.22
LuO, 2020
0.1 mol% **1.22**,
1.1 equivalent KOH,
80 °C,
12 h, water
Up to 95% yield

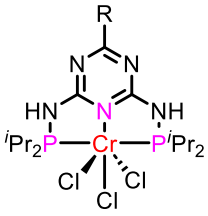

R = *p*-CF_3-C_6H_4

1.23
Kempe, 2020
3 mol% **1.23**,
0.5 equivalents KO^{t}Bu,
150 °C,
18 h, dioxane
Up to 94% yield

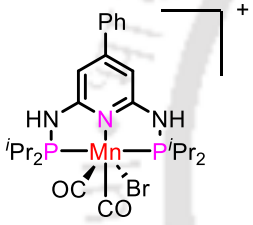

1.24
Kempe, 2018
3 mol% **1.24**,
1 equivalennt KO^{t}Bu, 80 °C,
18 h, THF
Up to 97% yield

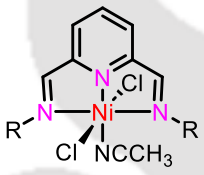

R = ^{i}Pr

1.25
Kumar, 2020
0.02 mol% **1.25**,
0.75 equivalent NaO^{t}Bu,
140 °C,
48 h, neat
Up to 80% yield

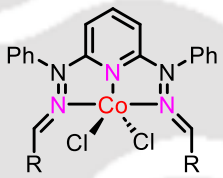

R = *p*-OEt-C_6H_4

1.26
Ghosh, 2021
4 mol% **1.26**,
0.5 equivalent KO^{t}Bu,
110 °C,
24 h, toluene
Up to 86% yield

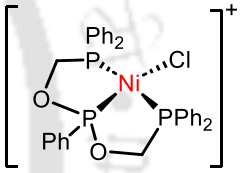

1.27
Mani, 2022
2.5 mol% **1.27**,
0.8 equivalent KO^{t}Bu,
140 °C,
24 h, toluene
Up to 92% yield

Figure 1.12. Representative examples of catalytic *N*-alkylation of amines with primary alcohols employing homogeneous complexes including pincer-metal complexes.[43, 49]

alcohols containing electron withdrawing and electron donating groups.[51] The *N*-alkylated amines were obtained in good to excellent yields (up to 94%) in presence of **1.23** (3 mol%) and 0.5 equivalents KO^{t}Bu in polar dioxane solvent at 150 °C in 18 h under N_2 (Figure 1.12).[51] In 2018, Kempe employed pincer ligated PNP-Mn complex **1.24** similar to **1.17** (Figure 1.12), for the synthesis of secondary amines (up to 97% yield) starting from primary amines with plethora of substituted alcohols in presence of one equivalent of KO^{t}Bu in polar solvent THF at 80 °C under 3 mol% catalyst loading.[52] Recently, nickel based methodologies have gained special attention as sustainable alternatives to the noble metal-based complexes owing to the higher

abundance of nickel and its inexpensive nature.[17, 53] However, due to strong bonding and thereby poor leaving group ability of alcohols poses a prime challenge for their transformation catalyzed by a nickel center.[54] In 2020, Kumar and co-workers described solvent-free *N*-alkylation of aniline derivatives with primary alcohols in addition to synthesizing a variety of benzimidazoles *via* hydrogen-borrowing strategy.[55] The pincer-nickel complex **1.25** (Figure 1.12) resulted in moderate to good yields (up to 90%) of the secondary amines under very low catalyst loading (0.002–0.02 mol%) in presence of 0.75 equivalents of NaO^{t}Bu. The highest yield (up to 90%) was observed for the amination of napthyl-1-methanol with 2-aminopyridine and very high turnovers (up to 34000) were observed in case of alkylation of 2-aminopyridine with 4-methoxybenzyl alcohol.[55] In the following year, Ghosh and co-workers synthesized pincer Co(II) complex **1.26** (Figure 1.12) and successfully applied it for the C-N bond formation towards the synthesis of *N*-alkylated amines (up to 85% yield).[56] The reaction was carried out using 4 mol% **1.26**, 0.5 equivalents KO^{t}Bu at 110 °C after 24 h under argon atmosphere.[56] Recently, Mani synthesized four and five coordinated Ni(II) pincer complexes and among them **1.27** (2.5 mol%) exhibited excellent catalytic activity for the *N*-alkylation of aromatic amines in presence of 0.8 equivalents of KO^{t}Bu at 140 °C in 24 h under nitrogen atmosphere.[57]

The *N*-alkylation of amines is currently an emerging research area and it is one of the most efficient protocols to generate secondary amines.[43] These compounds have remarkable significance in terms of applications in biological and pharmaceutical industries.[36c] In this regard, pincer-metal complexes have been at forefront in catalyzing such transformations and few of them have been discussed above as covering all of the reports is out of the scope of this chapter. Pincer-metal catalyzed transformation of alcohols and primary amines to secondary amines has been well-reviewed in past[42, 44, 50] and the current focus has shifted to employing pincer based 3*d* metals for *N*-alkylation of alcohols, and many reports have been published for the same.[44, 45]

1.3.1.3 Catalytic *β*–Alkylation of secondary alcohols with primary alcohols

Several research groups world-wide used the hydrogen borrowing technique to work on *C*-alkylation processes concurrently with research on *N*-alkylation.[28, 30] As with *N*-alkylation, *C*-alkylation also follows a similar pathway involving sequence of dehydrogenation, condensation and hydrogenation reactions, mediated by a transition metal complex.[42] In

comparison to the conventional alkylation of stoichiometrically synthesized enolates using alkyl halides, this process seems more appealing owing to the stability and easy availability of alcohol substrates and water is generated as the sole by-product (Scheme 1.11).[42]

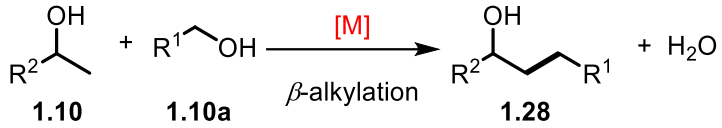

Scheme 1.11. General scheme for the transition metal catalyzed *β*-alkylation of secondary alcohols with primary alcohols also called as Guerbet reaction.

There have been a plethora of reports for the catalytic *β*-alkylation of secondary alcohols with primary alcohols, based on transition metal complexes having Ir,[58-67] Rh,[68] Ru,[25] Mn,[24, 49] Co,[24] Ni,[17, 49] and Cu[49] as metal center. In this regard, pincer ligated metal complexes have been at the forefront in the cross-coupling of alcohols resulting in *β*-alkylated alcohols with high yields and selectivity (Figures 1.13-1.14).[14, 17, 25] In 2008, Crabtree reported *β*-alkylation of 2° alcohols with 1° alcohols based on terpy pincer-ruthenium and pincer-iridium catalyst **1.29a-b** (Figure 1.13).[66] The use of 1 equivalent KOH along with 1 mol% **1.29a** resulted in 65% yield of **1.28** with 100% selectivity, whereas under similar conditions and lower loading of base (20 mol%), **1.29b** afforded 95% yield of the *β*-alkylated product with 93% selectivity.[66] In 2016, Yu and co- workers studied the *β*-alkylation of secondary alcohols with primary alcohols and achieved up to 91% yield of **1.28** using pincer-Ru(III) complex **1.30** (Figure 1.13).[69] They also further extended the current protocol towards the alkylation of cyclopentanol with benzyl alcohol to afford dialkylated secondary alcohols. Later, Kundu and co-workers synthesized a series of pincer-ruthenium catalysts and utilized them towards the *β*-alkylation of secondary alcohols with primary alcohols.[70] They observed that upon significantly decreasing the catalyst loading, the NHC ligand-based NNC pincer-ruthenium complex **1.31** (Figure 1.13) resulted in very high turnover of 288000 for the *C*-alkylation reaction under solvent-free conditions.[70] Moreover, the complex **1.31** exhibited a vast substrate scope (including aromatic, aliphatic and heterocyclic alcohols). On the similar lines, they discussed the role of metal-ligand cooperativity in the bifunctional pincer-ruthenium complex **1.20** (Figure 1.13), which was able to effectively bring about the *β*-alkylation of numerous secondary alcohols with very high selectivity and turnovers (up to 31500) in the presence of 0.5 equivalents NaOH in refluxing toluene after 1.5 h of the reaction.[71] In 2020, Kumar and co-workers studied the *β*-alkylation of 1-phenyl ethanol alcohol with benzyl alcohol employing phosphine-free NNN pincer-

ruthenium carbonyl complex **1.32** (Figure 1.13) based on *bis*(imino)pyridine ligand.[72a] At a loading of 0.00025 mol%, highest TON of 372000 was achieved with the complex **1.32** under solvent free conditions in presence of very low loading of NaOH (2.5 mol%). Recently, Bera described the catalytic *β*-alkylation of secondary alcohols with primary alcohols using Ir(III)-NHC complex (**1.33**) (Figure 1.13) along with potassium hydroxide as base.[72b] The complex **1.33** achieved exceptional activity due to the presence of pyripyridyl(benzamide)-functionalized NHC backbone in which dearomatization/aromatization of pyridine backbone occurs during the course of reaction. The catalytic systems exhibits a broad range of substrate scope under low base (10 mol%) and catalyst loading (0.05 mol%) in a short span of time *i.e* 30 min.[72b] They also extended the current protocol for the *α*-alkylation of ketones employing primary alcohols in addition to the synthesis of quinoline and lactone derivatives.[72b] In the same year, Ghosh and co-workers synthesized an amido-functionalized ruthenium carbene complex **1.34** (Figure 1.13) and studied it for the cross-coupling of variety of secondary and primary alcohols, where they obtained moderate to good yields (*ca.* 63–89%)of the *β*-alkylated product.[72c]

Although, there have been exemplary cases where the *β*-alkylation of secondary alcohols with primary alcohols has been efficiently catalyzed by noble metal based pincer complexes,[25] but current focus has shifted to employ easily available, less toxic and highly abundant 3*d*-metal based complexes.[25] In this context, homogeneous systems mainly comprising of pincer-ligated complexes based on Cr,[73] Mn,[24] Ni,[17] Co[14] and Zn[74] have been reported for such reactions (Figure 1.14). In 2017, Kempe and co-workers were the first to report the Co-catalyzed *β*-alkylation of alcohols using a PN_5P pincer-Co complex **1.35** (5 mol %) (Figure 1.14) in the presence of 1.1 equiv of KHMDS (potassium hexamethyldisilazane) to get up to 80% yield of the *β*-alkylated product.[75] The catalyst system was applicable to a broad range of substrates and was driven by hydrogen-borrowing strategy. Yu and co-workers were the first to report Mn-catalyzed *β*-alkylation reaction, where they synthesized a panel of phosphine-free Mn(I) complexes bearing a pyridyl-supported pyrazolyl-imidazolyl ligand.[76] Among the complexes screened, **1.36** (Figure 1.14) was found to be the most efficient towards the *β*-alkylation reaction. It was then employed towards the alkylation of various secondary alcohols with primary alcohols (43 examples) and up to 93% yield of the *β*-alkylated product was obtained using 2.1 mol% of catalyst loading in presence of KO^{t}Bu (30 mol%) at 110 °C with water as the sole by product. This protocol was further extended for one pot synthesis of flavan

derivatives from simple alcohols and for *β*-alkylation of cholesterol and its derivatives.[76] Later in 2019, Rueping and coworkers reported a novel Mn(I) complex (**1.37)** bearing a PNN pincer ligand (Figure 1.14) and employed it for the *β*-alkylation of secondary alcohols by primary alcohols *via* double hydrogen auto-transfer.[77] They obtained up to 99% conversion using 1 mol% of **1.37** in presence of KO^{t}Bu (25 mol%) at 135 °C and a broad range of substrates (29 examples) were converted into higher-value alcohols in good yields.[77]

In 2021, Ding reported a pincer-cobalt complex (0.7 mol %) supported by a $^{i\text{Pr}}$PPPN$^{\text{H}}$Py$^{\text{Me}}$ terdentate ligand (**1.38**) (Figure 1.14) for the *β*-alkylation of alcohols in up to 87% yield at 110°C at a very high loading (110 mol %) of KO^{t}Bu.[78] Later, Balaraman described the *β*-alkylation of alcohols utilizing $NiBr_2$/TMEDA (1:1) in the presence of 1 equivalent of KOH

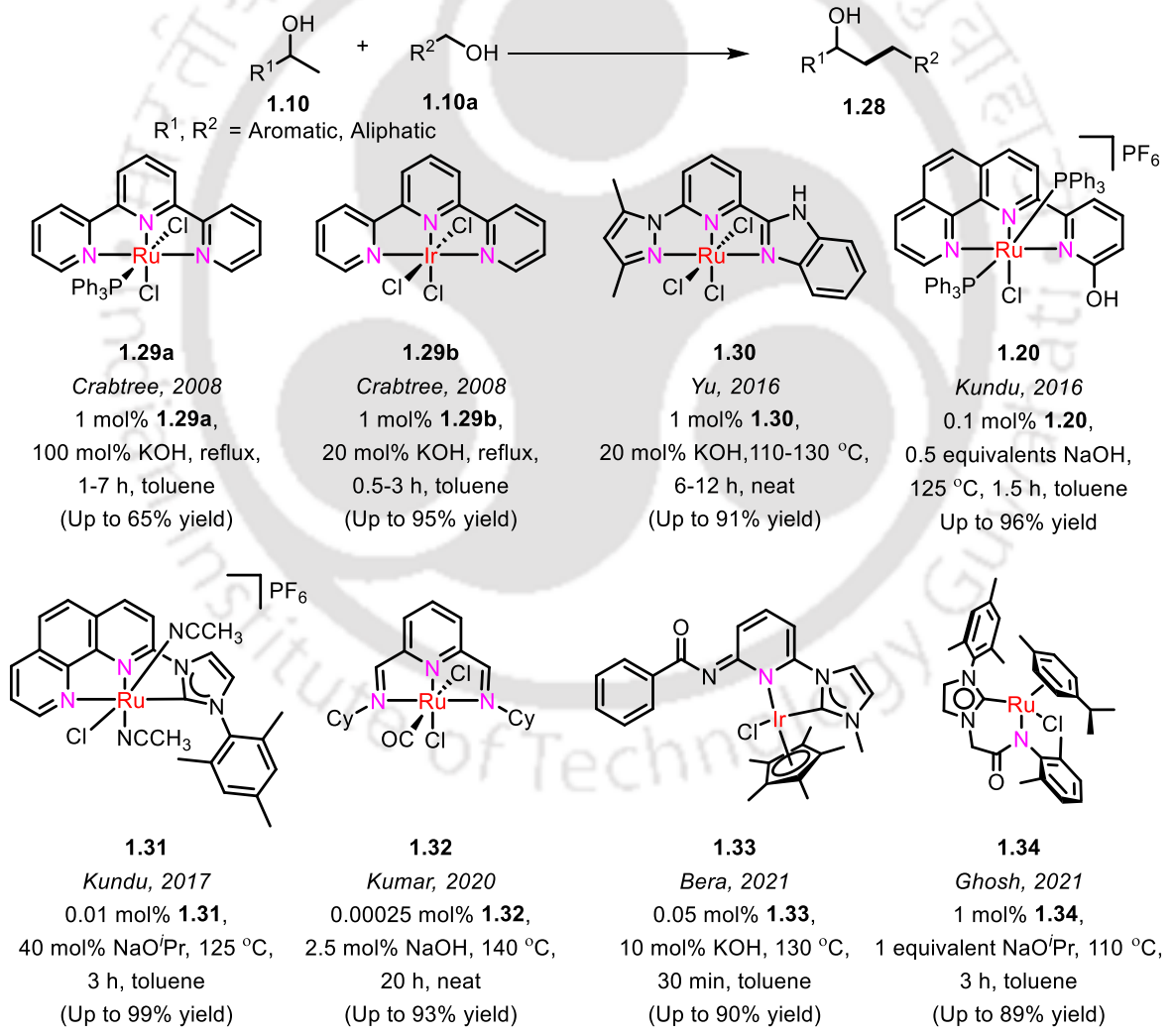

Figure 1.13. Representative examples of catalytic *β*-alkylation of secondary alcohols with primary alcohols employing homogeneous systems majorly comprising of pincer complexes, based on precious metals.[28]

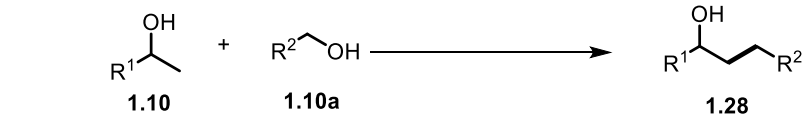

1.10 **1.10a** **1.28**

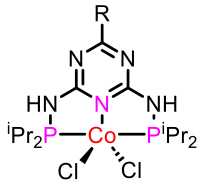

R = *p*-CF_3-C_6H_4

1.35
Kempe, 2017
5 mol% **1.35**,
1.1 equivalent KHMDS, 110 °C,
20 h, toluene
(Up to 80% yield)

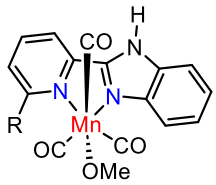

R = 3,5-Me_2pz

1.36
Yu, 2018
2.1 mol% **1.36**,
30 mol% KO^{t}Bu, 110 °C,
24 h, toluene
(Up to 93% yield)

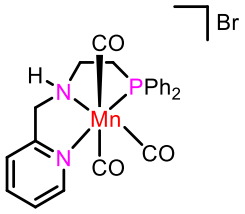

1.37
Rueping, 2019
1-3 mol% **1.37**,
25 mol% KO^{t}Bu, 135 °C,
20 h, toluene
(Up to 99% yield)

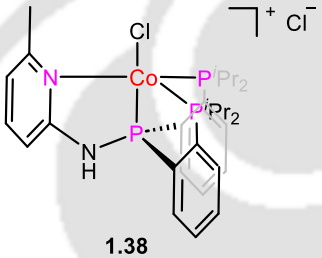

1.38
Ding, 2021
0.7 mol% **1.38**,
110 mol% KO^{t}Bu, 110 °C,
24 h, toluene
(Up to 87% yield)

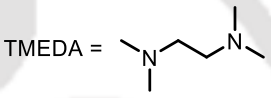

Balaraman, 2021
5 mol% **Ni**Br_2,
5 mol% TMEDA
1.1 equivalent KOH, 130 °C,
18 h, *n*-octane
(Up to 91% yield)

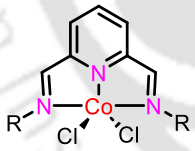

R = ^{i}Pr

1.39
Kumar, 2022
0.0025 mol% **1.39**,
2.5 mol% NaO^{t}Bu, 140 °C,
24 h, air, neat
(Up to 85% yield)

0.0025 mol% **1.39**,
2.5 mol% NaO^{t}Bu, microwave,
140 °C, 2 h, neat
(Up to 89% yield)

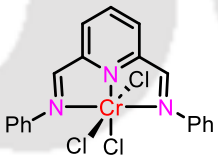

1.40
Kumar, 2022
0.005 mol% **1.40**,
5 mol% NaO^{t}Bu, 140 °C,
3 h, air, neat
(Up to 84% yield)

0.005 mol% **1.40**,
5 mol% NaO^{t}Bu, microwave,
140 °C, 1.5 h, neat
(Up to 91% yield)

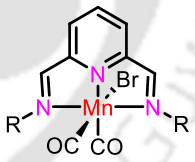

R = *p*-F-C_6H_4

1.41
Kumar, 2023
0.05 mol% **1.41**,
2.5 mol% NaO^{t}Bu, 140 °C,
12 h, air, neat
(Up to 92% yield)

0.05 mol% **1.41**,
2.5 mol% NaO^{t}Bu, microwave,
140 °C, 2 h, neat
(Up to 91% yield)

Figure 1.14. Representative 3*d* metal based homogeneous systems reported for catalytic *β*-alkylation of secondary alcohols with primary alcohols including pincer-metal complexes.[28]

at 130 °C using *n*-octane as solvent (Figure 1.14).[79] The $NiBr_2$/TMEDA (1:1) system tolerated a broad spectrum of substrates including aromatic, cyclic, acyclic, aliphatic alcohols and the protocol was extended towards the double alkylation of cyclopentanol with various alcohols.

In the following years, Kumar and co-workers synthesized a series of NNN pincer complexes consisting of chromium,[73] cobalt[80] and manganese[81] (**1.39-1.41**) (Figure 1.14) as central metal atom, for the catalytic *β*-alkylation of secondary alcohols with primary alcohols.[25] In 2022, Kumar reported the use of easily accessible $CoCl_2$ (0.01 mol%) towards the *β*-alkylation of alcohols affording high yields of **1.28** (up to 87%) and unprecedented turnovers (*ca.* 8700) in the presence of only 2.5 mol% of NaO^{t}Bu.[82] Later, similar studies were performed with NNN pincer-cobalt complex **1.39** (Figure 1.14)[80] and while $CoCl_2$ at a 0.0025 mol% loading and 2.5 mol % of NaO^{t}Bu at 140 °C resulted in 66% yield of **1.28** (26400 TON at 1100 TOF h^{-1}) in the *β*-alkylation of 1-phenyl ethanol with benzyl alcohol, its corresponding pincer complex **1.39** (0.0025 mol%) was highly efficient (*ca.* 1.3-fold *vs* $CoCl_2$) and afforded 85% yield of **1.28** (*ca.* 34000 TON at 1417 TOF h^{-1}) under similar conditions.[80] In the same year, Kumar and co-workers reported the first chromium catalyzed *β*-alkylation of secondary alcohols with primary alcohols, wherein they utilized simple base metal salt $CrCl_3.6H_2O$ and its corresponding NNN-pincer complex **1.40** (Figure 1.14) for the cross-coupling of secondary alcohol with primary alcohol.[73] This protocol afforded high yields of the *β*-alkylated product **1.28** under both conventional and microwave conditions. At 0.005 mol% loading of **1.40** and 5 mol% of NaO^{t}Bu at 140 °C, 90% yield (180000 TON in 1.5 h at 12000 TOs/h) and 84% yield (16800 TON in 3 h at 5600 TOs/h) of **1.40** was obtained under microwave heating and conventional heating respectively.[73] In the case of $CrCl_3.6H_2O$ under similar conditions, lower yields of **1.28** were obtained under both microwave (*ca.* 76%) as well as conventional heating (*ca.* 79%[73] Later in 2023, they reported Mn(I) complex (**1.41**) (Figure 1.14) based on *bis*(imino)pyridine ligand for the catalytic *C*-alkylation reaction.[81] The pincer-Mn(I) complex (**1.41**) displayed excellent activity (up to 92% yield) towards the catalytic *β*-alkylation of secondary alcohols by primary alcohols (35 substrates) at 0.05 mol% catalyst loading in presence of 2.5 mol% of NaO^{t}Bu under both conventional (air, 140 °C, 12h) and microwave heating (75 W, 2h).[81]

In conclusion, the catalytic *β*-alkylation of secondary alcohols with primary alcohols is an important organic synthetic reaction as it results in higher alcohols which find extensive applications in fine chemical and biofuel industries.[30b] The use of pincer-metal complexes (mainly ruthenium) for such transformations, has been reported by several researchers, namely

Crabtree,[66] Bera,[72b] Ghosh,[72c] Kundu,[70] Balaraman,[79] Kumar[72a] and many others. Over the past few years, many reviews have discussed the cross-coupling of alcohols utilizing pincer-metal complexes[28, 30a, 32] and in the current section a few of those examples have been elaborated. Recently, pincer-ligated earth abundant metal systems for the catalytic *β*-alkylation reactions have also gained attention and research in this area is still being explored.[25, 44] The detailed discussion of the same is covered in Chapter-IV.

1.3.1.4 Catalytic cross-coupling of alcohols to form *α*-alkylated and *β*-disubstituted ketones

As discussed above, acceptorless dehydrogenative coupling of alcohols is one of the most prominent synthetic methodologies in contemporary chemistry.[28] The hydrogen borrowing process involves the initial transition metal catalyzed dehydrogenation of alcohols to give the corresponding carbonyl compounds (Scheme 1.10).[42] This is followed by the base mediated aldol reaction to give *α*,*β*-alkylation ketones, which then undergo either partial hydrogenation to yield *α*-alkylated ketones (Scheme 1.12) or complete hydrogenation to afford *β*-alkylated alcohols (Scheme 1.11).[42] The cross-coupling of secondary alcohols follows similar process, resulting in *β*-disubstituted ketones.

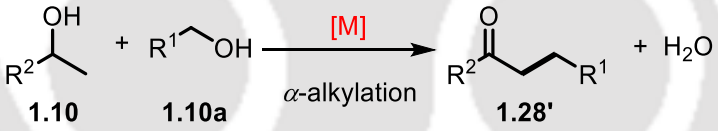

Scheme 1.12. General scheme for the transition metal catalyzed *β*-alkylation of secondary alcohols with primary alcohols.

In 2017, Achard reported the catalytic dehydrogenative cross-coupling of secondary alcohols with primary alcohols employing complex **1.42** (Figure 1.15) which resulted in selective synthesis of *α*-alkylated ketone (*via* with the concomitant formation of trace amount of *β*-alkylated alcohol.[72d] The complex was able to tolerate variety of substrates and afford moderate to good yields of the desired product with high selectivity.[72d] Later in 2019, Gunanathan and co-workers reported a Ru(II) catalyzed cross-coupling of two different secondary alcohols to *β*-disubstituted ketones using **1.43a** (Figure 1.15). They employed Ru-MACHO (1 mol%) as catalyst for coupling of variety of cyclic and acyclic secondary alcohols with benzylic secondary alcohols to yield cross-coupled ketone products in 30–90% yields.[72e] They extended the present protocol towards the self-coupling of secondary alcohols leading to the synthesis

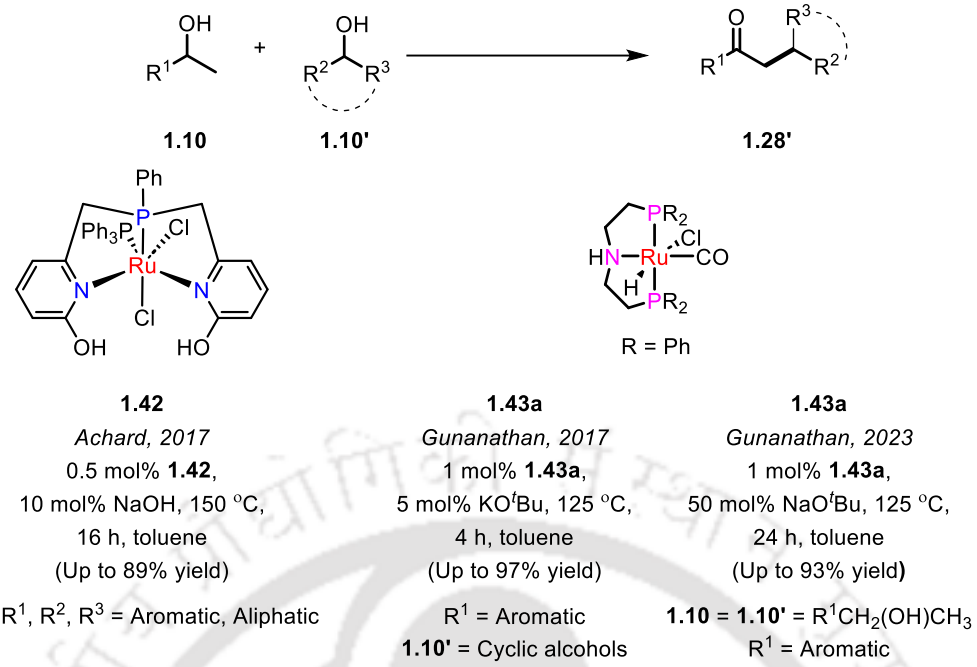

Figure 1.15. Selected examples reported for the synthesis of α-alkylated or β-disubstituted ketones *via* cross-coupling of alcohols.

of β-branched ketones.[72f] The complex **1.43a** (Figure 1.15) along with NaO^{t}Bu was effective towards the facile conversion of numerous functionalized aryl methanols, heteroaryl methanols, and linear and branched aliphatic secondary alcohols, resulting in water and hydrogen as the only by-products.[72f]

As discussed in previous and the current section, the acceptorless dehydrogenative coupling of alcohols is one of most prominent synthetic strategy towards the synthesis of ketones and alcohols.[42] The selective synthesis of α-alkylated and β-branched ketones is challenging and has been mainly described in past using homogeneous Ru(II) complexes comprising of mainly pincer complexes by the groups of Achard,[72d] Song,[72g] Gunanathan[72f] and others.[28] As, discussing all the examples is not in the scope of current chapter, a few of the representative examples have been discussed above.

1.3.2 Aqueous reforming of alcohols for the production of hydrogen

The environmental concerns and depleting fossil fuels have forced the scientific community to focus significantly on developing more sustainable and eco-friendly protocols. The alternate sources of energy explored till date, like solar, wind, tidal, nuclear, and geothermal, suffer from numerous limitations.[83] To eliminate the harmful effects of fossil fuel burning, focus has been shifted to hydrogen generation from waste as an immediate solution.[84] Hydrogen is regarded

as a clean fuel and an efficient energy carrier (120 MJ/kg) that can be converted into electricity by utilising various fuel cell technologies, thereby generating a significant amount of energy per unit mass.[85, 86] The use of hydrogen as a fuel has broadened the scope of energy sources, as it substantially reduces the emission of greenhouse gases and does not generate pollutants. Currently, the majority of H_2 is produced commercially using four main sources: natural gas, coal, oil and electrolysis.[87] As of 2022, fossil fuels are the major sources (*ca.* 95%) for the industrial-scale production of global hydrogen without carbon abatement.[88] The past few decades have witnessed a plethora of reports on the production and utilization of H_2 as a clean-burning sustainable energy source with high energy content (120 MJ/kg).[86, 89-91] Globally, the current emphasis is on sustainable hydrogen production from biomass[11-12] or *via* thermochemical, photocatalytic, or electrolytic splitting of water[92-94] using electricity from wind,[95, 96] solar,[95, 96] and geothermal energy.[92, 94, 97-99] The noteworthy advancement in green hydrogen production is, to a large extent, is limited by its storage and transportation, which includes low volumetric energy density, safe handling, and the requirement for expensive cryogenic and high-pressure compression cylinders.[100-103]

The storage of H_2 in the chemical bonds of small organic molecules and the transportation of these liquid organic hydrogen carriers (LOHCs) prior to their on-site dehydrogenation to generate on-demand H_2 while regenerating the LOHCs is an evolving and promising method in the quest for sustainable energy.[104] This process is of great interest due to the abundance of H_2-rich biomass feedstock. Moreover, the ability to produce H_2 from renewable resources makes this process environmentally friendly. These carbon-based compounds offer great prospects for efficient and sustainable H_2 production. In order to selectively generate H_2 from these molecules, researchers are actively focusing on developing novel catalytic processes that can offer potential advantages in terms of scalability, cost-effectiveness and environmental impact. By exploring the potential of small organic molecules, researchers aim to reduce the challenges and expand the range of possibilities for a future powered by H_2. In this regard, homogeneous catalysts, particularly those based on pincers, have proven to be efficient for catalyzing reactions involving release of H_2.[105]

1.3.2.1 Aqueous reforming of (m)ethanol for the production of hydrogen

In a broader concept of sustainable power management, the production of H_2 from renewable resources continues to be a challenging issue.[106] Alcohols are considered stable H_2-rich

molecules, and a significant research effort has been made in particular to generate hydrogen using alcohols as starting materials.[105] Since the storage of H_2 in the form of gas or liquid is associated with several safety implications owing to its flammable nature, the production of ''on-demand'' H_2 by directly using liquid organic hydrogen carriers (LOHCs, which could either be industrial wastes such as glycerol or readily available biomass derived products such as ethanol) provides a potentially promising route for hydrogen generation with concomitant production of value-added chemicals.[104] Among the plethora of catalysts that are at one's disposal, homogeneous catalysts, especially those containing pincer ligands have been efficient in catalyzing reactions involving the release of hydrogen, such as the aqueous reforming of (m)ethanol (Figure 1.16).[107]

In terms of alcohol reforming, methanol is seen as a viable option as it has a high gravimetric hydrogen capacity (12.6 wt%) and is therefore considered a promising candidate for H_2 generation.[89] Methanol is of great importance because of its easy availability from biomass and industrial sources.[108, 109] Depending on the circumstances of the reaction, dehydrogenation of methanol leads to the generation of different value-added products. Methanol can be dehydrogenated to CO and H_2, but carbon monoxide is detrimental for fuel cell applications.[110] Since, aqueous methanol-reforming entails complete dehydrogenation of methanol into CO_2 and H_2, it is an appealing method for storing hydrogen. Heterogeneous catalysts have been extensively used for methanol reforming and has been reviewed widely.[111]

A pioneering report that emerged in 2013 by Beller describes the use of pincer–Ru complexes (**1.43a-b**) (Figure 1.16) based on the MACHO ligand to catalyze the transformation of an mixture into H_2 and CO_2 (or CO_3^{2-}).[112] On optimizing the reaction conditions, it was observed that under similar reaction conditions, **1.43b** (1.8 ppm, 0.008 mol%) shows better activity (16.6% yield of H_2 at 2687 h^{-1}) in comparison to **1.43a** (8.23% yield of H_2 at 1051 h^{-1}) when employed in a 9 : 1 mixture of MeOH/H_2O (v/v) in the presence of 8.0 M KOH (1.4 equivalents with respect to water) after 3 h at 91 °C.[112] A remarkable activity was observed (up to 350000 TONs with 27% yield of hydrogen) when the reaction was performed with 9:1 MeOH/H_2O (v/v) under 0.008 mol% catalyst loading of **1.43b** after 23 days.[112] Later, Grutzmacher reported an anionic ruthenium complex [Ru(trop$_2$dad)], trop$_2$dad = 1,4-*bis*- (5*H*-dibenzo[*a,d*]cyclohepten-5-yl)-1,4-diazabuta-1,3-diene, **1.45** (Figure 1.16) for the aqueous-phase methanol reforming leading to 80% methanol conversion (84% H_2 yield) using 0.5 mol% **1.45** at 90 °C after 10 h.[113] This reaction proceeded without the additional use of base, and the

H_2/CO_2 gas mixture evolved was able to power an H_2/O_2 fuel cell.[113] Other significant pincer-ruthenium complexes

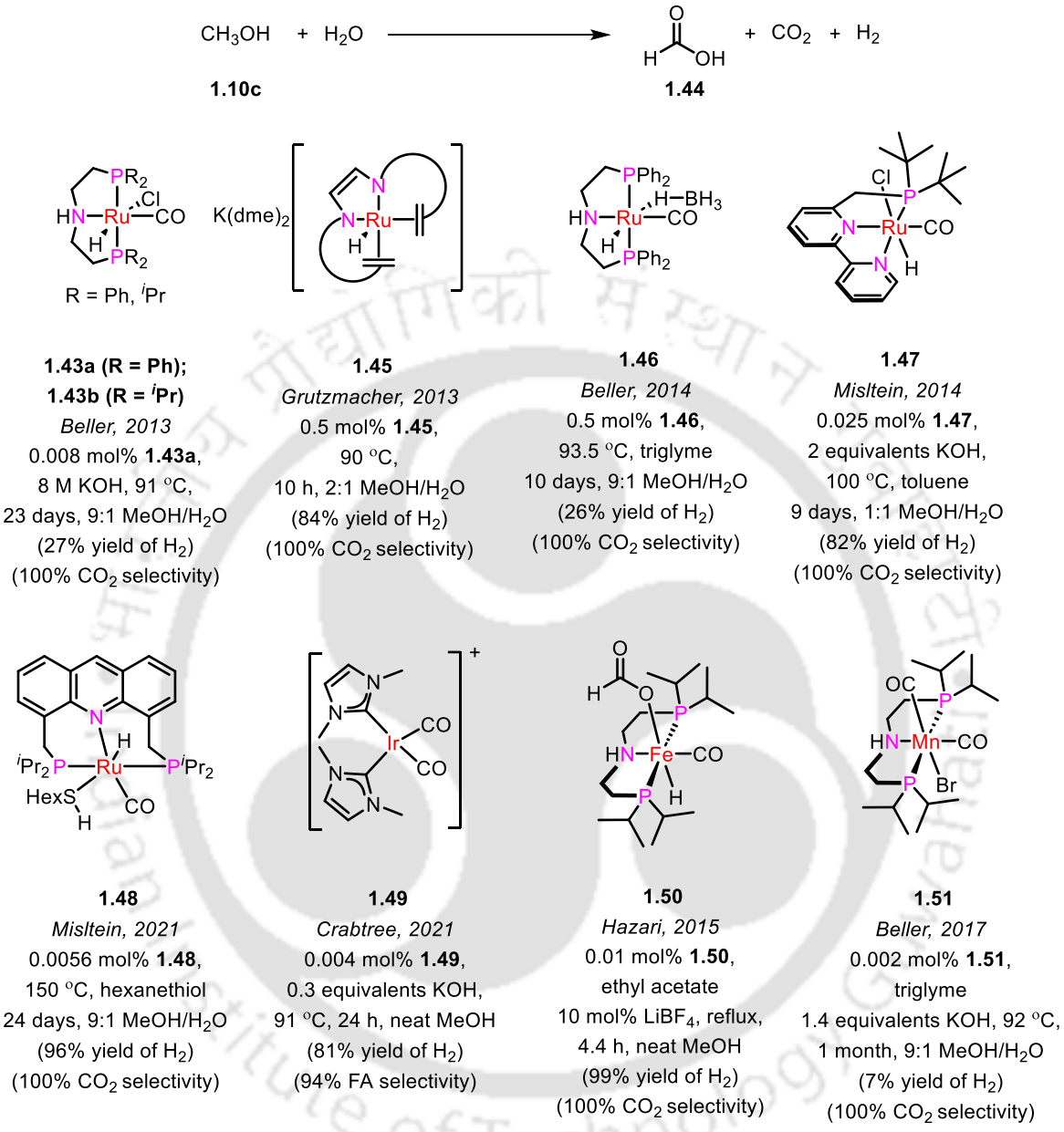

Figure 1.16. Selected examples (including pincer-metal systems) reported for the homogeneous catalytic aqueous methanol reforming.[105]

reported for this reaction include those by Beller, where he employed pincer–Ru-based catalyst, Ru-MACHO-BH, **1.46** (Figure 1.16), for base-free dehydrogenation of methanol.[114] The complex **1.46** (0.009 mol%) in combination with $Ru(H)_2(dppe)_2$ (0.009 mol%) afforded a total TON of >4200 (26% yield of H_2 relative to H_2O) under base free conditions at 93.5 °C after 10 h for a 9:1 MeOH/H_2O (v/v) mixture with only a trace amount of CO being formed (< 8

ppm).[114] In the same year, Milstein and co-workers reported the first example of a reusable homogeneous pincer Ru-PNN complex **1.47** (Figure 1.16) for aqueous reforming of methanol to H_2 and CO_2 (absorbed by base) at 100 °C without any requirement for catalyst isolation and purification.[115] The reforming of methanol in presence of 0.025 mol% of **1.47** and 2 equivalents of KOH, resulted in 77% yield of H_2 after 7 days. Moreover, when the organic layer of the reaction mixture was collected separately and reused directly, without using a catalyst and toluene, 82% yield of hydrogen was produced after nine days.[115] Thus, the catalyst was found to be reusable after several days of the reaction, and no loss in the activity of the catalyst was observed.

This was followed was several reports by Singh,[116] Qin and Zheng[117] and others, where homogeneous ruthenium complexes were employed for the catalytic reforming of methanol. In 2021, Milstein and co-workers described an acridine based pincer–ruthenium complex **1.48** (Figure 1.16) for the base-free methanol reforming reaction without utilizing additional solvents.[118] For a 9 : 1 MeOH/H_2O mixture, 96% yield of H_2 was obtained after heating the reaction mixture for more than 3 weeks in presence of 0.0056 mol% of **1.48** and an equivalent amount of hexanethiol, indicating the robustness and durability of the system.[118]

In the context of non-ruthenium based complexes, there are several complexes based on Ir, pincer complexes of Fe and Mn that were also reported (Figure 1.16).[105] In 2015, Crabtree reported an air- stable *bis*(N-heterocyclic carbene)-based iridium complex **1.49** (0.004 mol%) for the acceptorless dehydrogenation of methanol at 91 °C under basic conditions (6.7 M KOH, 0.3 equivalents relative to water) to produce hydrogen along with formic acid (81% yield at 3612 TONs) after 24 h.[119]

Despite the fact that the precious metals have been mainly studied for methanol reforming reaction, few examples have been reported by the groups of Hazari and Beller where they have utilized pincer-iron (**1.50**) and pincer-manganese (**1.51**) complexes based on MACHO ligand (Figure 1.16) for these reactions.[120-122] In case of the former, at 0.01 mol% catalyst loading in combination with 10 mol% $LiBF_4$, methyl formate and H_2 (*ca.* 99% yield and 20000 TON) were observed after heating for 4.4 h under reflux conditions.[121] On the other hand, 0.002 mol% of PNP pincer-based Mn catalyst **1.51** (Figure 1.16)[122] gave up to 7% yield of H_2 (up to 20000 TONs) in the presence of 10 equivalents of PNP^{i}Pr ligand and 1.4 equivalents of KOH after 1 month of prolonged reaction time for a 9 : 1 (v/v) (20 mL) mixture of methanol/water at 92 °C.[122]

Like methanol, bioethanol has gained attention as a promising hydrogen carrier owing to its relatively high hydrogen output (13 wt%).[123-126] It is generated on a large industrial scale *via* fermentation of biomass.[127] It is low-cost, readily available and has low toxicity.[128] The synthesis of acetic acid along with hydrogen *via* reforming of aqueous ethanol would have a large impact on industrial organic chemistry.[129] The transformation of ethanol to acetic acid has been extensively reported with heterogeneous based systems.[130, 131] The major drawback of heterogenous systems is their poor selectivity towards acetic acid and requirement of very high temperature (up to 350 °C).

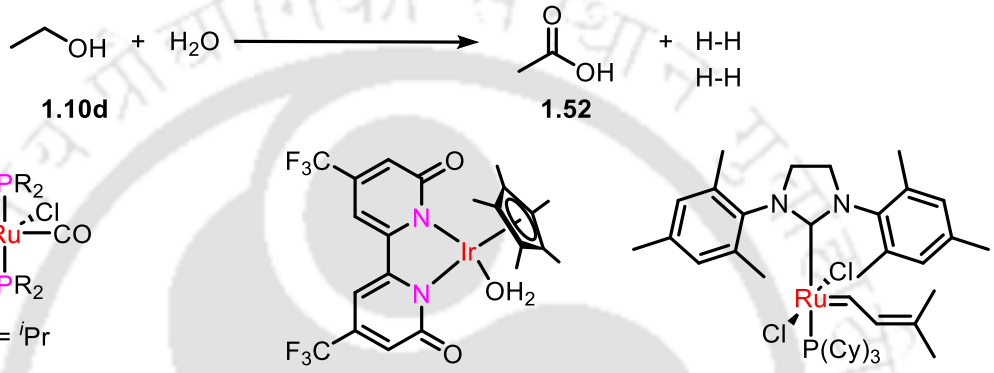

1.43b
Beller, 2014
0.005 mol% **1.43b**,
0.93 equivalents NaOH, 90 °C,
20 h, 1:3.2 EtOH/H_2O
(70% yield of H_2)
(70% yield of **1.52**)

1.53
Fujita, 2018
0.25 mol% **1.53**,
1.2 equivalents NaOH, 90 °C,
18 h, 1:111 EtOH/H_2O
(99% yield of H_2)
(99% yield of **1.52**)

1.54
Qin and Zheng, 2022
0.0008 mol% **1.54**,
0.9 equivalents KOH, 100 °C,
120 h, 1.2:1 EtOH/H_2O
(19% yield of H_2)
(15.5% yield of **1.52**)

Figure 1.17. Homogeneous catalysts reported for the aqueous ethanol reforming reaction.[105]

In the context of homogeneous based systems, ruthenium-based complexes have been mainly demonstrated for the aqueous ethanol reforming reaction resulting in acetic acid and hydrogen (Figure 1.17), with only one report with pincer-based system.[129, 132-134] The first report on catalytic ethanol reforming reaction employing a homogeneous system was published in 2014 (Figure 1.17). Here, Beller and co-workers studied several Ru and Ir-based complexes for the homogeneous catalytic conversion of bioethanol to yield acetic acid and hydrogen.[133] Notably, the pincer-ruthenium complex **1.43b** (Figure 1.17), earlier reported for methanol reforming,[112] was chosen as the optimized catalyst, owing to its high stability and its ability to form a free coordination site in the presence of a base.[133] Under the optimized conditions, a 5 : 5 EtOH/water mixture (v/v) led to 70% conversion of ethanol to acetic acid within 20 h at 90 °C. The analysis of the gas produced from the reaction showed the presence of very tiny amounts

of CO_2 and CO (below 10 ppm). In 2018, Fujita and coworkers reported an efficient bipyridonate ligated Ir complex **1.53** (Figure 1.17) for production of acetic acid with high yields from ethanol–water solution.[135] In the presence of 0.25 mol% **1.53** and 1.2 equivalents of NaOH, 99% yield of acetic acid and 95% yield of H_2 was observed after 18 h. In 2022, Zheng utilized an Ru-alkylidene complex **1.54** (0.0008 mol%) in the presence of 0.9 equivalents of KOH in a 1.2 : 1 EtOH: H_2O mixture, where they got up to 47295 TON (15.5% conversion of ethanol) and 19% yield of H_2 after five days at 100 °C (Figure 1.17).[134]

The reforming of alcohols, mainly methanol and ethanol using pincer-metal complexes continues to be the current favorite of the researchers and has gained significant attention over the past few years.[104, 105, 107] The production of clean-burning hydrogen under mild conditions using homogneous pincer complexes has a clear advantage over the traditional approach where harsh conditions are required with heterogeneous systems.[111] Apart from the selected examples discussed in this section, a detailed review of the previously reported catalytic systems for the reforming of methanol and ethanol has been covered in chapter II and III respectively.

1.3.3 Production of hydrogen from ethylene glycol

Ethylene glycol (EG) is the simplest and the most abundant vicinal diol, having high hydrogen storage capacity (6.5 wt%).[136] The liberation of H_2 from ethylene glycol, has gained a lot of interest recently as a potential candidate for sustainable energy and has been studied using both heterogeneous[137] and homogeneous[29] catalysts.

Homogeneous reforming of ethylene glycol for the production of hydrogen was first described by Cole-Hamilton and the group in 1988.[138] A variety of alcoholic substrates were tested using $[RuH_2(N_2)(PPh_3)_3]$ as a catalyst in presence of NaOH, and rates of hydrogen production (catalyst turnover h^{-1}) were reported. The rate was found to be considerably higher on employing Ru based catalyst for ethylene glycol (515.9 h^{-1}), and illumination aided the rate of hydrogen production still further (1185.3 h^{-1}).[138] From the point-of-view of pincer-metal complexes, Beller and co-workers in 2015 employed a pincer Ru-PNP catalyst, **1.43a** (Figure 1.18) for hydrogen production from ethylene glycol in diglyme at 125 °C and unprecedented catalytic activity was achieved (64,459 h^{-1} after 1 hour, yield of H_2 = 2.5% and 59,253 h^{-1} after 2 hours, yield of H_2 = 4.5 %) using less than 0.38 ppm (0.000038 mol%) of **1.43a** in presence of 0.16 equivalents of KOH (relative to ethylene glycol).[139] Although the glycolic acid generation was not confirmed, the developed protocol was found to be improved by about 54

times in terms of hydrogen generation with that reported by Cole-Hamilton's group (TOF 1185.3 h^{-1} after 2h).[139]

Very recently, Milstein and co-workers reported PNN pincer–Ru based aqueous reforming of ethylene glycol to glycolic acid and hydrogen gas with no CO_2 or CO emissions under milder reaction conditions.[140a] The reforming process resulted in a 91% yield of glycolic acid (TON = 182) with the evolution of 223 mL of pure hydrogen gas (yield = 93%) at 0.5 mol% catalyst loading and with 5 equivalents of the KOH in a 1 : 1 mixture of water (1 mL) and THF (1 mL) at 115 °C.[140a] They screened a variety of acridine-type Ru- PNP complexes and PNNH-based complexes and among all, **1.57** (Figure 1.18) showed superior performance in the reforming reaction.[140a]

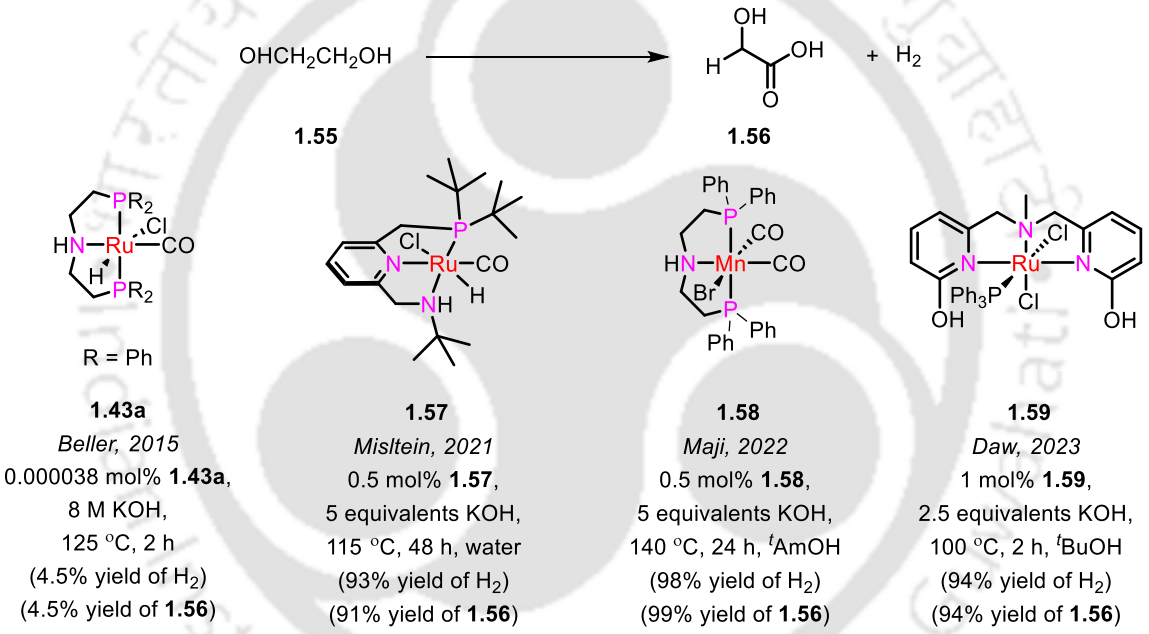

Figure 1.18. Pincer-based metal complexes reported for the production of hydrogen from ethylene glycol.[29]

Reforming of ethylene glycol to glycolic acid has so far relied on expensive metals. In 2022, Maji and co-workers have reported a series of complexes based on the third most abundant metal, manganese, and employed them for the reforming of ethylene glycol to glycolic acids.[141] A bench stable earth-abundant metal complex **1.58** (Figure 1.18) has catalyzed the reaction at 140 °C with the catalyst loading of 0.5 mol% in the presence of KOH (5 equivalents) in ^{t}AmOH. Among all the complexes, **1.58** is stabilized by the ^{Ph}MACHO ligand and gave the highest volume of hydrogen (240 mL, yield = 98%) with a TON > 198 and glycolic acid yield > 99% in 24 h.[141]

Very recently, Daw developed a bifunctional NNN pincer–Ru complex **1.59**, which showed high catalytic efficiency (25225 TON) for the selective production of H_2 from ethylene glycol (apart from sorbitol[142]) under mild reaction conditions along with the formation of glycolic acid (Figure 1.18).[143] In the presence of 1 mol% **1.59** and 2.5 equivalents of KOH, 94% yield of glycolic acid was obtained within 2 h at 100 °C using ^{t}BuOH as solvent.[143]

Ethylene glycol is one of the simplest vicinal diol and reports based on homogeneous reforming of ethylene glycol for the production of hydrogen are scarce.[29] The pincer-metal complexes have majorly been used for the transformation of ethylene glycol to glycolic acid and most of these reports have been covered in the current section. Recently in the past two years, Singh,[140b] Daw,[143] Maji[141] and others[29] have explored this polyol for the generation of hydrogen and is an emerging area in the field of alcohol reforming using pincer catalysts.

1.3.4 Transformation of glycerol to lactic acid and hydrogen

Glycerol is readily available as a result of the booming bio-diesel sector, which creates this polyol as a primary waste product.[144] Additionally, it is non-toxic and biodegradable and has a high boiling point, unlike ethanol and methanol. It is also produced as a waste product from a variety of processes, such as hydrogenolysis of cellulose[145] and fermentation processes using micro-organisms.[146] Thus, owing to the contribution from multiple sources including the recent boom in bio-diesel production, there is a large abundance of glycerol in global reservoirs. The versatile nature of glycerol has rightly made it to be considered as useful waste which can either be directly used as a fuel,[147, 148] a non-volatile solvent,[147, 148] a source of molecular hydrogen or be functionalized/transformed into a plethora of valuable raw materials including lactic acid.[144] Notably lactic acid finds wide utility in food, pharmaceutical and polymers industries.[149] Bioconversion and heterogeneous catalysts for glycerol to lactic acid are well explored and are limited by several challenges.[150] In order to achieve high selectivity towards lactic acid during its production from glycerol, minimization of some side reactions such as (i) C–C cleavage, (ii) over-oxidation and (iii) over-reduction reactions should be accomplished.[151] In this context, the homogeneous catalysts comprising of majorly pincer-metal systems (Figure 1.17) came into the picture, which can operate under milder conditions and also show higher selectivity for lactic acid.[29]

In a pioneering effort in 2014, Crabtree set the trend by putting forward the idea of using homogeneous iridium complexes for acceptorless dehydrogenation of glycerol to lactic acid

and hydrogen.[152] The first report employing a pincer-ligated complex for such transformation came in 2015, where Beller described the remarkable activity of PNP-Ru complex **1.43a** (Figure 1.19), where a TON of 270000 with about 67% yield of lactic acid was afforded after 24 h at 140 °C using NMP as a solvent.[139] They obtained similar yield of lactic acid in case of industrial glycerol under identical reaction conditions (0.00025 mol% **1.43a** and 1.08 equivalents NaOH). Later, Crabtree and Hazari came up with the first-ever report on the homogeneous catalysis of glycerol to lactic acid and hydrogen using a catalyst derived from base-metal iron (Figure 1.19).[153] Their attempt to convert glycerol to lactic acid using a PNP pincer–iron complex **1.50** (0.02 mol%) (Figure 1.19) in the presence of NaOH (base: glycerol = 1 : 1) at 140 °C for 3 h gave lactic acid with a high selectivity of 83% (TON = 880), with the glycerol conversion (*ca.* 24%) being lower than that reported with its pincer-ruthenium counterpart **1.43a**.[139]

In 2020, Kumar and co-workers synthesized NNN pincer–Ru complexes based on *bis*(imino)pyridine and 2,6-*bis*(benzimidazole- 2-yl)pyridine ligands and investigated their catalytic activity for the transformation of glycerol into lactic acid and hydrogen.[154] All the reactions were performed for 48 h at 140 °C, using 0.03 mol% of the considered pincer–Ru catalysts in the presence of 0.58 equivalents of KOH, and the best results (approximately 70% lactic acid yield with 97% selectivity towards lactic acid) were obtained for catalyst **1.62** (Figure 1.19). In the case when the KOH loading was increased to 1 equivalent, keeping the catalyst loading at 0.03 mol%, Kumar was successful in achieving a 90% yield of lactic acid with a high selectivity of 98% towards lactic acid at 92% conversion of glycerol in an open vessel in the presence of an inert atmosphere at 140 °C after 48 h.[154] In 2022, Deng and Fu used PNP–Mn complexes to accomplish the transformation of glycerol into sodium lactate.[155] A very high yield of sodium lactate (96%) with 98% selectivity was obtained in 24 hours when 5 mmol glycerol was allowed to react with 0.5 mol% **1.58** (Figure 1.19) in the presence of 1.1 equivalents of NaOH and 0.5 mL of dioxane as solvent at 160 °C. They were also successful in achieving 63% lactate yield with 98% selectivity after 36 hours with a very low catalyst loading of 0.025 mol% by elevating the temperature to 180 °C.[155]

After demonstrating remarkable activity with pincer-ruthenium complex **1.62** towards the selective transformation of glycerol to lactic acid,[154] Kumar has extended these studies by utilizing base-metal salts and complexes for this transformation.[156-158] In 2024, the group has reported commercially available $CoCl_2$ for both the acceptorless and transfer dehydrogenation

of glycerol to lactic acid.[157] In the acceptorless dehydrogenation of glycerol, 33% yield of lactic acid was observed with 44% selectivity in the presence of 0.5 mol% $CoCl_2$ and 0.75 equivalents of KOH while in the presence of acetone, which acts as a sacrificial acceptor, 93% yield of lactic acid was observed using 1.1 equivalents of NaO^{t}Bu and 0.5 mol% $CoCl_2$ at 160 °C.[157] In the same year, inspired by the success of with NNN pincer-Ru complexes,[154] Kumar synthesized *bis*(imino)pyridine-based NNN pincer-Mn(II) complexes and applied them towards the transformation of glycerol to lactic acid in presence of acetone.[156] Among the considered complexes, ^{Ph2}NNNMnCl_2 (**1.63**) (Figure 1.19) was found to be the most efficient. Remarkable yield of lactic acid (up to 92%) was observed with >99% selectivity at 0.5 mol% loading of **1.63** in the presence of an equivalent of NaOH at 140 °C in 24 h.[156] Under similar reaction conditions, the commercially available $MnCl_2.4H_2O$ gave 72% yield of lactic acid with 96% selectivity. The pincer-Mn(II) catalyst **1.63** was further investigated with a range of acceptors, and good to moderate yields were observed in those cases.[156] After this report, the same group synthesized novel pincer-Fe(II) complexes and studied them for the catalytic transfer dehydrogenation of glycerol to lactic acid.[158] Similar to the previous work based on pincer-manganese,[156] in this case also ^{Ph2}NNNFeCl_2 (**1.64**) (Figure 1.19) was found to be highly efficient and it gave 91% lactic acid with 99% selectivity. Further, very high turnover (up to 740000 TONs) were obtained on decreasing the catalyst loading to 0.0001 mol%, where 74% lactic acid was observed with 98% selectivity after 7 days.[158] In comparison to the catalytic system based on $CoCl_2$,[157] which was the first glycerol transfer dehydrogenation system reported, the current corresponding system based on pincer-Fe operates at a relatively lower catalyst loading and at a lower temperature.

In the nutshell, glycerol is currently easily available owing to the boom in bio-diesel sector[144] and is being used currently to produce several value-added chemicals including lactic acid.[29] To achieve high selectivity of lactic acid, pincer-metal systems have been most promising candidates due to their robustness and high stability, as discussed above.[29] In the past decade, there has been a growing interest for the catalytic conversion of glycerol to lactic acid either *via* acceptorless fashion[139, 152-155] or using a transfer dehydrogenating agent.[156-158] This is due to the fact that large quantities of glycerol is present in global reservoirs.[144] Therefore, this transformation continues to prosper and is a growing area in the applications of pincer-metal chemistry in the transformation of polyols.

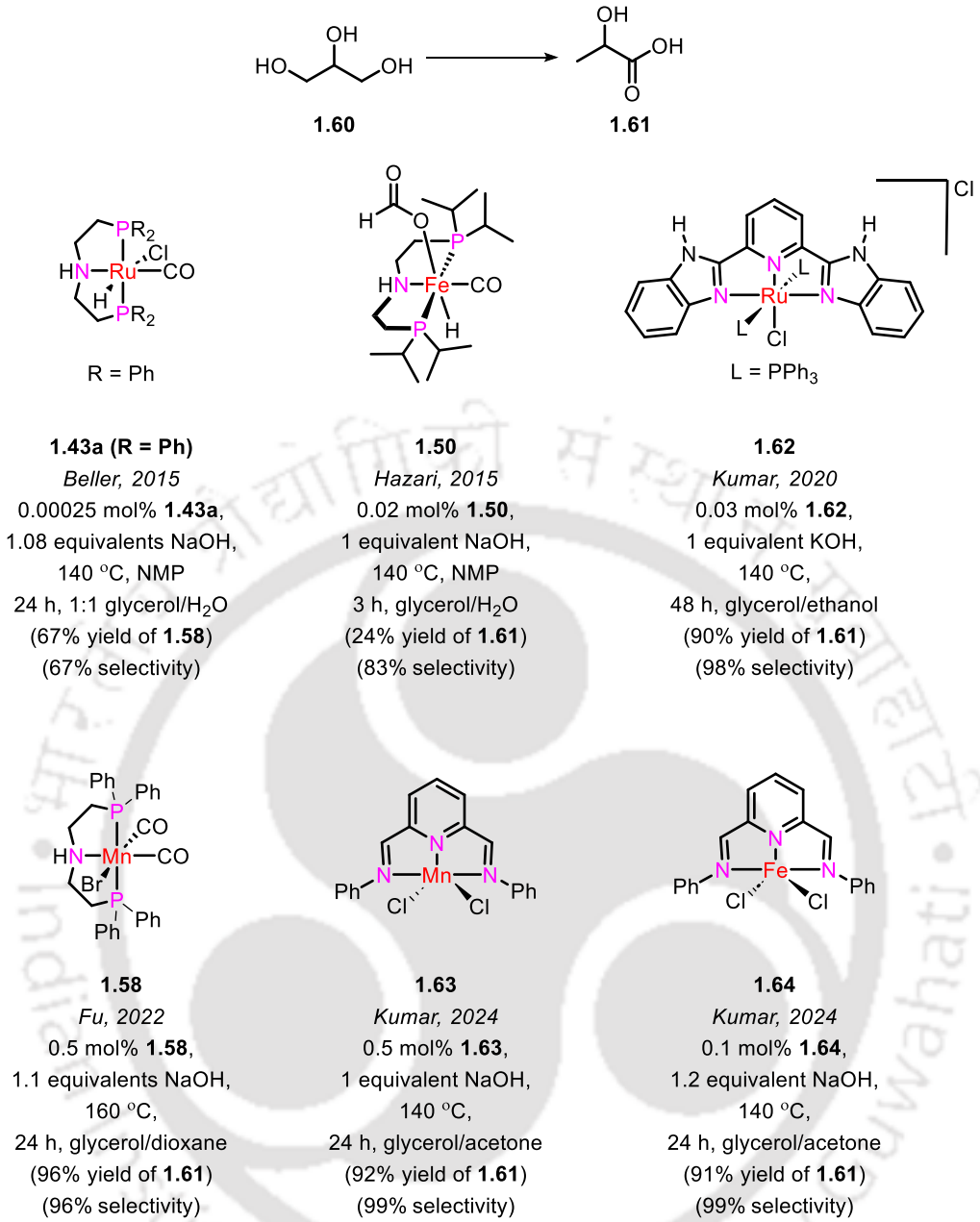

Figure 1.19. Pincer-based metal complexes reported for the transformation of glycerol to lactic acid.[29]

1.4 Summary

After the pioneering report by Moulton and Shaw in 1976,[10] catalysis using pincer-metal complexes have achieved a significant milestone and still continues to evolve over past few decades.[9,13-15] These versatile complexes continue to be the most preferred homogeneous catalysts and several reviews and pioneering reports exist in literature that describe the effectiveness of these complexes.[13-26] These complexes have exhibited outstanding catalytic properties in significant transformations including but not limited to dehydrogenation of

alcohols[32] and their tandem reactions such as *C*-alkylation,[30a, 25, 28, 43, 44] *N*-alkylation[30a, 45] and others. The use of pincer catalysts for the sustainable chemistry leading to the production of hydrogen from easily available and less toxic alcohols is currently an emerging area.[29] Each of these areas have witnessed a significant growth, thereby showcasing the vast scope of these complexes.[29] Therefore, an in-depth detailed review on each of the field is currently out of the scope of this thesis, and hence a concise overview that highlights the most relevant reactions with representative examples has been done. A detailed overview on the literature for the relevant reactions has been provided in greater detail in the appropriate chapters. Globally, significant amount research is still ongoing that continues to lay emphasis on each of these reactions independently. The versatile nature of pincer complexes and their vast application discussed above, lays the foundation for the objectives of current thesis.

1.5 Objectives

The current chapter has included a thorough literature survey that addresses transition metals and their pincer complexes towards plethora of organic transformations. Environmental concerns and diminishing non-renewable resources have made the current researchers to focus on developing more sustainable protocols. It is crucial to produce fuels and fine chemicals in an economical and ecologically responsible manner from inexpensive, plentiful renewable resources. Several complexes with a range of pincer-ligand-metals combinations have shown remarkable results in accomplishing this task. The high catalytic activity at mild reaction conditions, low catalyst loading and high selectivity are the main advantages of the pincer chemistry. The rich chemistry of pincer-ligated complexes is yet to be fully explored, mainly in context of sustainable chemical processes.

The aim of the current thesis is to explore the transformation of alcohols towards generation of hydrogen and value-added chemicals using pincer-metal complexes, and accordingly, attempts have been made to address the following questions:

- Is it possible to move away from phosphine-based ligand systems and study *bis*(imino)pyridine based NNN ligands as they are easy to synthesize?
- Will these NNN-ligated pincer-ruthenium complexes show good catalytic activity

  towards the reforming of various alcohols to generate H_2 and value-added chemicals with high selectivity without generation of carbon dioxide?

- Will it be possible to move away from precious metals and study the (de)hydrogenative transformation of alcohols using base-metal pincer complexes?

- Is it possible to achieve the *β*–alkylation of alcohols at low catalyst and base loading using cheap and abundant pincer-based *3d*-metal complexes?

1.6 References

1. Abbott, J. K. C.; Dougan, B. A.; Xue, Z.L. Chapter 13 - Synthesis of Organometallic Compounds. In *Modern Inorganic Synthetic Chemistry*, Xu, R.; Pang, W.; Huo, Q., Eds. Elsevier: Amsterdam, **2011**; pp 269-293.
2. Zeise, W. C. Von der Wirkung zwischen Platinchlorid und Alkohol, und von den dabei entstehenden neuen Substanzen. *Ann. Phys. Chem.* **1831,** *97*, 497-541.
3. Seyferth, D. The Grignard Reagents. *Organometallics* **2009,** *28*, 1598-1605.
4. Ziegler, K.; Holzkamp, E.; Breil, H.; Martin, H. Polymerisation von Äthylen und anderen Olefinen. *Angew. Chem*. **1955,** *67*, 426.
5. Soga, K.; Shiono, T. Ziegler-Natta catalysts for olefin polymerizations Prog. *Polym. Sci.* **1997,** *22*, 1503– 1546.
6. Knowles, W. S.; Noyori, R. Pioneering perspectives on asymmetric hydrogenation. *Acc. Chem*. Res. **2007,** *40*, 1238-1239.
7. Grubbs, R. H. Olefin-Metathesis Catalysts for the Preparation of Molecules and Materials. *Adv. Synth. Catal.* **2007,** *349*, 34-40.
8. Johansson Seechurn, C. C. C.; Kitching, M. O.; Colacot, T. J.; Snieckus, V. Palladium-Catalyzed Cross-Coupling: A Historical Contextual Perspective to the 2010 Nobel Prize. *Angew. Chem., Int. Ed.* **2012,** *51*, 5062-5085.
9. Das, K.; Kumar, A. Alkane dehydrogenation reactions catalyzed by pincer-metal complexes. In *Advances in Organometallic Chemistry*, Pérez, P. J., Ed. Academic Press, 2019; Vol. 72, Chapter 1, pp 1– 57.
10. Moulton, C. J.; Shaw, B. L. Transition Metal–carbon Bonds. Part XLII. Complexes of Nickel, Palladium, Platinum, Rhodium and Iridium with the Tridentate Ligand 2,6-Bis[(di-T-Butylphosphino)methyl]phenyl. *J. Chem. Soc., Dalton Trans*. **1976,** *11*, 1020– 1024.
11. van Koten, G.; Timmer, J. G.; Noltes, J. G.; Spek, A. L. A novel type of Pt–C interaction and a model for the final stage in reductive elimination processes involving C–C coupling at Pt; synthesis and molecular geometry of [1,N,N′-η-2,6-bis{(dimethylamino)methyl}-toluene]iodoplatinum(II) tetrafluoroborate. *J. Chem. Soc., Chem. Commun.* **1978**, 250-252.
12. van Koten, G. Tuning the Reactivity of Metals Held in a Rigid Ligand Environment. *Pure Appl. Chem.* **1989,** *61*, 1681-1694.
13. Peris, E.; Crabtree, R. H. Key factors in pincer ligand design. *Chem. Soc. Rev.* **2018,** *47*, 1959-1968.
14. Junge, K.; Papa, V.; Beller, M. Cobalt-Pincer Complexes in Catalysis. *Chem. - Eur. J.* **2019,** *25*, 122-143.
15. Nandi, P. G.; Arora, V.; Yasmin, E.; Kumar, A. Pincer-group(8) and pincer-group(9) metal complexes for catalytic alkane dehydrogenation reactions. In *Pincer-Metal Complexes*; Kumar, A., Ed.; Elsevier, 2022; Chapter 2, pp 69– 122.
16. Chang, J.; Ding, M.; Mao, J.-X.; Zhang, J.; Chen, X. Reactions and catalytic applications of a PNCNP pincer palladium hydride complex. *Dalton Trans.* **2022,** *51*, 17602-17608.
17. Arora, V.; Narjinari, H.; Nandi, P. G.; Kumar, A. Recent advances in pincer–nickel catalyzed reactions. *Dalton Trans.* **2021,** *50*, 3394-3428.
18. Kumar, A.; Bhatti, T. M.; Goldman, A. S. Dehydrogenation of Alkanes and Aliphatic Groups by Pincer-Ligated Metal Complexes. *Chem. Rev.* **2017,** *117*, 12357-12384.

19. Valdés, H.; García-Eleno, M. A.; Canseco-Gonzalez, D.; Morales-Morales, D. Recent Advances in Catalysis with Transition-Metal Pincer Compounds. *ChemCatChem*. **2018,** *10*, 3136-3172.
20. Choi, J.; MacArthur, A. H. R.; Brookhart, M.; Goldman, A. S. Dehydrogenation and Related Reactions Catalyzed by Iridium Pincer Complexes. *Chem. Rev.* **2011,** *111*, 1761-1779.
21. Gonzalez-Sebastian, L.; Morales-Morales, D. Cross-coupling reactions catalyzed by palladium pincer complexes. A review of recent advances. *J. Organomet. Chem.* **2019,** *893*, 39-51.
22. Younus, H. A.; Su, W.; Ahmad, N.; Chen, S.; Verpoort, F. Ruthenium pincer complexes: Synthesis and catalytic applications. *Adv. Synth. Catal*. **2015,** *357*, 283-330.
23. Filonenko, G. A.; van Putten, R.; Hensen, E. J. M.; Pidko, E. A. Catalytic (de)hydrogenation promoted by non-precious metals – Co, Fe and Mn: recent advances in an emerging field. *Chem. Soc. Rev.* **2018,** *47*, 1459-1483.
24. Mukherjee, A.; Milstein, D. Homogeneous Catalysis by Cobalt and Manganese Pincer Complexes. *ACS Catal.* **2018,** *8*, 11435-11469.
25. Narjinari, H.; Bisarya, A.; Arora, V.; Nandi, P. G.; Das, K.; Kumar, A. Current State-of-Art in the Guerbet-Type β-Alkylation of Secondary Alcohols with Primary Alcohols Catalyzed by Complexes Based on 3d Metals. In *Dehydrogenation Reactions with 3d Metals*, Sundararaju, B., Ed. Springer Nature Switzerland: Cham, 2024; pp 93-127.
26. Manar, K. K.; Cheng, J.; Yang, Y.; Yang, X.; Ren, P. Promising Catalytic Application by Pincer Metal Complexes: Recent Advances in Hydrogenation of Carbon-Based Molecules. *ChemCatChem* **2023,** *15*, e202300004.
27. Alig, L.; Fritz, M.; Schneider, S. First-row transition metal (de) hydrogenation catalysis based on functional pincer ligands. *Chem. Rev.* **2018,** *119*, 2681-2751.
28. Mullick, S.; Ghosh, A.; Banerjee, D. Recent advances in cross-coupling of alcohols via borrowing hydrogen catalysis. *Chem. Commun.* **2024,** *60*, 4002-4014.
29. Bisarya, A.; Karim, S.; Narjinari, H.; Banerjee, A.; Arora, V.; Dhole, S.; Dutta, A.; Kumar, A. Production of hydrogen from alcohols via homogeneous catalytic transformations mediated by molecular transition-metal complexes. *Chem. Commun.* **2024,** *60*, 4148-4169.
30. (a) Cook, A.; Newman, S. G. Alcohols as Substrates in Transition-Metal-Catalyzed Arylation, Alkylation, and Related Reactions. *Chemical Rev.* **2024,** *124*, 6078-6144. (b) Cramer, J.; Sager, C. P.; Ernst, B. Hydroxyl Groups in Synthetic and Natural-Product-Derived Therapeutics: A Perspective on a Common Functional Group. *J.Med. Chem.* **2019,** *62*, 8915-8930.
31. Rinaldi, R.; Jastrzebski, R.; Clough, M. T.; Ralph, J.; Kennema, M.; Bruijnincx, P. C.; Weckhuysen, B. M. Paving the Way for Lignin Valorisation: Recent Advances in Bioengineering, Biorefining and Catalysis. *Angew. Chem., Int. Ed.* **2016,** *55*, 8164-8215.
32. Trincado, M.; Bösken, J.; Grützmacher, H. Homogeneously Catalyzed Acceptorless Dehydrogenation of Alcohols: A Progress Report. *Coord. Chem. Rev.* **2021,** *443*, 213967
33. Vinayagamoorthi, R.; Viswanathan, B.; Krishnamurthy, K. R. Catalytic Conversion of Alcohols into Value-Added Products. In *Catalysis for Clean Energy and Environmental Sustainability: Biomass Convers. Green Chem. - Volume 1*, Pant, K. K.; Gupta, S. K.; Ahmad, E., Eds. Springer International Publishing: Cham, **2021**; pp 505-590.
34. Trincado, M.; Banerjee, D.; Grützmacher, H. Molecular catalysts for hydrogen production from alcohols. *Energy Environ. Sci.* **2014,** *7*, 2464-2503.
35. Zhang, J.; Gandelman, M.; Shimon, L. J. W.; Rozenberg, H.; Milstein, D. Electron-Rich, Bulky Ruthenium PNP-Type Complexes. Acceptorless Catalytic Alcohol Dehydrogenation. *Organometallics* **2004,** *23*, 4026-4033.
36. (a) Zhou, M.-J.; Liu, G.; Xu, C.; Huang, Z. Acceptorless Dehydrogenation of Aliphatics, Amines, and Alcohols with Homogeneous Catalytic Systems. *Synthesis* **2022,** *55*, 547-564. (b) Borthakur, I.; Kumari, S.; Kundu, S. Water as a solvent: transition metal catalyzed dehydrogenation of alcohols going green. *Dalton Trans.* **2022,** *51*, 11987-12020. (c) Lawrence, S. A. Amines: Synthesis, Properties and Applications; Cambridge University Press, 2004; p 269.
37. Wang, Z.; Pan, B.; Liu, Q.; Yue, E.; Solan, G. A.; Ma, Y.; Sun, W.-H. Efficient acceptorless dehydrogenation of secondary alcohols to ketones mediated by a PNN-Ru(ii) catalyst. *Catal. Sci. Technol.* **2017,** *7*, 1654-1661.

38. Wang, Q.; Chai, H.; Yu, Z. Acceptorless Dehydrogenation of N-Heterocycles and Secondary Alcohols by Ru(II)-NNC Complexes Bearing a Pyrazoyl-indolyl-pyridine Ligand. *Organometallics* **2018,** *37*, 584-591.
39. Balaraman, E.; Nandakumar, A.; Jaiswal, G.; Sahoo, M. K. Iron-catalyzed dehydrogenation reactions and their applications in sustainable energy and catalysis. *Catal. Sci. Technol.* **2017,** *7*, 3177-3195.
40. Chakraborty, S.; Lagaditis, P. O.; Förster, M.; Bielinski, E. A.; Hazari, N.; Holthausen, M. C.; Jones, W. D.; Schneider, S. Well-Defined Iron Catalysts for the Acceptorless Reversible Dehydrogenation-Hydrogenation of Alcohols and Ketones. *ACS Catal.* **2014,** *4*, 3994-4003.
41. Bruneau-Voisine, A.; Wang, D.; Roisnel, T.; Darcel, C.; Sortais, J.-B. Hydrogenation of ketones with a manganese PN3P pincer pre-catalyst. *Catal. Commun.* **2017,** *92*, 1-4.
42. Reed-Berendt, B. G.; Latham, D. E.; Dambatta, M. B.; Morrill, L. C. Borrowing Hydrogen for Organic Synthesis. *ACS Cent. Sci*. **2021,** *7*, 570-585.
43. Jafarzadeh, M.; Sobhani, S. H.; Gajewski, K.; Kianmehr, E. Recent advances in C/N-alkylation with alcohols through hydride transfer strategies. *Org. Biomol. Chem.* **2022,** *20*, 7713-7745.
44. Irrgang, T.; Kempe, R. 3d-Metal Catalyzed N- and C-Alkylation Reactions via Borrowing Hydrogen or Hydrogen Autotransfer. *Chem. Rev.* **2019,** *119*, 2524-2549.
45. Mahato, J.; Das, R.; Saha, T. K. 3d transition metal complexes as homogeneous catalysts in N-alkylation reactions using alcohols: A recent update. *Tetrahedron* **2024,** *165*, 134192.
46. Watanabe, Y.; Tsuji, Y.; Ohsugi, Y. The Ruthenium Catalyzed N-Alkylation and N-Heterocyclization of Aniline Using Alcohols and Aldehydes. *Tetrahedron Lett.* **1981,** *22*, 2667-2670.
47. Grigg, R.; Mitchell, T. R. B.; Sutthivaiyakit, S.; Tongpenyai, N. Transition Metal-Catalysed N-Alkylation of Amines by Alcohols. *J. Chem. Soc., Chem. Commun*. **1981**, 611-612.
48. Maji, M.; Chakrabarti, K.; Paul, B.; Roy, B. C.; Kundu, S. Ruthenium(II)-NNN-Pincer-Complex-Catalyzed Reactions Between Various Alcohols and Amines for Sustainable C−N and C−C Bond Formation. *Adv. Synth. Catal*. **2018,** *360*, 722-729.
49. Das, K.; Nandi, P. G.; Islam, K.; Srivastava, H. K.; Kumar, A. N–Alkylation of Amines Catalyzed by a Ruthenium–Pincer Complex in the Presence of in situ Generated Sodium Alkoxide. *Eur. J. Org. Chem.* **2019,** *2019*, 6855-6866.
50. Reed-Berendt, B. G.; Polidano, K.; Morrill, L. C. Recent advances in homogeneous borrowing hydrogen catalysis using earth-abundant first row transition metals. *Org. Biomol. Chem.* **2019,** *17*, 1595-1607.
51. Kallmeier, F.; Fertig, R.; Irrgang, T.; Kempe, R. Chromium-Catalyzed Alkylation of Amines by Alcohols. *Angew. Chem., Int. Ed*. **2020,** *59*, 11789-11793.
52. Fertig, R.; Irrgang, T.; Freitag, F.; Zander, J.; Kempe, R. Manganese-Catalyzed and Base-Switchable Synthesis of Amines or Imines via Borrowing Hydrogen or Dehydrogenative Condensation. *ACS Catal.* **2018,** *8*, 8525-8530.
53. Ananikov, V. P. Nickel: The "Spirited Horse" of Transition Metal Catalysis. *ACS Catal.* **2015,** *5*, 1964-1971.
54. Vellakkaran, M.; Singh, K.; Banerjee, D. An Efficient and Selective Nickel-Catalyzed Direct N-Alkylation of Anilines with Alcohols. *ACS Catal.* **2017,** *7*, 8152-8158.
55. Arora, V.; Dutta, M.; Das, K.; Das, B.; Srivastava, H. K.; Kumar, A. Solvent-Free N-Alkylation and Dehydrogenative Coupling Catalyzed by a Highly Active Pincer-Nickel Complex. *Organometallics* **2020,** *39*, 2162-2176.
56. Singh, A.; Maji, A.; Joshi, M.; Choudhury, A. R.; Ghosh, K. Designed Pincer Ligand Supported Co(II)-Based Catalysts for Dehydrogenative Activation of Alcohols: Studies on N-Alkylation of Amines, α-Alkylation of Ketones and Synthesis of Quinolines. *Dalton Trans.* **2021,** *50*, 8567-8587.
57. Panigrahi, D.; Mondal, M.; Gupta, R.; Mani, G. Four- and five-coordinate nickel(ii) complexes bearing new diphosphine–phosphonite and triphosphine–phosphite ligands: catalysts for N-alkylation of amines. *RSC Adv.* **2022,** *12*, 4510-4520.

58. Ruiz-Botella, S.; Peris, E. Unveiling the Importance of π-Stacking in Borrowing-Hydrogen Processes Catalysed by Iridium Complexes with Pyrene Tags. *Chem. Eur. J.* **2015,** *21*, 15263-15271.
59. Jiménez, M. V.; Fernández-Tornos, J.; Modrego, F. J.; Pérez-Torrente, J. J.; Oro, L. A. Oxidation and β-Alkylation of Alcohols Catalysed by Iridium(I) Complexes with Functionalised N-Heterocyclic Carbene Ligands. *Chem. Eur. J.* **2015,** *21*, 17877-17889.
60. Xu, C.; Goh, L. Y.; Pullarkat, S. A. Efficient Iridium-Thioether-Dithiolate Catalyst for β-Alkylation of Alcohols and Selective Imine Formation via N-Alkylation Reactions. *Organometallics* **2011,** *30*, 6499-6502.
61. Segarra, C.; Mas-Marzá, E.; Mata, J. A.; Peris, E., Shvo's Catalyst and [IrCp*Cl2(amidine)] Effectively Catalyze the Formation of Tertiary Amines from the Reaction of Primary Alcohols and Ammonium Salts. *Adv. Synth. Catal*. **2011,** *353*, 2078-2084.
62. Gong, X.; Zhang, H.; Li, X. Iridium phosphine abnormal N-heterocyclic carbene complexes in catalytic hydrogen transfer reactions. *Tetrahedron Lett.* **2011,** *52*, 5596-5600.
63. Gnanamgari, D.; Sauer, E. L. O.; Schley, N. D.; Butler, C.; Incarvito, C. D.; Crabtree, R. H. Iridium and Ruthenium Complexes with Chelating N-Heterocyclic Carbenes: Efficient Catalysts for Transfer Hydrogenation, β-Alkylation of Alcohols, and N-Alkylation of Amines. *Organometallics* **2009,** *28*, 321-325.
64. da Costa, A. P.; Sanaú, M.; Peris, E.; Royo, B. Easy preparation of Cp*-functionalized N-heterocyclic carbenes and their coordination to rhodium and iridium. *Dalton Trans.* **2009**, 6960-6966.
65. Pontes da Costa, A.; Viciano, M.; Sanaú, M.; Merino, S.; Tejeda, J.; Peris, E.; Royo, B. First Cp*-Functionalized N-Heterocyclic Carbene and Its Coordination to Iridium. Study of the Catalytic Properties. *Organometallics* **2008,** *27*, 1305-1309.
66. Gnanamgari, D.; Leung, C. H.; Schley, N. D.; Hilton, S. T.; Crabtree, R. H. Alcohol cross-coupling reactions catalyzed by Ru and Ir terpyridine complexes. *Org. Biomol. Chem.* **2008,** *6*, 4442-4445.
67. Fujita, K.-i.; Asai, C.; Yamaguchi, T.; Hanasaka, F.; Yamaguchi, R. Direct β-Alkylation of Secondary Alcohols with Primary Alcohols Catalyzed by a Cp*Ir Complex. *Org. Lett.* **2005,** *7*, 4017-4019.
68. Satyanarayana, P.; Reddy, G. M.; Maheswaran, H.; Kantam, M. L. Tris(acetylacetonato)rhodium(III)-Catalyzed α-Alkylation of Ketones, β-Alkylation of Secondary Alcohols and Alkylation of Amines with Primary Alcohols. *Adv. Synth. Catal.* **2013,** *355*, 1859-1867.
69. Wang, Q.; Wu, K.; Yu, Z. Ruthenium(III)-Catalyzed β-Alkylation of Secondary Alcohols with Primary Alcohols. *Organometallics* **2016,** *35*, 1251-1256.
70. Shee, S.; Paul, B.; Panja, D.; Roy, B. C.; Chakrabarti, K.; Ganguli, K.; Das, A.; Das, G. K.; Kundu, S. Tandem Cross Coupling Reaction of Alcohols for Sustainable Synthesis of β-Alkylated Secondary Alcohols and Flavan Derivatives. *Adv. Synth. Catal.* **2017,** *359*, 3888-3893.
71. Chakrabarti, K.; Paul, B.; Maji, M.; Roy, B. C.; Shee, S.; Kundu, S. Bifunctional Ru (ii) complex catalysed carbon–carbon bond formation: an eco-friendly hydrogen borrowing strategy. *Org. Biomol. Chem.* **2016,** *14*, 10988-10997.
72. (a) Das, K.; Yasmin, E.; Das, B.; Srivastava, H. K.; Kumar, A. Phosphine-free pincer-ruthenium catalyzed biofuel production: high rates, yields and turnovers of solventless alcohol alkylation. *Catal. Sci. Technol.* **2020,** *10*, 8347-8358. (b) Kaur, M.; Reshi, N. U. D.; Patra, K.; Bhattacherya, A.; Kunnikuruvan, S.; Bera, J. K. A Proton-Responsive Pyridyl(benzamide)-Functionalized NHC Ligand on Ir Complex for Alkylation of Ketone and Secondary Alcohols. *Chem. - Eur. J.* **2021,** *27*, 10737-10748. (c) Prakasham, A.; Ta, S.; Dey, S.; Ghosh, P. One pot tandem dual C-C and C-O bond reductions in the β-alkylation of secondary alcohols with primary alcohols by ruthenium complexes of amido and picolyl functionalized N-heterocyclic carbenes. *Dalton Trans.***2021**, *50*, 15640-15654. (d) Sahoo, A. R.; Lalitha, G.; Murugesh, V.; Bruneau, C.; Sharma, G. V.; Suresh, S.; Achard, M. Ruthenium Phosphine-Pyridone Catalyzed Cross-Coupling of Alcohols to form α-alkylated ketones *J. Org. Chem.* **2017,** *82*, 10727– 10731. (e) Thiyagarajan, S; Gunanathan, C. Catalytic Cross-Coupling of Secondary Alcohols. *J. Am. Chem. Soc.* **2019**, *141*, 3822–3827. (f)

Kumar, N.; Sankar, R. V.; Gunanathan, C. Ruthenium-Catalyzed Self-Coupling of Secondary Alcohols. *J. Org. Chem.* **2023**, *88*, 17155–17163. (g) Chang, W.; Gong, X.; Wang, S.; Xiao, L.-P.; Song, G. Acceptorless dehydrogenation and dehydrogenative coupling of alcohols catalysed by protic NHC ruthenium complexes. *Org. Biomol. Chem.* **2017,** *15*, 3466-3471.

73. Narjinari, H.; Tanwar, N.; Kathuria, L.; Jasra, R. V.; Kumar, A. Guerbet-Type β-alkylation of Secondary Alcohols Catalyzed by Chromium Chloride and its Corresponding NNN Pincer Complex. *Catal. Sci. Technol.* **2022,** *12*, 4753– 4762.
74. Jana, D.; Roy, S.; Naskar, S.; Halder, S.; Kanrar, G.; Pramanik, K. Potent pincer-zinc catalyzed homogeneous α-alkylation and Friedländer quinoline synthesis reaction of secondary alcohols/ketones with primary alcohols. *Org. Biomol. Chem.* **2024,** *22*, 6393-6408.
75. Freitag, F.; Irrgang, T.; Kempe, R. Cobalt-Catalyzed Alkylation of Secondary Alcohols with Primary Alcohols via Borrowing Hydrogen/Hydrogen Autotransfer. *Chem. - Eur. J.* **2017,** *23*, 12110-12113.
76. Liu, T.; Wang, L.; Wu, K.; Yu, Z. Manganese-Catalyzed β-Alkylation of Secondary Alcohols with Primary Alcohols under Phosphine-Free Conditions. *ACS Catal.* **2018,** *8*, 7201-7207.
77. El-Sepelgy, O.; Matador, E.; Brzozowska, A.; Rueping, M. C-Alkylation of Secondary Alcohols by Primary Alcohols through Manganese-Catalyzed Double Hydrogen Autotransfer. *ChemSusChem* **2019,** *12*, 3099-3102.
78. Pandey, B.; Xu, S.; Ding, K. Switchable β-alkylation of Secondary Alcohols with Primary Alcohols by a Well-Defined Cobalt Catalyst. *Organometallics* **2021,** *40*, 1207-1212.
79. Babu, R.; Subaramanian, M.; Midya, S. P.; Balaraman, E. Nickel-Catalyzed Guerbet Type Reaction: C-Alkylation of Secondary Alcohols via Double (de)Hydrogenation. *Org. Lett.* **2021,** *23*, 3320-3325.
80. Nandi, P. G.; Thombare, P.; Prathapa, S. J.; Kumar, A., Pincer-Cobalt-Catalyzed Guerbet-Type β-Alkylation of Alcohols in Air under Microwave Conditions. *Organometallics* **2022,** *41*, 3387-3398.
81. Bisarya, A.; Jasra, R. V.; Kumar, A., NNN Pincer-Manganese-Catalyzed Guerbet-Type β-Alkylation of Alcohols under Microwave Irradiation. *Organometallics* **2023,** *42*, 1818-1831.
82. Nandi, P. G.; Kumar, P.; Kumar, A. Ligand-free Guerbet-type reactions in air catalyzed by in situ formed complexes of base metal salt cobaltous chloride. *Catal. Sci. Technol.* **2022,** *12*, 1100-1108.
83. Rahman, A.; Farrok, O.; Haque, M. M. Environmental impact of renewable energy source based electrical power plants: Solar, wind, hydroelectric, biomass, geothermal, tidal, ocean, and osmotic. *Renew. Sust. Energy Rev.* **2022,** *161*, 112279.
84. Jones, L. W. Liquid Hydrogen as a Fuel for the Future: Replacement of hydrocarbon fuel for transportation systems by liquid hydrogen is proposed and discussed. *Science* **1971,** *174*, 367-370.
85. Dodds, P. E.; Staffell, I.; Hawkes, A. D.; Li, F.; Grünewald, P.; McDowall, W.; Ekins, P. Hydrogen and fuel cell technologies for heating: A review. *Int. J. Hydrogen Energy* **2015,** *40*, 2065-2083.
86. Singh, S.; Jain, S.; Ps, V.; Tiwari, A. K.; Nouni, M. R.; Pandey, J. K.; Goel, S. Hydrogen: A sustainable fuel for future of the transport sector. *Renew. Sust. Energy Rev* **2015,** *51*, 623-633.
87. Navarro, R. M.; Pena, M.; Fierro, J. L. G. Hydrogen production reactions from carbon feedstocks: fossil fuels and biomass. *Chem. Rev.* **2007,** *107*, 3952-3991.
88. Rosenow, J. Is heating homes with hydrogen all but a pipe dream? An evidence review. *Joule* **2022,** *6*, 2225-2228.
89. Satyapal, S.; Read, C.; Ordaz, G.; Stetson, N.; Thomas, G.; Petrovic, J. In *The US Department of Energy's National Hydrogen Storage Project: Goal, Progress and Future Plans*, The Fourth US-Korea Forum on Nanotechnology: Sustainable Energy, Honolulu 2007.
90. El-Shafie, M.; Kambara, S.; Hayakawa, Y. Hydrogen production technologies overview. *J. Power Energy Eng.* **2019,** *07*, 107-154.
91. Abdin, Z.; Zafaranloo, A.; Rafiee, A.; Mérida, W.; Lipiński, W.; Khalilpour, K. R. Hydrogen as an energy vector. *Renew. Sust.Energy Rev.* **2020,** *120*, 109620.
92. Dincer, I. Green methods for hydrogen production. *Int. J. Hydrogen Energy* **2012,** *37*, 1954-1971.

93. Kumar, S. S.; Lim, H. An overview of water electrolysis technologies for green hydrogen production. *Renew. Sust. Energy Rev.* **2022,** *8*, 13793-13813.
94. Qureshi, F.; Yusuf, M.; Kamyab, H.; Vo, D.-V. N.; Chelliapan, S.; Joo, S.-W.; Vasseghian, Y. J. Latest eco-friendly avenues on hydrogen production towards a circular bioeconomy: Currents challenges, innovative insights, and future perspectives. *Renew. Sust. Energy Rev.* **2022,** *168*, 112916.
95. Temiz, M.; Dincer, I. Development of solar and wind based hydrogen energy systems for sustainable communities. *Energy Convers. Manag.* **2022,** *269*, 116090.
96. Temiz, M.; Dincer, I. Development and assessment of an onshore wind and concentrated solar based power, heat, cooling and hydrogen energy system for remote communities. *J. Clean.Prod.* **2022,** *374*, 134067.
97. Xu, X.; Zhou, Q.; Yu, D., The future of hydrogen energy: Bio-hydrogen production technology. *Int. J. Hydrogen Energy* **2022,** *47*, 33677-33698.
98. El-Emam, R. S.; Özcan, H., Comprehensive review on the techno-economics of sustainable large-scale clean hydrogen production. *J. Clean.Prod.* **2019,** *220*, 593-609.
99. Caparrós Mancera, J. J.; Segura Manzano, F.; Andújar, J. M.; López, E.; Isorna, F. Sun, heat and electricity. A comprehensive study of non-pollutant alternatives to produce green hydrogen. *Int. J. Energy Res.* **2022,** *46*, 17999-18028.
100. Green, M. A. In *Hydrogen safety issues compared to safety issues with methane and propane*, AIP conference Proceedings2006 American Institute of Physics; pp 319-326.
101. Sadaghiani, M. S.; Mehrpooya, M. Introducing and energy analysis of a novel cryogenic hydrogen liquefaction process configuration. *Int. J. Hydrogen Energy y* **2017,** *42*, 6033-6050.
102. S S Sreedhar, I.; Kamani, K. M.; Kamani, B. M.; Reddy, B. M.; Venugopal, A. A Bird's Eye view on process and engineering aspects of hydrogen storage. *Renew. Sustain. Energy Rev.* **2018,** *91*, 838-860.
103. Li, H.; Cao, X.; Liu, Y.; Shao, Y.; Nan, Z.; Teng, L.; Peng, W.; Bian, J. Safety of hydrogen storage and transportation: An overview on mechanisms, techniques, and challenges. *Energy Rep.* **2022,** *8*, 6258-6269.
104. Sekine, Y.; Higo, T. Recent Trends on the Dehydrogenation Catalysis of Liquid Organic Hydrogen Carrier (LOHC): A Review. *Top. Catal.* **2021,** *64*, 470-480.
105. Yadav, V.; Sivakumar, G.; Gupta, V.; Balaraman, E. Recent Advances in Liquid Organic Hydrogen Carriers: An Alcohol-Based Hydrogen Economy. *ACS Catal.* **2021,** *11*, 14712-14726.
106. Levin, D. B.; Chahine, R. Challenges for renewable hydrogen production from biomass. *Int. J. Hydrogen Energy* **2010,** *35*, 4962-4969
107. Kumar, A.; Daw, P.; Milstein, D. Homogeneous Catalysis for Sustainable Energy: Hydrogen and Methanol Economies, Fuels from Biomass, and Related Topics. *Chem. Rev.* **2022,** *122*, 385-441.
108. Reed, T. B.; Lerner, R. M. Methanol: A Versatile Fuel for Immediate Use: Methanol can be made from gas, coal, or wood. It is stored and used in existing equipment. *Science* **1973,** *182*, 1299-1304.
109. Olah, G. A. Beyond oil and gas: the methanol economy. *Angew. Chem. Int. Ed.* **2005,** *44*, 2636-2639.
110. Cheng, X.; Shi, Z.; Glass, N.; Zhang, L.; Zhang, J.; Song, D.; Liu, Z.-S.; Wang, H.; Shen, J. A review of PEM hydrogen fuel cell contamination: Impacts, mechanisms, and mitigation. *J. Power Sources* **2007,** *165*, 739-756.
111. Li, H.; Ma, C.; Zou, X.; Li, A.; Huang, Z.; Zhu, L. On-board methanol catalytic reforming for hydrogen Production-A review. *Int. J. Hydrogen Energy* **2021,** *46*, 22303-22327.
112. Nielsen, M.; Alberico, E.; Baumann, W.; Drexler, H.-J.; Junge, H.; Gladiali, S.; Beller, M. Low-temperature aqueous-phase methanol dehydrogenation to hydrogen and carbon dioxide. *Nature* **2013,** *495*, 85-89.
113. Rodríguez-Lugo, R. E.; Trincado, M.; Vogt, M.; Tewes, F.; Santiso-Quinones, G.; Grützmacher, H. A homogeneous transition metal complex for clean hydrogen production from methanol–water mixtures. *Nat. Chem.* **2013,** *5*, 342-347.
114. Monney, A.; Barsch, E.; Sponholz, P.; Junge, H.; Ludwig, R.; Beller, M. Base-free hydrogen generation from methanol using a bi-catalytic system. *Chem. Commun.* **2014,** *50*, 707-709.

115. Hu, P.; Diskin-Posner, Y.; Ben-David, Y.; Milstein, D. Reusable homogeneous catalytic system for hydrogen production from methanol and water. *ACS Catal.* **2014,** *4*, 2649-2652.
116. Awasthi, M. K.; Rai, R. K.; Behrens, S.; Singh, S. K. Low-temperature hydrogen production from methanol over a ruthenium catalyst in water. *Catal. Sci. Technol.* **2021,** *11*, 136-142.
117. Wang, Q.; Lan, J.; Liang, R.; Xia, Y.; Qin, L.; Chung, L. W.; Zheng, Z. New Tricks for an Old Dog: Grubbs Catalysts Enable Efficient Hydrogen Production from Aqueous-Phase Methanol Reforming. *ACS Catal.* **2022,** *12*, 2212-2222.
118. Luo, J.; Kar, S.; Rauch, M.; Montag, M.; Ben-David, Y.; Milstein, D. Efficient Base-Free Aqueous Reforming of Methanol Homogeneously Catalyzed by Ruthenium Exhibiting a Remarkable Acceleration by Added Catalytic Thiol. *J. Am. Chem. Soc.* **2021,** *143*, 17284-17291.
119. Campos, J. s.; Sharninghausen, L. S.; Manas, M. G.; Crabtree, R. H. Methanol dehydrogenation by iridium N-heterocyclic carbene complexes. *Inorg. Chem.* **2015,** *54*, 5079-5084.
120. Alberico, E.; Sponholz, P.; Cordes, C.; Nielsen, M.; Drexler, H. J.; Baumann, W.; Junge, H.; Beller, M. Selective hydrogen production from methanol with a defined iron pincer catalyst under mild conditions. *Angew. Chem., Int. Ed.* **2013,** *125*, 14412-14416.
121. Bielinski, E. A.; Förster, M.; Zhang, Y.; Bernskoetter, W. H.; Hazari, N.; Holthausen, M. C. Base-free methanol dehydrogenation using a pincer-supported iron compound and Lewis acid co-catalyst. *ACS Catal.* **2015,** *5*, 2404-2415.
122. Andérez-Fernández, M.; Vogt, L. K.; Fischer, S.; Zhou, W.; Jiao, H.; Garbe, M.; Elangovan, S.; Junge, K.; Junge, H.; Ludwig, R.; Beller, M. A stable manganese pincer catalyst for the selective dehydrogenation of methanol. *Angew. Chem., Int. Ed.* **2017,** *129*, 574-577.
123. Ni, M.; Leung, D. Y. C.; Leung, M. K. H. A review on reforming bio-ethanol for hydrogen production. *Int. J. Hydrogen Energy* **2007,** *32*, 3238-3247.
124. Rossetti, I.; Tripodi, A. Catalytic Production of Renewable Hydrogen for Use in Fuel Cells: A Review Study. *Top. Catal.* **2022**.
125. Palma, V.; Ruocco, C.; Cortese, M.; Martino, M. Bioalcohol Reforming: An Overview of the Recent Advances for the Enhancement of Catalyst Stability. *Catalysts* **2020,** *10*, 665.
126. Palanisamy, A.; Soundarrajan, N.; Ramasamy, G.,Analysis on production of bioethanol for hydrogen generation. *Environ. Sci. Pollut. Res.* **2021,** *28*, 63690-63705.
127. Bai, F. W.; Anderson, W. A.; Moo-Young, M. Ethanol fermentation technologies from sugar and starch feedstocks. *Biotechnol. Adv.* **2008,** *26*, 89-105.
128. Ibeto, C.; Ofoefule, A.; Agbo, K. A global overview of biomass potentials for bioethanol production: a renewable alternative fuel. *Trends Appl. Sci. Res.* **2011,** *6*, 410-425.
129. Budiman, A. W.; Nam, J. S.; Park, J. H.; Mukti, R. I.; Chang, T. S.; Bae, J. W.; Choi, M. J. Review of Acetic Acid Synthesis from Various Feedstocks Through Different Catalytic Processes. *Catal. Surv. Asia* **2016,** *20*, 173-193.
130. Nomura, T.; Zhao, Y.; Minami, E.; Kawamoto, H., Reaction Mechanisms and Production of Hydrogen and Acetic Acid from Aqueous Ethanol Using a Rn-Sn/TiO2 Catalyst in a Continuous Flow Reactor. In *Catalysts* **2024**; Vol. 14.
131. Dagle, R. A.; Winkelman, A. D.; Ramasamy, K. K.; Lebarbier Dagle, V.; Weber, R. S. Ethanol as a Renewable Building Block for Fuels and Chemicals. *Ind. Eng. Chem. Res.* **2020,** *59*, 4843-4853.
132. Hu, P.; Ben-David, Y.; Milstein, D. General Synthesis of Amino Acid Salts from Amino Alcohols and Basic Water Liberating H2. *J. Am. Chem. Soc.* **2016,** *138*, 6143-6146.
133. Sponholz, P.; Mellmann, D.; Cordes, C.; Alsabeh, P. G.; Li, B.; Li, Y.; Nielsen, M.; Junge, H.; Dixneuf, P.; Beller, M. Efficient and Selective Hydrogen Generation from Bioethanol using Ruthenium Pincer-type Complexes. *ChemSusChem* **2014,** *7*, 2419-2422.
134. Wang, Q.; Xia, Y.; Chen, Z.; Wang, Y.; Cheng, F.; Qin, L.; Zheng, Z. Hydrogen Production via Aqueous-Phase Reforming of Ethanol Catalyzed by Ruthenium Alkylidene Complexes. *Organometallics* **2022,** *41*, 914-919.
135. Kuwahara, M.; Nishioka, M.; Yoshida, M.; Fujita, K.-i. A Sustainable Method for the Synthesis of Acetic Acid Based on Dehydrogenation of an Ethanol–Water Solution Catalyzed by an Iridium Complex Bearing a Functional Bipyridonate Ligand. *ChemCatChem* **2018,** *10*, 3636-3640.

136. Zou, Y.-Q.; von Wolff, N.; Anaby, A.; Xie, Y.; Milstein, D. Ethylene glycol as an efficient and reversible liquid-organic hydrogen carrier. *Nat. Catal.* **2019,** *2*, 415-422.
137. Vaidya, P. D.; Lopez-Sanchez, J. A. Review of Hydrogen Production by Catalytic Aqueous-Phase Reforming. *ChemistrySelect* **2017,** *2*, 6563-6576
138. Morton, D.; Cole-Hamilton, D. J. Molecular hydrogen complexes in catalysis: highly efficient hydrogen production from alcoholic substrates catalysed by ruthenium complexes. *J. Chem. Soc., Chem. Commun.* **1988**, 1154-1156.
139. Li, Y.; Nielsen, M.; Li, B.; Dixneuf, P. H.; Junge, H.; Beller, M. Ruthenium-catalyzed hydrogen generation from glycerol and selective synthesis of lactic acid. *Green Chem.* **2015,** *17*, 193-198.
140. (a) Zou, Y. Q.; von Wolff, N.; Rauch, M.; Feller, M.; Zhou, Q. Q.; Anaby, A.; Diskin-Posner, Y.; Shimon, L. J.; Avram, L.; Ben-David, Y.; Milstein, D. Homogeneous Reforming of Aqueous Ethylene Glycol to Glycolic Acid and Pure Hydrogen Catalyzed by Pincer-Ruthenium Complexes Capable of Metal–Ligand Cooperation. *Chem. -Eur. J.* **2021,** *27*, 4715-4722. (b) Kumar, A.; Priya, B.; Singh, S. K. Ruthenium-Catalyzed Transformation of Ethylene Glycol for Selective Hydrogen Gas Production in Water. *ACS Sustainable Chem.* **2023,** *11*, 3999-4008.
141. Waiba, S.; Maiti, M.; Maji, B. Manganese-Catalyzed Reformation of Vicinal Glycols to α-Hydroxy Carboxylic Acids with the Liberation of Hydrogen Gas. *ACS Catal.* **2022,** *12*, 3995-4001.
142. Sahoo, S. T.; Mohanty, A.; Sharma, R.; Rout, S. R.; Dandela, R.; Daw, P. A Bifunctional Ruthenium Catalyst for Effective Renewable Hydrogen Production from Biomass-Derived Sorbitol. *Organometallics* **2023,** *42*, 745-751.
143. Sahoo, S. T.; Mohanty, A.; Sharma, R.; Daw, P. A Switchable Route for Selective Transformation of Ethylene Glycol to Hydrogen and Glycolic Acid by Bifunctional Ruthenium Catalyst. *Dalton Trans.* **2023,** *52*, 15343-15347.
144. Crabtree, R. H., Transfer Hydrogenation with Glycerol as H-Donor: Catalyst Activation, Deactivation and Homogeneity. *ACS Sustainable Chem. Eng.* **2019,** *7*, 15845-15853.
145. Alonso, D. M.; Wettstein, S. G.; Dumesic, J. A., Bimetallic catalysts for upgrading of biomass to fuels and chemicals. *Chem. Soc. Rev.* **2012,** *41*, 8075-8098.
146. Wang, Z.; Zhuge, J.; Fang, H.; Prior, B. A., Glycerol production by microbial fermentation: A review. *Biotechnol. Adv.* **2001,** *19*, 201-223.
147. Pagliaro, M.; Ciriminna, R.; Kimura, H.; Rossi, M.; Della Pina, C., From Glycerol to Value-Added Products. *Angew. Chem., Int. Ed.* **2007,** *46*, 4434-4440.
148. Jérôme, F.; Pouilloux, Y.; Barrault, J. Rational Design of Solid Catalysts for the Selective Use of Glycerol as a Natural Organic Building Block. *ChemSusChem* **2008,** *1*, 586-613.
149. Dusselier, M.; Van Wouwe, P.; Dewaele, A.; Makshina, E.; Sels, B. F. Lactic acid as a platform chemical in the biobased economy: the role of chemocatalysis. *Energ Environ. Sci.* **2013,** *6*, 1415-1442.
150. Abdel-Rahman, M. A.; Sonomoto, K., Opportunities to overcome the current limitations and challenges for efficient microbial production of optically pure lactic acid. *J.Biotechnol.* **2016,** *236*, 176-192.
151. Razali, N.; Abdullah, A. Z., Production of lactic acid from glycerol via chemical conversion using solid catalyst: A review. *Appl. Catal., A* **2017,** *543*, 234-246.
152. Sharninghausen, L. S.; Campos, J.; Manas, M. G.; Crabtree, R. H. Efficient selective and atom economic catalytic conversion of glycerol to lactic acid. *Nat. Commun.* **2014,** *5*, 5084.
153. Sharninghausen, L. S.; Mercado, B. Q.; Crabtree, R. H.; Hazari, N. Selective conversion of glycerol to lactic acid with iron pincer precatalysts. *Chem. Commun.* **2015,** *51*, 16201-16204.
154. Dutta, M.; Das, K.; Prathapa, S. J.; Srivastava, H. K.; Kumar, A. Selective and High Yield Transformation of Glycerol to Lactic Acid Using NNN Pincer Ruthenium Catalysts. *Chem. Commun.* **2020,** *56*, 9886-9889.
155. Deng, C.-Q.; Deng, J.; Fu, Y. Manganese-catalysed dehydrogenative oxidation of glycerol to lactic acid. *Green Chem.* **2022,** *24*, 8477-8483.
156. Bisarya, A.; Dhole, S.; Kumar, A. Efficient net transfer-dehydrogenation of glycerol: NNN pincer–Mn and manganese chloride as a catalyst unlocks the effortless production of lactic acid and isopropanol. *Dalton Trans.* **2024,** *53*, 12698-12709.

157. Narjinari, H.; Dhole, S.; Kumar, A. Acceptorless or Transfer Dehydrogenation of Glycerol Catalyzed by Base Metal Salt Cobaltous Chloride – Facile Access to Lactic Acid and Hydrogen or Isopropanol. *Chem. -Eur. J.* **2024,** *30*, e202302686.
158. Venkateshappa, B.; Bisarya, A.; Nandi, P. G.; Dhole, S.; Kumar, A. Production of Lactic Acid via Catalytic Transfer Dehydrogenation of Glycerol Catalyzed by Base Metal Salt Ferrous Chloride and Its NNN Pincer-Iron Complexes. *Inorg. Chem.* **2024,** *63*, 15294-15310.

Chapter II

Pincer–Ruthenium Catalyzed Reforming of Methanol to Formic Acid and Hydrogen

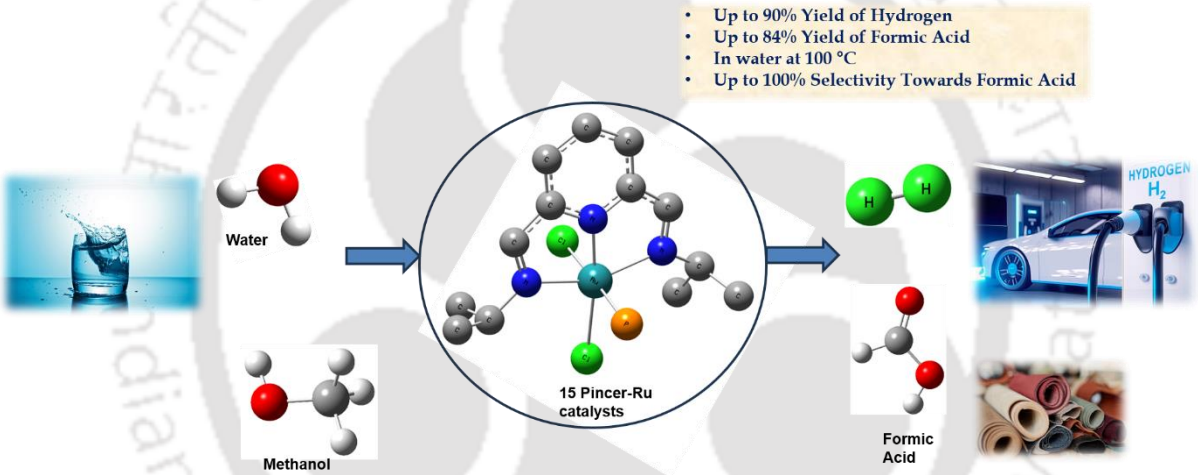

The content of this chapter has been adapted from "*Pincer-Ruthenium-Catalyzed Reforming of Methanol-Selective High-Yield Production of Formic Acid and Hydrogen*" by Arora, V.; Yasmin, E.; Tanwar, N.; Hathwar, V.R.; Wagh, T.; Dhole, S.; Dhole, S.; Kumar, A. *ACS Catal.* **2023**, *13*, 3605-3617.

2.1 Introduction

Due to the ever-increasing global energy demand and the rapid rate at which fossil fuel reserves are being depleted, there is a great need for the emergence of alternative and clean sources of energy which are sustainable and also would lessen the burden of global pollution.[1, 2] Alternative energy sources explored till date, like solar, wind, tidal, nuclear, and geothermal, suffer from several limitations.[3] Thus, a realistic alternative would be utilizing a combination of renewable energy sources and fossil fuels, leading to an uninterrupted production and storage of energy.[4-6] Several reports have emerged over the last few years on the production of H_2 as a clean-burning sustainable energy source with high energy content (120 MJ/kg).[7-10] Globally, the current emphasis is on sustainable hydrogen production from biomass[11-12] or *via* thermochemical, photocatalytic, or electrolytic splitting of water[11-13] using electricity from wind,[14, 15] solar,[14, 15] and geothermal energy.[11, 13, 16-18] The significant advancement in green hydrogen production is, to a large extent, overshadowed by the limitations associated with its storage and transportation, which include but are not limited to low volumetric energy density, safe handling, and the need for expensive cryogenic and high-pressure compression cylinders.[19-22] Alternative hydrogen adsorption-based technologies suffer from drastic conditions, low hydrogen storage capacities, low energy efficiency, and high cost.[23, 24] An emerging area of hydrogen carrier systems is its storage in the chemical bonds of tiny organic molecules.[5, 25, 26] This is typically accomplished by catalytic dehydrogenation of light organic hydrogen carriers.[5, 25, 26] Among the various catalysts that are at one's disposal, homogeneous catalysts, especially those based on pincers (chelating ligands that bind the metal through three adjacent donor sites in a meridional geometry) have been efficient in catalyzing reactions involving the release of hydrogen, such as the aqueous reforming of methanol (Scheme 2.1).[4]

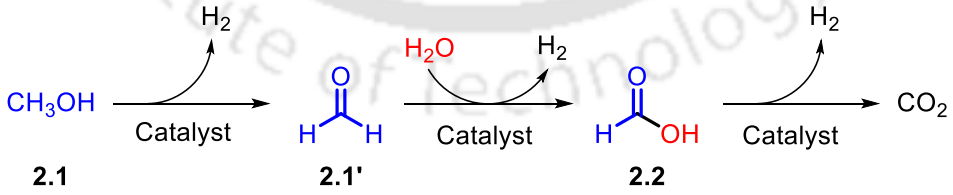

Scheme 2.1. Schematic representation of methanol reforming.

Methanol has up to 12.6% H_2 content and hence has been used as an efficient hydrogen storage medium as it is capable of meeting the ultimate Department of Energy targets (5.5 wt %) for H_2 storage on-board vehicles.[7] Rightly, its reforming has been reported by a number of groups

employing homogeneous complexes, resulting in hydrogen production in high yields and TON.

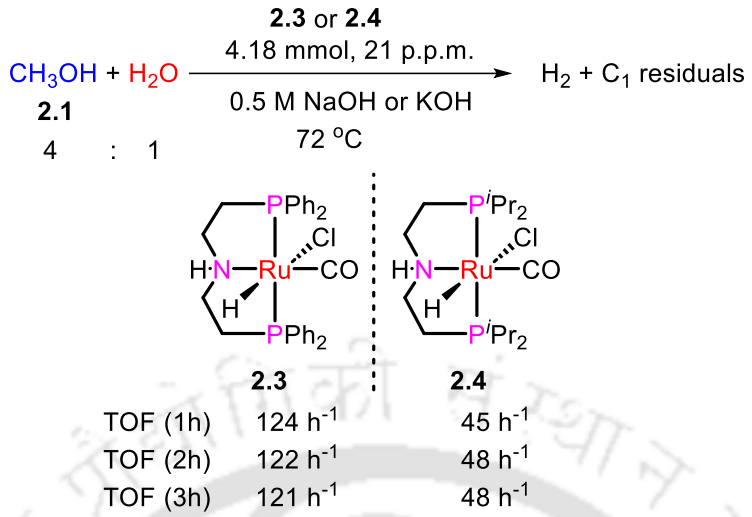

Scheme 2.2. Aqueous reforming of methanol using pincer-Ru complexes reported by Beller.[27]

A pioneering report that emerged in 2013 by Beller describes the use of pincer–Ru complexes based on the MACHO ligand to catalyze the transformation of an MeOH/H_2O mixture into H_2 and CO_2 (or CO_3^{2-}).[27] In the presence of catalytic amounts of ruthenium complex (21 ppm) and 0.5 M base, a 4 : 1 methanol–water mixture is dehydrogenated to formaldehyde, which is further dehydrogenated to formic acid and finally to carbon dioxide with an overall release of three equivalents of hydrogen. A variety of pincer–Ru catalysts were screened by varying MeOH/H_2O mixtures along with different bases and among all, **2.3** and **2.4** have shown significant catalytic activity (Scheme 2.2). On optimizing the reaction conditions, it was found that under identical conditions, **2.4** (1.8 ppm, 0.008 mol%) shows better activity (16.6% yield of H_2 at 2687 h^{-1}) in comparison to **2.3** (8.23% yield of H_2 at 1051 h^{-1}) when employed in a 9 : 1 mixture of MeOH/H_2O in the presence of 8.0 M KOH (1.4 equivalents with respect to water) after 3 h at 91 °C. Upon increasing the water content (MeOH/H_2O = 3 : 2), poor catalytic activity was observed with **2.3** (28 ppm, 0.0028 mol%) with the turnover frequency (after 1 h) reaching only up to 90 h^{-1}, explaining the poor solubility of **2.3**. Again, upon employing **2.4** (28 ppm, 0.0028 mol%) under similar conditions (MeOH/H_2O = 3 : 2), an eight-fold improvement of activity was observed with a turnover frequency of 732 h^{-1} at 86.5 °C.[27] Although with lower activity, a diluted methanol system (MeOH:H_2O = 1 : 9) in the presence of 8.0 M KOH (1.4 equivalents with respect to water) still afforded significant hydrogen evolution after 3 h of the reaction (201 h^{-1}; 1.3% H_2 with respect to the limiting reagent) at 95 °C. A remarkable activity was observed (4734 h^{-1} with 9.1% yield of hydrogen) when the

reaction was performed with neat methanol under similar conditions after 3 h. All the reactions were performed at a temperature range of 65–95 °C, and pure hydrogen was detected in all the cases.[27]

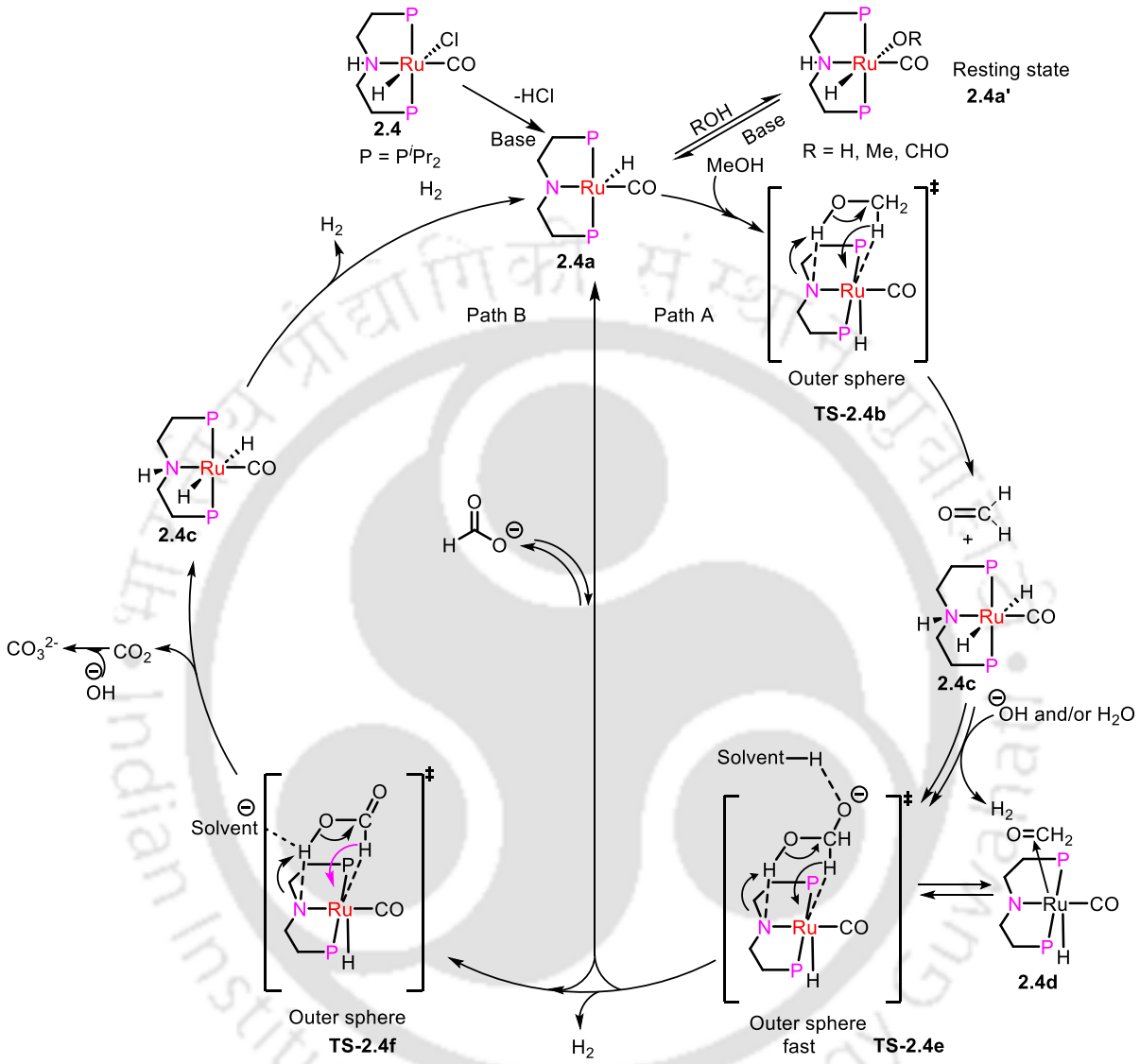

Scheme 2.3. Mechanism proposed by Beller for the aqueous reforming of methanol using pincer-Ru complex **2.4**.[27]

Based on several control experiments, a reaction mechanism was proposed (Scheme 2.3) where the first step involves the activation of catalyst **2.4** in the presence of base to generate the catalytically active amido species **2.4a**, which dehydrogenates methanol to afford hydrogen and formaldehyde. The removal of the first hydrogen molecule is proposed to occur *via* the outer sphere concerted mechanism involving **TS-2.4b**, without methanol getting directly coordinated to the metal centre. Further attack of hydroxide species will generate the gem-diol(ate), which will be stabilized by the solvent cage of MeOH/H_2O as depicted in **TS-2.4e**.

This will again undergo an outer sphere dehydrogenation step and lead to the generation of the second hydrogen molecule along with the formation of formate ions to regenerate the catalytically active species **2.4a** *via* path **A** (Scheme 2.3). Intermediate **2.4a** may now again enter the catalytic cycle involving path **A**. Alternatively **2.4a** may react with the formate ion to undergo decarboxylation *via* **TS-2.4f** followed by the removal of the third hydrogen molecule *via* formation of hydride species **2.4c** (path **B**, Scheme 2.3).[27] Considering the fact that free formate is detected and that there is formation of substantial amounts of carbon dioxide, Beller concluded that the rate of formate dehydrogenation (path **B**, Scheme 2.3) is faster than the rate of methanol dehydrogenation (path **A**, Scheme 2.3).

An anionic Ru complex [Ru(trop$_2$dad)], trop$_2$dad = 1,4-*bis*- (5*H*-dibenzo[*a,d*]cyclohepten-5-yl)-1,4-diazabuta-1,3-diene, **2.5** (Figure 2.10) was reported by Grutzmacher for the aqueous-phase methanol reforming leading to 80% methanol conversion (84% H_2 yield) using 0.5 mol% **2.5** at 90 °C after 10 h.[28] This reaction proceeded without the additional use of base, and the H_2/CO_2 gas mixture evolved was able to power an H_2/O_2 fuel cell.[28] Attempts were made to elucidate the mechanistic details of the reaction involving **2.5** by density functional theory based molecular dynamics (DFT-MD) and solvent effects.[28] They concluded that the solvent (methanol and water) participates actively in the reaction by forming hydrogen bonds with the complex, which helps in the stabilization of the transition state involved in the catalytic cycle, thereby assisting the C–H activation process.[28] Meijer and co-workers also focused their study on the solvent effects of the methanol reforming reaction, concluding that the involvement of polar protic solvents largely influences the energetics of the reaction due to hydrogen bonding with the solvent molecules.[29]

Soon after, Beller and co-workers reported another pincer– Ru-based catalyst, Ru-MACHO-BH, **2.6** (Figure 2.10), for base-free dehydrogenation of methanol.[30] The catalyst is similar to **2.3** reported for base-mediated dehydrogenation of methanol, but since the catalyst is free from the chloride ligand, it eliminates the need for base required for its activation. Both the catalysts **2.6** and **2.3** exhibited similar activity (with H_2 yield at 6% and 7% respectively) in the presence of 1.4 equivalents of KOH for a 9 : 1 MeOH/H_2O system at 0.009 mol% catalyst loading at 93.5 °C after 3 h. Further, the use of triglyme as a solvent resulted in a slight increase in the yield of H_2 (up to 8%) owing to the better solubility of **2.6**. Under similar conditions, in the absence of base, 0.009 mol% of **2.6** exhibited lesser activity (0.1% yield of H_2) for a 9 : 1 MeOH/H_2O system at 93.5 °C.[30] However, under identical conditions, upon increasing the

catalyst loading from 0.0009 mol% (5 mol) to 0.172 mol% 0.172 mol% (95 μmol), significant acceleration in the reactivity was observed (3.4% yield of H_2).[30] In order to get higher turnover

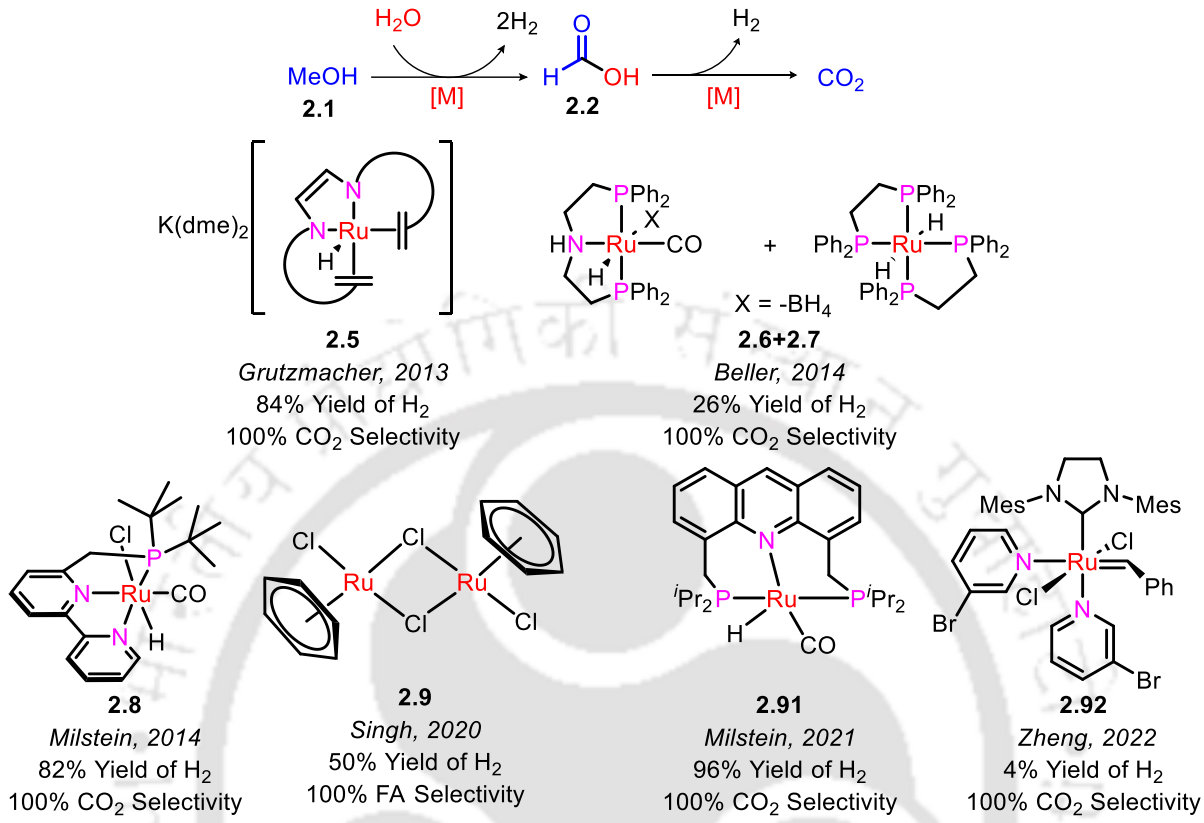

Figure 2.10. Ru-based complexes reported for aqueous-phase methanol reforming.

numbers, authors envisioned that the catalytic step that involves the formic acid dehydrogenation needs to be accelerated in a different fashion. Therefore, a bi-catalytic system was introduced in which **2.6** interacts with $Ru(H)_2(dppe)_2$ **2.7** in a synergistic manner under base free conditions and a total TON of >4200 (26% yield of H_2 relative to H_2O) was observed with only a trace amount of CO content (< 8 ppm).[30]

In a parallel effort in the same year, Milstein and co-workers reported the first example of a reusable homogeneous Ru-PNN pincer complex for reforming methanol to H_2 and CO_2 (absorbed by base) at 100 °C without any requirement for catalyst isolation and purification.[31] Initially, for a 1 : 5.5 MeOH/H_2O system, reaction was performed at 0.2 mol% **2.8** in the presence of 2 equivalents of NaOH for 24 hours under solvent-free conditions at 115 °C, and no formation of hydrogen was detected.[31] However, the addition of THF under similar reaction conditions has resulted in 71% hydrogen generation after two days. This is indicative of the better solubility of the catalyst in the presence of THF in the reaction medium.[31] Upon

decreasing the loading of **2.8** to 0.05 mol% in the presence of 2 equivalents of NaOH in THF at 115 °C, a decrement in the yield of hydrogen (28%) was observed after four days. Under similar conditions, further optimization led to the findings that toluene was a better solvent, resulting in a 68% yield of hydrogen after four days at the catalyst loading of 0.05 mol%. When 2 equivalents of KOH was used in place of NaOH, 70% hydrogen was produced after seven days and 77% after nine days in toluene at 115 °C.[31] Moreover, when the organic layer of the reaction mixture was collected separately and reused directly, without using a catalyst and toluene, 82% yield of hydrogen was produced after nine days.[31] Thus, the catalyst was found to be reusable after several days of the reaction, and no loss in the activity of the catalyst was observed. Overall, about 1.53 g of MeOH was found to be fully converted to H_2 and CO_2 in the **2.8** (0.01 mol%) catalyzed reaction in the presence of KOH (2 equivalents) in toluene at 115 °C with the TON reaching up to 29000 after 30 days.[31]

In the year 2020, Singh and co-workers reported methanol reforming employing *in situ* generated ruthenium nano-particles using an organometallic precursor $[(\eta^6\text{-benzene})RuCl_2]_2$ **2.9**.[32] Initially, when the reaction was carried out in a 2 : 1 MeOH/H_2O mixture in the presence of 1.2 equivalents of KOH at 110 °C, 73 mol H_2 per mol Ru was observed (TOF 9 h^{-1}, yield = 16%). The change in the colour of the reaction mixture from dark brown to a black suspension suggested the formation of Ru nanoparticles, which was further confirmed by TEM analysis (*ca.* 18.7 nm).[32] Further investigation was performed by adding a 2-hydroxypyridine ligand and a significant boost in the initial TOF was observed (18 h^{-1}) with the release of 0.66 moles of H_2 per mole of methanol (106 moles of H_2 per mole of Ru, yield = 23%) in the **2.9** catalyzed reforming of 2 : 1 MeOH/H_2O in the presence of 1.2 equivalents of KOH at 110 °C. Under otherwise identical conditions, when the reaction was performed with 1 : 1 MeOH/H_2O, the activity was further increased reaching a TON of 134 moles of H_2 per mole of Ru (TOF 20 h^{-1}, yield = 29%).[32] Increasing the temperature of this 1 : 1 MeOH/H_2O reaction mixture from 110 °C to 130 °C has accelerated the H_2 production rate leading to 49 h^{-1} and 229 moles of H_2 (yield = 50%) per mole of Ru.[32] However, upon further increasing the water content, a 1 : 2 MeOH/H_2O mixture led to lower catalytic activity (14 h^{-1}).

Later, Milstein and co-workers have reported an acridine based pincer–ruthenium complex **2.91** for the base-free methanol reforming reaction without utilizing additional solvents.[33] The reaction was performed in a closed system at 150 °C and surprisingly, adding a catalytic amount of thiol (1 equivalent relative to **2.91**) to a 4 : 1 MeOH/H_2O mixture in the presence of 0.0056

mol% **2.91** led to the formation of 330 mL of gas containing H_2 and CO_2 in a 3 : 1 volumetric ratio after heating for 12 hours. Ultimately, a TOF of about 337 h^{-1} (40%) was obtained, which was found to be 80 times more than that obtained in the absence of thiol using 0.02 mol% **2.91** after 24 h (15 mL of gas containing H_2 and CO_2 in a 3 : 1 volumetric ratio with TOF = 4 h^{-1} and 2% H_2 yield).[33] Further optimization of the reaction conditions indicated that upon lowering the water content by using a 9 : 1 MeOH/H_2O mixture, better catalytic activity could be achieved (470 mL of gas containing H_2 and CO_2 in a 3 : 1 volumetric ratio with TOF = 480 h^{-1} and 58% H_2 yield). This improvement in the catalytic activity upon increasing the methanol concentration can be attributed to the better solubility of **2.91** in methanol. After heating the reaction mixture for more than 3 weeks, over 10 L of H_2 gas with a TON of 4130000 (yield = 96% relative to water) was produced, indicating the robustness and durability of the system.[33]

Recently, Zheng and co-workers have reported the application of a well-known third-generation Grubb's catalyst **2.92** for hydrogen generation *via* aqueous phase methanol reforming.[34] The reaction was performed in a 9 : 1 MeOH/H_2O mixture at 100 °C in the presence of 1.4 equivalents of KOH and **2.92** (0.009 mol%) for 3 h. The best TOF_{3h} of 139 h^{-1} (corresponding to approximately 1.3% yield of H_2) was achieved using **2.92** with negligible formation of CO (0.8 X 10^{-4} ppm).[34] The addition of 3-bromopyridine or PCy_3 was found to cease the hydrogen evolution, suggesting the significance of the dissociation of 3-bromo pyridine or PCy_3 in the catalytic cycle.[34] Further optimization of the reaction condition was carried out by varying the base and by changing the ratio of the MeOH/H_2O mixture. It was observed that both the 9 : 1 MeOH/H_2O mixture and neat methanol in the presence of 1.4 equivalents of KOH have given the best TOF_{3h} values (139 h^{-1} and 144 h^{-1} respectively), which correspond to 1.25% (relative to water) and 0.3% yields (relative to methanol) of H_2 respectively.[34] The reaction was performed for an extended period of time to examine the stability of the catalyst, and it was found that at 0.003 mol% loading of **2.92**, very high TON of 11424 after 72 h, which corresponds to 3.8% conversion of methanol was observed.[34] On the basis of several experimental and computational studies, a mechanism was proposed, which commences with the dissociation of 3-bromopyridine from **2.92** followed by the salt-metathesis to generate the active species **2.92b**. This undergoes a β-hydride elimination *via* rearrangement to give a Ru-monohydride species **2.92e** along with the release of formaldehyde. The subsequent interaction of a methanol molecule with **2.92e** follows a methanol-assisted metathesis pathway and lead to the evolution of the first molecule of hydrogen. A similar process occurs for the generation of other two hydrogen molecules (Scheme 2.4).

Apart from Ru-based pincer complexes, there are several other complexes based on Ir and Rh that were also reported (Figure 2.11). One of the oldest reports for this reaction was with a Rh

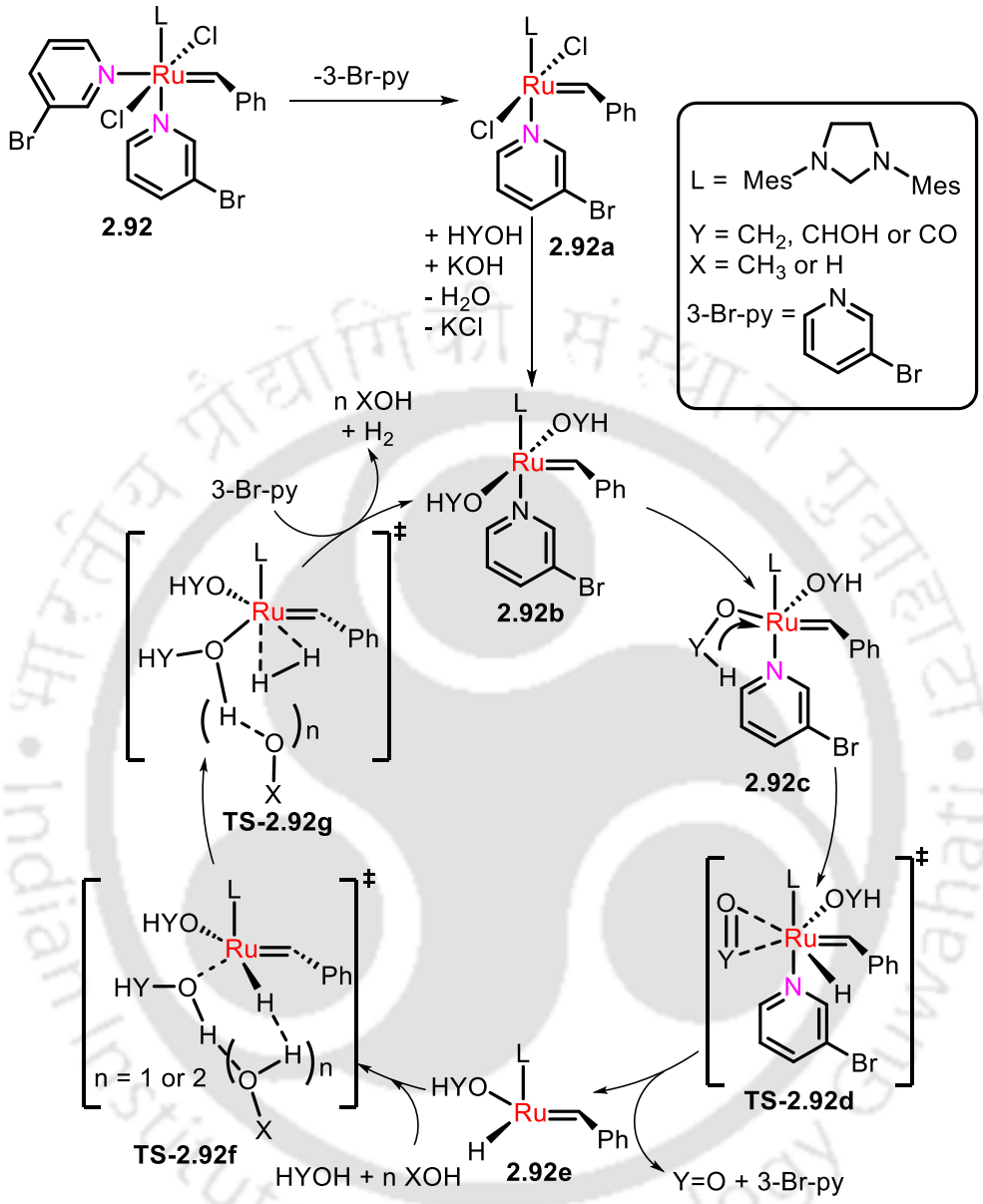

Scheme 2.4. Mechanism involved in the aqueous reforming of methanol by the third-generation Grubb's catalyst **2.92** as proposed by Zheng.[34]

complex (**2.93**) by Cole-Hamilton in 1987.[35] The complex **2.93** was found to give a TOF of 7 h^{-1}. In 2015, Crabtree and co-workers employed an air- stable *bis*(N-heterocyclic carbene)-based iridium complex **2.94** (0.004 mol%) for the acceptorless dehydrogenation of neat methanol at 91 °C under basic conditions (6.7 M KOH, 0.3 equivalents relative to water) to produce hydrogen (81% yield at 3612 TONs) after 24 h.[36] Furthermore, they applied their system to carry out the transfer dehydrogenation of ketones and imines, along with aniline methylation, with all the reactions giving very high yields.[36] In the same year, Fujita and Yama-

guchi reported complex **2.95** (0.1 mol%), which gave 64% yield of H_2 with a TON of 10510 for the reforming of a 1 : 4 MeOH/ H_2O mixture after 150 h in the presence of 0.5 mol% NaOH at 100 °C.[37]

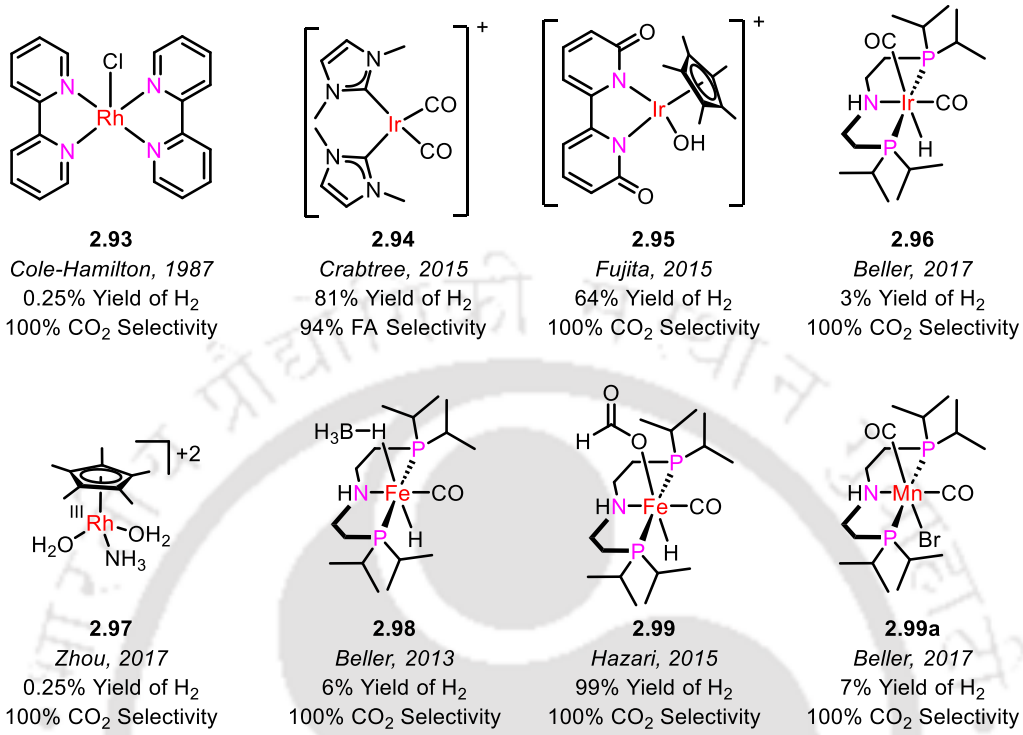

Figure 2.11. Catalysts other than Ru reported for aqueous-phase methanol-reforming.

In 2017, Beller and co-workers employed an Ir-based PNP-MACHO complex **2.96** (0.008 mol %) for the methanol reforming reaction and a TON of 1400 (*ca.* 3.5% yield of H_2) was achieved in the presence of 9 mol% KOH for a 9 : 1 mixture of MeOH/H_2O at 94 °C.[38] Upon increasing the base loading to 1.4 equivalents, the turn-overs increased to 1900 (*ca.* 5% yield of H_2).[38] In the same year, Zhou and co-workers developed a Rh-base catalyst [Cp*Rh-(NH_3)(H_2O)$_2$] **2.97** for methanol reforming reaction without using any external base.[39] In the 0.03 mol% **2.97** catalysed reforming of methanol using a 3 : 1 MeOH/H_2O mixture at 70 °C, hydrogen was produced in 1% yield at 83.2 h^{-1} with no formation of CO.[39] The reaction was found to be more active under faintly acidic conditions.[39]

Despite the fact that the precious metals have historically been at the cutting edge of catalysis, their scarcity, high cost, low abundance and toxicity pose questions about sustainability. This has sparked significant interest towards the development of base metal catalysts for several (de)hydrogenation and related reactions. In this regard, the very first report with an earth-abundant catalyst for methanol reforming was reported by Beller and co-workers, where they

developed an Fe-based pincer catalyst **2.98**, which at a loading of 0.002 mol% was found to achieve a TON of 10000 (ca. 6% H_2 yield) after 46 h in the presence of 1.4 equivalents of 8 M KOH for a 9 : 1 MeOH/ H_2O mixture at 91 °C.[40] However, the **2.98** catalyst was not as stable as its Ru counterpart, also reported by Beller (Figure 2.10).[27]

Soon after, Bernskoetter, Hazari and Holthausen reported a series of stable pincer-iron complexes for the dehydrogenation of methanol in the presence of Lewis acid without any requirement of the base.[41] The requirement of Lewis acid is only for the activation of the catalyst and has nothing to do with the reaction mechanism. In the absence of water, 0.01 mol% **2.99** in combination with 10 mol% $LiBF_4$ dehydrogenates MeOH to methyl formate and H_2 (*ca.* 99% yield and 20000 TON) after heating for 4.4 h under reflux conditions.[41] Under similar conditions, in the presence of water, catalyst **2.99**, in combination with 10 mol% $LiBF_4$ fully converts MeOH into H_2 and CO_2 with the TON reaching up to 30000 (ca. 99% yield of H_2) after 52 h.[41] Upon further lowering the loading of **2.99** to 0.006 mol%, a TON of 51000 is obtained but with a reduced yield of 50%, which is the highest TON reported for a base metal catalyst.[41] The stark contrast in the yields observed in case of **2.98**[40] and **2.99**[41] is due to the fact that in case of latter, $LiBF_4$ is used as additive which helps in the activation of the catalyst by facilitating the decarboxylation of the formate complex **2.99** to access the catalytically active species.[41] Typically the former is an off-cycle species and owing to its inefficient activation, lower yields are obtained.[40, 41]

In the year 2017, Beller reported a PNP pincer-based Mn catalyst for the methanol reforming reaction (Figure 2.11). A range of manganese catalysts and their precursors were tested.[42] Upon optimizing the reaction conditions, catalyst **2.99a** (0.03 mol%) in the presence of 10 equivalents of PNP^{i}Pr ligand and 1.4 equivalents of KOH was found to exhibit the highest TON of 138 (*ca.* 1.4% yield of H_2) after 5 h of reaction in a 9 : 1 mixture of methanol/water at 90 °C.[42] In stark contrast, the precursor $Mn(CO)_5Br$, was found to show a decline in the activity in the presence of additional PNP^{i}Pr ligand (up to 68 TON after 5 h with 0.7% H_2 yield).[42]

2.2 Objectives

In the context of the role of pincer-metal complexes in catalytic reforming of methanol, it is noteworthy that majority of the reports involve moderately good π-accepting phosphine flanking groups in combination with a central N that is either a σ-donating amine or a pyridyl-N.[4] Moreover, the reports demonstrating the use of pincer-ruthenium complexes towards the

selective formation of formic acid and hydrogen are scarce. In this regard, the current chapter aims to address the following questions.

- Will replacing the π-accepting phosphine flanking groups with σ-donor groups (eg. weaker σ-donor imines), while keeping the central pyridyl N intact affect the catalytic activity?
- Will these NNN-ligated pincer-ruthenium complexes (Figure 2.12) show good catalytic activity towards the aqueous methanol reforming to generate H_2 and formic acid with high selectivity without generation of greenhouse gas carbon dioxide?
- Will these *bis*(imino)pyridine based NNN pincers would be innocent that offer a distinctly different metal-centered reactivity in stark contrast to the corresponding phosphine-based ligands which are typically non-innocent and operate via metal−ligand cooperation?
- What is the mechanism involved in the current study?
- Can one extrapolate the current study to generation of D_2, which is not readily available?

2.3 Results and Discussion

2.3.1 Synthesis and characterization of pincer–ruthenium acetonitrile complexes based on *bis*(imino)pyridine ligands

The NNN pincer–Ru acetonitrile complexes (**2.102b–d**) were synthesized in good yields by the treatment of the corresponding ligands[43-48] with [Ru(*p*-cymene)Cl_2]$_2$ in acetonitrile under reflux conditions overnight (Scheme 2.5), followed by washing with diethyl ether. The complexes **2.102b–d** were fully characterized by high-resolution mass spectrometry (HRMS), infrared (IR), ^{1}H, and ^{13}C{H} nuclear magnetic resonance (NMR) studies.

Good-quality single crystals were obtained by slow diffusion of 1 mL pentane into a 1 mL dichloromethane solution of 10 mg of the pincer–ruthenium complex **2.102c**. We were also successful in obtaining well-defined single crystals of **2.101f**, the synthesis of which has been earlier reported from our group.[45] The structures of both **2.102c** and **2.101f** were unambiguously determined by single-crystal X-ray diffraction studies (Figure 2.13).

2.3.2 Catalytic activity of pincer–ruthenium complexes (2.100, 2.101, and 2.102) towards aqueous-phase methanol reforming reaction

The novel pincer-ruthenium acetonitrile-based complexes (**2.102**) along with the previously reported complexes (Figure 2.12) have been employed towards the catalytic reforming of methanol for generation of hydrogen. The initial optimization of pincer–ruthenium (**2.100**, **2.101**, and **2.102**) catalyzed aqueous-phase methanol reforming was commenced by heating a

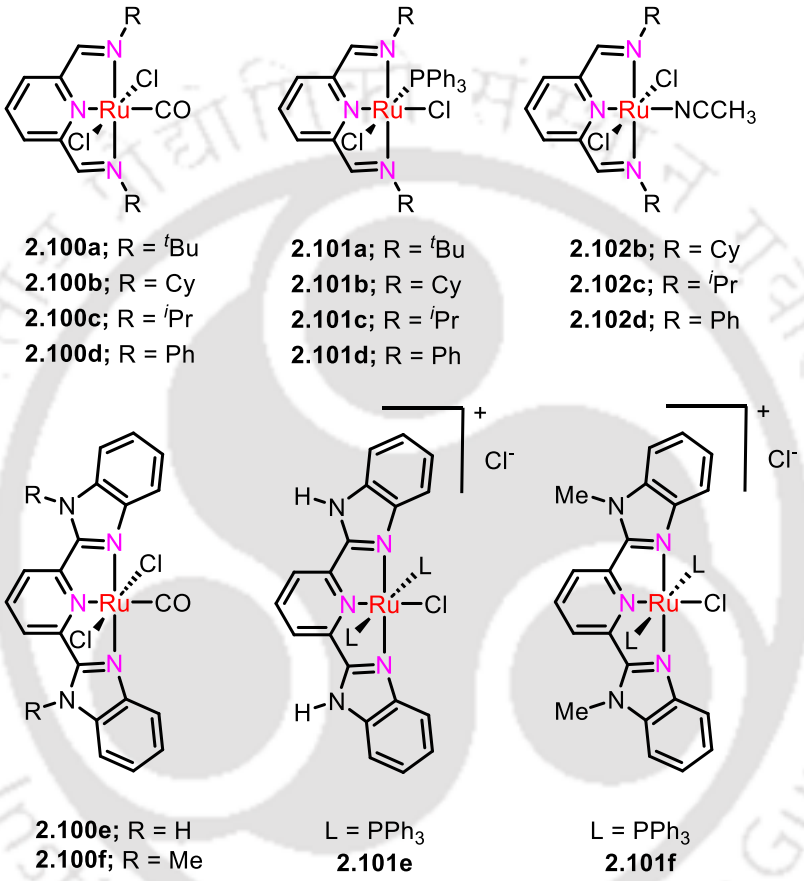

Figure 2.12. Pincer-ruthenium complexes employed in the current study.

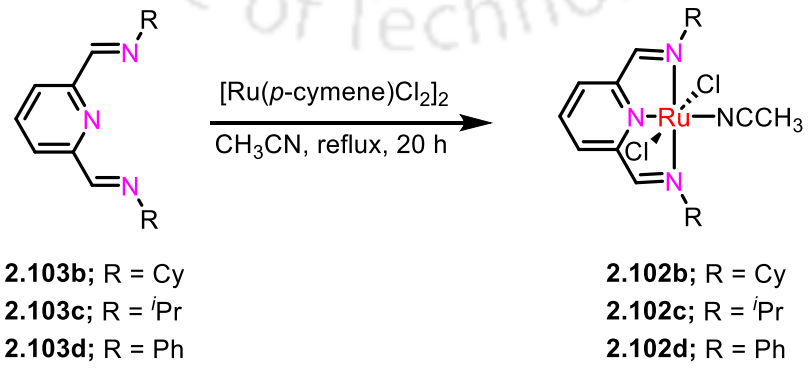

Scheme 2.5. General synthetic route towards NNN pincer–ruthenium acetonitrile complexes.

mixture of MeOH and H_2O (in a 2:1 ratio) containing an equivalent of base (with respect to water) in the presence of 0.04 mol % of ^{Cy2}NNNRuCl$_2$(CO) (**2.100b**) as the catalyst (Table 2.2) at 100 °C. Among the various bases screened, KO^{t}Bu showed better reactivity (entry 3 *vs.* entries 1–7, Table 2.2). When the reaction was further optimized at various loadings of KO^{t}Bu, the best result was obtained while using 0.5 equivalents of KO^{t}Bu (entry 9 *vs.* entries 3, 10, and 11, Table 2.2).

Further optimization of various pincer–ruthenium catalysts was carried out with MeOH and H_2O in a 2:1 ratio using 0.5 equivalents of KO^{t}Bu (Table 2.3). The best catalytic activity among the carbonyl complexes (**2.100a-f**) was exhibited by ^{Ph2}NNNRuCl$_2$(CO) (**2.100d**) which gave yields of hydrogen and formic acid that were about 4.7 folds (entry 4 *vs* entry 2, Table 2.3) higher in comparison to that obtained with **2.100b**. On the other hand, the corresponding yields obtained with **2.100a**, **2.100c**, and **2.100e** were about three-folds (entries 1, 3, and 5 *vs.* entry

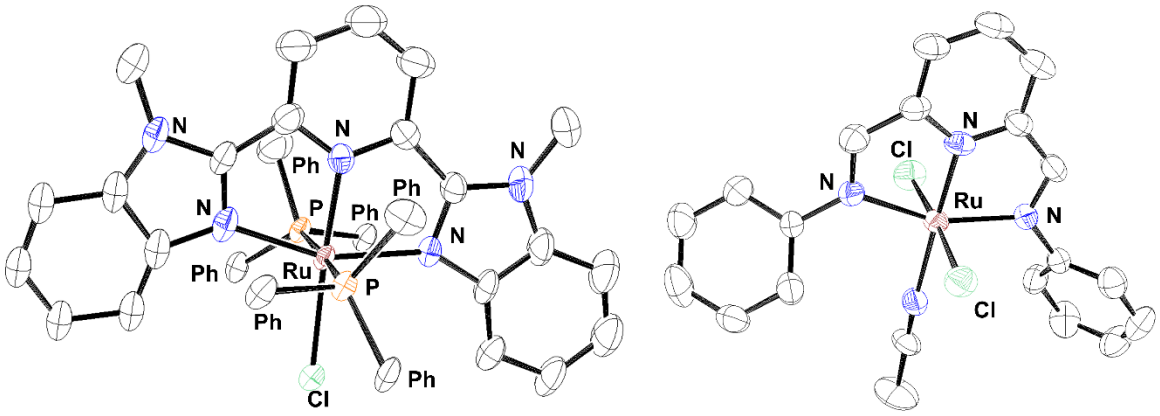

Figure 2.13. Crystal structures of **2.101f** and **2.102d** with ORTEP drawn at 50% probability. The phenyl groups on all phosphorus, all the hydrogen atoms, counter ion and the solvent molecules are omitted for the sake of clarity.

Table 2.1. Selected crystallographic bond distances (Å) and bond angles (°) of complexes **2.101f** and **2.102d**

2.102d		**2.101f**	
Ru–N (Å) Pyridine	1.917(5)	Ru–N (Å) (Pyridine)	2.007(12)
Ru–N (imine) (Å)	2.053(5) 2.081(5)	Ru–N (imine) (Å)	2.100(12) 2.127(11)
Ru–Cl (Å)	2.3732(18) 2.3794(17)	Ru–Cl (Å)	2.445(4)
Ru–N (Å) (acetonitrile nitrogen)	2.089(6)	Ru–P (Å)	2.428(4) 2.422(4)

(Imine)N-Ru-N(Imine) (°)	157.4(2)	(Imine)N-Ru-N(Imine) (°)	158.3(5)
Ru-N≡CCH_3 (°)	177.68(19)	P-Ru-P (°)	176.15(13)
		(Pyridine)N-Ru-Cl (°)	176.1(3)

Table 2.2: The **2.100b** catalyzed aqueous-phase reforming of methanol using various bases

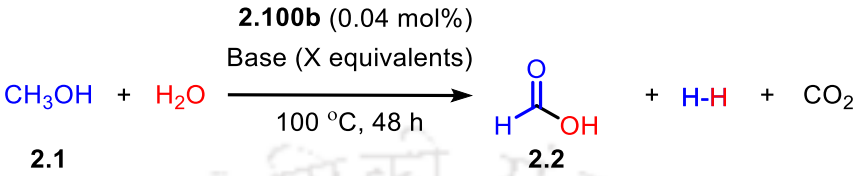

Entry	Base (X equivalents)	mmol of gas	% Yield of H_2[a]	% Yield of **2.2**[b]	% Yield of CO_2[c]
1	NaOH (1)	0.17	1.89	1.89	0
2	NaO^{t}Bu (1)	0.14	1.48	1.48	0
3	KO^{t}Bu (1)	0.37	3.4[d]	2.2	1.2
4	NaOEt (1)	0.23	2.5	2.5	0
5	Na_2CO_3 (1)	0.04	0.42	0.42	0
6	K_2CO_3 (1)	0.05	0.6	0.6	0
7	KOH (1)	0.03	0.3	0.3	0
8	NaO^{t}Bu (0.2)	0.15	1.63	1.63	0
9	KO^{t}Bu (0.5)	0.31	3.29	3.29	0
10	KO^{t}Bu (0.2)	0.12	1.28	1.28	0
11	KO^{t}Bu (0.1)	0.01	0.1	0.1	0

Reaction conditions: Methanol (0.375 mL, 9.27 mmol), H_2O (0.083 mL, 4.635 mmol), base (X equivalents), and **2.100b** (0.0009g, 0.0019 mmol, 0.04 mol %) at 100 °C. Gas evolution was determined by burette measurements. [a]Yield was calculated as moles of H_2 (as determined from GC and the amount of gas evolved)/moles of H_2O. [b]The yield of **2.2** is calculated by ^{1}H NMR spectroscopy using sodium acetate as a standard. [c]The amount of carbon dioxide formed in the reaction was calculated taking in account the subsequent dehydrogenation of HCOOH to H_2 and CO_2. $n(CO_2)$ = (mmol of gas − 2*mmol of formic acid)/4; yield of CO_2 = $n(CO_2)$/n(H_2O). [d]Calculated as weighted average of % hydrogen generated from formic acid and % hydrogen generated from carbon dioxide.

2, Table 2.3) lower. Further, upon employing the analogous PPh_3 complexes **2.101a-f** (Table 2.3, entries 7–12), better yields (*ca.* 23.7% each, 7.9 folds higher in comparison with **2.100b**) of hydrogen and HCOOH were obtained with complex **2.101b** (entry 8 *vs* entry 2, Table 2.3).

The corresponding yields obtained in the reaction catalyzed by **2.101d** were comparable with

Table 2.3: Aqueous-phase reforming of methanol using various pincer-ruthenium catalysts

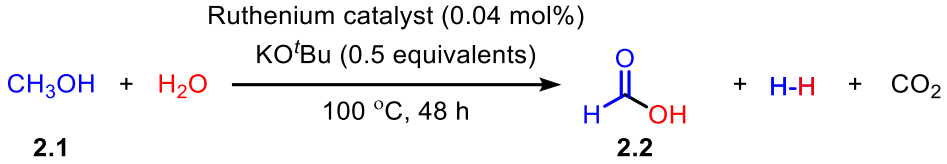

Entry	Ruthenium catalyst (0.04 mol%)	mmols of gas	% Yield of H_2[a]	% Yield of **2.2**[b]	% Yield of CO_2[c]
1	**2.100a**	0.1	1	1	0
2	**2.100b**	0.31	3	3	0
3	**2.100c**	0.1	1	1	0
4	**2.100d**	1.3	14	14	0
5	**2.100e**	0.1	1	1	0
6	**2.100f**	0.8	9	9	0
7	**2.101a**	0.2	3	3	0
8	**2.101b**	2.2	24	24	0
9	**2.101c**	0.7	8	8	0
10	**2.101d**	1.9	21	21	0
11	**2.101e**	0.7	8	8	0
12	**2.101f**	1.2	13	13	0
13	**2.102b**	0.6	7	7	0
14	**2.102c**	0.5	6	6	0
15	**2.102d**	0.2	2	2	0
16	$RuCl_2(PPh_3)_3$	0.2	3	3	0
17	$RuCl_3.3H_2O$	0.4	2.5[d]	1	1.5
18	[Ru(*p*-cymene)Cl_2]$_2$	1.09	12	12	0

Reaction conditions: Methanol (0.375 mL, 9.27 mmol), H_2O (0.083 mL, 4.635 mmol), KO^{t}Bu (0.260 g, 2.32 mmol, 0.5 equivalents), and Ru catalyst (0.0009g, 0.0019 mmol, 0.04 mol %) at 100 °C. Gas evolution was determined by burette measurements. [a]Yield was calculated as moles of H_2 (as determined from GC and the amount of gas evolved)/moles of H_2O. [b]The yield of **2.2** is calculated by ^{1}H NMR spectroscopy using sodium acetate as a standard. [c]The amount of carbon dioxide formed in the reaction was calculated taking in account the subsequent dehydrogenation of **2.2** to H_2 and CO_2. $n(CO_2)$ = (mmol of gas − 2*mmol of **2.2**)/4; yield of CO_2 = $n(CO_2)$/n(H_2O). [d]Calculated as weighted average of % hydrogen generated from formic acid and % hydrogen generated from carbon dioxide.

that observed with **2.101b** (*ca.* 21%, entry 10 *vs.* entry 8, Table 2.3). The reactivity of **2.101f** was comparable to **2.100d** (entry 12 *vs.* entry 4, Table 2.3). In case of corresponding acetonitrile analogues (**2.102b-d**), lower yields were obtained when compared to **2.101b** (entries 13–15 *vs* entry 8, Table 2.3). The commercially available ruthenium precursors $RuCl_3.3H_2O$,

$RuCl_2(PPh_3)_3$ and $[Ru(p\text{-cymene})Cl_2]_2$ demonstrated lower reactivity in comparison to the corresponding pincer–ruthenium complexes (entries 16–18 *vs* entries 1–15, Table 2.3). Among all the complexes screened, $^{Cy2}NNNRuCl_2(PPh_3)$ (**2.101b**) turned out to be the most active catalyst (23.7% yield of H_2 and HCOOH, entry 8, Table 2.3).

Further variations in reaction conditions (Table 2.4) were performed with 0.04 mol % loading of **2.101b** and 0.5 equivalents KO^{t}Bu and MeOH/H_2O (2:1). To begin with, the influence of the temperature on the catalytic performance was studied. Notably, the yields of hydrogen and formic acid at 120 °C and at 140 °C were comparable to those observed at 100 °C in the **2.101b**-catalyzed aqueous-phase methanol reforming reaction (entries 2 and 3 *vs.* entry 1, Table 2.4). Hence, further optimizations were performed at 100 °C for the **2.101b**-catalyzed aqueous-phase methanol reforming reaction. Notably, systematic improvements in yields were observed when the base loading was increased to 1 equivalent and further to 1.5 equivalents of KO^{t}Bu leading to 43% and 66%, respectively, of hydrogen and formic acid each (entries 4–5, Table 2.4). It is noteworthy that, in these reactions, the selectivity toward formic acid is almost quantitative. A further increase in base loading was not investigated owing to the poor solubility of KO^{t}Bu at higher concentrations.

There was a gradual increase in yield of hydrogen when the catalyst loading was increased (entries 5–10, Table 2.4) albeit with a compromise in formic acid selectivity. The best yield of hydrogen and formic acid at 100% selectivity towards the latter was about 81% each and was obtained for the reforming of a 2:1 methanol/water mixture containing 1.5 equivalents of KO^{t}Bu catalyzed by 0.2 mol % of **2.101b**. At 0.8 mol % of **2.101b**, though hydrogen was obtained in a yield of 89%, the yield of formic acid was however low (64% at 72% selectivity) owing to subsequent dehydrogenation to carbon dioxide (*ca*. 25%, entry 9, Table 2.4). There was hardly any increment in yield when the reaction was repeated with 2 mol% of **2.101b**, ultimately leading to 90% hydrogen and 73% formic acid at 80% selectivity (entry 10, Table 2.4). The generation of hydrogen from aqueous methanol was studied at higher concentrations of methanol (*ca.* 3:1 with respect to water), and good yields (84%) of hydrogen along with 82% of formic acid at 95% selectivity was achieved (entry 11, Table 2.4). Further increase in methanol/H_2O to 4:1 lead to lower yields of hydrogen with no selectivity towards formic acid (entry 12, Table 2.4). Lower yields of hydrogen were observed in case of neat methanol highlighting the importance of water in the reaction (entry 13, Table 2.4). On the other hand, no reaction was observed when only water was used as the reactant (entry 14, Table 2.4).

Table 2.4: Aqueous-phase methanol reforming catalyzed by **2.101b** under various conditions.

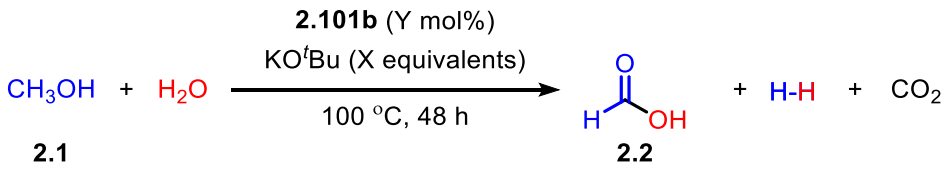

Entry	**2.101b** (Y mol%)	KO^{t}Bu (X equivalents)	mmols of gas	% Yield of H_2[a]	% Yield of **2.2**[b]	% Yield of CO_2[c]
1	0.04	0.5	2.2	24	24	0
2[d]	0.04	0.5	2.14	23	23	0
3[e]	0.04	0.5	1.91	21	21	0
4	0.04	1.0	3.98	43	43	0
5[f]	0.04	1.5	3.04	66	66	0
6[f]	0.1	1.5	3.2	69	69	0
7[f]	0.2	1.5	3.8	81[m]	81	0
8[f]	0.4	1.5	4.98	82[g]	56	24
9[f]	0.8	1.5	5.3	89[g]	64	25
10[f]	2.0	1.5	5.0	90[g]	73	18
11[h]	0.8	1.5	4.05	84[g]	81 ± 2[l]	4
12[i]	0.8	1.5	3.4	51	1	50
13[j]	0.8	0.75	3.4	29	21	8
14[k]	0.8	0.75	0	0	0	0

Reaction conditions: Methanol (0.375 mL, 9.27 mmol), H_2O (0.083 mL, 4.635 mmol), KO^{t}Bu (X equivalents), and **2.101b** ((0.0009g, 0.0019 mmol, 0.04 mol %) at 100 °C. Gas evolution was determined by burette measurements. [a]Yield was calculated as moles of H_2 (as determined from GC and the amount of gas evolved)/moles of H_2O. [b]The yield of **2.2** is calculated by ^{1}H NMR spectroscopy using sodium acetate as a standard. [c]The amount of carbon dioxide formed in the reaction was calculated taking in account the subsequent dehydrogenation of HCOOH to H_2 and CO_2. $n(CO_2)$ = (mmol of gas − 2*mmol of formic acid)/4; yield of CO_2 = $n(CO_2)$/n(H_2O). [d]Reaction was performed at 120 °C. [e]Reaction was performed at 140 °C. [f]Reaction conditions: methanol (0.188 mL, 4.64 mmol), H_2O (0.083 mL, 2.32 mmol), KO^{t}Bu (0.390 g, 3.48 mmol) and **2.101b** (0.0009–0.046 mmol, 0.04–2 mol%) were used. [g]Calculated as weighted average of % hydrogen generated from formic acid and % hydrogen generated from carbon dioxide. [h]6.95 mmol of MeOH, 2.32 mmol of water, 3.48 mmol of KO^{t}Bu, and 0.018 mmol of **2.101b** were used. [i]9.268 mmol of MeOH, 2.32 mmol of water, 3.48 mmol of KO^{t}Bu, and 0.018 mmol of **2.101b** were used. [j]Only 4.64 mmol of MeOH and 0.037 mmol of **2.101b** were used. [k]Only 4.64 mmol of water and 0.037 mmol of **2.101b** were used. [l]Average of three runs. [m]This corresponds to 3.8 mmol of hydrogen, which was further confirmed by obtaining 3.8 mmol of ethyl benzene starting from 4 mmol of styrene in the presence of Pd/C at 120 °C.

2.3.3 Control experiments and mechanistic studies on the pincer–ruthenium catalyzed aqueous-phase methanol reforming reaction.

Scheme 2.6 depicts the proposed mechanism catalyzed by **2.101a–d**, which demonstrates fairly

good activity among all the considered catalysts. In an influential pioneering computational study, Lei very nicely elucidates the nature of the pincer–ruthenium catalyzed aqueous-phase methanol dehydrogenation to carbon dioxide and dihydrogen.[49] We set up on to computationally probe the factors that influence the selective formation of formic acid that is observed in the current study on pincer–ruthenium catalyzed aqueous-phase methanol dehydro--genation. For this purpose, DFT calculations were performed employing the PBE method using the Def2SVP basis set with a polarization function (Figure 2.14).

The first step involves the loss of PPh_3 from **2.101c** to afford a 16-electron pentacoordinate species consisting of two chloride ligands (**2.101c′**). The barrier for this dissociation is computed to be 22.16 kcal/mol at 100 °C. The dissociation of PPh_3 was confirmed by ^{31}P NMR studies (Figure 2.15) and HRMS studies (Figure 2.16). In the presence of methanol (**2.1**) and KO^{t}Bu, the dichloride species undergoes salt metathesis to form the Ru–methoxide species **2.103c**. The calculation of the energetics of the salt metathesis is not undertaken not only because this is typically a facile reaction but also because of the complex nature of the base (a cocktail of alkali−metal alkoxides in the reaction mixture) and the corresponding product salts (solvated or otherwise) involved.

The Ru–methoxide intermediate (**2.103c**) undergoes *β*–H elimination to give formaldehyde (**2.1′**) along with the formation of Ru–H species **2.105c** *via* **TS-2.104c**. This process is slightly uphill (ΔG_{100} = 7.56 kcal/mol) with a barrier of 17.70 kcal/mol (Figure 2.14). The formaldehyde (**2.1′**) can react with water either independently or in the presence of **2.105c**. While independent reaction of **2.1′** with one water leads to methanediol (**2.1″**) with a barrier of 33.14 kcal/mol, the corresponding reaction (**2.105c** → **TS-2.106c** → **2.107c**) in the presence of **2.105c** leads to **2.1″** coordinated **2.102c**, with a comparable barrier (32.25 kcal/mol) (Figure 2.14).

With an additional water molecule, while the corresponding barrier is much lower (11.77 kcal/mol) in the absence of **2.105c**, the pincer-ruthenium catalyzed reaction **2.105c** → **TS-2.106′c** → **2.107c** is almost barrierless. Effectively, the presence of a second equivalent of water helps in lowering the barrier *via* a six-membered transition state for the conversion of formaldehyde (**2.1′**) to methanediol (**2.1″**) both in the presence and in the absence of **2.105c**. It is likely that **2.1″** is formed *via* the barrierless steps **2.105c** → **TS-2.106′c** → **2.107c** in the presence of an additional water molecule and remains coordinated to Ru in **2.107c**.

Subsequent σ-bond metathesis of the O−H bond in coordinated **2.1″** with the Ru–H bond of **2.107c** *via* **TS-2.108c** results in intermediate **2.109c** and the evolution of the first molecule of hydrogen, with a barrier of 23.85 kcal/mol and is an uphill process (ΔG_{100} = 7.81 kcal/mol). This is followed by a *β*-hydride elimination from the alkoxide coordinated to **2.109c**, leading to the formation of formic acid **2.2** (quantitatively detected in ^{1}H NMR) and the Ru–H species **2.105c** in a downhill process (ΔG_{100} = – 9.02 kcal/mol) with a barrier of $\Delta G^{\ddagger}_{100}$ =11.40 kcal/mol (**TS-2.110c**). This lowest-energy (Figure 2.14) intermediate **2.105c** is detected by NMR as **2.105b′** (Figure 2.15). The resulting Ru–H species **2.105c** has two pathways available at its disposal. Apparently in a favorable path, the Ru–H bond in **2.105c** can undergo a σ-bond metathesis with the O−H of the methanol to generate back the Ru-methoxide species **2.103c** and the second molecule of hydrogen *via* **TS-2.114c** ($\Delta G^{\ddagger}_{100}$ = 18.64 kcal/mol) in an uphill reaction (ΔG_{100} = 3.10 kcal/mol). This completes the catalytic cycle for formic acid generation, which is an overall downhill process (ΔG_{100} = – 0.33 kcal/mol) starting from equivalent amounts of methanol and water that also give rise to two equivalents of hydrogen.

Alternatively, liberation of second molecule of hydrogen and formation of Ru-formate **2.112c** *via* further σ-bond metathesis of the O−H of formic acid with the Ru–H bond in **2.105c** is likely to be difficult as it has a higher barrier (**TS-2.111c**, $\Delta G^{\ddagger}_{100}$ = 23.41 kcal/mol). This is in good agreement with the slight or no carbon dioxide observed during the reaction. However, when all the water is consumed, the formic acid cycle (**2.103c** → **TS-2.104c** → **2.105c** → **TS-2.106′c** → **2.107c** → **TS-2.108c** → **2.109c** → **TS-2.110c** → **2.105c** → **TS-2.114c** → **2.103c**) stops and then the cycle involving the formation of CO_2 (**2.103c** → **TS-2.104c** → **2.105c** → **TS-2.106′c** → **2.107c** → **TS-2.108c** → **2.109c** → **TS-2.110c** → **2.105c** → **TS-2.111c** → **2.112c** → **TS-2.113c** → **2.105c** → **TS-2.114c** → **2.103c**) may take over. This explains the observation of carbon dioxide at higher catalyst loadings (entries 8, 9, and 10, Table 2.4) and at lower concentrations of water (entries 11 and 12, Table 2.4).

The *β*-hydride elimination from the formate in **2.112c** *via* TS- **2.113c** ($\Delta G^{\ddagger}_{100}$ = 18.08 kcal/mol) with the concomitant release of carbon dioxide is a downhill reaction (ΔG_{100} = −14.75 kcal/mol). Finally, the Ru−H in intermediate **2.105c** undergoes σ-bond metathesis with the O–H of methanol to regenerate Ru-methoxide species **2.103c** *via* **TS-2.114c** along with the liberation of the third molecule of hydrogen. This is computed to be uphill (ΔG_{100} = 3.10 kcal/mol with a barrier of 18.63 kcal/mol). The overall process involving the generation of a mole of carbon dioxide and 3 moles of hydrogen from a mole each of methanol and water is downhill (ΔG_{100}

= –17.00 kcal/mol). Single-point calculations at a higher level with Def2TZVP were also performed (Figure 2.17), and interestingly, the level of the calculation does not affect the trend of the result.

Either for the cycle involving the formation of a mole of formic acid and 2 moles of hydrogen or for the cycle that results in a mole of carbon dioxide and 3 moles of hydrogen, the σ-bond metathesis of the O–H bond in coordinated **2.1″** with the Ru− H bond of **2.107c** (**2.107c** → **TS-2.08c** → **2.109c**) appears to be the rate-determining step (RDS) with a barrier of 23.85 kcal/mol. Figure 2.14 clearly indicates **2.107c** and/or **2.105c** (formed *via* **TS-2.110c**) to be the resting states of the reaction, and not surprisingly, while **2.107b′**, the derivative of **2.107b**, is observed in HRMS analysis (Scheme 2.4 and Figure 2.16), the lowest energy intermediate **2.105c** is detected by NMR as **2.105b′** (Figure 2.15).

This is well-complemented by the deuterium labelling studies that indicate a k_H/k_D value of 1.81 when CH_3OH was replaced with CD_3OD in the reaction. A combined kinetic and DFT (*vide infra*) analysis indicates that the methanol C–H bond activation occurs as a part of the mechanism[50] and is not a part of the RDS[50] (Figure 2.18a), while the O-H bond activation is the RDS and contributes majorly to the observed k_H/k_D value of 1.81.

The ratio of the TOF (8.00 mmol/48 h) of gas evolution for the **2.101b** catalyzed reaction of CH_3OH (13.92 mmol) with water (4.64 mmol) in the presence of KO^{t}Bu (6.96 mmol) at 100 °C to the corresponding TOF (3.78 mmol/48 h) of gas evolution starting from CD_3OD (13.92 mmol) and water (4.64 mmol) is 2.1 (equations 1 *vs* 2, Scheme 2.7). This KIE of 2.1 very nicely correlates with the ratio (1.81) of the corresponding slopes of the initial rate of gas evolution (Figure 2.18a).

Only 38% retention of deuterium in formic acid, upon use of CD_3OD + H_2O (equation 2, Scheme 2.7) and its lack thereof while employing CH_3OH + D_2O (equation 3, Scheme 2.7) suggests that while the steps (**2.103c** → **TS-2.104c** → **2.105c** → **TS-2.106c** → **2.107c**) are reversible, the transformation (**2.107c** → **TS-2.108c** → **2.109c** → **TS-2.110c** → **2.105c**) is facile and irreversible. Similar results were obtained by Zheng[34] and Singh[32] where they observed that CD_3OD is more influential than D_2O in altering the rate of reaction. Not surprisingly, complete retention of deuterium was observed in formic acid in the reaction of CD_3OD + D_2O catalyzed by **2.101b** at 100 °C (equation 4, Scheme 2.7).

Apparently, the reaction is primarily homogeneous and the major contributor to the observed reactivity was well-defined molecular pincer–Ru catalysts (equations 1 *vs* 5, Scheme 2.7) with minor contribution from heterogeneous Ru nanoparticles (NPs). Accordingly, the tiny amounts of black particles formed in the **2.101b** catalyzed reaction (entry 11, Table 2.4 and equation 1, Scheme 2.7) were analyzed by transmission electron microscopy (TEM) (Figure S1.34, Appendix I), separated, and used as a catalyst for methanol reforming under conditions identical as entry 11, Table 2.4. The poor reactivity (equation 6, Scheme 2.7) is suggestive of the fact that the formation of black Ru NPs is a deactivation step in the **2.101b**-catalyzed methanol reforming reaction.

Kinetic experiments were performed to determine the rate order of the reaction with respect to the concentration of the catalyst and methanol in a NMR tube. For the sake of ease of operation in a NMR tube, the reactions were performed using 0.5 equivalents of KO^{t}Bu rather than 1.5 equivalents. Using the initial rate method, it was found that the plots of the initial rate of formation of formic acid *vs* [**2.101b**] (Figures 2.18b and 2.20) and the initial rate of formation of formic acid *vs* [methanol] (Figures 2.18c and 2.21) is linear, which is indicative of first-order dependence on the concentrations of both **2.101b** and methanol.

Steric bulk on the imine N could play a key role in deciding the barrier of the overall RDS involving the σ-bond metathesis of the O–H bond in coordinated **2.1″** with the Ru–H bond of **2.107** *via* **TS-108.** Considering the fact that the reaction is performed in water under an atmosphere of air, it is likely that a combination of steric factors and the relative stability toward moisture/air dictates the observed difference in reactivity of the various considered catalysts.

Obtaining the desired amount of deuterium for specialized experiments[51] is often a challenge, not only owing to the fact that D_2 is less readily commercially available across all geographical locations but also because it is typically available in select expensive pack sizes. Taking into consideration, the immense applications of labelling organic compounds with hydrogen isotopes in numerous areas, from materials science to medicinal chemistry,[51] the ability of the current catalytic system to produce pure hydrogen was put into valuable application toward the on-site synthesis of desired amounts of D_2. Subsequent incorporation of the deuterium generated into various unsaturated molecules led to valuable compounds, including but not limited to reduced quinoline derivatives, which are key structural features of many natural and unnatural compounds with important biological properties such as antibacterial, antifungal, and anticancer activity (Scheme 2.8).[52]

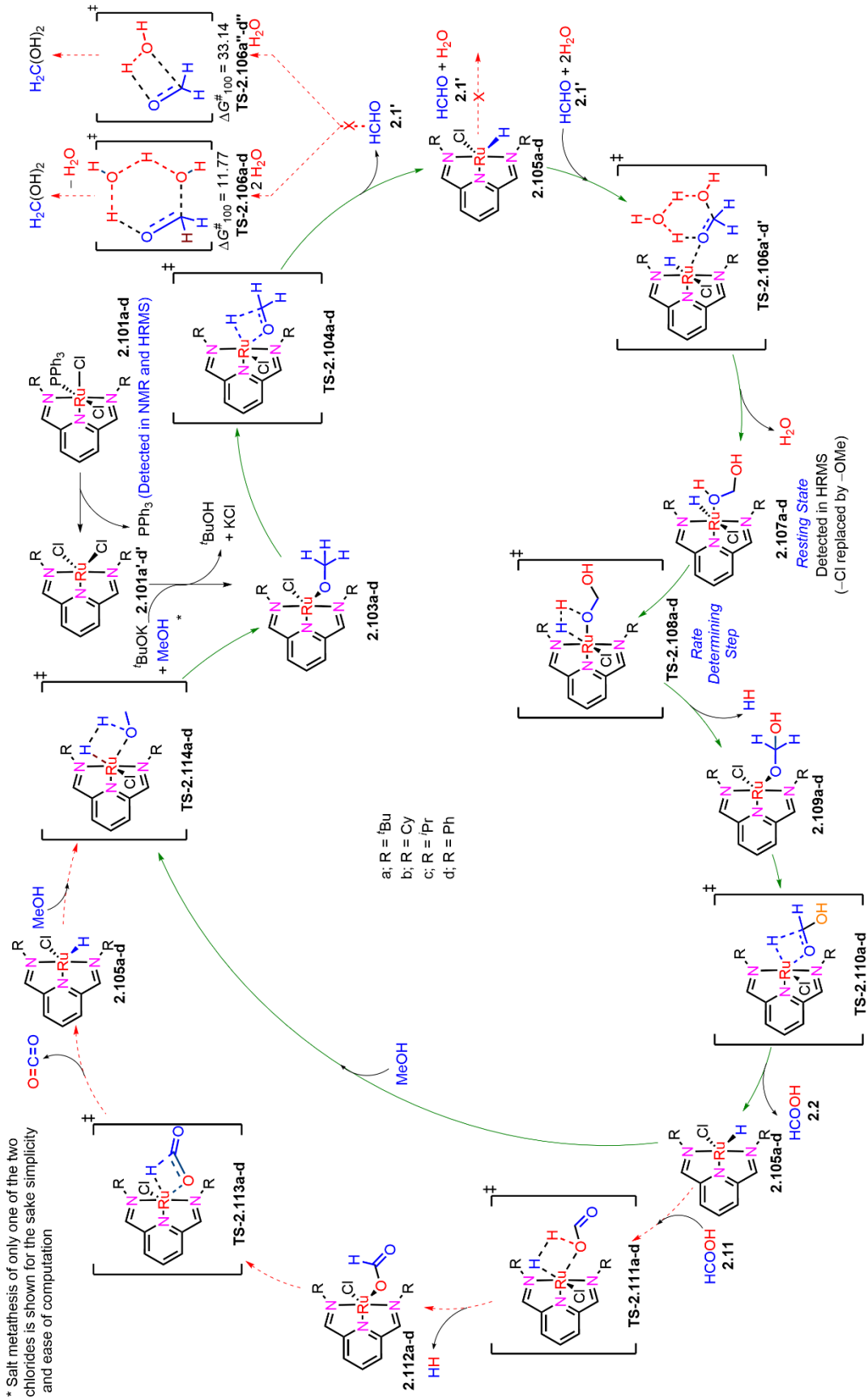

Scheme 2.6. Plausible mechanism involved in the **2.101** catalyzed reforming of methanol.

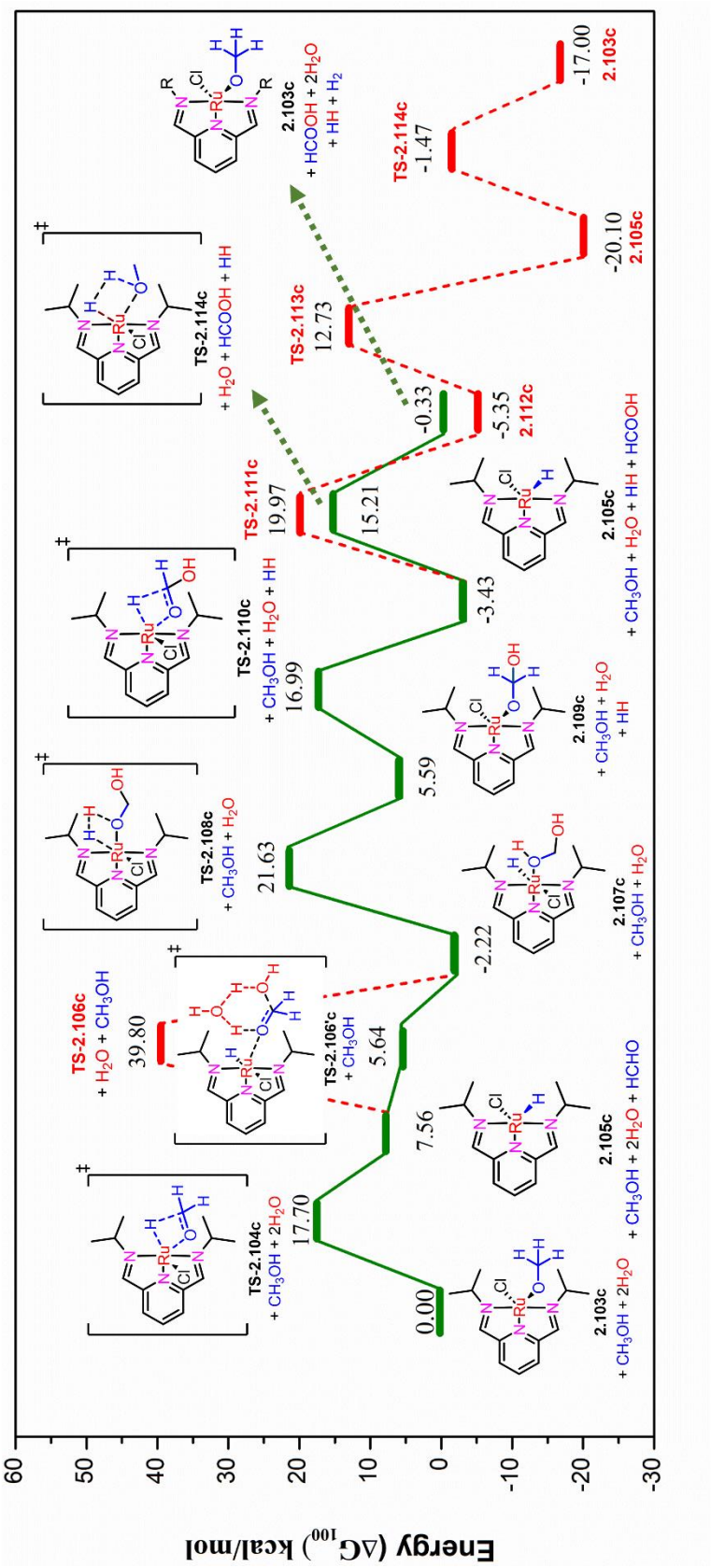

Figure 2.14. Free energy (ΔG_{100}) profile of the **2.101c** catalyzed reforming of methanol at 100 °C employing PBE method using the Def2SVP basis set. Structures of intermediates and transition states of only the favorable path (green solid lines) leading to formic acid are provided. The unfavorable path of the methanol to formic acid transformation and the path involving the methanol to carbon dioxide conversion is shown as red dotted lines.

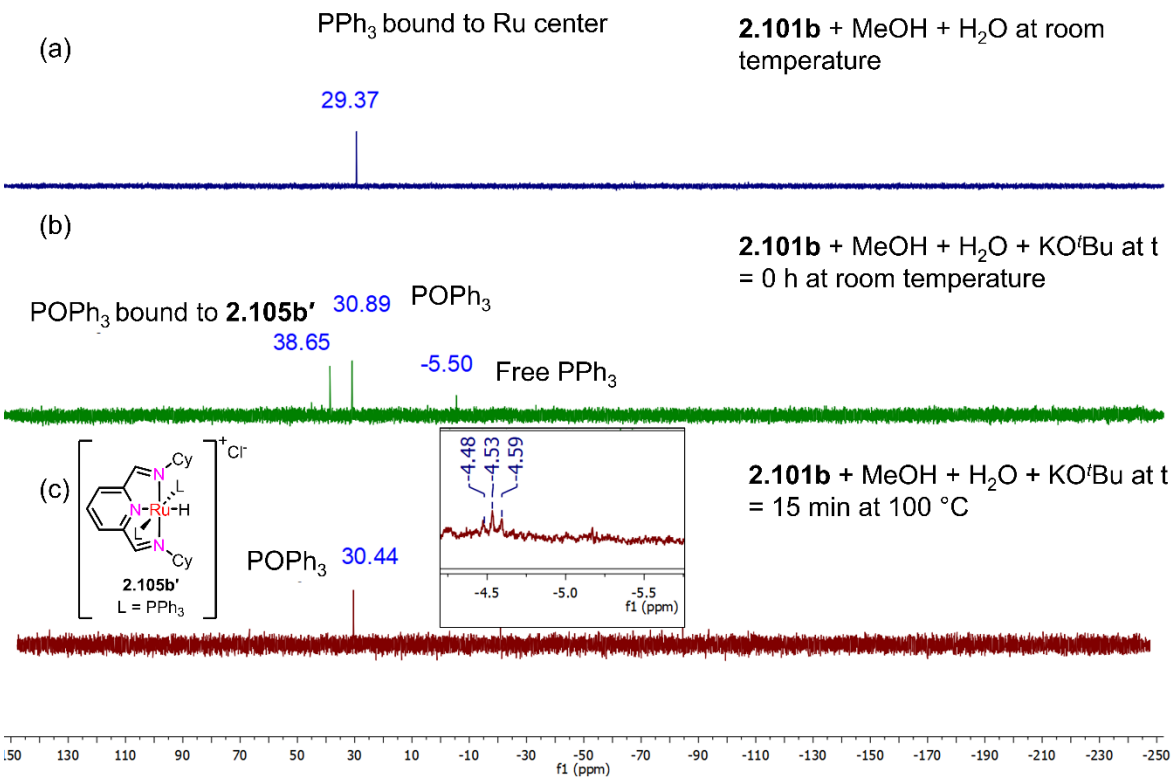

Figure 2.15. ^{31}P NMR spectra of (a) **2.101b** (80 mM) in MeOH/H_2O (b) **2.101b** (80 mM) in CH_3OH (9.27 mmol) with water (4.64 mmol) in the presence of KO^{t}Bu (2.32 mmol) at room temperature. (c) **2.101b** (80 mM) in CH_3OH (9.27 mmol) with water (4.64 mmol) in the presence of KO^{t}Bu (2.32 mmol) at 100 °C. The inset has the region of the corresponding ^1H NMR depicting the hydride signal.

2.4 Conclusion

NNN pincer–ruthenium complexes of the type (^{R2}NNN)$RuCl_2(CH_3CN)$ based on *bis*(imino)pyridine ligands have been synthesized and characterized. Along with their phosphine and carbonyl counterparts, these pincer ruthenium acetonitrile complexes were tested for the value-addition of methanol *via* its reforming in the presence of a base. In comparison with the considered catalysts, the best efficiency was observed with (^{Cy2}NNN)$RuCl_2(PPh_3)$. KO^{t}Bu (0.5 equivalents with respect to water) was found to give superior results at temperatures as low as 100 °C among the bases screened. For a mixture of methanol and water in a 2:1 ratio (^{Cy2}NNN)$RuCl_2(PPh_3)$ (0.2 mol%) gave a yield of up to 81% each of hydrogen and formic acid at 100% selectivity in the presence of KO^{t}Bu (1.5 equivalents with respect to water) at 100 °C. However, under identical conditions, a higher loading of (^{Cy2}NNN)$RuCl_2(PPh_3)$ (2 mol%) gave up to 90% of hydrogen and 73% of formic acid at 80% selectivity. In contrast, use of a 3:1 methanol/water mixture resulted in good yields (84%) of

hydrogen with 82% formic acid at 95% selectivity at a 0.8 mol% loading of(^{Cy2}NNN)RuCl$_2$(PPh$_3$). The yields of hydrogen/ deuterium calculated by measuring the volume of gas evolved are very consistent and comparable to the yields of products obtained by using them for reducing the various unsaturated compounds.

Valuable information was obtained from detailed mechanistic studies. Evidence for the homogeneous nature of the reaction involving well-defined molecular catalysts was obtained not only from Hg poisoning experiment (equation 5, Scheme 2.7), but also from kinetic studies that demonstrated a first-order dependence of rate on the concentrations of both (^{Cy2}NNN)RuCl$_2$(PPh$_3$) and methanol. Deuterium labelling studies were indicative of an average KIE of 1.96 that is because methanol C–H bond activation occurs as a part of the mechanism but not as a part of the RDS. This is very well complemented by DFT studies that compute that either for the cycle leading to formic acid and 2 mol of hydrogen or for the cycle that results in carbon dioxide and 3 moles of hydrogen, the σ- bond

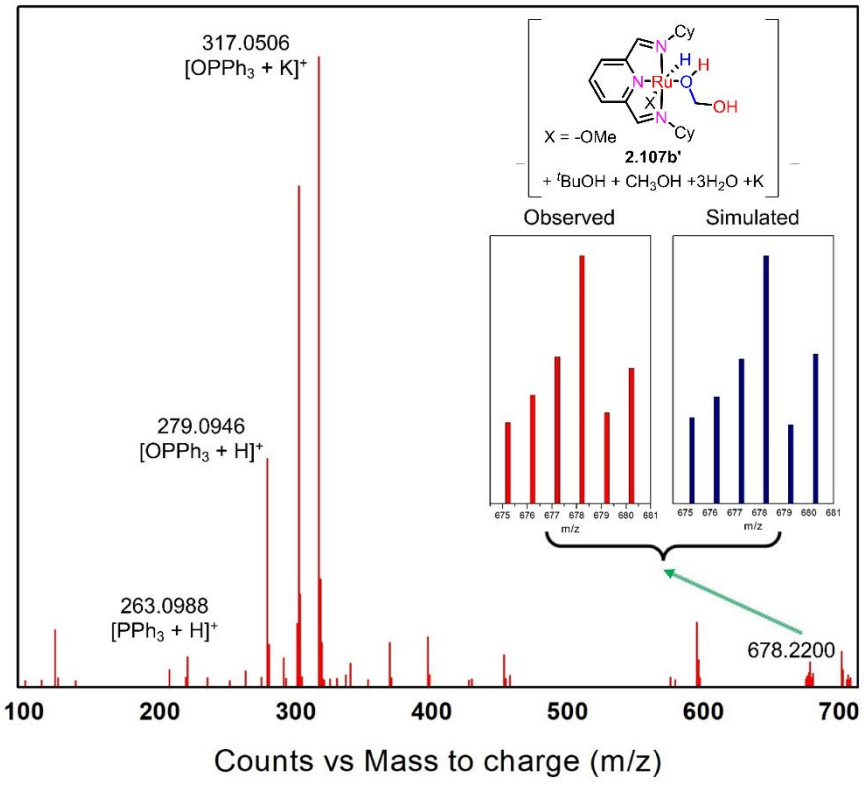

Figure 2.16. HRMS analysis of reaction mixture containing methanol (0.282 mL, 6.96 mmol), H_2O (0.042 mL, 2.32 mmol), KO^{t}Bu (0.390 g, 3.48 mmol) and **2.101b** (0.0136 g, 0.019 mmol, 0.8 mol%) at 100 °C after 2 h.

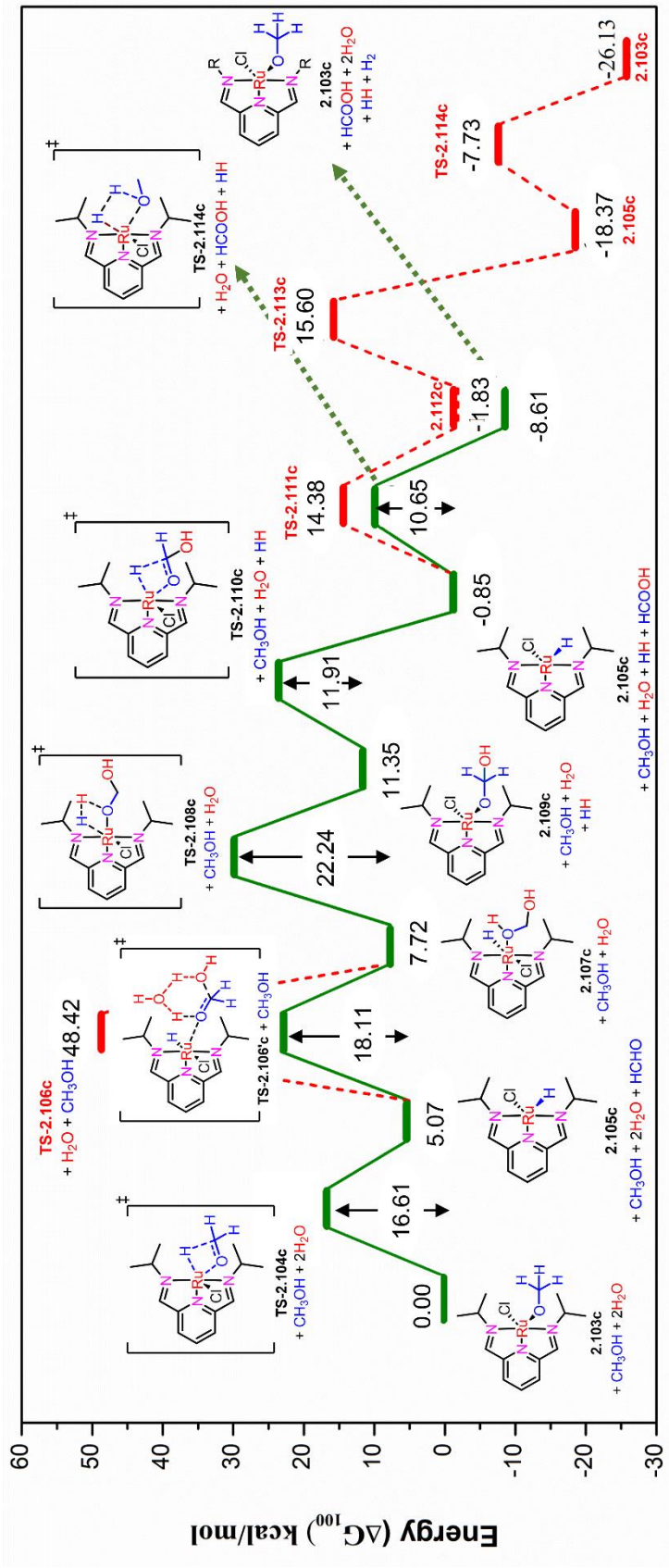

Figure 2.17. Free energy (ΔG_{100}) profile of the **2.101c** catalyzed reforming of methanol at 100 °C employing PBE method using the Def2TZVP basis set. Structures of intermediates and transition states of only the favorable path (green solid lines) leading to formic acid are provided. The unfavorable path of the methanol to formic acid transformation and the path involving the methanol to carbon dioxide conversion is shown as red dotted lines.

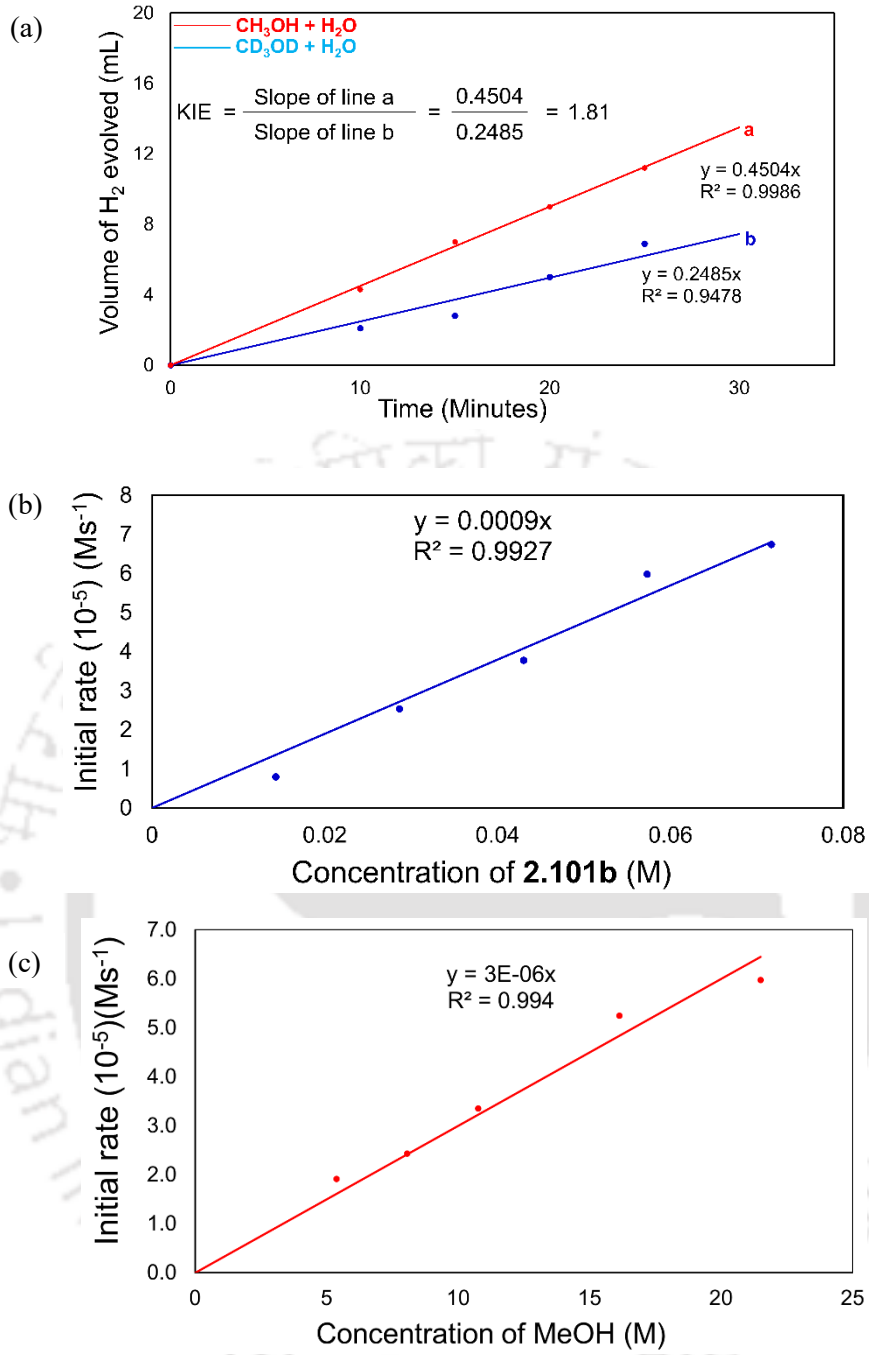

Figure 2.18. (a) Plot depicting the initial rate of gas evolution in the **2.101b** (0.027 g, 0.037 mmol, 0.8 mol%) catalyzed reaction of CH_3OH (13.92 mmol) with water (4.64 mmol) in the presence of KO^{t}Bu (6.96 mmol) at 100 °C and in the **2.101b** (0.027 g, 0.037 mmol, 0.8 mol%) catalyzed reaction of CD_3OD (13.92 mmol) with water (4.64 mmol) in the presence of KO^{t}Bu (6.96 mmol) at 100 °C. Also see Figure 2.19. (b) Variation of initial rate of formation of formic acid with concentration of **2.101b** (reaction condition: methanol (0.433 mL, 10.71 mmol), D_2O (0.065 mL, 3.57 mmol), KO^{t}Bu (0.2 g, 1.78 mmol), and **2.101b** (0.2, 0.4, 0.6, 0.8, and 1 mol %) at 100 °C in a NMR tube). Also see Figure 2.20. (c) Variation of the initial rate of formation of formic acid with concentration of methanol (reaction condition: methanol (0.108−0.433 mL, 2.67–10.71 mmol), D_2O (0.065 mL, 3.57 mmol), KO^{t}Bu (0.2 g, 1.78 mmol), and **2.101b** (0.8 mol %) at 100 °C in a NMR tube). Dioxane is used as a makeup solvent at lower concentrations of methanol. Also see Figure 2.21.

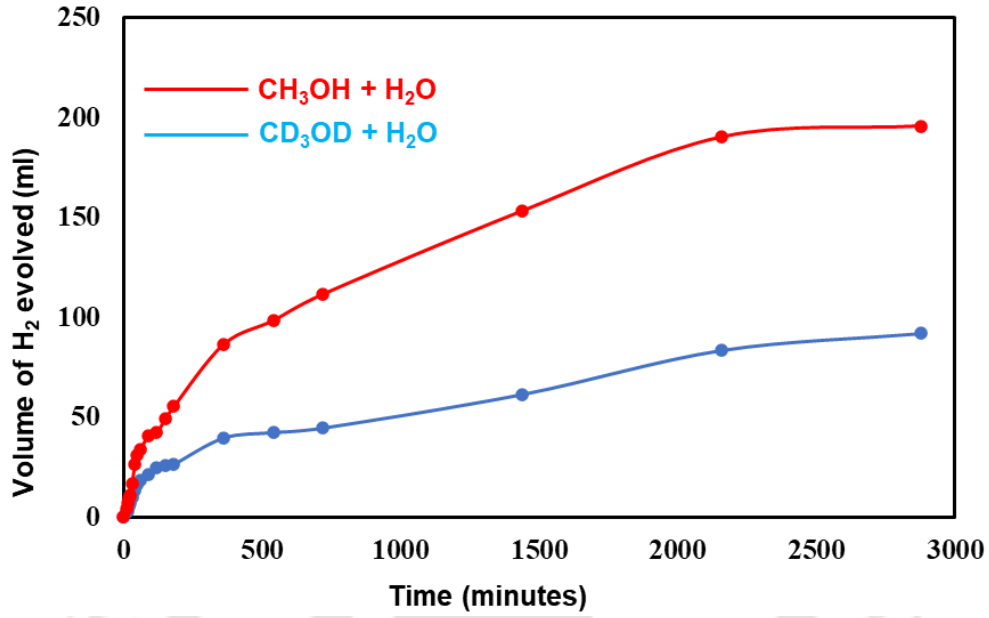

Figure 2.19. Reaction profile of gas evolution in the **2.101b** (0.027 g, 0.037 mmol, 0.8 mol%) catalysed reaction of CH_3OH (13.92 mmol) with water (4.64 mmol) in the presence of KO^{t}Bu (6.953 mmol) at 100 °C and in the **2b** (0.027 g, 0.037 mmol, 0.8 mol%) catalysed reaction of CD_3OD (13.92 mmol) with water (4.64 mmol) in the presence of KO^{t}Bu (6.953 mmol) at 100 °C.

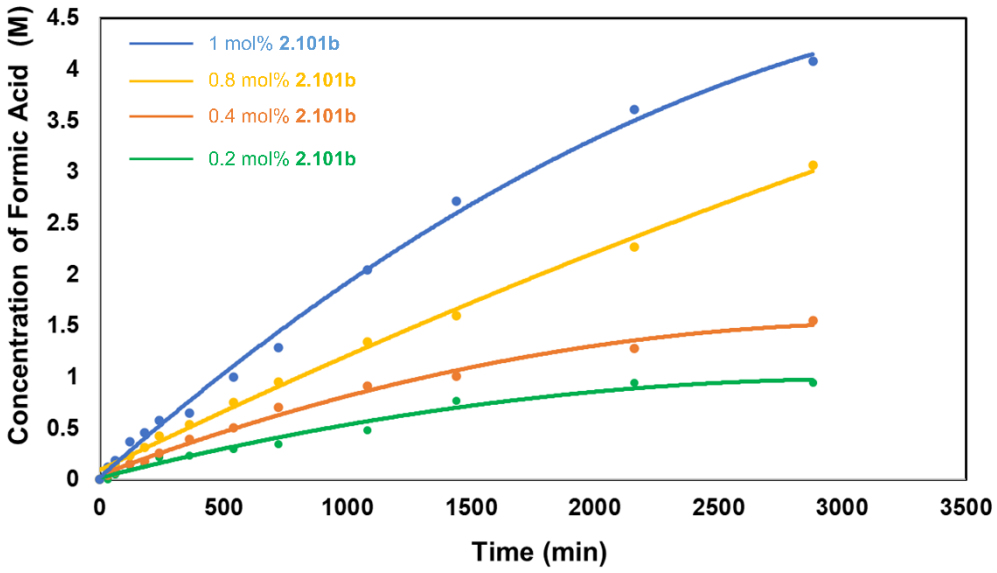

Figure 2.20. Reaction profile of formic acid formation in the **2.101b** (1 mol%, 0.8 mol%, 0.4 mol% and 0.2 mol%) catalysed reaction of CH_3OH (10.71 mmol) with D_2O (3.57 mmol) in the presence of KO^{t}Bu (1.79 mmol) at 100 °C.

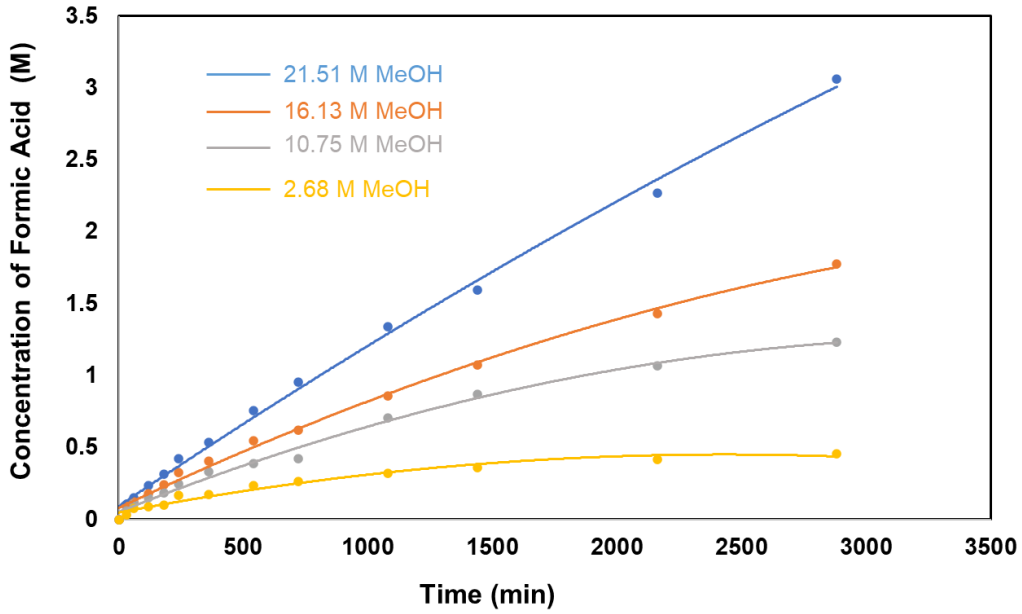

Figure 2.21. Reaction profile of formic acid formation in the **2.101b** (0.021g, 0.029 mmol, 0.8 mol%) catalysed reaction of CH_3OH (10.71 mmol, 8.03 mmol, 5.36 mmol, 2.68 mmol) with D_2O (3.57 mmol) in the presence of KO^{t}Bu (1.79 mmol) at 100 °C. Dioxane was added to maintain equal volume in all the cases.

metathesis leading to the elimination of the first molecule of hydrogen is the RDS. The unprecedented selectivity toward formic acid in these pincer–ruthenium catalyzed methanol reforming stems from the choice of the Ru–H bond in (^{Cy2}NNN)RuCl(H) to undergo a σ-bond metathesis either with the O−H of methanol (that completes the formic acid cycle) or with the O–H of formic acid that leads to carbon dioxide. Its preference for the former is mainly dictated by kinetics, which is more favored by 4.58 kcal/mol. We report a powerful catalytic system that comprises of an NNN pincer-ruthenium phosphine catalyst based on *bis*(imino)pyridine ligand for the high yield transformation of a mole of methanol and water to 2 moles of hydrogen and a mole of formic acid at unprecedented selectivity at a temperature as low 100 °C. This could open up exciting avenues for the reforming of methanol into clean-burning hydrogen and high-value formic acid.

2.5 Experimental Section

2.5.1 General procedure and materials

All the manipulations were carried out under purified Ar using either a standard double manifold or a glove box. The solvents such as tetrahydrofuran (THF), hexane and toluene were dried *via* double distillation over Na/benzophenone prior to the experiment.[53] Methanol was dried and distilled under argon according to the literature procedure.[53] All other chemicals such

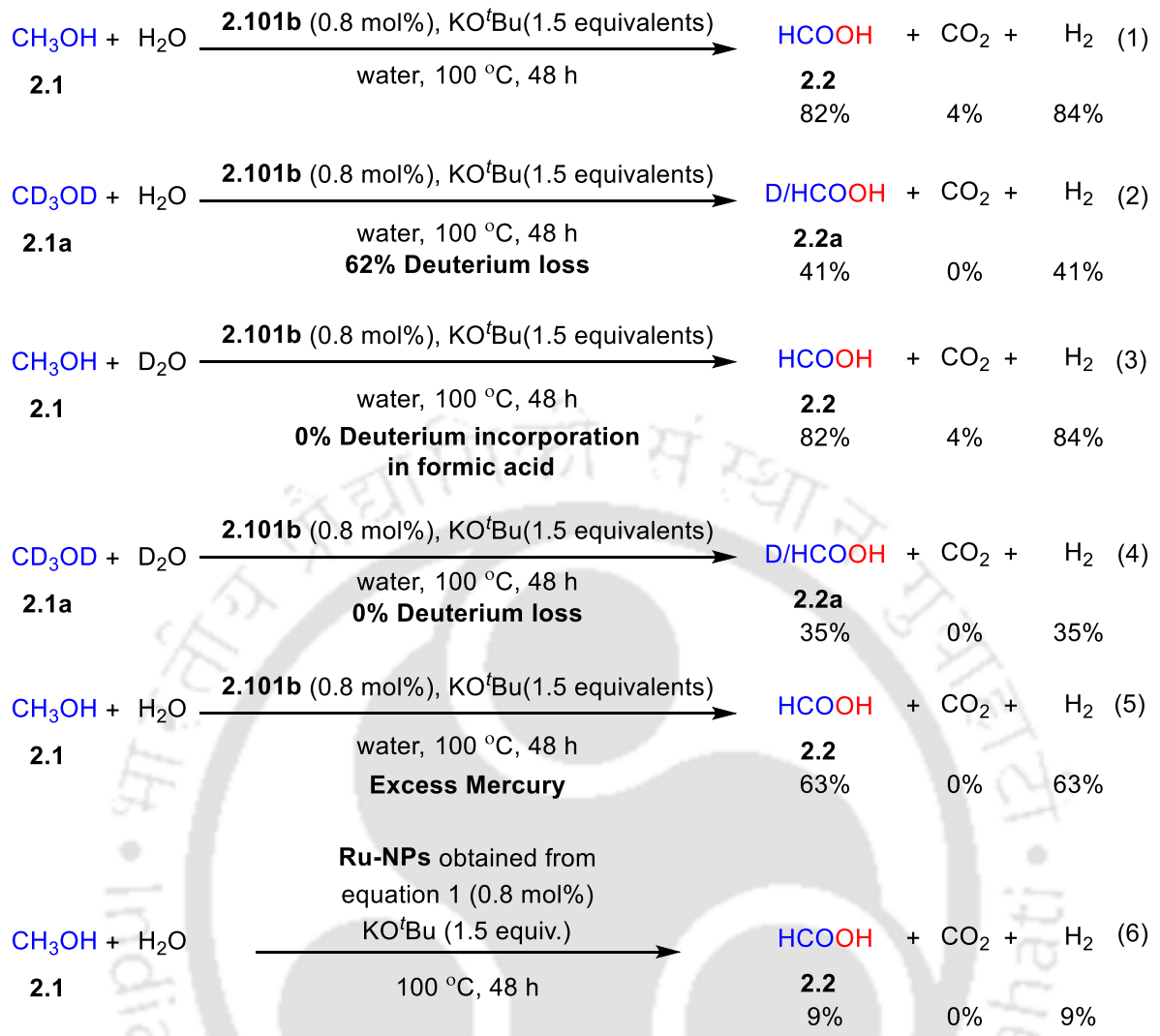

Scheme 2.7. Control experiments

as $RuCl_3 \cdot 3H_2O$, $[Ru(benzene)Cl_2]_2$, $[RuCl_2(p\text{-cymene})]_2$, pyridine-2,6-dicarboxylic acid, D_2O, ethanol-d_6 and $CDCl_3$ were purchased from MERCK or Sigma-Aldrich and used as such. All catalytic reactions were set up either under an Ar atmosphere or under air using dried glassware. The complexes $RuCl_2(PPh_3)_3$, **2.100a–f**, **2.101a–f**, and **2.102b–d** were prepared according to the literature procedure.[43-48, 54-64]

2.5.2 Physical measurements

^1H, ^2H, $^{13}C\{H\}$ and ^{31}P were recorded on a Bruker ASCEND 600 operating at 600 MHz for ^1H, 150 MHz for $^{13}C\{H\}$ and 564 MHz for ^{31}P or on a Bruker AVANCE 400 operating at 400 MHz for ^1H, 100 MHz for $^{13}C\{H\}$, 376 MHz for ^{31}P or on a Bruker AVANCE 500 operating at 500 MHz for ^1H, 125 MHz for $^{13}C\{H\}$, 470 MHz for ^{31}P. HRMS measurements were performed using an Agilent Accurate-Mass Q-TOF ESI–MS 6546. GC analyses were performed on an

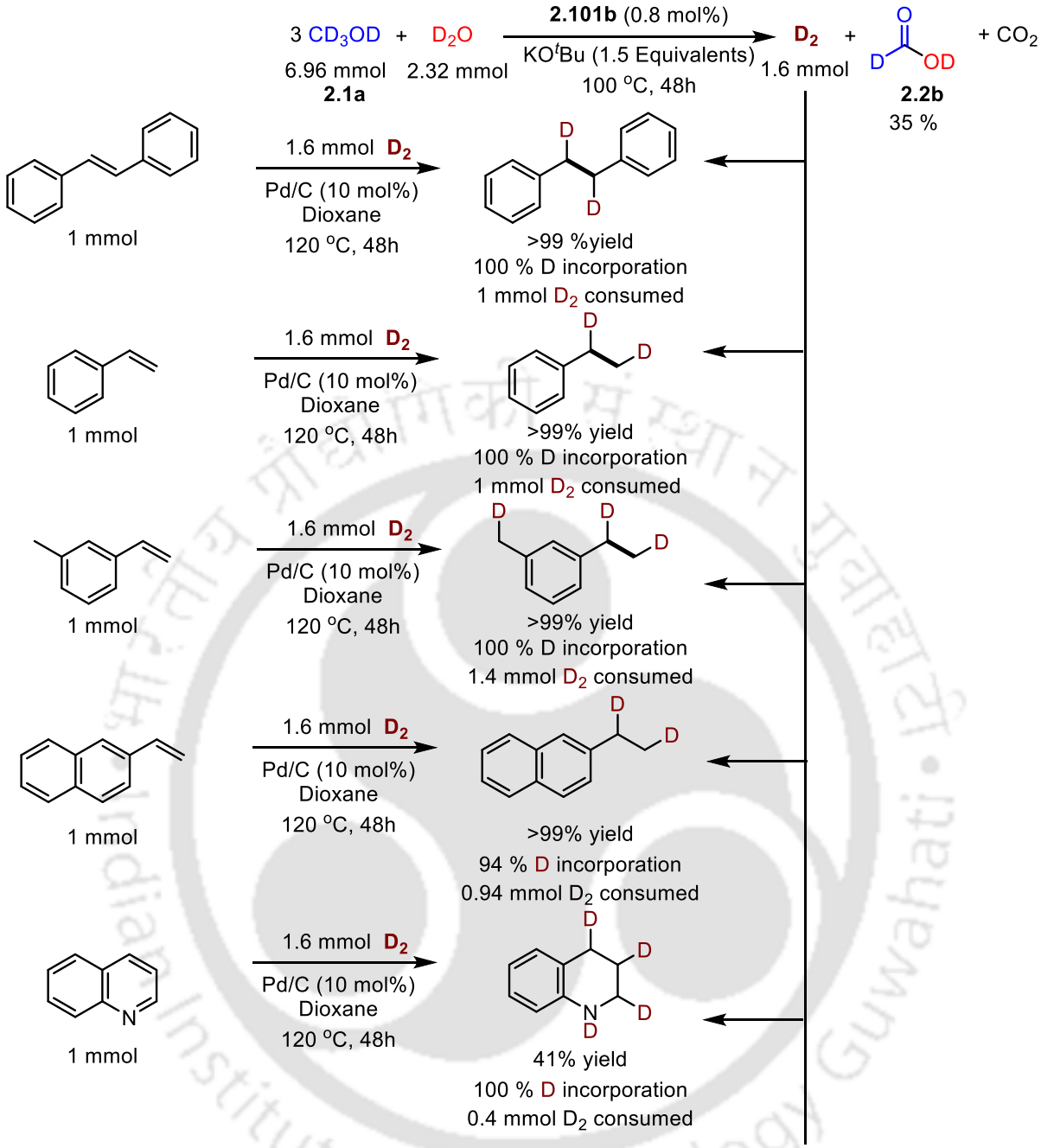

Scheme 2.8. On-site generation of deuterium for labelling various unsaturated compounds.

Agilent 7820-GC instrument fitted with an Agilent Front SS7 inlet N_2 HP-PLOT Q column (30 m length × 530 µm × 40 µm) using the following method: Agilent 7820-GC back detector: TCD starting temperature: 40 °C; time at starting temp: 0 min; ramp: 40 °C min^{-1} up to 250 °C with holding time = 5 min; flow rate (carrier): 25 mL min^{-1} (N_2); split ratio: 195; inlet temperature: 40 °C; detector temperature: TCD: 250 °C, FID: 250 °C.

2.5.3 General procedure for the synthesis of (^{R2}NNN)RuCl$_2$(CH$_3$CN) complexes (2.102b; R = Cy, 2.102c; R = ^{i}Pr and 2.102d; R = Ph). The complex **2.102b** were prepared by the

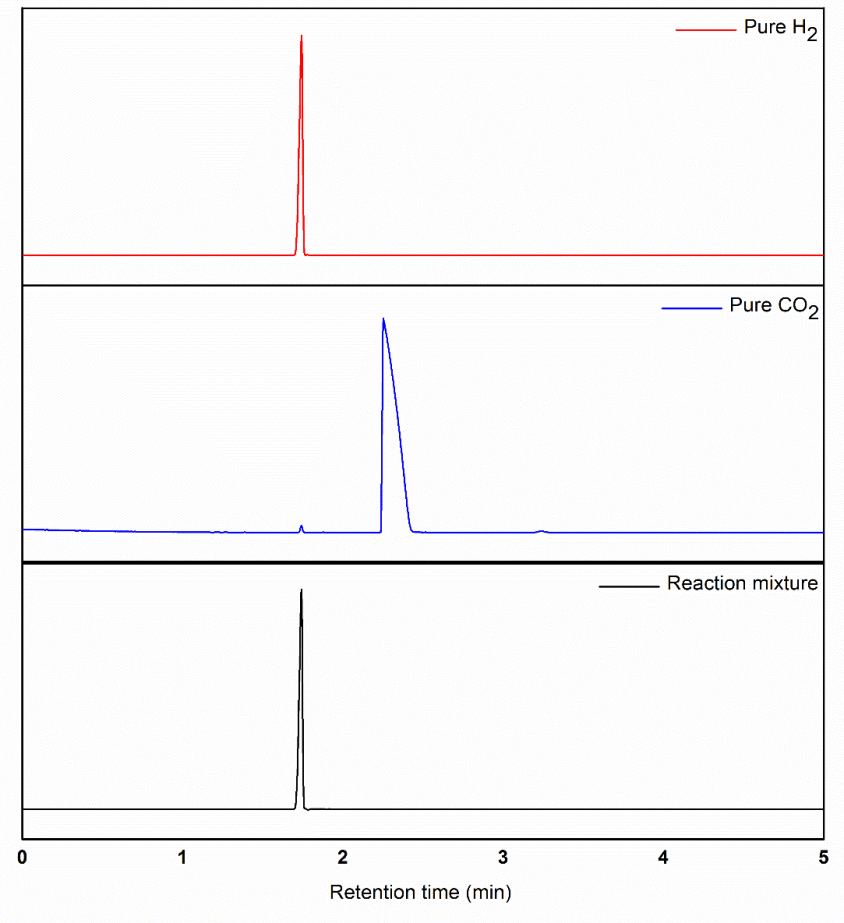

Figure 2.22. GC-TCD analysis of gas evolved from reaction along with corresponding analysis of pure H_2 and CO_2 gas. Reaction condition: Entry 11, Table 2.4.

reaction of corresponding ligands **2.103a** (0.100 g, 0.393 mmol) with $[RuCl_2(p\text{-cymene})]_2$ (0.120 g, 0.196 mmol), using acetonitrile as the solvent and stirring overnight under reflux conditions. The solvent was evaporated under reduced pressure, and the dark brown solid (**2.102b**) was washed with diethyl ether (3 × 3 mL). The residue was dried under a vacuum and 3a isolated as a black solid with a 64% yield (0.128 g). A similar procedure was followed for the synthesis of **2.102b-d**.

(^{Cy2}NNN)RuCl$_2$(CH$_3$CN) (2.102b). (0.128 g) 64% yield. NMR analysis shows the presence of two isomers (*cis* and *trans*) in a 1:2 ratio. ^{1}H NMR (600 MHz, $CDCl_3$): δ 8.57 (s, 2H, N=C*H*), 8.34 (s, 4H, N=C*H*), 8.02−7.95 (m, 2H, Ar), 7.79 (s, 1H, Ar), 7.59 (d, J = 7.8 Hz, 4H, Ar), 7.43 (t, *J* = 7.7 Hz, 2H, Ar), 3.96 (ddt, *J* = 11.3, 8.0, 3.3 Hz, 6H, NC*H*$(CH_2)_5$), 2.91 (s, 3H, C*H*$_3$CN), 2.83 (s, 6H, C*H*$_3$CN), 2.26−2.28 (m, *J* = 8.4, 4.3 Hz, 9H, NCH(C*H*$_2)_5$), 2.14−2.17 (m, 6H, NCH(C*H*$_2)_5$), 1.99−1.93 (m, 12H, NCH(C*H*$_2)_5$), 1.91−1.84 (m, 14H, NCH(C*H*$_2)_5$), 1.47−1.40 (m, 12H, NCH(C*H*$_2)_5$), 1.25 (d, *J* = 6.9 Hz, 7H, NCH(C*H*$_2)_5$). ^{13}C{H} NMR (151 MHz,

CDCl3): δ 161.91, 159.47 (N=*C*H), 128.99, 127.82, 126.28 (Ar), 122.35 (CH_3CN), 72.54 (N*C*H$(CH_2)_5$), 33.52, 26.07, 25.93, 25.52, 25.26, 24.10, 23.57 (NCH(*C*H$_2)_5$), 4.90 (*C*H$_3$CN). HRMS (ESI): m/z calculated for [**2.102b** − Cl]$^+$ = [$C_{21}H_{30}ClN_4Ru$]$^+$, 475.1202; found, 475.1352; m/z calculated for [**2.102b** − Cl + CH_3CN]$^+$ = [$C_{23}H_{33}ClN_5Ru$]$^+$, 516.1468; found, 516.1628.

(*i*^{Pr2}NNN)RuCl$_2$(CH$_3$CN) (2.102c). (0.117 g, black solid) 81% yield. NMR analysis shows the presence of two isomers (*cis* and *trans*) in a 1:2 ratio. ^{1}H NMR (600 MHz, $CDCl_3$): δ 8.56 (s, 2H, N=C*H*), 8.37 (s, 4H, N=C*H*), 7.96 (d, J = 7.4 Hz, 2H, Ar), 7.78 (t, J = 7.1 Hz, 1H, Ar), 7.60 (d, J = 7.8 Hz, 4H, Ar), 7.44 (t, J = 7.8 Hz, 2H, Ar), 4.39−4.30 (m, 6H, NC*H*$(CH_3)_2$), 2.91 (s, 3H, C*H*$_3$CN), 2.84 (s, 6H, C*H*$_3$CN), 1.61 (d, J = 6.5 Hz, 22H, NCH(C*H*$_3)_2$), 1.56 (d, J = 5.0 Hz, 14H, NCH(C*H*$_3)_2$). ^{13}C{H} NMR (151 MHz, $CDCl_3$); δ 163.26, 161.83, 160.60, 159.55 (N=*C*H), 134.01, 129.00, 128.08, 125.42 (Ar), 122.41 (CH_3CN), 77.29, 77.08, 76.87, 65.29, 64.63 (N*C*H$(CH_2)_3$), 23.19, 22.94, 22.91 (NCH(*C*H$_2)_3$), 5.17, 4.79 (*C*H$_3$CN). HRMS (ESI): m/z calculated for [**2.102c**–Cl–CH_3CN]$^+$ = [$C_{13}H_{19}ClN_3Ru$]$^+$, 354.0311; found, 354.0304; m/z calculated for [**2.102c**–Cl]$^+$ = [$C_{15}H_{22}ClN_4Ru$]$^+$, 395.0576; found, 395.0575; m/z calcd for [**2.102c**–Cl+CH_3CN]$^+$ = [$C_{17}H_{25}ClN_5Ru$]$^+$, 436.0842; found, 436.0845.

(Ph^{2}NNN)RuCl$_2$(CH$_3$CN) (2.102d). (0.116 g, purple solid) 69% yield. ^{1}H NMR (400 MHz, $CDCl_3$): δ 8.38 (s, 2H, N=C*H*), 7.73 (d, J = 7.9 Hz, 2H, Ar), 7.65 (d, J = 8.4 Hz, 4H, Ar), 7.48 (t, J = 7.9 Hz,1H, Ar), 7.34 (dd, J = 11.9, 7.3 Hz, 6H, Ar), 2.31 (s, 3H, C*H*$_3$CN). ^{13}C{H} NMR (151 MHz, $CDCl_3$): δ 160.30, 154.78, 150.96 (N=*C*H), 137.50, 129.42, 127.07, 123.43 (Ar), 121.33 (CH_3CN), 77.37, 77.16, 76.95 (Ar), 1.16 (*C*H$_3$CN). HRMS (ESI): m/z calcd for [**2.102d**–Cl–CH_3CN]$^+$ = [$C_{19}H_{15}ClN_3Ru$]$^+$, 421.9998; found, 421.9986; m/z calcd for [**2.102d**–Cl]$^+$ = [$C_{21}H_{18}ClN_4Ru$]$^+$, 463.0263; found, 463.0261; m/z calculated for [**2.102d**–Cl+CH_3CN]$^+$ = [$C_{23}H_{21}ClN_5Ru$]$^+$, 504.0529; found, 504.0525.

2.5.4 General procedure for the aqueous methanol reforming reaction.

In a 5 mL pear-shaped vessel attached to a condenser, KO^{t}Bu (0.390 g, 3.48 mmol) and **2.101b** (0.04−0.8 mol%; 0.0007−0.0136 g; 0.9−18.5 μmol) were added inside the glove box. This was followed by the addition of dry methanol (**2.1**) (0.188 mL, 4.635 mmol) or (0.282 mL, 6.951 mmol) and distilled water (0.042 mL, 2.317 mmol) under an Ar atmosphere. The mixture was heated in a pre-heated oil bath at 100 °C, and the gas evolved was quantified by the water displacement method, and the composition of the gas generated was analyzed by GC. The

reaction was run till no more evolution of gas was observed (typically 48 h) and was then cooled down to room temperature. An aliquot (10 mg approx.) was withdrawn from the reaction mixture, and the yield of the formic acid was determined by ^{1}H NMR using D_2O as the solvent and sodium acetate (known amount added in the NMR tube) as a standard.

2.5.5 General procedure for the on-site generation of deuterium and its incorporation in unsaturated substrates.

In a 5 mL pear-shaped vessel (A) attached to a condenser, KO^{t}Bu (0.390 g, 3.48 mmol), **2.101b** (0.8 mol %; 0.0136 g; 18.5 μmol), and anhydrous methanol-d_4(5a) (0.282 mL, 6.951 mmol) were added inside the glove box. This was followed by the addition of D_2O (0.042 mL, 2.317 mmol) under an Ar atmosphere. On the other hand, Pd/C (10 mol %; 0.0106 g; 0.1 mmol), unsaturated substrate (1 mmol), and 1,4- dioxane (0.5 mL) were added to a 30 mL bomb vessel B under an Ar atmosphere. The deuterium gas generated in the flask A at 100 °C was fed to bomb vessel B at 120 °C for 48 h and then cooled down to room temperature. An aliquot (10 mg approx.) was withdrawn from the reaction mixture of A, and the NMR yield of the formic acid-d_2 was determined by ^{2}H NMR using H_2O as the solvent and D_2O (known amount added in the NMR tube) as a standard. The ^{1}H NMR analysis was also done to check the formation of formic acid (if any). An aliquot (10 mg approx.) was withdrawn from the reaction mixture of B, and the NMR yield of the deuterated product was determined by ^{1}H NMR using $CDCl_3$ as the solvent and toluene (known amount added in the flask) as the standard. The ^{2}H NMR analysis was also done to check the deuterium incorporation in the product.

2.5.6. General procedure of the kinetic studies performed for the 2.101b catalyzed transformation of methanol to formic acid.

2.5.6.1 Variation of catalyst concentration. In a J-Young Teflon valve NMR tube, KO^{t}Bu (0.200 g, 1.79 mmol) and **2.101b** (0.2−1 mol %; 0.0050−0.0261 g; 7.14−35.7 μmol) were added inside the glove box. This was followed by the addition of dry methanol (**2.1**) (0.433 mL, 10.71 mmol) and D_2O (0.065 mL, 3.57 mmol) under an Ar atmosphere. The tube was heated in a preheated oil bath at 100 °C. ^{1}H NMR of the reaction mixture was recorded at different time intervals using sodium acetate as a standard.

2.5.6.2 Variation of MeOH concentration. In a J-Young Teflon valve NMR tube, KO^{t}Bu (0.200 g, 1.79 mmol) and **2.101b** (0.8 mol %; 0.0209 g; 28.56 μmol) were added inside the

glove box. This was followed by the addition of dry methanol (**2.1**) (0.433–0.108 mL, 10.71–2.67 mmol) and D_2O (0.065 mL, 3.57 mmol) under an Ar atmosphere. Dioxane was used as a make-up solvent at lower concentrations of methanol. The tube was heated in a preheated oil bath at 100 °C. ^1H NMR of the reaction mixture was recorded at different time intervals using sodium acetate as a standard.

2.5.7. Computational details

The geometries of all the considered complexes were fully optimized employing the DFT(PBE)[65] method on the Gaussian-09 package.[66] The Def2SVP[67-69] basis set with a polarization function were used for the metal (Ru) and non-metal atoms respectively. The empirical dispersion-GD3 was used in all molecular geometry optimization and energy computations. The transition states were located using the synchronous transit-guided quasi-Newton (QST2). Frequency calculations were also performed to differentiate minima structures or transition states on the potential energy surface. ΔG values were calculated by using the sum of electronic and thermal free energies. These values were computed at 100 °C to meet the experimental conditions. Single-point calculations were also performed at a higher level with Def2TZVP.

Supporting information containing NMR spectra, GC, HRMS analysis, and Cartesian coordinates of the computed complexes for chapter II is available as Appendix I and can be found at:

https://drive.google.com/file/d/1ppAVRIRsJuQ7DK_-J4LtayNnSOUh6GvV/view?usp=sharing

2.6 References

1. Ragauskas, A. J.; Williams, C. K.; Davison, B. H.; Britovsek, G.; Cairney, J.; Eckert, C. A.; Frederick Jr, W. J.; Hallett, J. P.; Leak, D. J.; Liotta, C. L.; Mielenz, J.R.; Murphy, R.; Templer, R.; Tschaplinski,T. The path forward for biofuels and biomaterials. *Science* **2006,** *311*, 484-489.
2. Kumar, A.; Bhatti, T. M.; Goldman, A. S. Dehydrogenation of Alkanes and Aliphatic Groups by Pincer-Ligated Metal Complexes. *Chem. Rev.* **2017,** *117*, 12357-12384.
3. Rahman, A.; Farrok, O.; Haque, M. M. Environmental impact of renewable energy source based electrical power plants: Solar, wind, hydroelectric, biomass, geothermal, tidal, ocean, and osmotic. *Renewable and Sustainable Energy Rev.* **2022,** *161*, 112279.
4. Kumar, A.; Daw, P.; Milstein, D. Homogeneous Catalysis for Sustainable Energy: Hydrogen and Methanol Economies, Fuels from Biomass, and Related Topics. *Chem. Rev.* **2022,** *122*, 385-441.
5. Yadav, V.; Sivakumar, G.; Gupta, V.; Balaraman, E. Recent Advances in Liquid Organic Hydrogen Carriers: An Alcohol-Based Hydrogen Economy. *ACS Catal.* **2021,** *11*, 14712-14726.
6. Das, K.; Kumar, A. Chapter One - Alkane dehydrogenation reactions catalyzed by pincer-metal complexes. In *Advances in Organometallic Chemistry*, Pérez, P. J., Ed. Academic Press 2019; Vol. 72, pp 1-57.

7. Satyapal, S.; Petrovic, J.; Read, C.; Thomas, G.; Ordaz, G. The US Department of Energy's National Hydrogen Storage Project: Progress towards meeting hydrogen-powered vehicle requirements. *Catal. Today* **2007**, *120*, 246-256.
8. El-Shafie, M.; Kambara, S.; Hayakawa, Y. Hydrogen production technologies overview. *J. Power Energy Eng.* **2019,** *07*, 107-154.
9. Singh, S.; Jain, S.; Ps, V.; Tiwari, A. K.; Nouni, M. R.; Pandey, J. K.; Goel, S. Hydrogen: A sustainable fuel for future of the transport sector. *Renew. Sustain. Energy Rev.* **2015,** *51*, 623-633.
10. Abdin, Z.; Zafaranloo, A.; Rafiee, A.; Mérida, W.; Lipiński, W.; Khalilpour, K. R., Hydrogen as an energy vector. *Renew. Sustain. Energy Rev.* **2020,** *120*, 109620.
11. Dincer, I. Green methods for hydrogen production. *Int. J. Hydrogen Energy* **2012,** *37*, 1954-1971.
12. Qureshi, F.; Yusuf, M.; Kamyab, H.; Vo, D.-V. N.; Chelliapan, S.; Joo, S.-W.; Vasseghian, Y. Latest eco-friendly avenues on hydrogen production towards a circular bioeconomy: Currents challenges, innovative insights, and future perspectives. *Renew. Sustain. Energy Rev.* **2022,** *168*, 112916.
13. Kumar, S. S.; Lim, H. An overview of water electrolysis technologies for green hydrogen production. *Renew. Sustain. Energy Rev.* **2022,** *8*, 13793-13813.
14. Temiz, M.; Dincer, I. Development of solar and wind based hydrogen energy systems for sustainable communities. *Energy Convers. Manag.* **2022,** *269*, 116090.
15. Temiz, M.; Dincer, I. Development and assessment of an onshore wind and concentrated solar based power, heat, cooling and hydrogen energy system for remote communities. *J. Clean. Prod.* **2022,** *374*, 134067.
16. Xu, X.; Zhou, Q.; Yu, D. The future of hydrogen energy: Bio-hydrogen production technology. *Int.J. Hydrogen Energy* **2022,** *47*, 33677-33698.
17. El-Emam, R. S.; Özcan, H. Comprehensive review on the techno-economics of sustainable large-scale clean hydrogen production. *J. Clean. Prod.* **2019,** *220*, 593-609.
18. Caparrós Mancera, J. J.; Segura Manzano, F.; Andújar, J. M.; López, E.; Isorna, F., Sun, heat and electricity. A comprehensive study of non-pollutant alternatives to produce green hydrogen. *Int. J. Energy Res.* **2022,** *46*, 17999-18028.
19. Green, M. A. Hydrogen safety issues compared to safety issues with methane and propane. In *AIP conference Proceedings 2006 American Institute of Physics*; American Institute of Physics 2006, pp 319-326.
20. Sadaghiani, M. S.; Mehrpooya, M. Introducing and energy analysis of a novel cryogenic hydrogen liquefaction process configuration. *Int. J. Hydrogen Energy* **2017,** *42*, 6033-6050.
21. S Sreedhar, I.; Kamani, K. M.; Kamani, B. M.; Reddy, B. M.; Venugopal, A. A Bird's Eye view on process and engineering aspects of hydrogen storage. *Renew. Sustain. Energy Rev.* **2018,** *91*, 838-860.
22. Li, H.; Cao, X.; Liu, Y.; Shao, Y.; Nan, Z.; Teng, L.; Peng, W.; Bian, J. Safety of hydrogen storage and transportation: An overview on mechanisms, techniques, and challenges. *Energy Rep.* **2022,** *8*, 6258-6269.
23. Ren, J.; Musyoka, N. M.; Langmi, H. W.; Mathe, M.; Liao, S. Current research trends and perspectives on materials-based hydrogen storage solutions: A critical review. *Int.J. Hydrogen Energy* **2017,** *42*, 289-311.
24. Sinigaglia, T.; Lewiski, F.; Santos Martins, M. E.; Mairesse Siluk, J. C. Production, storage, fuel stations of hydrogen and its utilization in automotive applications-a review. *Int.J. Hydrogen Energy* **2017,** *42*, 24597-24611.
25. Gianotti, E.; Taillades-Jacquin, M. l.; Rozière, J.; Jones, D. J. High-purity hydrogen generation via dehydrogenation of organic carriers: a review on the catalytic process. *ACS Catal.* **2018,** *8*, 4660-4680.
26. Modisha, P. M.; Ouma, C. N.; Garidzirai, R.; Wasserscheid, P.; Bessarabov, D. The prospect of hydrogen storage using liquid organic hydrogen carriers. *Energy Fuels* **2019,** *33*, 2778-2796.
27. Nielsen, M.; Alberico, E.; Baumann, W.; Drexler, H.-J.; Junge, H.; Gladiali, S.; Beller, M. Low-temperature aqueous-phase methanol dehydrogenation to hydrogen and carbon dioxide. *Nature* **2013,** *495*, 85-89.

28. Rodríguez-Lugo, R. E.; Trincado, M.; Vogt, M.; Tewes, F.; Santiso-Quinones, G.; Grützmacher, H. A homogeneous transition metal complex for clean hydrogen production from methanol–water mixtures. *Nat. Chem.* **2013,** *5*, 342-347.
29. Sinha, V.; Govindarajan, N.; de Bruin, B.; Meijer, E. J. How solvent affects c–h activation and hydrogen production pathways in homogeneous ru-catalyzed methanol dehydrogenation reactions. *ACS Catal.* **2018,** *8*, 6908-6913.
30. Monney, A.; Barsch, E.; Sponholz, P.; Junge, H.; Ludwig, R.; Beller, M. Base-free hydrogen generation from methanol using a bi-catalytic system. *Chem. Commun.* **2014,** *50*, 707-709.
31. Hu, P.; Diskin-Posner, Y.; Ben-David, Y.; Milstein, D. Reusable homogeneous catalytic system for hydrogen production from methanol and water. *ACS Catal.* **2014,** *4*, 2649-2652.
32. Awasthi, M. K.; Rai, R. K.; Behrens, S.; Singh, S. K. Low-temperature hydrogen production from methanol over a ruthenium catalyst in water. *Catal. Sci. Technol.* **2021,** *11*, 136-142.
33. Luo, J.; Kar, S.; Rauch, M.; Montag, M.; Ben-David, Y.; Milstein, D. Efficient Base-Free Aqueous Reforming of Methanol Homogeneously Catalyzed by Ruthenium Exhibiting a Remarkable Acceleration by Added Catalytic Thiol. *J. Am. Chem. Soc.* **2021,** *143*, 17284-17291.
34. Wang, Q.; Lan, J.; Liang, R.; Xia, Y.; Qin, L.; Chung, L. W.; Zheng, Z. New Tricks for an Old Dog: Grubbs Catalysts Enable Efficient Hydrogen Production from Aqueous-Phase Methanol Reforming. *ACS Catal.* **2022,** *12*, 2212-2222.
35. Morton, D.; Cole-Hamilton, D. J. Rapid thermal hydrogen production from alcohols catalysed by [Rh (2, 2′-bipyridyl) 2] Cl. *J. Chem. Soc., Chem. Commun.* **1987**, 248-249.
36. Campos, J. s.; Sharninghausen, L. S.; Manas, M. G.; Crabtree, R. H. Methanol dehydrogenation by iridium N-heterocyclic carbene complexes. *Inorg. Chem.* **2015,** *54*, 5079-5084.
37. Fujita, K. i.; Kawahara, R.; Aikawa, T.; Yamaguchi, R. Hydrogen production from a methanol–water solution catalyzed by an anionic iridium complex bearing a functional bipyridonate ligand under weakly basic conditions. *Angew. Chem., Int. Ed.* **2015,** *54*, 9057-9060.
38. Prichatz, C.; Alberico, E.; Baumann, W.; Junge, H.; Beller, M. Iridium–PNP pincer complexes for methanol dehydrogenation at low base concentration. *ChemCatChem* **2017,** *9*, 1891-1896.
39. Zhan, Y.-L.; Shen, Y.-B.; Li, S.-P.; Yue, B.-H.; Zhou, X.-C. Hydrogen generation from methanol reforming under unprecedented mild conditions. *Chin. Chem. Lett.* **2017,** *28*, 1353-1357.
40. Alberico, E.; Sponholz, P.; Cordes, C.; Nielsen, M.; Drexler, H. J.; Baumann, W.; Junge, H.; Beller, M. Selective hydrogen production from methanol with a defined iron pincer catalyst under mild conditions. *Angew. Chem., Int. Ed.* **2013,** *125*, 14412-14416.
41. Bielinski, E. A.; Förster, M.; Zhang, Y.; Bernskoetter, W. H.; Hazari, N.; Holthausen, M. C. Base-free methanol dehydrogenation using a pincer-supported iron compound and Lewis acid co-catalyst. *ACS Catal.* **2015,** *5*, 2404-2415.
42. Andérez-Fernández, M.; Vogt, L. K.; Fischer, S.; Zhou, W.; Jiao, H.; Garbe, M.; Elangovan, S.; Junge, K.; Junge, H.; Ludwig, R.; Beller, M. A stable manganese pincer catalyst for the selective dehydrogenation of methanol. *Angew. Chem., Int. Ed.* **2017,** *129*, 574-577.
43. Das, K.; Dutta, M.; Das, B.; Srivastava, H. K.; Kumar, A. Efficient Pincer-Ruthenium Catalysts for Kharasch Addition of Carbon Tetrachloride to Styrene. *Adv. Synth. Catal.* **2019,** *361*, 2965-2980.
44. Das, K.; Nandi, P. G.; Islam, K.; Srivastava, H. K.; Kumar, A. N–Alkylation of Amines Catalyzed by a Ruthenium–Pincer Complex in the Presence of in situ Generated Sodium Alkoxide. *Eur. J. Org. Chem.* **2019,** *2019*, 6855-6866.
45. Das, K.; Yasmin, E.; Das, B.; Srivastava, H. K.; Kumar, A. Phosphine-free pincer-ruthenium catalyzed biofuel production: high rates, yields and turnovers of solventless alcohol alkylation. *Catal. Sci. Technol.* **2020,** *10*, 8347-8358.
46. Dutta, M.; Das, K.; Prathapa, S. J.; Srivastava, H. K.; Kumar, A. Selective and High Yield Transformation of Glycerol to Lactic Acid Using NNN Pincer Ruthenium Catalysts. *Chem. Commun.* **2020,** *56*, 9886-9889.
47. Das, K.; Yasmin, E.; Kumar, A. Pincer-Ruthenium Catalyzed Oxygen Mediated Dehydrative Etherification of Alcohols and Ortho-Alkylation of Phenols. *Adv. Synth. Catal.* **2022,** *364*, 3895-3909.

48. Das, K.; Kathuria, L.; Jasra, R. V.; Dhole, S.; Kumar, A., Microwave-assisted pincer-ruthenium catalyzed Guerbet reaction for the upgradation of bio-ethanol to bio-butanol. *Catal. Sci. Technol.* **2023,** *13*, 1763-1776.
49. Lei, M.; Pan, Y.; Ma, X. The nature of hydrogen production from aqueous-phase methanol dehydrogenation with ruthenium pincer complexes under mild conditions. *Eur. J. Inorg. Chem.* **2015,** *2015*, 794-803.
50. Simmons, E. M.; Hartwig, J. F. On the Interpretation of Deuterium Kinetic Isotope Effects in C□H Bond Functionalizations by Transition-Metal Complexes. *Angew. Chem., Int. Ed.* **2012,** *51*, 3066-3072.
51. Kopf, S.; Bourriquen, F.; Li, W.; Neumann, H.; Junge, K.; Beller, M. Recent Developments for the Deuterium and Tritium Labeling of Organic Molecules. *Chem. Rev.* **2022,** *122*, 6634-6718.
52. Muthukrishnan, I.; Sridharan, V.; Menéndez, J. C. Progress in the Chemistry of Tetrahydroquinolines. *Chem. Rev.* **2019,** *119*, 5057-5191.
53. Armarego, W. L. F.; Chai, C. Purification of Inorganic and Metal-Organic Chemicals. In *Purification of Laboratory Chemicals*, 7th ed.; Armarego, W. L. F.; Chai, C., Eds. Butterworth-Heinemann: Boston, 2013; pp 555-661.
54. Johansson, A. J.; Zuidema, E.; Bolm, C. On the Mechanism of Ruthenium-Catalyzed Formation of Hydrogen from Alcohols: A DFT Study. *Chem.- Eur. J.* **2010,** *16*, 13487-13499.
55. Paul, B.; Shee, S.; Panja, D.; Chakrabarti, K.; Kundu, S. Direct Synthesis of N,N-Dimethylated and β-Methyl N,N-Dimethylated Amines from Nitriles Using Methanol: Experimental and Computational Studies. *ACS Catal.* **2018,** *8*, 2890-2896.
56. He, X.; Li, Y.; Fu, H.; Zheng, X.; Chen, H.; Li, R.; Yu, X. Synthesis of Unsymmetrical N-Heterocyclic Carbene–Nitrogen–Phosphine Chelated Ruthenium(II) Complexes and Their Reactivity in Acceptorless Dehydrogenative Coupling of Alcohols to Esters. *Organometallics* **2019,** *38*, 1750-1760.
57. Paul, B.; Panja, D.; Kundu, S. Ruthenium-Catalyzed Synthesis of N-Methylated Amides using Methanol. *Org. Lett.* **2019,** *21*, 5843-5847.
58. Arora, V.; Dutta, M.; Das, K.; Das, B.; Srivastava, H. K.; Kumar, A. Solvent-Free N-Alkylation and Dehydrogenative Coupling Catalyzed by a Highly Active Pincer-Nickel Complex. *Organometallics* **2020,** *39*, 2162-2176.
59. Arora, V.; Narjinari, H.; Kumar, A. Pincer-Nickel Catalyzed Selective Guerbet-Type Reactions. *Organometallics* **2021,** *40*, 2870-2880.
60. Nandi, P. G.; Thombare, P.; Prathapa, S. J.; Kumar, A. Pincer-Cobalt-Catalyzed Guerbet-Type β-Alkylation of Alcohols in Air under Microwave Conditions. *Organometallics* **2022,** *41*, 3387-3398.
61. Narjinari, H.; Tanwar, N.; Kathuria, L.; Jasra, R. V.; Kumar, A. Guerbet-type β-alkylation of secondary alcohols catalyzed by chromium chloride and its corresponding NNN pincer complex. *Catal. Sci. Technol.* **2022,** *12*, 4753-4762.
62. Arora, V.; Yasmin, E.; Tanwar, N.; Hathwar, V. R.; Wagh, T.; Dhole, S.; Kumar, A. Pincer–Ruthenium-Catalyzed Reforming of Methanol─Selective High-Yield Production of Formic Acid and Hydrogen. *ACS Catal.* **2023,** *13*, 3605-3617.
63. Bisarya, A.; Jasra, R. V.; Kumar, A. NNN Pincer-Manganese-Catalyzed Guerbet-Type β-Alkylation of Alcohols under Microwave Irradiation. *Organometallics* **2023,** *42*, 1818-1831.
64. Nandi, P. G.; Jasra, R. V.; Kumar, A. Pincer–Ruthenium-Catalyzed β-Methylation of Alcohols. *Organometallics* **2023,** *42*, 3138-3152.
65. Perdew, J. P.; Burke, K.; Ernzerhof, M. Generalized gradient approximation made simple. *Phys. Rev. Lett.* **1996,** *77*, 3865.
66. Frisch, M. J.; Trucks, G. W., Schlegel, H. B.; Scuseria, G. E.; Robb, M. A.; Cheeseman, J. R.; Scalmani, G.; Barone, V.; Mennucci, B.; Petersson, G. A.; Nakatsuji, H.; Caricato, M.; Li, X.; Hratchian, H. P.; Izmaylov, A. F.; Bloino, J.; Zheng, G.; Sonnenberg, J. L.; Hada, M.; Ehara, M.; Toyota, K.; Fukuda, R.; Hasegawa, J.; Ishida, M.; Nakajima, T.; Honda, Y.; Kitao, O.; Nakai, H.; Vreven, T.; Montgomery, J. A., Jr.; Peralta, J. E.; Ogliaro, F.; Bearpark, M.; Heyd, J. J.; Brothers, E.; Kudin, K. N.; Staroverov, V. N.; Keith, T.; Kobayashi, R.; Normand, J.; Raghavachari, K.; Rendell, A.; Burant, J. C.; Iyengar, S. S.; Tomasi, J.; Cossi, M.; Rega, N.; Millam, J. M.; Klene, M.; Knox, J. E.; Cross, J. B.; Bakken, V.; Adamo, C.; Jaramillo, J.; Gomperts, R.; Stratmann, R.

E.; Yazyev, O.; Austin, A. J.; Cammi, R.; Pomelli, C.; Ochterski, J. W.; Martin, R. L.; Morokuma, K.; Zakrzewski, V. G.; Voth, G. A.; Salvador, P.; Dannenberg, J. J.; Dapprich, S.; Daniels, A. D.; Farkas, O.; Foresman, J. B.; Ortiz, J. V.; Cioslowski, J.; Fox, D. J. Gaussian 09, Revision D.01; Gaussian, Inc.: Wallingford, CT, **2013**.

67. Hay, P. J.; Wadt, W. R. Ab initio effective core potentials for molecular calculations. Potentials for the transition metal atoms Sc to Hg. *J. Chem. Phys.* **1985,** *82*, 270-283.
68. Hay, P. J.; Wadt, W. R. Ab initio effective core potentials for molecular calculations. Potentials for K to Au including the outermost core orbitals. *J. Chem. Phys.* **1985,** *82*, 299-310.
69. Wadt, W. R.; Hay, P. J. Ab initio effective core potentials for molecular calculations. Potentials for main group elements Na to Bi. *J. Chem. Phys.* **1985,** *82*, 284-298.

Chapter III

Pincer–Ruthenium Catalyzed Reforming of Ethanol to Acetic Acid and Hydrogen

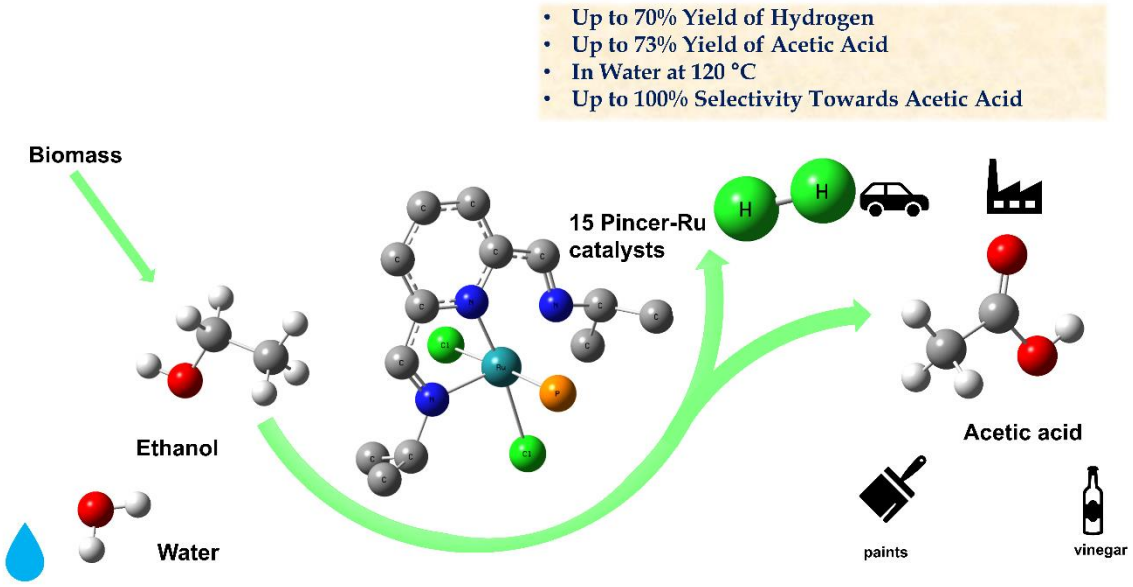

This work has been adapted from "*Reforming of Ethanol to Hydrogen and Acetic Acid Catalyzed by Pincer-Ruthenium Complexes*" by Arora, V.; Dhole, S.; Dhole, S.; Kumar, A. *Catal. Sci. Technol.* **2023**, *13*, 6699-6711.

3.1 Introduction

H_2 is considered as an important fuel due to its several benefits such as abundance and high energy density (120 MJ/kg).[1-3] It is considered as a clean fuel as the only by-product formed during its combustion is water.[1-3] As discussed in chapter II, liquid organic hydrogen carriers (LOHCs) such as methanol and ethanol are most preferred source of generating H_2 when required, due to their high H_2 content (12.6% and 13% respectively) and easy availability.[4-6] Among the different renewable alcohols, bioethanol has gained attention as an emerging hydrogen carrier because of its relatively high hydrogen output (13 wt%).[7-10] Primary investigations on the liberation of hydrogen from ethanol were reported in the 1970s and 1980s,[11, 12] and as compared to methanol, research on ethanol dehydrogenation lags far behind.[13, 14] Bioethanol is produced on a large scale *via* fermentation of biomass, such as biodegradable waste from food and agriculture based industries.[15] It is cheap, readily available in high quality and possesses low toxicity.[16] One benefit of ethanol's water content is that it can be utilized straight for the aqueous reforming reactions, negating the requirement of rigorous purifying methods.[17]

Acetic acid, which can be potentially obtained from the aqueous reforming of ethanol along with the production of hydrogen, is an organic compound which is produced and consumed on a large industrial scale.[18, 19] Its global consumption in 2020 was over 18 million tons globally.[20] It is primarily employed for the production of vinyl acetate, which is then polymerized to polyvinyl acetate, an important ingredient of paints and coatings[21] Along with this, it is also used in the production of various esters,[22] acetic anhydride[23] and polyethylene terephthalate (PET).[21]

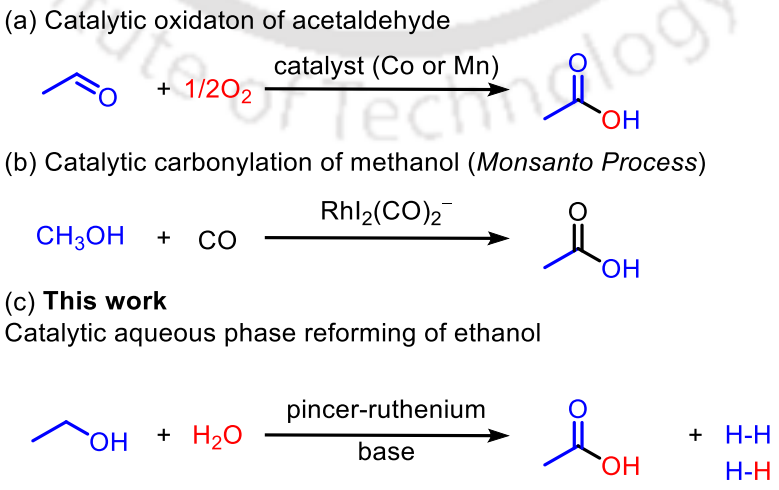

Scheme 3.1. Catalytic methods reported in literature for production of acetic acid.[18]

In the past, the industrial production of acetic acid has been majorly performed utilizing catalytic oxidation of acetaldehyde and oxygen (Scheme 3.1a).[18] Currently, the production of acetic acid is mainly accomplished *via* rhodium-catalyzed Monstano process (Scheme 3.1b).[18, 24, 25] Monsanto process was commercialized in 1966 employing an improved Rh-based homogeneous catalyst for a liquid-phase methanol carbonylation with CH_3I-promoted rhodium catalyst. While the reaction can be carried out using a plethora of Rh(I) or Rh(III) complexes, under reaction conditions they are almost invariably transformed to the active catalyst $[RhI_2(CO)_2]^{-1}$.[21] The main drawback of the process is that it requires harsh reaction conditions (180–220 °C and 30–40 atm) and difficult separation of corrosive liquid-phase products such as methyl iodide, hydrogen iodide from the homogeneous catalyst.[13] Moreover, the starting material used *i.e* rhodium is highly expensive.

Therefore, under these circumstances, developing a novel method for the production of acetic acid starting from ethanol as a raw material would be highly beneficial. This is due to the fact that, ethanol can be easily produced from renewable plant resources.[15] The synthesis of acetic acid along with hydrogen *via* reforming of aqueous ethanol would have a large impact on industrial organic chemistry (Scheme 3.1c). The transformation of ethanol to acetic acid has been extensively reported with heterogeneous based systems.[26, 27] In 2013, Brei reported the aqueous reforming of ethanol over $Cu/ZnO\text{-}ZrO_2\text{-}Al_2O_3$ catalyst at 250–320 °C, where up to 73% yield of acetic acid was obtained with 80% selectivity.[28] They observed the formation of various by-products such as ethyl acetate, acetaldehyde, methyl ethyl ketone, and butanol. Recently, a series of CuCr catalysts have been reported by Ye and co-workers for the transformation of ethanol to acetic acid.[29] They observed complete conversion of ethanol but only 48.6% yield of acetic acid was obtained at 350 °C after 6 h. The major limitation of heterogenous based catalysts is their low selectivity towards acetic acid along with the requirement of very high temperature (up to 350 °C).

In the context of homogeneous based systems, ruthenium-based complexes have been mainly employed for the aqueous ethanol reforming reaction to afford acetic acid and hydrogen (Figure 3.10).[25, 30-32]. The first report on ethanol reforming reaction mediated by a homogeneous molecular catalyst was published in 2014 (Figure 3.10). Here, Beller described several Ru and Ir-based complexes for the homogeneous catalytic conversion of bioethanol to yield acetic acid and hydrogen.[31] Initially, the catalytic activity of all the complexes was screened in a 9 : 1 EtOH/water mixture (v/v) in the presence of 0.0025 mol% of various Ru catalysts along with

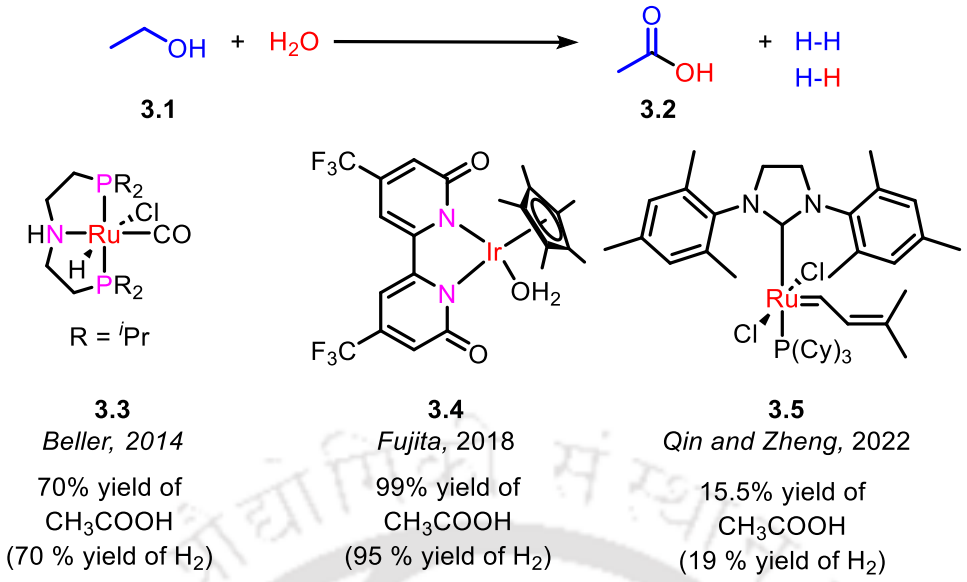

Figure 3.10. Homogeneous catalysts reported for the aqueous ethanol reforming reaction.

NaOH (0.36 equivalents with respect to water) at 90 °C.[31] Apart from the complex based on iridium, all the Ru complexes have shown good to high catalytic activity. Notably, the hydrochloride complex **3.3**, which exhibited a TOF_{3h} of 1170 h^{-1} (335 ml of gas evolution, yield of H_2 = 9%), was chosen as the optimized catalyst, owing to its high stability and its ability to form a free coordination site in the presence of a base.[31] The influence of increasing the water content was also tested in 7.5 : 2.5, 5 : 5, and 1 : 9 EtOH/water mixtures (v/v) and a decrease in the TOF_{3h} was observed in all the cases leading to 936 h^{-1}, 587 h^{-1} and 115 h^{-1} respectively.[31] However, lower water concentration (say for example a 9 : 1 EtOH/water mixture (v/v)) resulted in several side products such as 1-butanol and ethyl acetate. Surprisingly, a 5 : 5 EtOH/water mixture (v/v) resulted in H_2 and acetic acid as the only products. Under the optimized conditions, a 5 : 5 EtOH/water mixture (v/v) led to 70% conversion of ethanol to acetic acid within 20 h at 90 °C. They performed an additional long-reaction time experiment with **3.3** under the optimized conditions that resulted in 80000 TON after 98 h of reaction time.[31] The analysis of the gas evolved revealed the presence of very tiny amounts of CO_2 and CO (below 10 ppm). The developed protocol was also successful for the dehydrogenation of fermented bioethanol.[31]

Very recently, Zheng and co-workers demonstrated aqueous ethanol reforming using an Ru-alkylidene complex **3.5** (0.0008 mol%) in the presence of 0.9 equivalents of KOH in a 1.2 : 1 EtOH: H_2O mixture, where they obtained up to 47295 TON (15.5% conversion of ethanol) and 19% yield of H_2 after performing the reaction for five days at 100 °C (Figure 3.10).[32] The

control experiments were performed using the mixture of CH_3CHO/H_2O and CH_3CH_2OH/H_2O under the optimized conditions without any catalyst and in the presence of KOH, where only trace amounts of H_2 were detected.[32] In case of latter, neither acetaldehyde nor ethyl acetate was observed. These studies show that no side-reactions are occurring during the process and hydrogen obtained is solely due to the reforming of ethanol to acetic acid. The kinetic experiments indicate that the reaction is second order with first order in both ethanol and water, which is well complemented by the isotope labelling studies, where a KIE value of 2.87 has been obtained.[32] Furthermore, following the reaction at different temperatures and using the Arrhenius plot, an activation energy of 13.0 kcal mol^{-1} was obtained.[32] On the basis of NMR studies and control experiments, Zheng and co-workers have proposed a mechanism for the ethanol reforming reaction (Scheme 3.2), where initially, the salt metathesis of the base with **3.5** leads to **3.5a**.[32] Furthermore, CH_3CHO is generated *via* the *β*-hydride elimination to produce a hydrido complex **3.5b**.[32] A second ethanol molecule then coordinates to the ruthenium centre to form **3.5c** and the first molecule of hydrogen gets released. A second *β*-hydride elimination occurs, which affords **3.5d**, to which a molecule of water coordinates and leads to the generation of a second molecule of H_2 and geminal diol complex **3.5e**. Finally, acetic acid is formed upon further *β*-hydride elimination along with the regeneration of **3.5b**.[32]

In the context of non-Ru-based complexes, . Fujita extended the above studies to the dehydrogenation of various primary aliphatic and aromatic alcohols to the corresponding carboxylic acids as well, where they obtained moderate to excellent yields. Furthermore, complex **3.4** was also tested for its recyclability and even after 3 runs, 100% yield of hydrogen was obtained for the ethanol reforming reaction. Moreover, an independent reaction using acetaldehyde, a key intermediate in the reaction, has been performed, where in the presence of 111 equivalents of H_2O, 0.25 mol% **3.4** and 1.2 equivalents of NaOH, 88% of acetic acid along with 84% of H_2 were obtained.[33] The proposed catalytic cycle involves the formation of *in-situ* generated Ir–H species **3.4c** during the dehydrogenation of ethanol to acetaldehyde (Scheme 3.3).[33]

3.2 Objectives

In chapter II, a series of NNN pincer-ruthenium complexes (Figure 3.11) have been demonstrated towards the aqueous reforming of methanol resulting in highly selective formation of formic acid and hydrogen in high yields.[34] In this context, the current chapter aims to investigate the applicability of these complexes towards the reforming of ethanol.

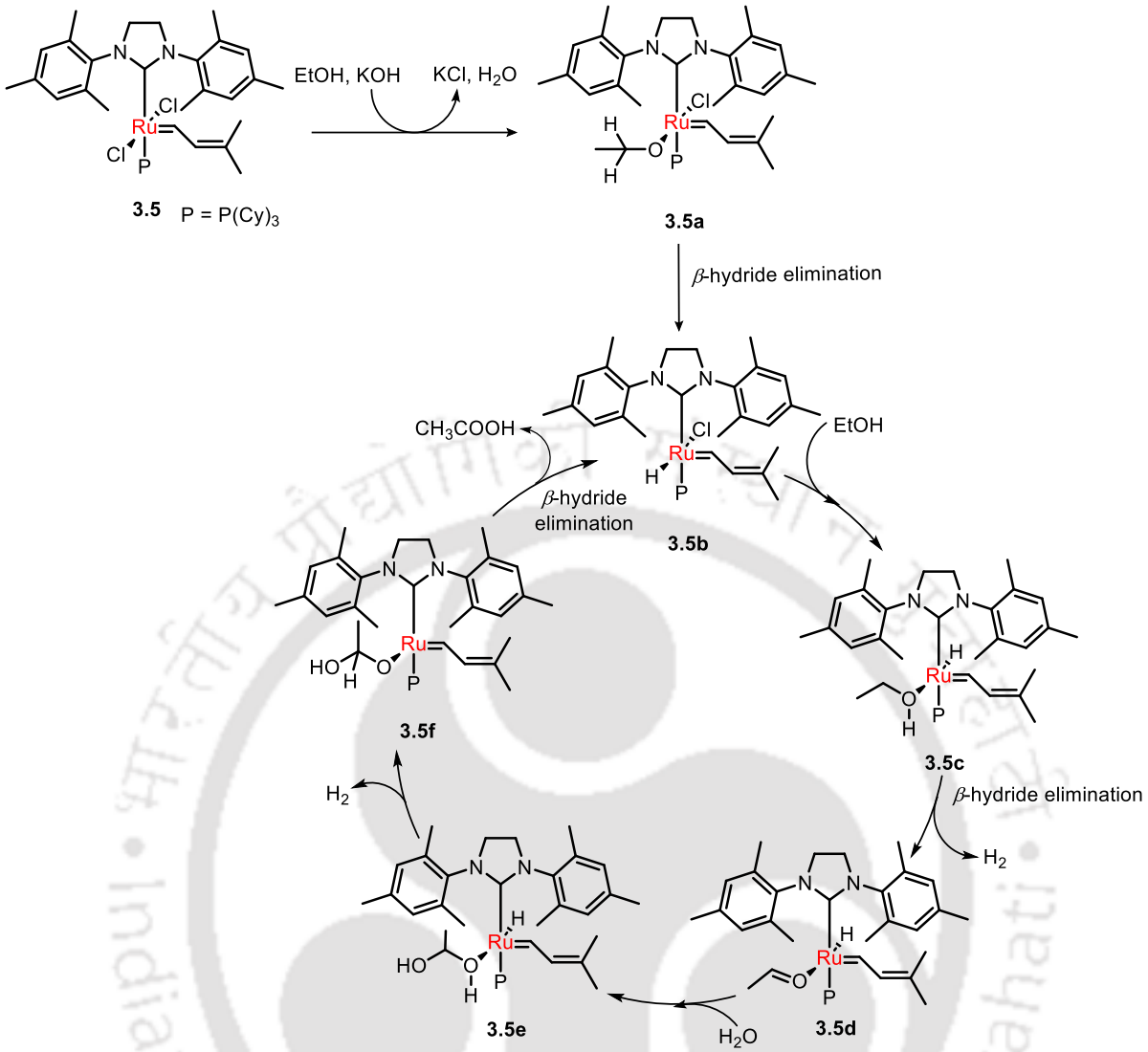

Scheme 3.2. Plausible reaction mechanism reported by Zheng for the **3.5** catalyzed aqueous phase reforming of ethanol.[32]

As discussed above, the heterogeneous systems reported in past, operate under very high temperature affording acetic acid with low yields and selectivity. Whereas, homogeneous systems have several advantages over heterogenous counterparts such as low catalyst loading, mild reaction conditions and high yield and selectivity of acetic acid. Therefore, it would be interesting to employ these environmentally benign and easy to synthesize *bis*(imino)pyridine based pincer-ruthenium complexes with the following questions in mind.

- Will these NNN-ligated pincer-ruthenium complexes show good catalytic activity towards the ethanol reforming to generate H_2 and acetic acid with high selectivity and without generation of any carbon dioxide?
- Is it possible to obtain detailed kinetic and mechanistic (experimental and computation-

-al) understanding of the process?

- Can one extrapolate the current study to reforming of other primary alcohols?

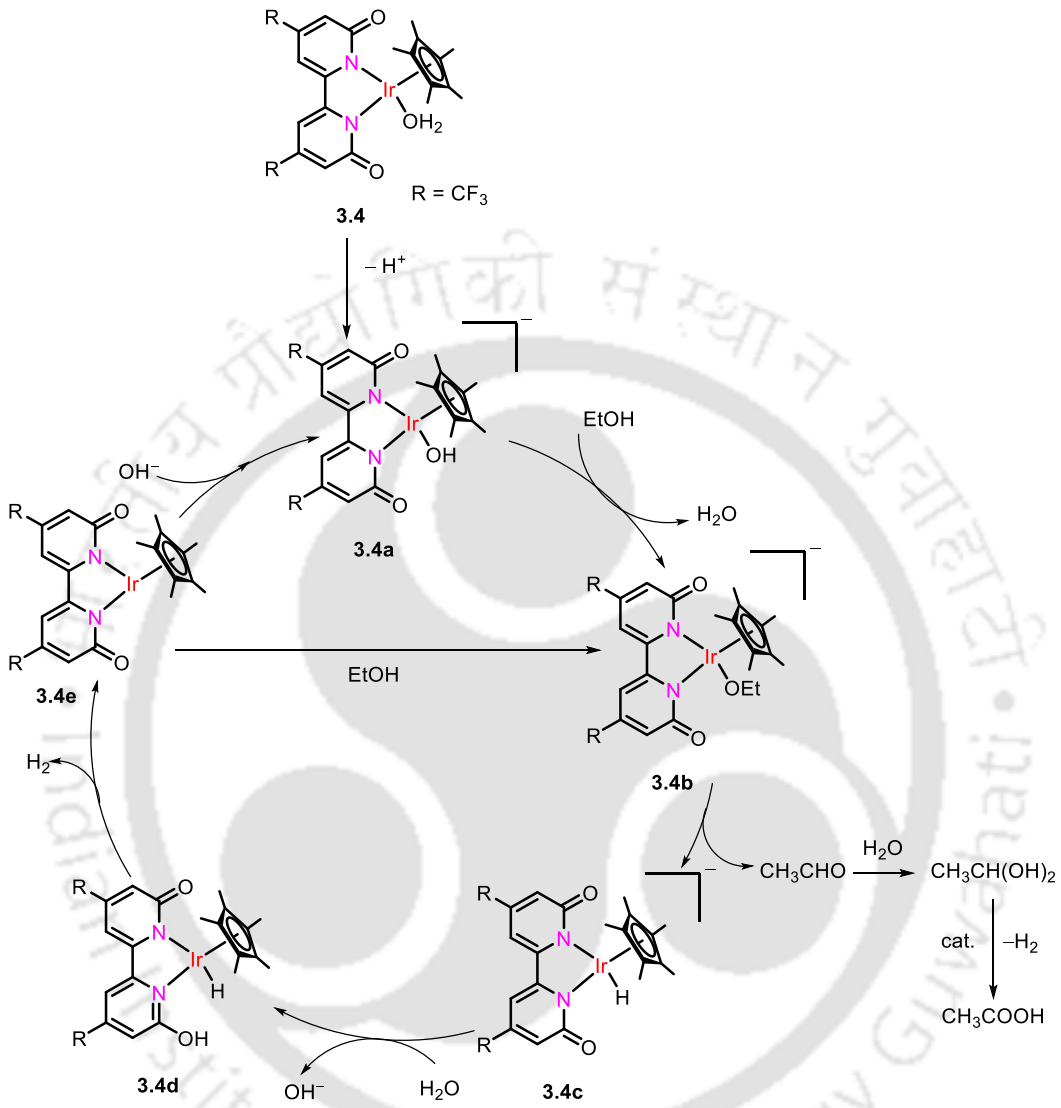

Scheme 3.3. Plausible reaction mechanism reported by Fujita for the catalytic reforming of ethanol using **3.4**.[33]

3.3 Results and Discussion

3.3.1 Aqueous-phase ethanol reforming catalyzed by NNN pincer-ruthenium complexes and their precursors

In chapter II, it has been demonstrated that among the considered NNN pincer-ruthenium complexes (Figure 3.11), the complex **3.7b** (0.2 mol%) could efficiently catalyze the methanol reforming reaction giving very high yields of formic acid (up to 81%, with 100% selectivity)

and hydrogen (up to 90%) in the presence of KO^{t}Bu (1.5 equivalents). Encouraged by these observations, we commenced the optimization of reaction conditions for the reforming of ethanol under the influence of numerous bases using pincer-ruthenium complex **3.7b** as a catalyst (Table 3.1). The studies were initiated by probing the reaction of EtOH and H_2O (in 2 : 1 ratio) in the presence of 0.5 equivalents of KO^{t}Bu and 0.2 mol% of **3.7b** at 120 °C that led to a moderately good yield of acetic acid apart from hydrogen (entry 1, Table 3.1). In comparison to the yields of acetic acid and hydrogen obtained when KO^{t}Bu was employed, while the productivity upon use of 0.5 equivalents of NaO^{t}Bu was about half (compare entry 2 with entry 1, Table 3.1), the corresponding yields were two-thirds when either KOH or Na

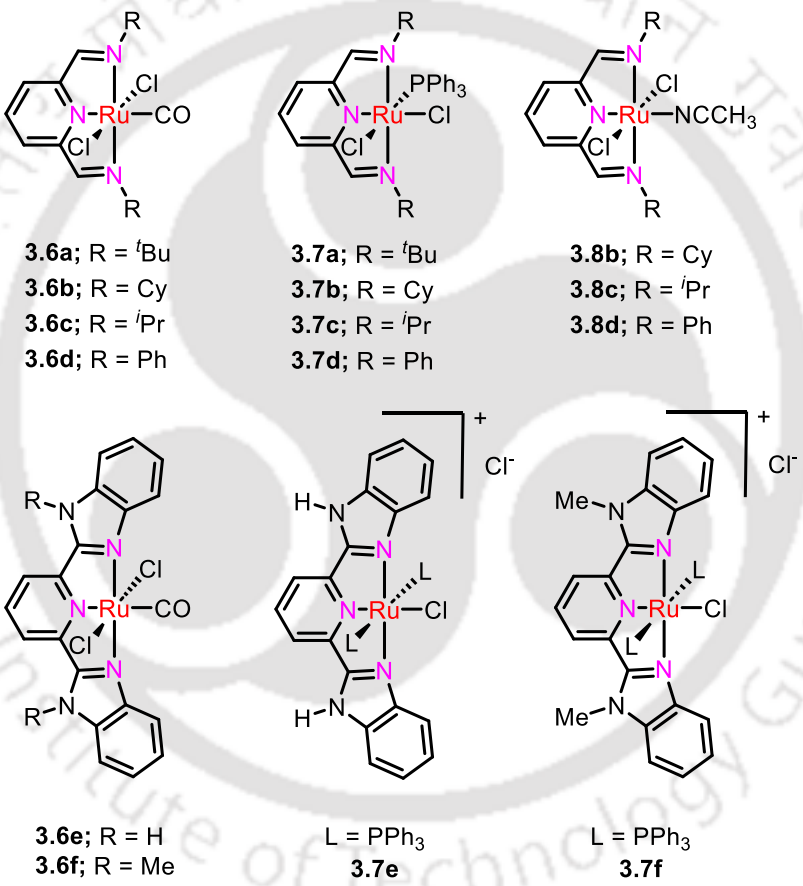

Figure 3.11. Pincer-ruthenium complexes employed in the current study.

(where a base is generated *in-situ*) was used (compare entries 4 and 10 with entry 1, Table 3.1). On the other hand, the use of NaOEt resulted in only one-thirds of the yield in comparison to the yields obtained in reactions carried out with KO^{t}Bu (compare entry 5 with entry 1, Table 3.1). Trace amounts of acetic acid and hydrogen were observed when the **3.7b** (0.2 mol%) catalyzed ethanol reforming was performed with NaOH, Na_2CO_3, K_2CO_3, Cs_2CO_3 and

$NaHCO_3$ (entries 3 and 6–9, Table 3.1). A systematic increase in yields of acetic acid and hydrogen was observed upon a gradual increase in the base loading (entries 11 and 12, Table 3.1). A maximum of 73% yield of acetic acid and 70% yield of H_2 was observed in the **3.7b**

Table 3.1: The **3.7b** catalyzed aqueous-phase reforming of ethanol using various bases

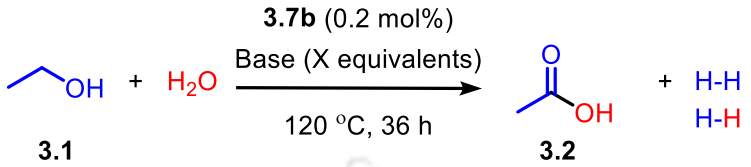

Entry	Base (X equiv.)	mmol of gas	% Yield of H_2[a]	% Yield of **3.2**[b]
1	KO^{t}Bu (0.5)	0.99	21	19
2	NaO^{t}Bu (0.5)	0.54	12	11
3	NaOH (0.5)	0.02	Trace	Trace
4	KOH (0.5)	0.64	14	14
5	NaOEt (0.5)	0.30	6.58	6.59
6	Na_2CO_3 (0.5)	0.01	Trace	Trace
7	K_2CO_3 (0.5)	0.13	1.12	2.7
8	Cs_2CO_3 (0.5)	0.01	Trace	Trace
9	Na (0.5)	0.71	15	15
10	KO^{t}Bu (1.0)	1.72	37	35
11	KO^{t}Bu (1.5)	3.24	70	73
12	KOH (1.0)	0.79	17	17
13	KOH (1.5)	1.19	26	25

Reaction conditions: Ethanol (0.271 mL, 4.64 mmol), H_2O (0.042 mL, 2.32 mmol), base (X equivalents), and **3.7b** (0.0034g, 0.0046 mmol, 0.2 mol%) at 120 °C. Gas evolution was determined by burette measurements after deducting the blank contribution. [a]Yield was calculated as moles of H_2 (as observed from GC and the amount of gas evolved)/moles of H_2O. [b]Yield of acetic acid was calculated from ^{1}H NMR using DMSO as standard.

(0.2 mol%) catalyzed reforming of ethanol + water (2 : 1) in the presence of 1.5 equivalents of KO^{t}Bu at 120 °C (entry 12, Table 3.1). Performing the reaction with 1 and 1.5 equivalents of KOH gave lower yields (entries 13 and 14, Table 3.1) for the reforming of ethanol. Under the best optimized conditions (entry 11, Table 3.1), further optimization of the ethanol reforming reaction was carried out using several pincer-ruthenium complexes and their precursors (Table 3.2). In addition, the commercially available Ru precursors like $RuCl_3 \cdot 3H_2O$, $RuCl_2(PPh_3)_3$, [Ru(*p*-cymene)Cl_2]$_2$ and [Ru(benzene)Cl_2]$_2$ also gave lower yields of acetic acid and hydrogen

Table 3.2: Aqueous-phase reforming of ethanol using various pincer-ruthenium catalysts

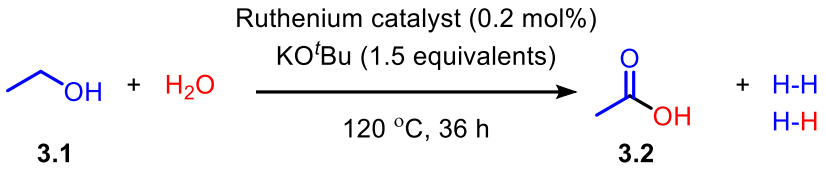

Entry	**[Ru]** (0.2 mol%)	mmols of gas	Yield of H_2[a] (%)	Yield of **3.2**[b] (%)
1	**3.6a**	0.80	17	18
2	**3.6b**	1.67	36	35
3	**3.6c**	2.00	43	43
4	**3.6d**	1.37	30	28
5	**3.6e**	3.22	69	70
6	**3.6f**	1.31	28	25
7	**3.7a**	2.77	60	59
8	**3.7b**	3.24	70	73
9	**3.7c**	2.67	58	58
10	**3.7d**	2.17	47	49
11	**3.7e**	2.20	48	47
12	**3.7f**	2.88	62	61
13	**3.8b**	1.01	22	23
14	**3.8c**	0.32	7	9
15	**3.8d**	1.40	30	32
16	$RuCl_2(PPh_3)_3$	0.46	10	10
17	$RuCl_3.3H_2O$	2.35	51	46
18	[Ru(*p*-cymene)Cl_2]$_2$	1.68	36	48
19	[Ru(benzene)Cl_2]$_2$	0.94	21	14
20	**3.6b**[c]	3.11	67	66
21	**3.8b**[c]	3.35	72	71
22	**3.6e**[d]	1.88	41	44
23	Only ligand	-	-	-

Reaction conditions: Ethanol (0.271 mL, 4.64 mmol), H_2O (0.042 mL, 2.32 mmol), KO^{t}Bu (0.390 g, 3.48 mmol, 1.5 equivalents), and ruthenium catalyst (0.0046 mmol, 0.2 mol%) at 120 °C. Gas evolution was determined by burette measurements after deducting the blank contribution. [a]Yield was calculated as moles of H_2 (as observed from GC and the amount of gas evolved)/moles of H_2O. [b]Yield of acetic acid was calculated from ^{1}H NMR using DMSO as standard. [c]1 equivalent of PPh_3 relative to **3.6b**/**3.8b** was added. [d]2 equivalent of PPh_3 relative to **3.6e** was added.

(entries 16–19, Table 3.2). The reaction with only ligand was also performed (entry 23, Table 3.2), where no product was observed.

Among the carbonyl complexes (**3.6a–f**) (entries 1–6, Table 3.2), the use of (^{Bim2}NNN)RuCl$_2$(CO) (**3.6e**) resulted in the maximum yield of acetic acid (69%) and hydrogen (70%) under the optimized conditions (entry 5, Table 3.2). A comparison of the ethanol reforming activity of pincer-ruthenium phosphine complexes **3.7a–f** (entries 7–12, Table 3.2), revealed that the best results (ca. 73% acetic acid and 70% H_2, entry 8, Table 3.2) were obtained with **3.7b** (0.2 mol%) as a catalyst in the presence of 1.5 equivalents of KO^{t}Bu at 120 °C after

Table 3.3: The **3.7b** catalyzed aqueous-phase reforming of ethanol under various conditions

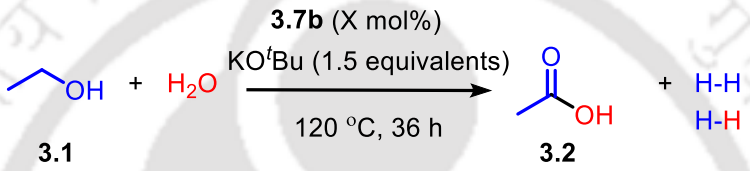

Entry	**3.7b** (X mol%)	mmols of gas	Yield of H_2[a] (%)	Yield of **3.2**[b] (%)
1	0.2	3.24	70	73
2[c]	0.2	3.14	68	73
3[c,d]	0.2	0.73	16	16
4[c,e]	0.2	3.42	74	77
5[c,f]	0.2	3.04	66	61
6[c,g]	0.2	3.24	70	69
7	0.1	2.77	60	59
8	0.4	3.11	67	71
9	0.6	3.22	70	66
10	0.8	3.10	67	67
11[c,h]	Only EtOH	1.07	23	26
12[c,i]	Only water	-	-	-

Reaction conditions: Ethanol (0.271 mL, 4.64 mmol), H_2O (0.042 mL, 2.32 mmol), KO^{t}Bu (0.390 g, 3.48 mmol, 1.5 equivalents), and **3.7b** (X mol%) at 120 °C. Gas evolution was determined by burette measurements after deducting the blank contribution. [a]Yield was calculated as moles of H_2 (as observed from GC and the amount of gas evolved)/moles of H_2O. [b]Yield of acetic acid was calculated from ^{1}H NMR using DMSO as standard. [c]Reaction was performed in air. [d]Reaction was set up at 100 °C. [e]Reaction was set up at 140 °C. [f]6.95 mmol of ethanol, 2.32 mmol of water, 3.48 mmol of KO^{t}Bu and 0.005 mmol of **3.7b** were used. [g]9.27 mmol of ethanol, 2.32 mmol of water, 3.48 mmol of KO^{t}Bu and 0.005 mmol of **3.7b** were used. [h]4.64 mmol of ethanol, 3.48 mmol of KO^{t}Bu and 0.005 mmol of **3.7b** were used. [i]2.32 mmol of water, 3.48 mmol of KO^{t}Bu and 0.005 mmol of **3.7b** were used.

36 h. The corresponding acetonitrile pincer-ruthenium complexes (**3.8b–d**) exhibited poor catalytic activity (entries 13–15, Table 3.2) as compared to **3.7b** (entry 8, Table 3.2) and **3.6e.** When the best optimized conditions were repeated under air, the yields of hydrogen and acetic acid were comparable with no change in selectivity (entry 1 *vs*. 2, Table **3.3**). While repeating the reaction under air at 100 °C resulted in lower reactivity of **3.7b** (0.2 mol%) (entry 1 *vs.* 3, Table **3.3**), the corresponding reactivity of **3.7b** (0.2 mol%) at 140 °C was comparable to its reactivity at 120 °C (entry 1 *vs.* 4, Table 3.3). Further the yields of hydrogen and acetic acid were unchanged when the ratio of ethanol to water was varied to 4:1 (entry 1 *vs.* 6, Table 3.3) in the **3.7b** (0.2 mol%) catalyzed reactions at 120 °C. Upon lowering the loading of **3.7b** to 0.1 mol% there was a slight decrease in the yield of hydrogen (60%) and acetic acid (59%, entry 1 *vs.* 7, Table 3.3). However, at higher loadings of **3.7b**, the aqueous ethanol (2:1) reforming activity was comparable (entry 1 *vs.* 8, 9 and 10, Table 3.3) at 120 °C in the presence of 1.5

Table 3.4: The **3.7b** catalyzed aqueous-phase reforming of various alcohols

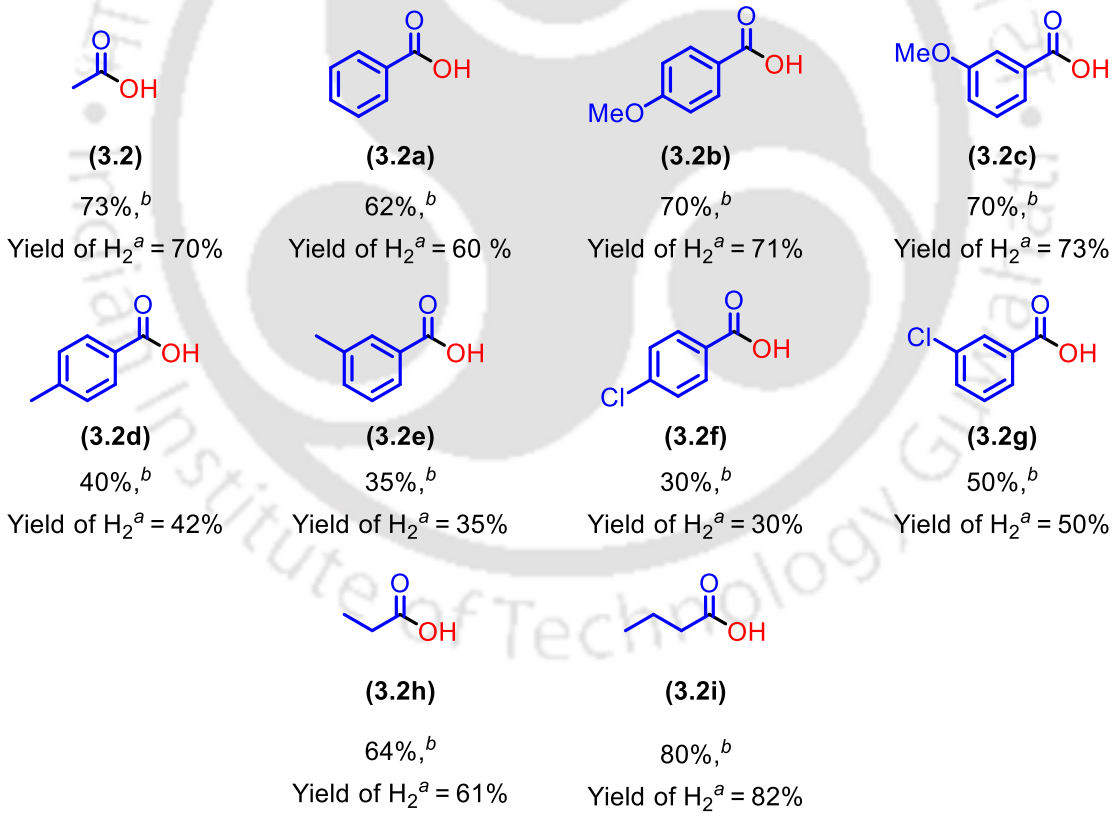

Reaction conditions: Alcohol (4.64 mmol), H_2O (0.042 mL, 2.32 mmol), KO^{t}Bu (0.390 g, 3.48 mmol, 1.5 equivalents), and **3.7b** (0.0034g, 0.0046 mmol, 0.2 mol%) at 120 °C. Gas evolution was determined by burette measurements after deducting the blank contribution. [a]Yield was calculated as moles of H_2 (as observed from GC and the amount of gas evolved)/moles of H_2O. [b]Yield of the product was calculated from ^{1}H NMR using DMSO as standard. For aromatic acids, the yield was similarly determined but after work-up of the reaction mixture with 6M HCl.

equivalents of KO^{t}Bu. This is in contrast to the observed increase in yield of H_2 and **3.2** with increase in loading of **3.7b** at a lower loading of KO^{t}Bu (0.5 equivalents) (Figure 3.13a). In the absence of water but in the presence of 1.5 equivalents of KO^{t}Bu, **3.7b** (0.2 mol%) catalyzed the transformation of ethanol giving hydrogen and acetic acid in 23% and 26% yields respectively (entry 11, Table 3.3). On the other hand, there was no reactivity when the reaction was repeated just with water (entry 12, Table 3.3). The optimized protocol (entry 8, Table 3.2) was employed to bring about the aqueous reforming of a range of aromatic and aliphatic secondary alcohols in moderate to good yields (Table 3.4).

3.3.2 Control experiments

In Chapter II, it has been demonstrated that the NNN pincer-ruthenium complex **3.7b** (0.2 mol%) could efficiently catalyze the aqueous reforming of methanol and the reactivity was hardly affected by the presence of excess mercury that is indicative of the homogeneity of the reaction mixture. Attempts to determine the order of the **3.7b** catalyzed ethanol reforming reaction using the initial rate method revealed a linear dependence of the rate of formation of **3.2** on the concentration of both **3.7b** (Figure 3.12a) and ethanol (Figure 3.12b), indicating the reaction to be first order with respect to both **3.7b** and ethanol. These observations also imply that the reaction is primarily homogeneous.

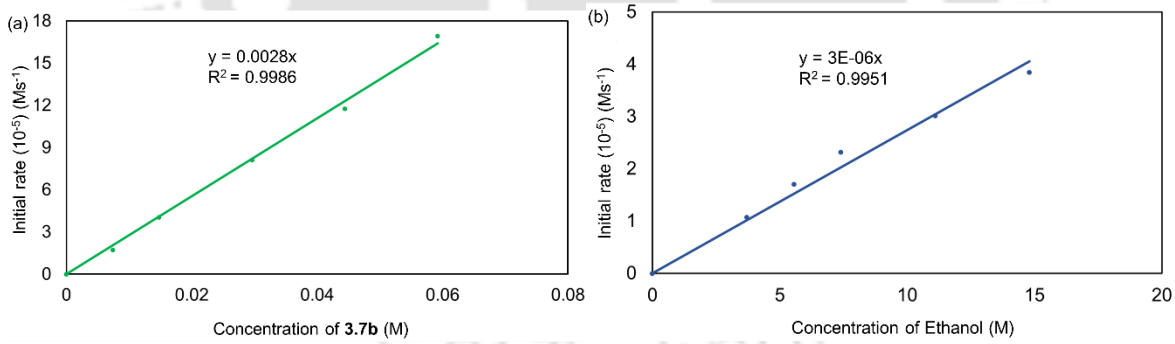

Figure 3.12. (a) Variation of the initial rate of formation of acetic acid with the concentration of **3.7b** (reaction conditions: ethanol (0.416 mL, 7.14 mmol), D_2O (0.065 mL, 3.57 mmol), KO^{t}Bu (0.2 g, 1.78 mmol) and **3.7b** (0.1–0.8 mol%; 0.0026–0.0208 g; 3.56–28.56 μmol) at 120 °C in a NMR tube) (Also see Figure 3.13a). (b) Variation of the initial rate of formation of acetic acid with the concentration of ethanol (reaction conditions: ethanol (0.104–0.416 mL, 1.78–7.14 mmol), D_2O (0.065 mL, 3.57 mmol), KO^{t}Bu (0.2 g, 1.78 mmol) and **3.7b** (0.0052 g, 7.12 μmol, 0.2 mol%) at 120 °C in a NMR tube). Dioxane is used as a make-up solvent at lower concentrations of ethanol (Also see Figure 3.13b). The reactions were performed using 0.5 equivalents of KO^{t}Bu rather than 1.5 equivalents for the sake of ease of operation in NMR tube.

Under the optimized conditions (entry 8, Table 3.2), the use of D_2O instead of H_2O did not have a significant effect either on the rate of reaction (Figure S2.26, Appendix II), or on the productivity (equation 1 *vs.* 2, Scheme 3.4). On the other hand, the use of CD_3CD_2OD in comb-

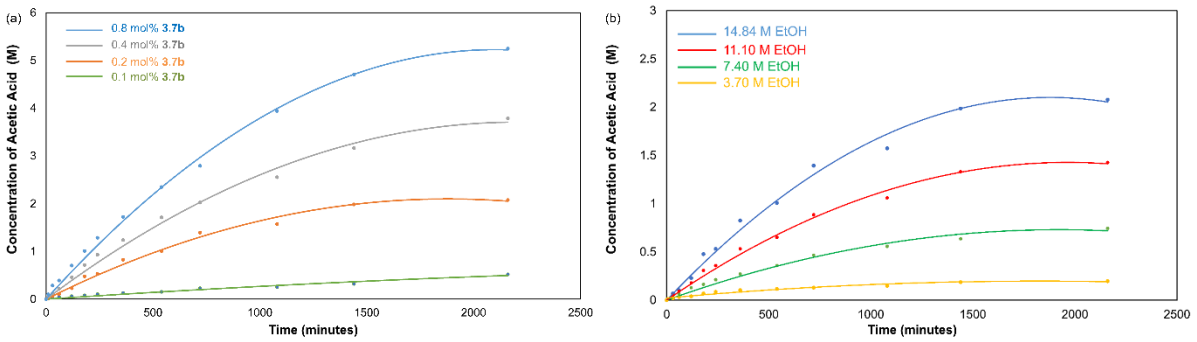

Figure 3.13. (a) Reaction profile of acetic acid formation at different concentrations of **3.7b** (reaction conditions: ethanol (0.416 mL, 7.14 mmol), D_2O (0.065 mL, 3.57 mmol), KO^{t}Bu (0.2 g, 1.78 mmol) and **3.7b** (0.1–0.8 mol%; 0.0026–0.0208 g; 3.56–28.56 μmol) at 120 °C in a NMR tube) (b) Reaction profile of acetic acid formation at different concentrations of ethanol (reaction conditions: ethanol (0.104–0.416 mL, 1.78–7.14 mmol), D_2O (0.065 mL, 3.57 mmol), KO^{t}Bu (0.2 g, 1.78 mmol) and **3.7b** (0.0052 g, 7.12 μmol, 0.2 mol%) at 120 °C in a NMR tube). Dioxane is used as a make-up solvent at lower concentrations of ethanol. The reactions were performed using 0.5 equivalents of KO^{t}Bu rather than 1.5 equivalents for the sake of ease of operation in NMR tube.

-ination with either D_2O or H_2O markedly slowed the reaction (equation 1 *vs*. 3 and 4, Scheme 3.4), producing a KIE value of 5.1 (Figure 3.14, equation 1 *vs*. 3, Scheme 3.4) as determined from the ratio of the TOF (36 h) in the **3.7b** catalyzed reaction of CD_3CD_2OD with H_2O. Similar value of KIE was obtained from the ratio of TOF (1 h) in the **3.7b** catalyzed reaction of CD_3CD_2OD with H_2O (*ca*. 5.4). This KIE nicely correlates with the KIE of 5.0 (obtained from the ratio of the corresponding slopes of the initial rate of gas evolution, Figure 3.14) and KIE of 5.6 (obtained from the ratio of yields of **3.2** and **3.2j**, equation 1 *vs*. 3, Scheme 3.4) resulting in an overall KIE of 5.23. The contribution of both C-H bond breaking occurring in the mechanism and O-H bond activation which is part of the r.d.s (Scheme 3.15), gives rise to this overall KIE of 5.23. Similarly, the reforming of CD_3CD_2OD with D_2O showed an overall KIE of 4.47 (Figure S2.27, Appendix II).

3.3.3 Plausible mechanism involved in the pincer-ruthenium catalyzed aqueous-phase ethanol reforming reaction

Based on Chapter-II and previous reports,[34] a catalytic cycle has been proposed employing **3.7a–d**, which exhibited good activity among the complexes studied (Scheme 3.5). In addition, the catalytic cycle has been probed computationally (Figures 3.16, 3.20 and 3.24) using the

PBE method with LANL2DZ and 6-311G(d,p) basis sets for metal and non-metal atoms respectively. The first step comprises of the formation of 16-electron penta-coordinate species **3.71a–d** *via* dissociation of PPh_3 from **3.7c** with a barrier of 21.96 kcal mol^{-1}.

The ^{31}P NMR studies (Figure 3.17 and Figure 3.18) and HRMS experiments (Figure 3.19) were performed to validate the dissociation of PPh_3. In the ^{31}P NMR of the reaction catalyzed by **3.7b**, two peaks at –5.48 ppm (corresponding to free PPh_3) and 29.65 ppm were observed after

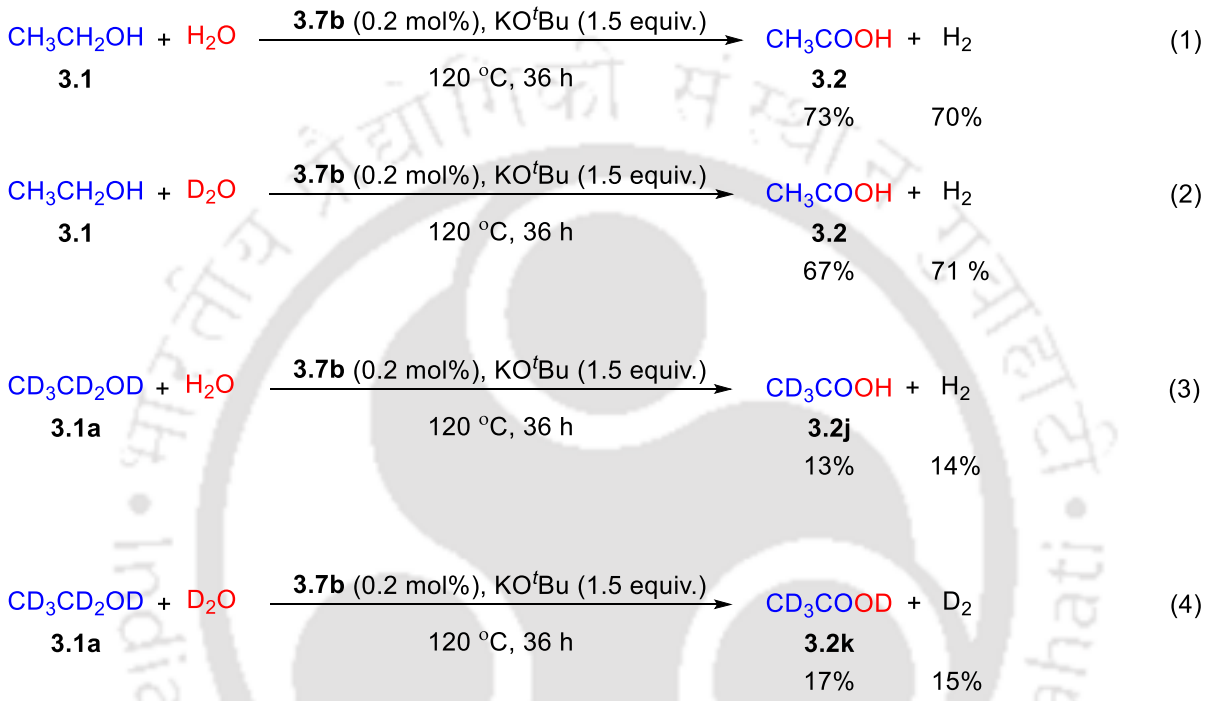

Scheme 3.4. Control experiments.

addition of a base at room temperature (Figure 3.17b). After the reaction mixture was heated at 120 °C for 15 min, 3 peaks were observed at –5.46 ppm (corresponding to free PPh_3), 30.97 ppm (corresponding to PPh_3 bound to Ru in **3.712b**) and 38.68 ppm (corresponding to PPh_3 bound to Ru in **3.713b**) (Figure 3.17c). The hydrides corresponding to both **3.712b** and **3.713b** were observed in the ^{1}H NMR spectrum (Figure 3.17d). A similar observation was made in the ^{31}P NMR studies carried out with the catalytic reaction mixture containing **3.7f** (Figure 3.18). In this case, two peaks at 30.74 ppm (corresponding to free $POPh_3$) and 53.09 ppm (corresponding to PPh_3 bound to Ru in **3.7fa**) were observed after addition of a base at room temperature (Figure 3.18b). After the reaction mixture was heated at 120 °C for 15 min, similar peaks were observed. The hydride corresponding to **3.7fa** was observed in the ^{1}H NMR spectrum (Figure 3.18d).

The dichloride species then gets engaged in salt-metathesis with ethanol (**3.1**) and a base to

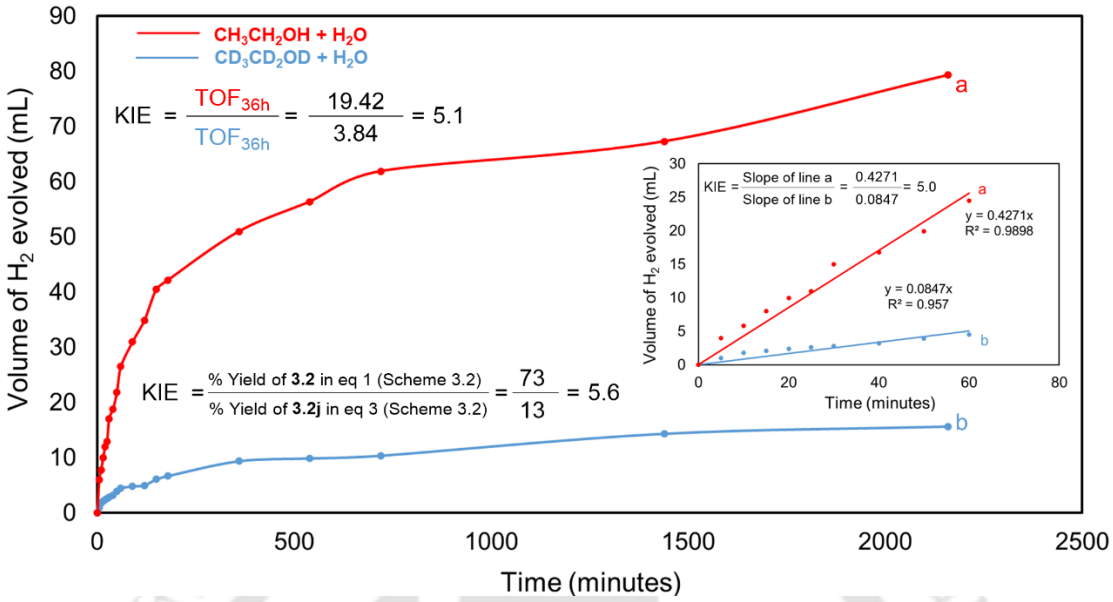

Figure 3.14. A comparative plot of the initial rate of gas evolution for the **3.7b** (0.0034 g, 0.0046 mmol, 0.2 mol%) catalyzed reaction of C_2H_5OH (0.27 mL, 4.64 mmol) with water (0.042 mL, 2.32 mmol) in the presence of KO^{t}Bu (0.390 g, 3.48 mmol) at 120 °C and for the **3.7b** (0.0034 g, 0.0046 mmol, 0.2 mol%) catalyzed reaction of C_2D_5OD (0.27 mL, 4.64 mmol) with water (0.042 mL, 2.32 mmol) in the presence of KO^{t}Bu (0.390 g, 3.48 mmol) at 120 °C. (Also see Figure S2.27, Appendix II).

form Ru-ethoxide species (**3.72a–d**) which are also detected in HRMS as its derivative [**3.72b′**–Cl]$^+$ (Scheme 3.5 and Figure 3.19). The *β*-H elimination in Ru-ethoxide species (**3.72a–d**) results in the generation of acetaldehyde (**3.1′**) and Ru-H species **3.74a–d** via **TS-3.73a–d** (Scheme 3.5). The barrier for this transformation **3.72b** → **3.74b** is computed to be 14.08 kcal mol^{-1} (**TS-3.3b**) at 120 °C (Figure 3.16). The acetaldehyde (**3.1′**) formed above then reacts with water to form ethane-1,2-diol *via* a 6-membered transition state (**TS-3.5a–d**) involving two water molecules (Scheme 3.5). The interaction of **3.1′** with two water molecules rather than one is taken into account owing to the lower barrier in the case of the former with methanol (discussed in Chapter II, Figure 2.14). With ethanol, the barrier for **3.74b** → **3.76b** is computed to be 13.78 kcal mol^{-1} (**TS-3.75b**) (Figure 3.16). This is followed by the alcoholysis of the O–H bond bound to the metal center in **3.76a–d** with the Ru–H bond, liberating the first molecule of H_2 and intermediates **3.78a–d** via **TS–3.77a–d** (Scheme 3.5). This process proceeds via a barrier of 23.19 kcal mol^{-1} (**TS-3.77b**) and **3.76b** → **3.78b** is an uphill process (ΔG_{120} = 9.37 kcal mol^{-1}) (Figure 3.16).

Subsequently, the *β*-H elimination from **3.78a–d** could occur thereby converting ethane-1,2-diol to acetic acid (**3.2**) and giving back the Ru–H species **3.74a–d** while going through **TS–3.79a–d** (Scheme 3.5). This step **3.78b → 3.74b** is a downhill process with an activation barrier of $\Delta G^{\ddagger}_{120}$ = 9.54 kcal mol^{-1} (**TS-3.79b**). This intermediate (**3.74b**) has the lowest energy and is likely to be the resting state of the reaction. Not surprisingly in the **3.7b/3.7f** catalyzed ethanol reforming, the Ru–H species **3.74b** could be detected as their phosphine adducts **3.712b/3.7fa** in the NMR analysis (Figure 3.17 and Figure 3.18) and HRMS analysis ([**3.714b**–Cl]$^+$, [**3.712b**+H_2O+Na]$^+$ and [**3.713b**–Cl]$^+$, Figure 3.19).

Further, the Ru-ethoxide species **3.72a–d** are regenerated by the alcoholysis with an additional ethanol molecule *via* **TS-3.711a–d** (Scheme 3.5). The step **3.74b → 3.72b** is an uphill process (ΔG_{120} = 8.24 kcal mol^{-1}) with a relatively high barrier (**TS–3.711b**; $\Delta G^{\ddagger}_{120}$ = 23.25 kcal mol^{-1}) (Figure 3.5). This completes the cycle for the reforming of ethanol to acetic acid which is an overall downhill process (ΔG_{120} = –7.77 kcal mol^{-1}) liberating two equivalents of hydrogen.

Considering the fact that both **TS–3.77b** and **TS–3.711b** have comparable energies while taking into account the greater normalized value of the former (19.03 kcal mol^{-1}) with respect to the latter (7.24 kcal mol^{-1}), the rate determining step (RDS) of the above cycle appears to be the alcoholysis of the O–H bond in **3.76b** which proceeds *via* **TS–3.77b** and has a barrier of 23.19 kcal mol^{-1}. Zheng reported a KIE of 3.41 for the reforming of CD_3OD with D_2O where the metathesis step leading to evolution of hydrogen was the RDS rather than the C–H activation.[35] On a similar note, one could explain the KIE of 4.47 for reforming of CD_3CD_2OD with D_2O in the current studies which points to the possibility that C–H bond activation is not occurring in the RDS though it is likely to occur in one of the segments (here during *β*–H elimination from **3.72b** and **3.78b**) of the catalytic cycle. The mechanism of the reaction catalyzed by **3.7c** is very similar with a rate-determining barrier of 25.67 kcal mol^{-1} that corresponds to the alcoholysis of the O–H bond in **3.74c** with ethanol which proceeds via **TS–3.711c** (Figure 3.24).

A very similar reaction catalyzed by **3.7b** is initiated by the dissociation of PPh_3 (as evident from ^{1}H NMR (Figure 3.17) and HRMS (Figure 3.19)), and the corresponding reactions catalyzed by **3.6b** proceed *via* the dissociation of the carbonyl group to give rise to a pentacoordinate 16-electron pincer Ru-dichloride as inferred from the IR studies (Figure 3.20 for **3.6b** and Figure 3.21 for **3.6c**). Hence, apart from the initial generation of penta-coordinate

dichloride species **3.71b**, the mechanisms of the **3.6b** catalyzed reactions are very similar to that catalyzed by **3.7b**. As CO is a gas, the lack of reactivity of the former may be related to the absence of neutral groups (such as PPh_3 in the case of the latter) to stabilize the 16-electron pincer–Ru species and preserve it as 18-electron pincer–Ru species (say **3.74b** as **3.713b** Scheme 3.5, Figure 3.17 and 3.19) that facilitates its re-entry whenever it goes out of the cycle. Not surprisingly, addition of PPh_3 (1 equivalent relative to the catalyst) to the reactions catalyzed by **3.6b** and **3.8b** resulted in yields comparable to that obtained with **3.7b** as a catalyst (compare entry 8, Table 3.2 with entries 20 and 21, Table 3.2). Thus, the activity of both **3.6b** and **3.8b** could be enhanced by the addition of one equivalent of PPh_3 (relative to the catalyst) to match the reactivity of **3.7b**.

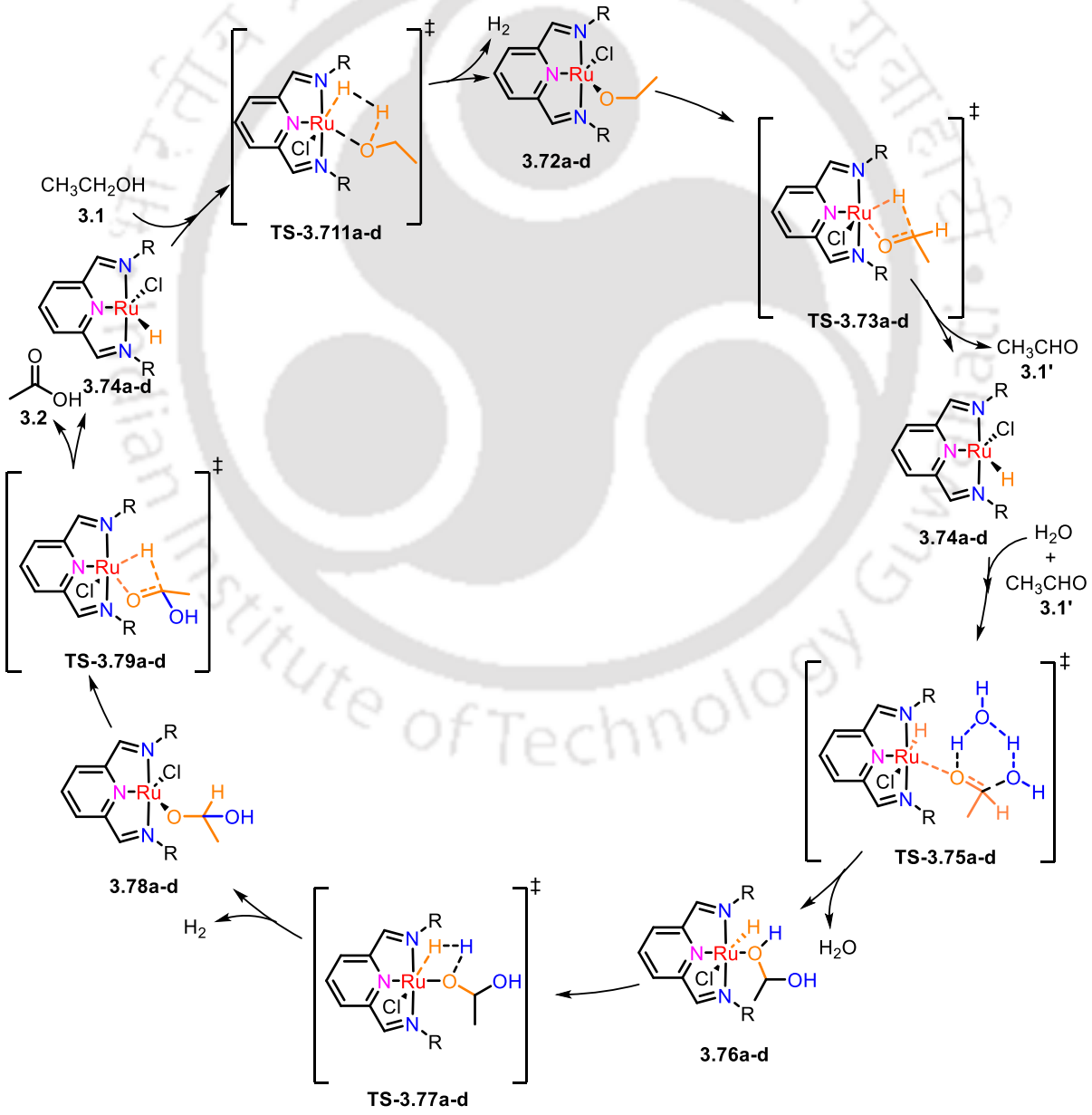

Scheme 3.15. Plausible mechanism involved in the **3.7a-d** catalyzed ethanol reforming.

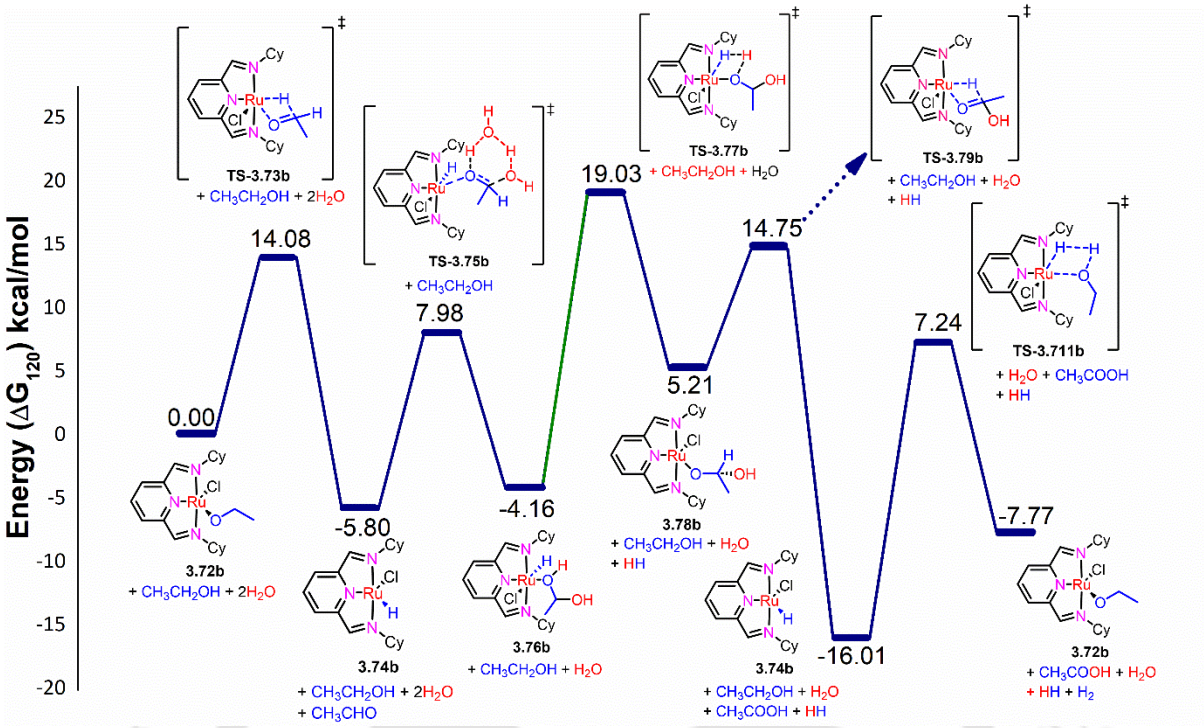

Figure 3.16. Free energy (ΔG_{120}) profile of the **3.7b** catalyzed reforming of ethanol at 120 °C.

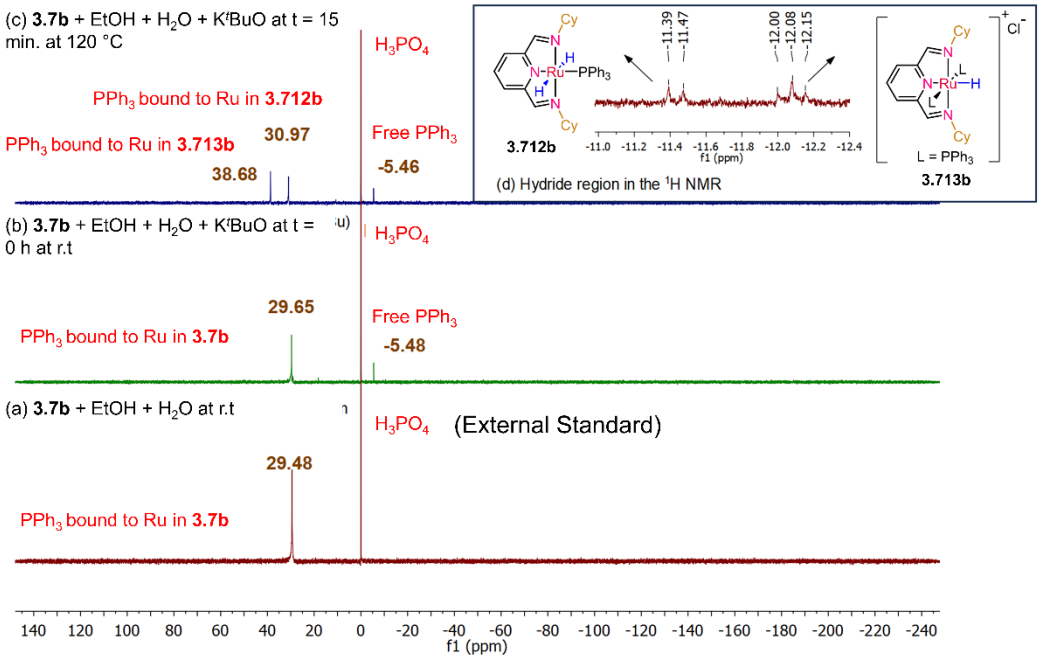

Figure 3.17. NMR studies of the reaction mixture containing ethanol (0.271 mL, 4.64 mmol), H_2O (0.042 mL, 2.32 mmol), and **3.7b** (0.0136 g, 0.019 mmol, 0.8 mol%) depicting (a) ^{31}P NMR at room temperature (t = 0 h), (b) ^{31}P NMR at room temperature (t = 0 h) in the presence of KO^{t}Bu (0.390 g, 3.48 mmol, 1.5 equivalents), (c) ^{31}P NMR at 120 °C for 15 minutes in the

presence of KO^{t}Bu (0.390 g, 3.48 mmol, 1.5 equivalents) and (d) ^{1}H NMR at 120 °C for 15 minutes in the presence of KO^{t}Bu (0.390 g, 3.48 mmol, 1.5 equivalents).

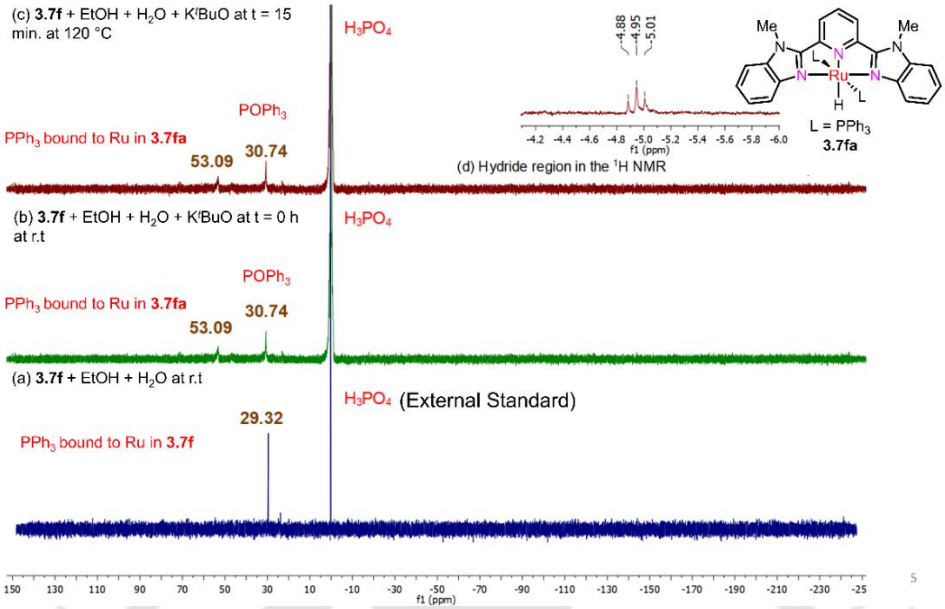

Figure 3.18. NMR studies of the reaction mixture containing ethanol (0.271 mL, 4.64 mmol), H_2O (0.042 mL, 2.32 mmol), and **3.7f** (0.0192 g, 0.019 mmol, 0.8 mol%) depicting (a) ^{31}P NMR at room temperature (t = 0 h), (b) ^{31}P NMR at room temperature (t = 0 h) in the presence of KO^{t}Bu (0.390 g, 3.48 mmol, 1.5 equivalents), (c) ^{31}P NMR at 120 °C for 15 minutes in the presence of KO^{t}Bu (0.390 g, 3.48 mmol, 1.5 equivalents) and (d) ^{1}H NMR at 120 °C for 15 minutes in the presence of KO^{t}Bu (0.390 g, 3.48 mmol, 1.5 equivalents).

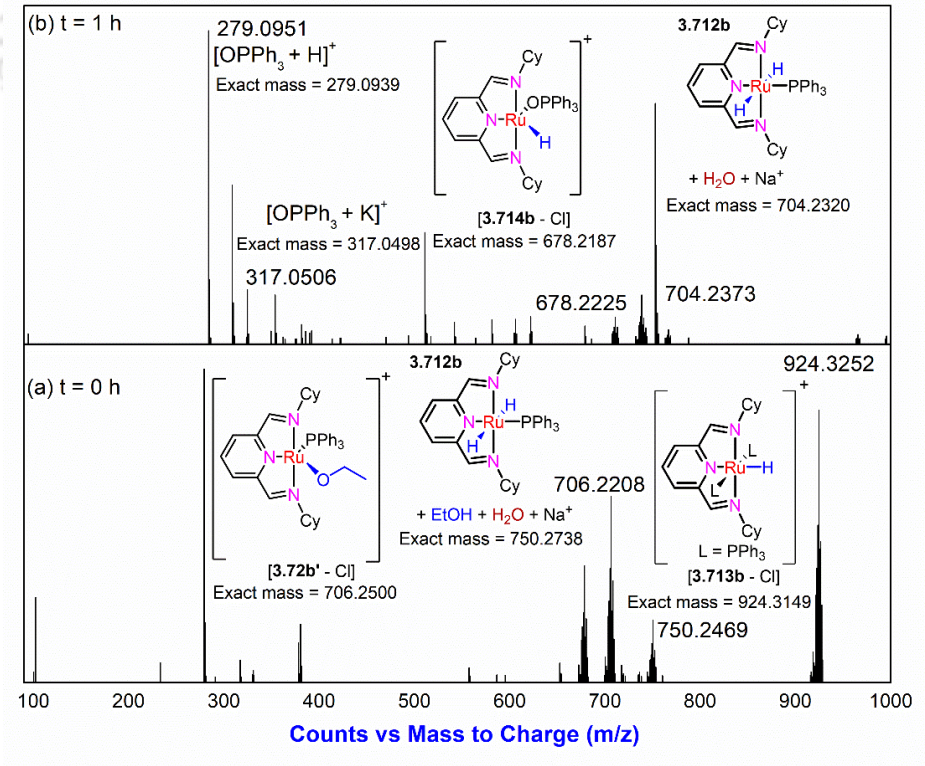

Figure 3.19. HRMS of the reaction mixture containing ethanol (0.271 mL, 4.64 mmol), H_2O (0.042 mL, 2.32 mmol), KO^{t}Bu (0.390 g, 3.48 mmol, 1.5 equivalents), and **3.7b** (0.0136 g, 0.019 mmol, 0.8 mol%) maintained at (a) room temperature (t = 0 h) and (b) at 120 °C for 1 h.

Similar to **3.6c**, the carbonyl of **3.6e** was found to undergo dissociation under the reaction conditions as indicated by IR studies (Figure 3.22). Analysis of the free energy profile of the **3.6e** catalyzed reaction indicated the alcoholysis of the O–H bond in **3.76e** with ethane-1,2-diol through **TS–3.77e** (Figure 3.23) with a barrier of 24.18 kcal mol^{-1} to be the RDS. In contrast to the penta-coordinate 16-electron pincer Ru resting states derived from *bis*(imino)pyridine ligands (**3.74b**, –16.01 kcal mol^{-1}, Figure 3.16 and **3.74c**, –15.06 kcal mol−1, Figure 3.24), the corresponding penta-coordinate 16-electron pincer Ru resting state originating from 2,6-*bis*(benzimidazole-2-yl) pyridine ligands appears to be more stable (**3.74e**, –17.9 kcal mol^{-1}, Figure 3.23). This means that even in the absence of a neutral ligand, **3.74e** may be relatively stable in comparison to **3.74b/3.74c**. In fact, the presence of neutral ligands may further stabilize it and prevent its re-entry into the catalytic cycle. Hence despite the fact that, after the generation of the intermediate **3.72e** *via* loss of PPh_3, the cationic complex **3.7e** would follow a similar catalytic cycle to that traversed by **3.6e**, the productivity of **3.7e** (48% H_2, entry 11, Table 3.2) is not on-par in comparison to **3.6e** (69% H_2, entry 5, Table 3.2). The inferior productivity of **3.7e** in comparison to **3.6e** despite having a similar catalytic cycle

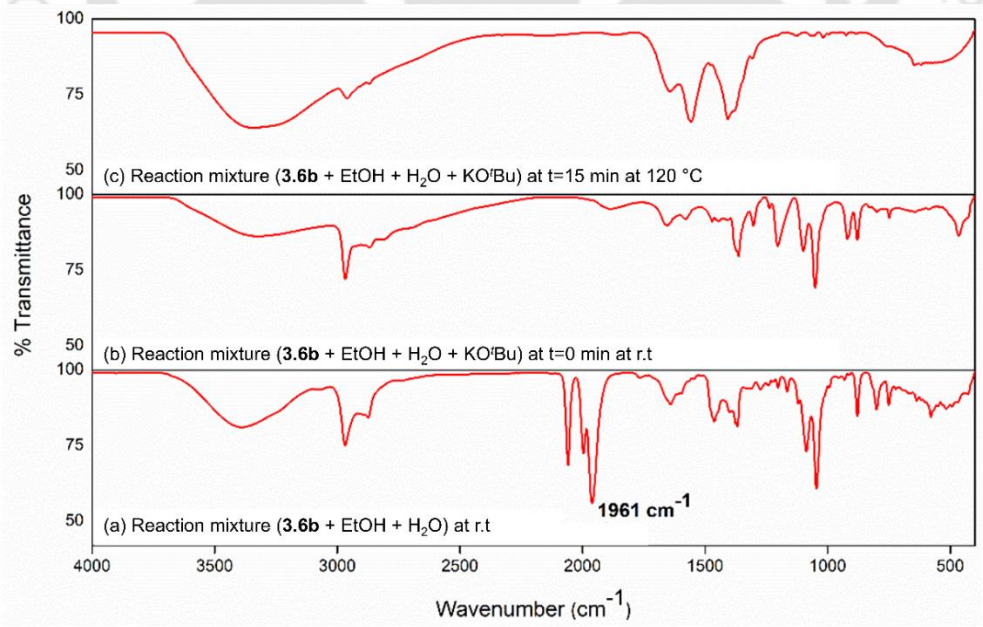

Figure 3.20. IR spectra of (a) **3.6b** (0.0136 g, 0.019 mmol, 0.8 mol%) in ethanol (0.271 mL, 4.64 mmol) with water (0.042 mL, 2.32 mmol) (b) **3.6b** (0.0136 g, 0.019 mmol, 0.8 mol%) in ethanol (0.271 mL, 4.64 mmol) with water (0.042 mL, 2.32 mmol) in the presence of KO^{t}Bu (0.390 g, 3.48 mmol, 1.5 equivalents) at room temperature. (c) **3.6b** (0.0136 g, 0.019 mmol,

0.8 mol%) in ethanol (0.271 mL, 4.64 mmol) with water (0.042 mL, 2.32 mmol) in the presence of KO^{t}Bu (0.390 g, 3.48 mmol, 1.5 equivalents) after 15 min at of heating 120 °C.

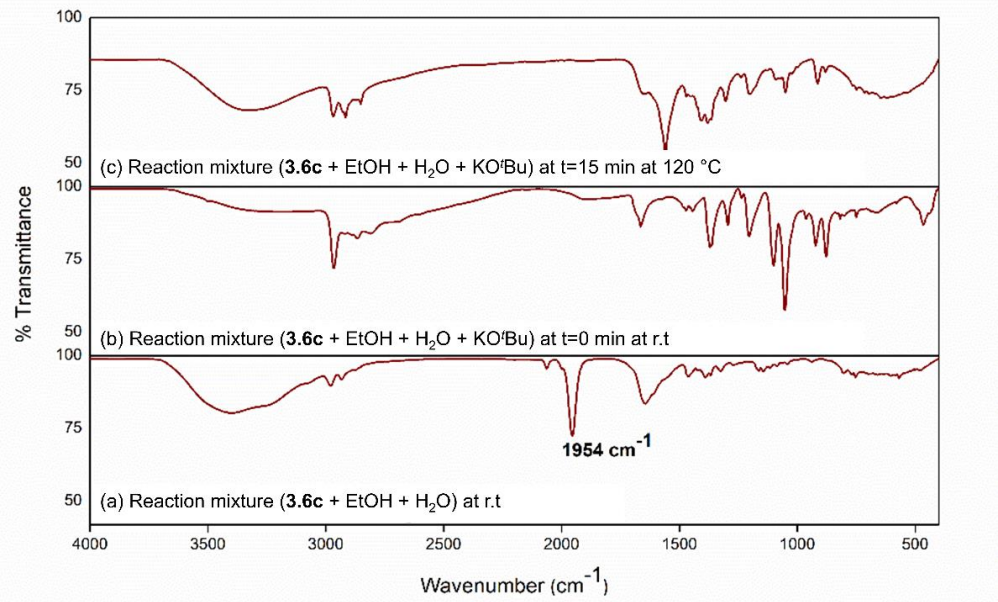

Figure 3.21. IR spectra of (a) **3.6c** (0.0121 g, 0.019 mmol, 0.8 mol%) in ethanol (0.271 mL, 4.64 mmol) with water (0.042 mL, 2.32 mmol) (b) **3.6c** (0.0121 g, 0.019 mmol, 0.8 mol%) in ethanol (0.271 mL, 4.64 mmol) with water (0.042 mL, 2.32 mmol) in the presence of KO^{t}Bu (0.390 g, 3.48 mmol, 1.5 equivalents) at room temperature. (c) **3.6c** (0.0121 g, 0.019 mmol, 0.8 mol%) in ethanol (0.271 mL, 4.64 mmol) with water (0.042 mL, 2.32 mmol) in the presence of KO^{t}Bu (0.390 g, 3.48 mmol, 1.5 equivalents) after 15 min at of heating 120 °C.

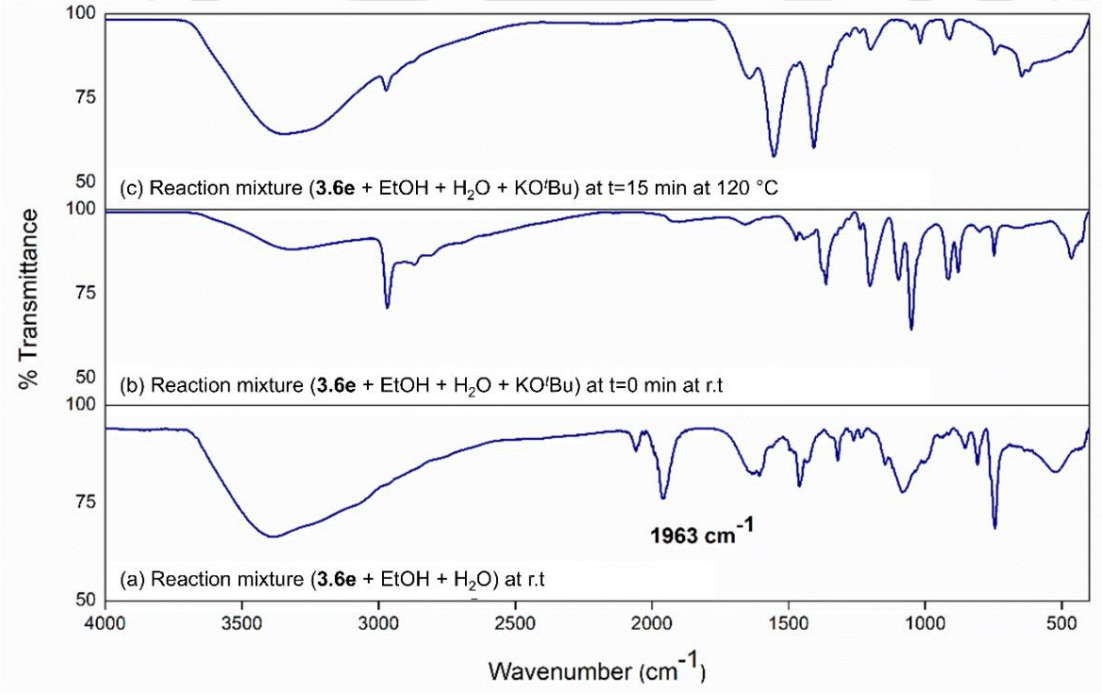

Figure 3.22. IR spectra of (a) **3.6e** (0.0094 g, 0.019 mmol, 0.8 mol%) in ethanol (0.271 mL, 4.64 mmol) with water (0.042 mL, 2.32 mmol) (b) **3.6e** (0.0094 g, 0.019 mmol, 0.8 mol%) in ethanol (0.271 mL, 4.64 mmol) with water (0.042 mL, 2.32 mmol) in the presence of KO^{t}Bu (0.390 g, 3.48 mmol, 1.5 equivalents) at room temperature. (c) **3.6e** (0.0094 g, 0.019 mmol, 0.8

mol%) in ethanol (0.271 mL, 4.64 mmol) with water (0.042 mL, 2.32 mmol) in the presence of KO^{t}Bu (0.390 g, 3.48 mmol, 1.5 equivalents) after 15 min at of heating 120 °C.

(Figure 3.23) may thus be mapped not only to the need of activation *via* double dissociation of PPh_3 groups from the former but also to the presence of resting-state stabilizing PPh_3 groups in the former and its lack thereof in the case of the latter. Apparently, in this case, addition of PPh_3 (2 equivalents with respect to the catalyst) to the reactions catalyzed by **3.6e** resulted in yields comparable to that obtained with **3.7e** as a catalyst (compare entry 11, Table 3.2 with entry 22, Table 3.2). In other words, the activity of **3.6e** could be retarded by the addition of two equivalents of PPh_3 to match the reactivity of **3.7e**. It is interesting to note that the barriers for each of the steps in the cycle catalyzed by **3.7b** and **3.6e** are much less than the corresponding barrier of the reaction catalyzed by **3.7c** (Figure 3.16, Figure 3.23, Figure 3.24 and Table S2.10, Appendix II). This explains the better activity of **3.7b** and **3.6e** in comparison to **3.7c**. Furthermore, the highest normalized barriers of **3.7b** (19.03 kcal mol^{-1}, Figure 3.16) and **3.6e** (19.79 kcal mo^{l-1}, Figure 3.23) are comparable and are much lower than the highest normalized barrier of **3.7c** (23.26 kcal mol^{-1}, Figure 3.24). This is well-reflected in the comparable activities of **3.7b** (70% H_2, entry 8, Table 3.2) and **3.6e** (69% H_2, entry 5, Table 3.2) both of which are higher than **3.7c** (58% H_2, entry 9, Table 3.2).

Recently, Zheng has studied the experimental activation Gibbs free energy at room temperature, $\Delta G^{\ddagger}_{25}$ = 32.0 kcal mol^{-1} which differs by about 3.2 kcal mol^{-1} from the computed

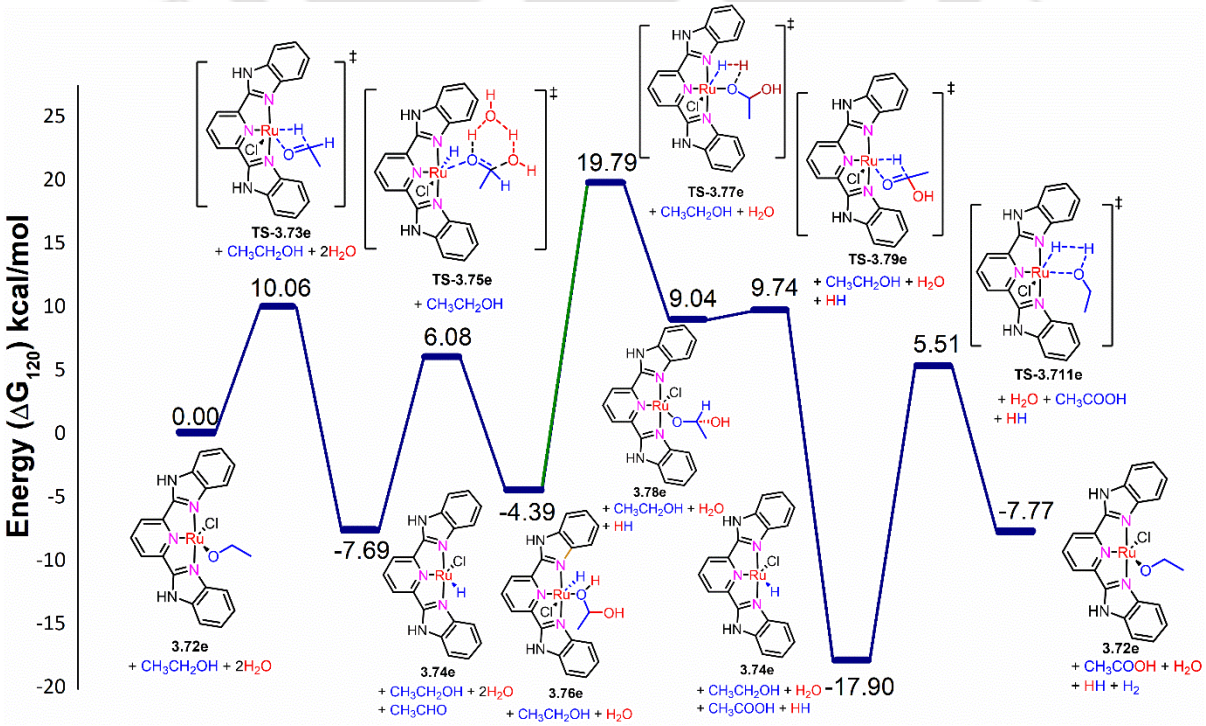

Figure 3.23. Free energy (ΔG_{120}) profile of the **3.6e** catalyzed reforming of ethanol at 120 °C.

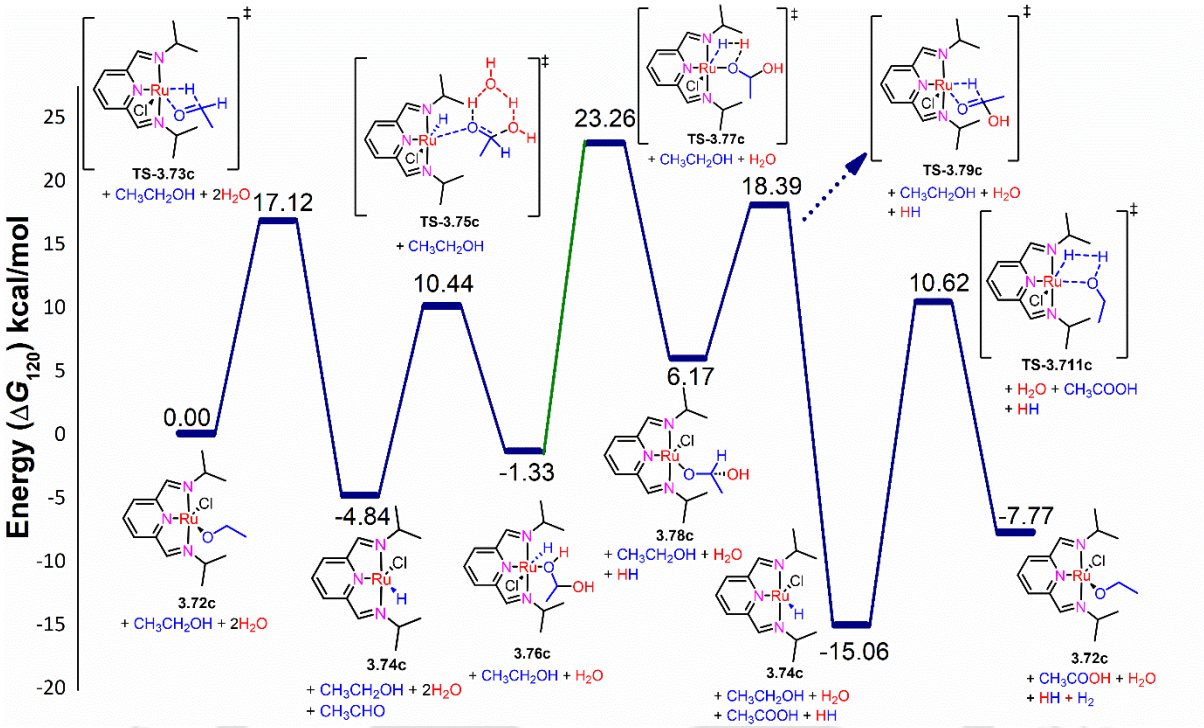

Figure 3.24. Free energy (ΔG_{120}) profile of the **3.7c** catalyzed reforming of ethanol at 120 °C.

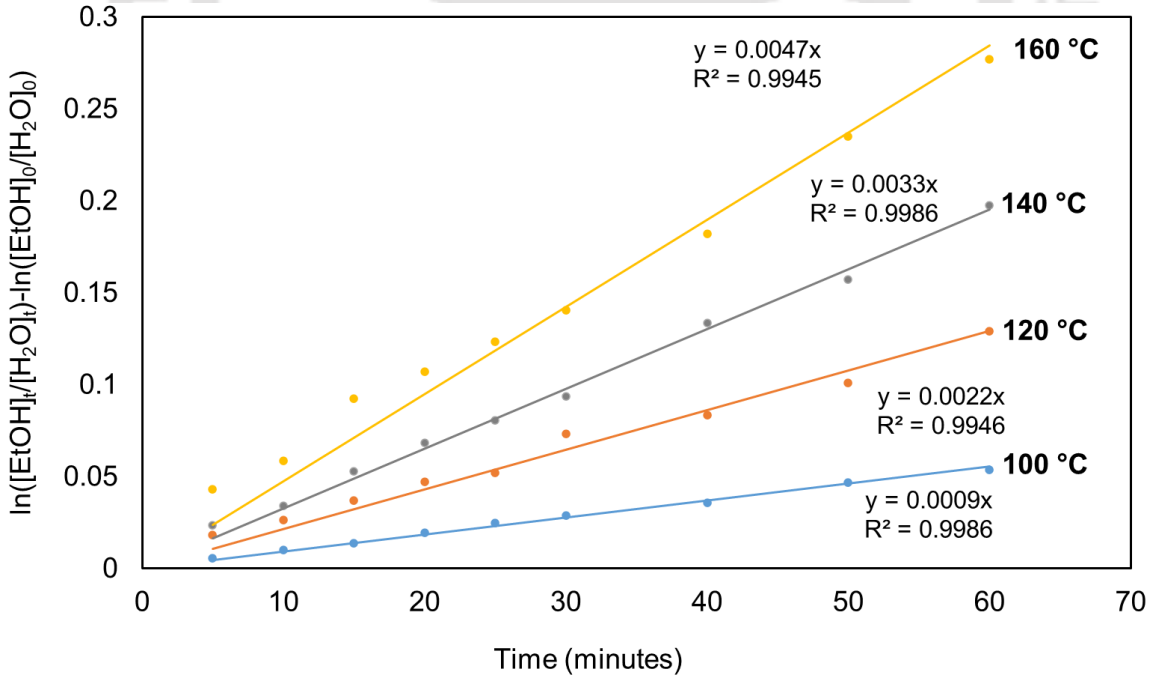

Figure 3.25 Plot for the calculation of rate constant by linear fitting based on equation 1. Reaction conditions: **3.7b** (0.0034 g, 0.0046 mmol, 0.2 mol%), EtOH (0.271 mL, 4.64 mmol)

with H_2O (0.042 mL, 2.32 mmol) in the presence of KO^{t}Bu (0.390 g, 3.48 mmol) at 100 °C,120 °C, 140 °C and, 160 °C. The H_2 evolved in first 1 hour of the reaction has been considered.

barrier ($\Delta G^{\ddagger}_{25}$ = 28.8 kcal mol^{-1}) for the reforming of methanol catalyzed by Ru(II) alkylidene complexes.[35] The same protocol has been employed in the current study to calculate the activation Gibbs free energy at room temperature for the ethanol reforming reaction catalyzed by **3.7b**.

For this purpose, the activation energy (E_a) for the **3.7b** catalyzed ethanol reforming was determined using the Arrhenius plot (Figure 3.25). The value of rate constants at different temperature were obtained from the slopes of the graph shown in Figure 3.25 based on equation 1. Further, Arrhenius equation (equation 2) was employed to obtain an activation energy (E_a) of 8.68 kcalmol^{-1} by linear fitting of ln$k$ versus (1000/T), where k = rate constant, R = gas constant (1.9872 calmol^{-1}K^{-1}) and T = temperature in K. The thermodynamic parameters, including activation Gibbs free energy ($\Delta G^{\ddagger}$), activation enthalpy ($\Delta H^{\ddagger}$) and activation entropy ($\Delta S^{\ddagger}$), were calculated by using the Eyring equation (equation 3), where k = rate constant, k_B = Boltzmann constant, h = Planck's constant, R = gas constant (1.9872 calmol^{-1}K^{-1}) and T = temperature in K.[35] The plot of ln(k/T) vs. (1000/T), gave the value of $\Delta H^{\ddagger}$ = 7.89 kcalmol^{-1} and $\Delta S^{\ddagger}$ = -0.55 kcalmol^{-1}K^{-1}. The Gibbs free energy, $\Delta G^{\ddagger}_{25}$ was calculated using $\Delta G^{\ddagger} = \Delta H^{\ddagger} - T\Delta S^{\ddagger}$, which was found to be 24.28 kcalmol^{-1}.

$$\ln \frac{[EtOH]_t}{[H_2O]_t} = k([EtOH]_0 - [H_2O]_0).t + \ln \frac{[EtOH]_0}{[H_2O]_0} \quad (1)$$

$$\ln k = \ln A - \frac{1000.E_a}{RT} \quad (2)$$

$$\ln \frac{k}{T} = \ln \frac{k_B}{h} + \frac{\Delta S^{\ddagger}}{T} - \frac{\Delta H^{\ddagger}}{R}\left(\frac{1}{T}\right) \ldots\ldots\ldots\ldots\ldots \quad (3)$$

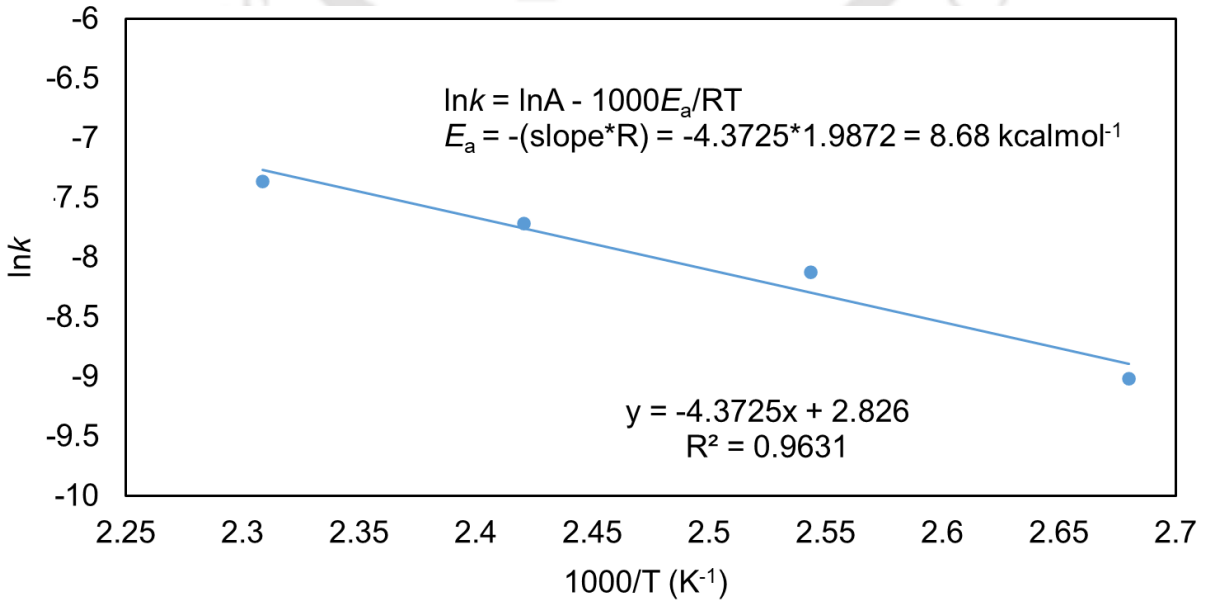

Figure 3.26. Arrhenius plot of ln*k vs.* 1000/T based on equation 2, at T = 373.15 K, 393.15 K, 413.15 K and 415.15 K.

The experimental activation Gibbs free energy at room temperature for the **3.7b** catalyzed ethanol reforming, $\Delta G^{\ddagger}_{25} = 24.28$ kcal mol^{-1}, differs by 1.1 kcal mol^{-1} from the computed value ($\Delta G^{\ddagger}_{25} = 23.17$ kcal mol^{-1}).

3.4 Conclusion

Pincer-ruthenium complexes based on *bis*(imino)pyridine ligands and 2,6-*bis*(benzimidazole--2-yl) ligands readily convert aqueous feed-agnostic ethanol selectively to clean-burning hydrogen and industrially valuable acetic acid. In comparison with the considered catalysts, (^{Cy2}NNN)RuCl$_2$(PPh$_3$) gave the best yield of up to 70% of H_2 and 73% of acetic acid in the presence of KO^{t}Bu (1.5 equivalents with respect to water) at 120 °C for the 2 : 1 mixture of

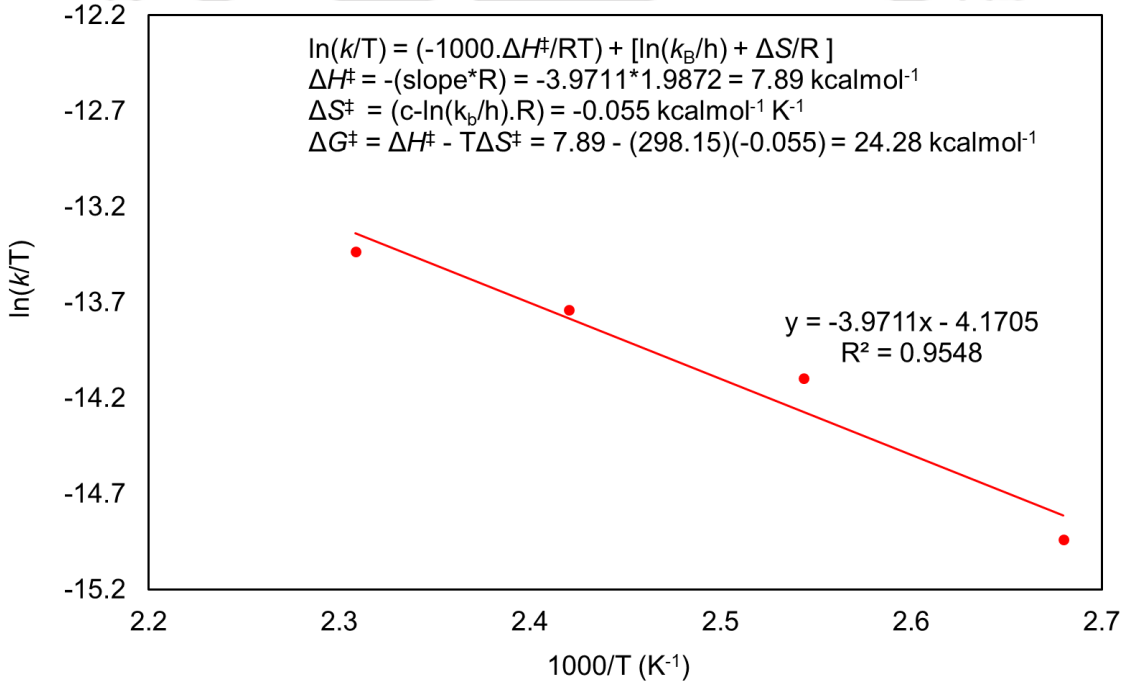

Figure 3.27. Eyring plot of ln(*k*/T) *vs.* 1000/T based on equation 3, at T = 373.15 K, 393.15 K, 413.15 K and 415.15 K.

ethanol and water. Under identical conditions, the use of a 4 : 1 ethanol/water mixture afforded comparable yields of hydrogen (70%) and acetic acid (69%). Proof for the homogeneity of the reaction involving distinct molecular catalysts was obtained from the kinetic studies that revealed a first-order dependence of rate on the concentrations of both (^{Cy2}NNN)RuCl$_2$(PPh$_3$)

and ethanol. An average KIE of 5.23 was obtained from deuterium-labelling experiments which along with the DFT studies point towards the involvement of C–H bond activation of ethanol in the catalytic cycle. The alcoholysis step leading to the evolution of the first molecule of hydrogen along with the concomitant formation of (^{Cy2}NNN)RuCl(H) with an energy barrier of 23.19 kcal mol^{-1} has been computed to be the RDS. The HRMS and NMR studies of the reaction mixture have been successful in aiding the detection of (^{Cy2}NNN)RuCl(H) as its phosphine adduct, which apparently is the resting-state of the catalytic cycle, and are well in agreement with DFT studies. This work comprises a robust NNN *bis*(imino)pyridine pincer-ruthenium phosphine catalytic system for the aqueous ethanol reforming that not only offers great promise but also opens up exciting possibilities towards the generation of hydrogen, a sustainable fuel, and industrially important acetic acid.

3.5 Experimental Section

3.5.1 General procedure and materials

All the manipulations were carried out under purified Ar using either a standard double manifold or a glove box. The solvents such as tetrahydrofuran (THF), hexane and toluene were dried via double distillation over Na/benzophenone prior to the experiment.[36] Ethanol was dried and distilled under argon according to the literature procedure.[36] All other chemicals such as $RuCl_3 \cdot 3H_2O$, [Ru(benzene)Cl_2]$_2$, [$RuCl_2$(*p*-cymene)]$_2$, pyridine-2,6-dicarboxylic acid, D_2O, ethanol-d_6 and $CDCl_3$ were purchased from MERCK or Sigma-Aldrich and used as such. All catalytic reactions were set up either under an Ar atmosphere or under air using dried glassware. The complexes $RuCl_2(PPh_3)_3$, **3.6a–f**, **3.7a–f**, and **3.8b–d** were prepared according to the literature procedure.[34, 37-52]

3.5.2 Physical measurements

^{1}H, ^{2}H, ^{13}C{H} and ^{31}P were recorded on a Bruker ASCEND 600 operating at 600 MHz for ^{1}H, 150 MHz for ^{13}C{H}, and 564 MHz for ^{31}P or on a Bruker AVANCE 400 operating at 400 MHz for ^{1}H, 100 MHz for ^{13}C{H}, 376 MHz for ^{31}P or on a Bruker AVANCE 500 operating at 500 MHz for ^{1}H, 125 MHz for ^{13}C{H}, 470 MHz for ^{31}P. HRMS measurements were performed using an Agilent Accurate-Mass Q-TOF ESI–MS 6546. GC analyses were performed on an Agilent 7820-GC instrument fitted with an Agilent Front SS7 inlet N_2 HP-PLOT Q column (30 m length × 530 μm × 40 μm) using the following method: Agilent 7820-GC back detector: TCD starting temperature: 40 °C; time at starting temp: 0 min; ramp: 40 °C min^{-1} up to 250 °C

with holding time = 5 min; flow rate (carrier): 25 mL min^{-1} (N_2); split ratio: 195; inlet temperature: 40 °C; detector temperature: TCD: 250 °C, FID: 250 °C. Fourier Transform Infrared (FT-IR) spectra were analysed on a Perkin Elmer Spectrum Two FT-IR spectrometer at room temperature in the region 400–4000 cm^{-1}.

3.5.3 General procedure for the aqueous ethanol reforming reaction

In a 5 mL pear-shaped vessel attached to a condenser, KO^{t}Bu (0.390 g, 3.48 mmol) and **3.7b** (0.2–0.8 mol%; 0.0034–0.0136 g; 4.6–18.5 μmol) were added inside the glove box. This was followed by addition of dry ethanol (**3.1**) (0.271 mL, 4.634 mmol) and distilled water (0.042 ml, 2.317 mmol) under air. The mixture was heated in a pre-heated oil bath at 120 °C and the gas evolved was quantified by the water displacement method, and the composition of the gas generated was analyzed by GC analysis (Figure 3.28). The reaction was run till no more evolution of gas was observed (typically 36 h) and was then cooled down to room temperature. An aliquot (approximately 10 mg) was withdrawn from the reaction mixture and the yield of acetic acid was determined by ^{1}H NMR using D_2O as a solvent and dimethyl sulfoxide (known amount added in the vessel) as a standard.

3.5.4 General procedure for the kinetic studies performed for the 3.7b catalyzed aqueous ethanol reforming reaction

3.5.4.1 Variation of catalyst concentration. In a screw cap NMR tube, KO^{t}Bu (0.200 g, 1.78 mmol) and **3.7b** (0.1–0.8 mol%; 0.0026–0.0208 g; 3.56–28.56 μmol) were added inside the glove box. This was followed by addition of dry ethanol (**3.1**) (0.416 mL, 7.14 mmol) and D_2O (0.065 mL, 3.57 mmol). The tube was heated in a pre-heated oil bath at 120 °C. ^{1}H NMR of the reaction mixture was recorded at different time intervals using dimethyl sulfoxide as a standard.

3.5.4.2 Variation of ethanol concentration. In a screw cap NMR tube, KO^{t}Bu (0.200 g, 1.78 mmol) and **3.7b** (0.0052 g, 7.12 μmol, 0.2 mol%) were added inside the glove box. This was followed by addition of dry ethanol (**3.1**) (0.416–0.104 mL, 7.14–1.78 mmol) and D_2O (0.065 mL, 3.57 mmol). Dioxane was used as a make-up solvent at lower concentrations of ethanol. The tube was heated in a pre-heated oil bath at 120 °C. ^{1}H NMR of the reaction mixture was recorded at different time intervals using dimethyl sulfoxide as a standard.

3.5.5. Computational details

The geometries of all the considered complexes were fully optimized employing the DFT(PBE)[53] method on the Gaussian-09 package.[54] The LANL2DZ[55-57] and 6-311G(d,p) basis sets with a polarization function were used for the metal (Ru) and non-metal atoms respectively. The empirical dispersion-GD3 was used in all molecular geometry optimization and energy computations. The transition states were located using the synchronous transit-guided quasi-Newton (QST2) and Genecp (gen keyword with effective core potential) was used to define the basis set. The method and basis set were chosen on the basis of previous reports on pincer complexes.[37, 40, 49-51] Frequency calculations were also performed to differentiate minima structures or transition states on the potential energy surface. ΔG values were calculated by using the sum of electronic and thermal free energies. These values were computed at 120 °C to meet the experimental conditions.

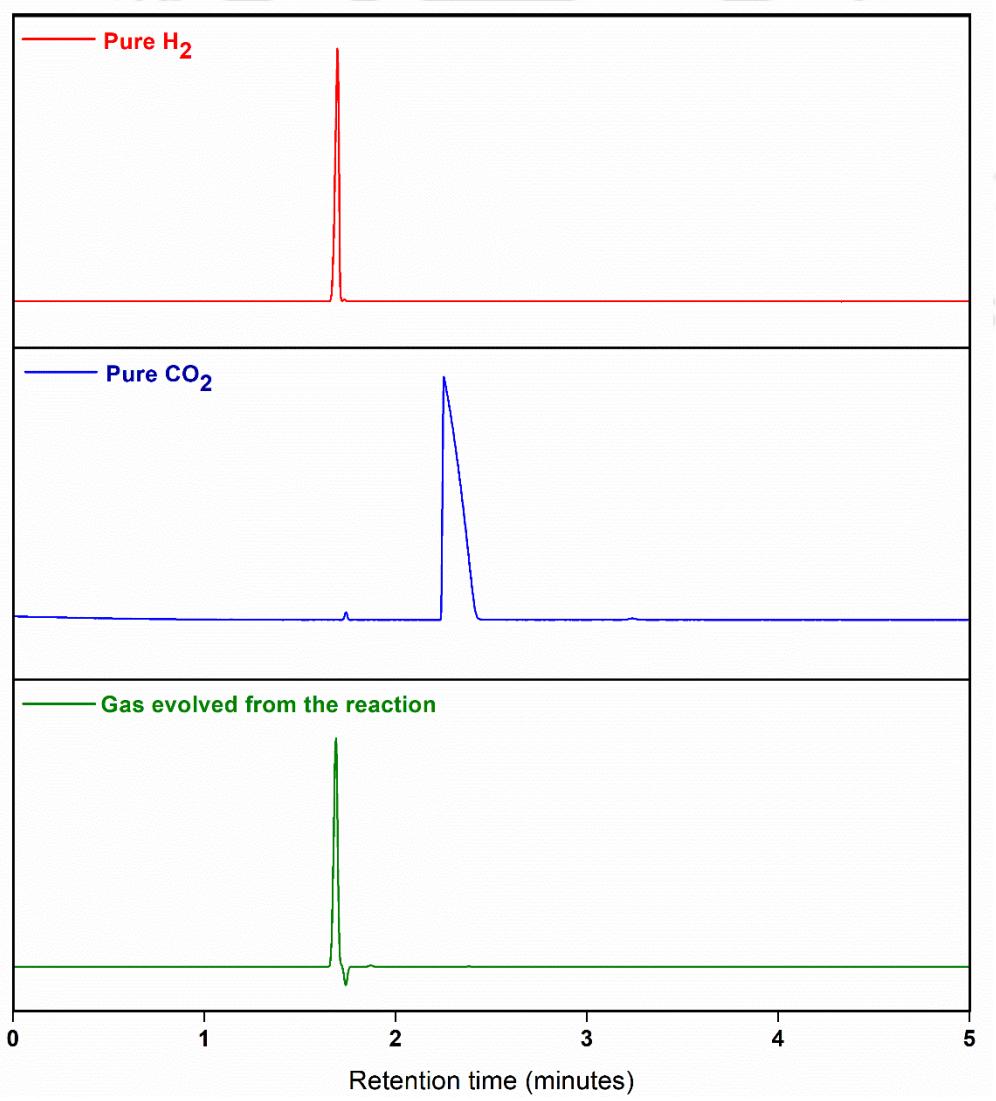

Figure 3.28. GC-TCD analysis of gas evolved from the ethanol reforming reaction along with the corresponding analysis of pure H_2 and CO_2 gas. Reaction condition: Ethanol (0.271 mL,

4.64 mmol), H_2O (0.042 mL, 2.32 mmol), KO^{t}Bu (0.390 g, 4.64 mmol, 1.5 equivalents), and **3.7b** (0.0034 g, 0.0046 mmol, 0.2 mol %) at 120 °C (Entry 1, Table 3.3).

Supporting information containing NMR spectra, GC and HRMS analysis, Kinetics data and Cartesian coordinates of the computed complexes for chapter III is available as Appendix II and can be found at:

https://drive.google.com/file/d/1ppAVRIRsJuQ7DK_-J4LtayNnSOUh6GvV/view?usp=sharing

3.6 References

1. Jones, L. W. Liquid Hydrogen as a Fuel for the Future: Replacement of hydrocarbon fuel for transportation systems by liquid hydrogen is proposed and discussed. *Science* **1971,** *174*, 367-370.
2. Satyapal, S.; Petrovic, J.; Read, C.; Thomas, G.; Ordaz, G. The US Department of Energy's National Hydrogen Storage Project: Progress towards meeting hydrogen-powered vehicle requirements. *Catal. Today* **2007,** *120*, 246-256.
3. Singh, S.; Jain, S.; Venkateswaran, P.; Tiwari, A. K.; Nouni, M. R.; Pandey, J. K.; Goel, S. Hydrogen: A sustainable fuel for future of the transport sector. *Renew. Sustain. Energy Rev.* **2015,** *51*, 623-633.
4. Modisha, P. M.; Ouma, C. N.; Garidzirai, R.; Wasserscheid, P.; Bessarabov, D. The prospect of hydrogen storage using liquid organic hydrogen carriers. *Energy Fuels* **2019,** *33*, 2778-2796.
5. Yadav, V.; Sivakumar, G.; Gupta, V.; Balaraman, E. Recent Advances in Liquid Organic Hydrogen Carriers: An Alcohol-Based Hydrogen Economy. *ACS Catal.* **2021,** *11*, 14712-14726.
6 Gianotti, E.; Taillades-Jacquin, M. l.; Rozière, J.; Jones, D. J. High-purity hydrogen generation via dehydrogenation of organic carriers: a review on the catalytic process. *ACS Catal.* **2018,** *8*, 4660-4680.
7. Ni, M.; Leung, D. Y. C.; Leung, M. K. H. A review on reforming bio-ethanol for hydrogen production. *Int. J. Hydrogen Energy* **2007,** *32*, 3238-3247.
8. Rossetti, I.; Tripodi, A. Catalytic Production of Renewable Hydrogen for Use in Fuel Cells: A Review Study. *Top. Catal.* **2022**, 1-20.
9. Palma, V.; Ruocco, C.; Cortese, M.; Martino, M. Bioalcohol Reforming: An Overview of the Recent Advances for the Enhancement of Catalyst Stability. *Catalysts* **2020,** *10*, 665.
10. Palanisamy, A.; Soundarrajan, N.; Ramasamy, G., Analysis on production of bioethanol for hydrogen generation. *Environ. Sci. Pollut. Res.* **2021,** *28*, 63690-63705.
11. Morton, D.; Cole-Hamilton, D. J. Molecular hydrogen complexes in catalysis: highly efficient hydrogen production from alcoholic substrates catalysed by ruthenium complexes. *J. Chem. Soc., Chem. Commun.* **1988**, 1154-1156.
12. Dobson, A.; Robinson, S. D. Complexes of the platinum metals. 7. Homogeneous ruthenium and osmium catalysts for the dehydrogenation of primary and secondary alcohols. *Inorg. Chem.* **1977,** *16*, 137-142.
13. Sordakis, K.; Tang, C.; Vogt, L. K.; Junge, H.; Dyson, P. J.; Beller, M.; Laurenczy, G. Homogeneous Catalysis for Sustainable Hydrogen Storage in Formic Acid and Alcohols. *Chem. Rev.* **2018,** *118*, 372-433.
14. Kumar, A.; Daw, P.; Milstein, D. Homogeneous Catalysis for Sustainable Energy: Hydrogen and Methanol Economies, Fuels from Biomass, and Related Topics. *Chem. Rev.* **2022,** *122*, 385-441.
15. Bai, F. W.; Anderson, W. A.; Moo-Young, M., Ethanol fermentation technologies from sugar and starch feedstocks. *Biotechnol. Adv.* **2008,** *26*, 89-105.
16. Ibeto, C.; Ofoefule, A.; Agbo, K. A global overview of biomass potentials for bioethanol production: a renewable alternative fuel. *Trends Appl. Sci. Res.* **2011,** *6*, 410-425.

17. Lamy, C.; Coutanceau, C.; Leger, J. M. The direct ethanol fuel cell: a challenge to convert bioethanol cleanly into electric energy. In *Catalysis for Sustainable Energy Production*; Barbaro, P.; Bianchini, C., Eds.; WILEY-VCH Verlag GmbH & Co. kGaA: Weinheim, **2009**; pp. 1-42.
18. Berre, C.; Serp, P.; Kalck, P.; Torrence, G. Acetic acid. In *Ullmann's Encyclopedia of Industrial Chemistry*. WILEY-VCH Verlag GmbH & Co. kGaA: Weinheim, **2014**; vol. 74, pp. 1-34.
19. Wittcoff, H. A.; Reuben, B. G.; Plotkin, J. S. *Industrial Organic Chemicals*, 3rd ed.; John Wiley & Sons, Inc.: Hokoben, NJ, **2012**.
20. Pal, P.; Nayak, J. Acetic Acid Production and Purification: Critical Review Towards Process Intensification. Sep. *Purif. Rev.* **2017**, *46*, 44– 61.
21. Yoneda, N.; Kusano, S.; Yasui, M.; Pujado, P.; Wilcher, S. Recent advances in processes and catalysts for the production of acetic acid. *Appl. Catal., A* **2001,** *221*, 253-265.
22. Hung, W.-J.; Lai, I. K.; Chen, Y.-W.; Hung, S.-B.; Huang, H.-P.; Lee, M.-J.; Yu, C.-C., Process Chemistry and Design Alternatives for Converting Dilute Acetic Acid to Esters in Reactive Distillation. *Ind. Eng. Chem. Res.* **2006,** *45*, 1722-1733.
23. Hardy, W. Acetic Anhydride. *Ind. Eng. Chem. Res.* **1957,** *49*, 51A-52A.
24. Maitlis, P. M.; Haynes, A.; Sunley, G. J.; Howard, M. J. Methanol carbonylation revisited: thirty years on. *J. Chem. Soc., Dalton Trans.* **1996**, 2187-2196.
25. Budiman, A. W.; Nam, J. S.; Park, J. H.; Mukti, R. I.; Chang, T. S.; Bae, J. W.; Choi, M. J. Review of Acetic Acid Synthesis from Various Feedstocks Through Different Catalytic Processes. *Catal. Surv. Asia* **2016,** *20*, 173-193.
26. Nomura, T.; Zhao, Y.; Minami, E.; Kawamoto, H. Reaction Mechanisms and Production of Hydrogen and Acetic Acid from Aqueous Ethanol Using a Rn-Sn/TiO2 Catalyst in a Continuous Flow Reactor. *Catalysts* **2024**, *14*, 249.
27. Dagle, R. A.; Winkelman, A. D.; Ramasamy, K. K.; Lebarbier Dagle, V.; Weber, R. S. Ethanol as a Renewable Building Block for Fuels and Chemicals. *Ind. Eng. Chem. Res.* **2020**, *59*, 4843–4853.
28. Brei, V. L.; Sharanda, M. E.; Prudius, S. V.; Bondarenko, E. A. Synthesis of acetic acid from ethanol-water mixture over Cu/ZnO-ZrO2-Al2O3 catalyst. *Appl. Catal. A* **2013**, *458*, 196-200.
29. Xiang, N.; Xu, P.; Ran, N.; Ye, T. Production of acetic acid from ethanol over CuCr catalysts via dehydrogenation-(aldehyde–water shift) reaction. *RSC Adv.* **2017,** *7*, 38586-38593.
30. Hu, P.; Ben-David, Y.; Milstein, D. General Synthesis of Amino Acid Salts from Amino Alcohols and Basic Water Liberating H2. *J. Am. Chem. Soc.* **2016,** *138*, 6143-6146.
31. Sponholz, P.; Mellmann, D.; Cordes, C.; Alsabeh, P. G.; Li, B.; Li, Y.; Nielsen, M.; Junge, H.; Dixneuf, P.; Beller, M. Efficient and Selective Hydrogen Generation from Bioethanol using Ruthenium Pincer-type Complexes. *ChemSusChem* **2014,** *7*, 2419-2422.
32. Wang, Q.; Xia, Y.; Chen, Z.; Wang, Y.; Cheng, F.; Qin, L.; Zheng, Z. Hydrogen Production via Aqueous-Phase Reforming of Ethanol Catalyzed by Ruthenium Alkylidene Complexes. *Organometallics* **2022,** *41*, 914-919.
33. Kuwahara, M.; Nishioka, M.; Yoshida, M.; Fujita, K.-i. A Sustainable Method for the Synthesis of Acetic Acid Based on Dehydrogenation of an Ethanol–Water Solution Catalyzed by an Iridium Complex Bearing a Functional Bipyridonate Ligand. *ChemCatChem* **2018,** *10*, 3636-3640.
34. Arora, V.; Yasmin, E.; Tanwar, N.; Hathwar, V. R.; Wagh, T.; Dhole, S.; Kumar, A. Pincer–Ruthenium-Catalyzed Reforming of Methanol─Selective High-Yield Production of Formic Acid and Hydrogen. *ACS Catal.* **2023,** *13*, 3605-3617.
35. Wang, Q.; Lan, J.; Liang, R.; Xia, Y.; Qin, L.; Chung, L. W.; Zheng, Z. New tricks for an old dog: Grubbs catalysts enable efficient hydrogen production from aqueous-phase methanol reforming. *ACS Catal.* **2022,** *12*, 2212-2222.
36. Armarego, W. L. F.; Chai, C., Chapter 5 - Purification of Inorganic and Metal-Organic Chemicals. In *Purification of Laboratory Chemicals (Seventh Edition)*, Armarego, W. L. F.; Chai, C., Eds. Butterworth-Heinemann: Boston, **2013**; pp 555-661.
37. Das, K.; Nandi, P. G.; Islam, K.; Srivastava, H. K.; Kumar, A. N–Alkylation of Amines Catalyzed by a Ruthenium–Pincer Complex in the Presence of in situ Generated Sodium Alkoxide. *Eur. J. Org. Chem.* **2019,** *2019*, 6855-6866.

38. Das, K.; Yasmin, E.; Das, B.; Srivastava, H. K.; Kumar, A. Phosphine-free pincer-ruthenium catalyzed biofuel production: high rates, yields and turnovers of solventless alcohol alkylation. *Catal. Sci. Technol.* **2020,** *10*, 8347-8358.
39. Dutta, M.; Das, K.; Prathapa, S. J.; Srivastava, H. K.; Kumar, A. Selective and high yield transformation of glycerol to lactic acid using NNN pincer ruthenium catalysts. *Chem. Commun.* **2020,** *56*, 9886-9889.
40. Das, K.; Kathuria, L.; Jasra, R. V.; Dhole, S.; Kumar, A. Microwave-assisted pincer-ruthenium catalyzed Guerbet reaction for the upgradation of bio-ethanol to bio-butanol. *Catal. Sci. Technol.* **2023,** *13*, 1763-1776.
41. Arora, V.; Narjinari, H.; Kumar, A. Pincer-Nickel Catalyzed Selective Guerbet-Type Reactions. *Organometallics* **2021,** *40*, 2870-2880.
42. Nandi, P. G.; Kumar, P.; Kumar, A. Ligand-free Guerbet-type reactions in air catalyzed by in situ formed complexes of base metal salt cobaltous chloride. *Catal. Sci. Technol.* **2022,** *12*, 1100-1108.
43. Nandi, P. G.; Thombare, P.; Prathapa, S. J.; Kumar, A. Pincer-Cobalt-Catalyzed Guerbet-Type β-Alkylation of Alcohols in Air under Microwave Conditions. *Organometallics* **2022,** *41*, 3387-3398.
44. Narjinari, H.; Tanwar, N.; Kathuria, L.; Jasra, R. V.; Kumar, A. Guerbet-type β-alkylation of secondary alcohols catalyzed by chromium chloride and its corresponding NNN pincer complex. *Catal. Sci. Technol.* **2022,** *12*, 4753-4762.
45. Bisarya, A.; Jasra, R. V.; Kumar, A. NNN Pincer-Manganese-Catalyzed Guerbet-Type β-Alkylation of Alcohols under Microwave Irradiation. *Organometallics* **2023,** *42*, 1818-1831.
46. Arora, V.; Dutta, M.; Das, K.; Das, B.; Srivastava, H. K.; Kumar, A. Solvent-Free N-Alkylation and Dehydrogenative Coupling Catalyzed by a Highly Active Pincer-Nickel Complex. *Organometallics* **2020,** *39*, 2162-2176.
47. Das, K.; Dutta, M.; Das, B.; Srivastava, H. K.; Kumar, A. Efficient Pincer-Ruthenium Catalysts for Kharasch Addition of Carbon Tetrachloride to Styrene. *Adv. Synth. Catal* **2019,** *361*, 2965-2980.
48. Das, K.; Yasmin, E.; Kumar, A., Pincer-Ruthenium Catalyzed Oxygen Mediated Dehydrative Etherification of Alcohols and Ortho-Alkylation of Phenols. *Adv. Synth. Catal.* **2022,** *364*, 3895-3909.
49. Johansson, A. J.; Zuidema, E.; Bolm, C. On the Mechanism of Ruthenium-Catalyzed Formation of Hydrogen from Alcohols: A DFT Study. *Chem. -Eur. J.* **2010,** *16*, 13487-13499.
50. Paul, B.; Shee, S.; Panja, D.; Chakrabarti, K.; Kundu, S. Direct Synthesis of N,N-Dimethylated and β-Methyl N,N-Dimethylated Amines from Nitriles Using Methanol: Experimental and Computational Studies. *ACS Catal.* **2018,** *8*, 2890-2896.
51. He, X.; Li, Y.; Fu, H.; Zheng, X.; Chen, H.; Li, R.; Yu, X. Synthesis of Unsymmetrical N-Heterocyclic Carbene–Nitrogen–Phosphine Chelated Ruthenium(II) Complexes and Their Reactivity in Acceptorless Dehydrogenative Coupling of Alcohols to Esters. *Organometallics* **2019,** *38*, 1750-1760.
52. Paul, B.; Panja, D.; Kundu, S., Ruthenium-Catalyzed Synthesis of N-Methylated Amides using Methanol. *Org. Lett.* **2019,** *21*, 5843-5847.
53. Perdew, J. P.; Burke, K.; Ernzerhof, M. Generalized gradient approximation made simple. *Phys. Rev. Lett.* **1996,** *77*, 3865-3868.
54. Frisch, M. J.; Trucks, G. W., Schlegel, H. B.; Scuseria, G. E.; Robb, M. A.; Cheeseman, J. R.; Scalmani, G.; Barone, V.; Mennucci, B.; Petersson, G. A.; Nakatsuji, H.; Caricato, M.; Li, X.; Hratchian, H. P.; Izmaylov, A. F.; Bloino, J.; Zheng, G.; Sonnenberg, J. L.; Hada, M.; Ehara, M.; Toyota, K.; Fukuda, R.; Hasegawa, J.; Ishida, M.; Nakajima, T.; Honda, Y.; Kitao, O.; Nakai, H.; Vreven, T.; Montgomery, J. A., Jr.; Peralta, J. E.; Ogliaro, F.; Bearpark, M.; Heyd, J. J.; Brothers, E.; Kudin, K. N.; Staroverov, V. N.; Keith, T.; Kobayashi, R.; Normand, J.; Raghavachari, K.; Rendell, A.; Burant, J. C.; Iyengar, S. S.; Tomasi, J.; Cossi, M.; Rega, N.; Millam, J. M.; Klene, M.; Knox, J. E.; Cross, J. B.; Bakken, V.; Adamo, C.; Jaramillo, J.; Gomperts, R.; Stratmann, R. E.; Yazyev, O.; Austin, A. J.; Cammi, R.; Pomelli, C.; Ochterski, J. W.; Martin, R. L.; Morokuma, K.; Zakrzewski, V. G.; Voth, G. A.; Salvador, P.; Dannenberg, J. J.; Dapprich, S.; Daniels, A. D.;

Farkas, O.; Foresman, J. B.; Ortiz, J. V.; Cioslowski, J.; Fox, D. J. Gaussian 09, Revision D.01; Gaussian, Inc.: Wallingford, CT, **2013**.

55. Hay, P. J.; Wadt, W. R. Ab initio effective core potentials for molecular calculations. Potentials for the transition metal atoms Sc to Hg. *J. Chem. Phys.* **1985,** *82*, 270-283.
56. Hay, P. J.; Wadt, W. R. Ab initio effective core potentials for molecular calculations. Potentials for K to Au including the outermost core orbitals. *J. Chem. Phys.* **1985,** *82*, 299-310.
57. Wadt, W. R.; Hay, P. J. Ab initio effective core potentials for molecular calculations. Potentials for main group elements Na to Bi. *J. Chem. Phys.* **1985,** *82*, 284-298.

Chapter IV

Synthesis of Pincer-Nickel Complexes and Their Application in the Selective β–Alkylation of Secondary Alcohols with Primary Alcohols

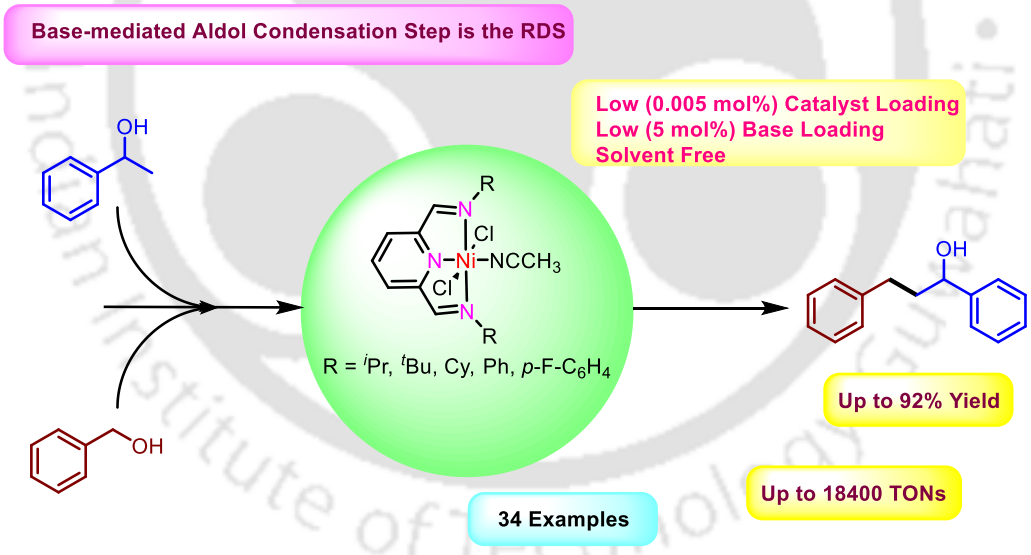

The content of this chapter has been adapted from "*Pincer-Nickel Catalyzed Selective Guerbet-Type Reactions*" by Arora, V.; Narjinari, H.; Kumar, A. *Organometallics* **2021**, *40*, 2870-2880.

4.1 Introduction

The formation of C-C bonds starting from alcohols play an important role in synthetic organic chemistry having varied applications in fuel, fine chemicals, medicinal, agrochemicals, and pharmaceuticals.[1] The traditional process employed for the synthesis of *β*-alkylated alcohols involves multistep synthetic procedure, but this leads to the consumption of costly and toxic reagents along with the generation of a large amount of stochiometric waste (Scheme 4.10).[2-4]

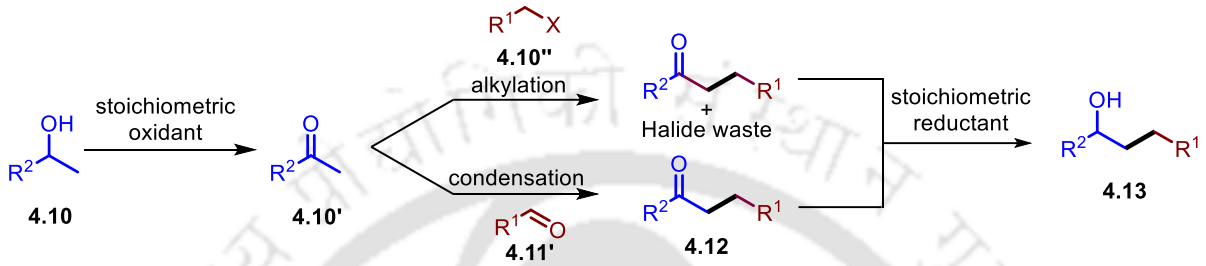

Scheme 4.10. Traditional methods reported in literature for the synthesis of *β*-alkylated alcohols.[5]

Transition metal-catalyzed *β*-alkylation of alcohols has attracted the most attention among the many procedures. Alcohols can be used to generate higher *β*-alkylated alcohols *via* acceptorless dehydrogenative coupling, which is an intriguing strategy due to its environmentally beneficial approach.[6, 7] The process begins with the transition-metal mediated initial dehydrogenation of both (primary and secondary) alcohols to the corresponding carbonyl intermediates. These unsaturated compounds then undergoes aldol condensation to afford corresponding unsaturated ketones which further gets hydrogenated to afford the *β*-alkylated alcohols (Scheme 4.11).[6]

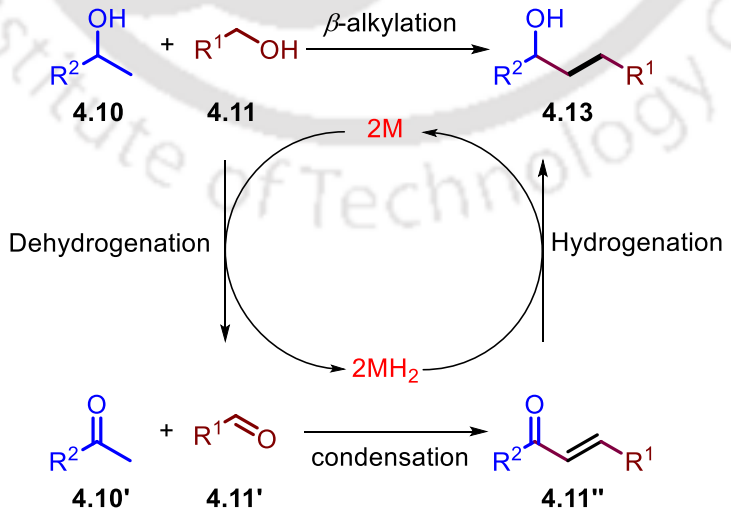

Scheme 4.11. Generalized C-C bond forming pathway *via* hydrogen borrowing strategy.[6]

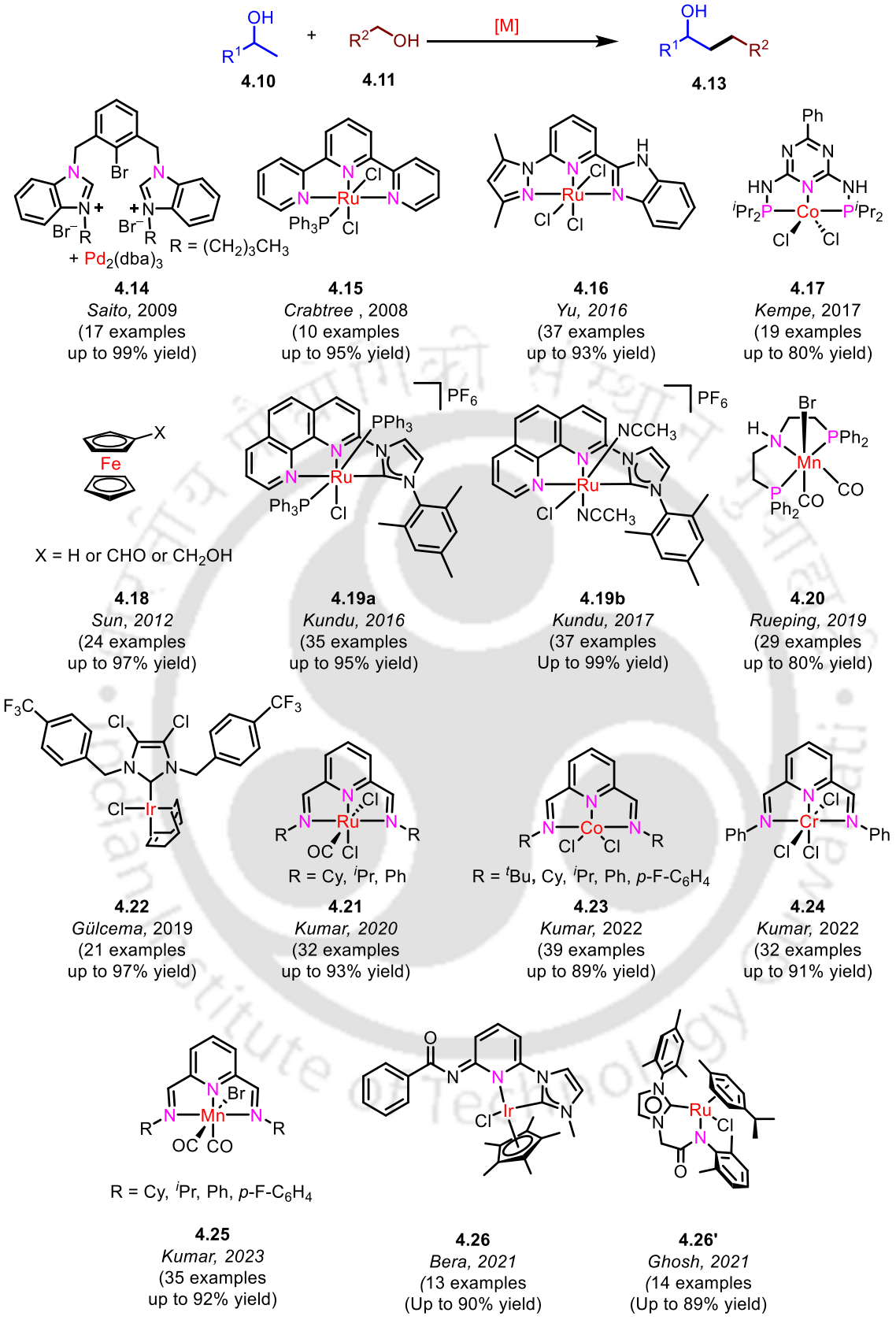

Figure 4.10. Selected examples reported for the *β*–alkylation of secondary alcohols with primary alcohols.[7]

A range of transition metal complexes based on Ir,[8-17] Rh,[18] Ru,[5, 19-25] Pd,[26] Mn,[27, 28] Co,[29] Fe,[30] Ni,[31] and Cu[32] have been reported for the *β*-alkylation of secondary alcohols with primary alcohols (Figure 4.10). Majority of all these reports have been mediated by noble metal catalysts and therefore it would be highly desirable to replace them with earth-abundant transition metals, such as Cu, Ni, Fe, and Mn.[33]

In 2003, Shim and Cho were the first to describe the *β*-alkylation of secondary alcohols with primary alcohols using $RuCl_2(PPh_3)_3$ (5 mol%) in the presence of 1-dodecene in dioxane and 3 equivalents of NaOH at 80 °C for 40 h (Scheme 4.12). The catalytic system demonstrated a vast substrate scope and was effective towards aliphatic, aromatic and cyclic carbinols.[34]

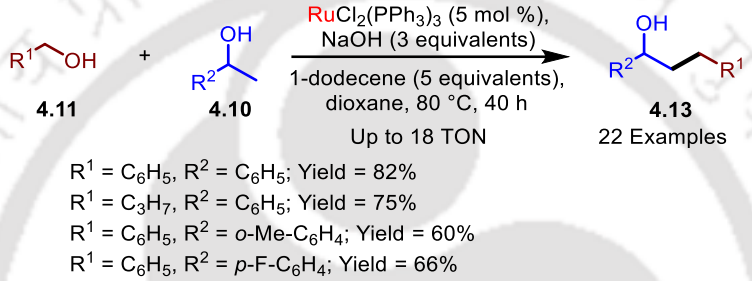

Scheme 4.12. $RuCl_2(PPh_3)_3$ catalyzed *β*-alkylation of alcohols reported by Cho and Shim.[34]

In 2016, Kundu and co-workers reported an atom-economical alkylation of secondary alcohols with primary alcohols employing the bifunctional pincer-ruthenium complex **4.19a**.[21] The complex exhibited metal-ligand cooperativity and tolerated several aromatic, aliphatic and heteroatomic alcohols. In the presence of 0.1 mol% of **4.19a** and 0.5 equivalents, very high yields of the *β*-alkylated alcohols were obtained within 90 minutes at 125 °C (Scheme 4.13). They further extended the current scope to the double alkylation of cyclopentanol with various primary alcohols.[21] In next year, the same group demonstrated these reactions using similar complex (**4.19b**) having acetonitrile groups instead of phosphine groups (Scheme 4.13).[23] In comparison to **4.19a** (0.1 mol%), the complex **4.19b** afforded high yields of the desired products at a lower loading (0.01 mol%) in the presence of 0.4 equivalents of NaO^iPr but in a longer time (1.5 h *vs.* 3 h). They obtained very high turnover of 288000 for the *C*-alkylation reaction upon significantly decreasing the catalyst loading under solvent-free conditions.[23]

In 2020, Kumar and co-workers reported the *β*-alkylation of 1-phenyl ethanol with benzyl alcohol employing *bis*(imino)pyridine based NNN pincer-ruthenium carbonyl complexes and phosphine complexes. The highest TON of 372000 was achieved with the pincer complex

$^{(Cy2NNN}RuCl_2(CO)$ **(4.21)** under solvent-free conditions under very low base loading (2.5 mol%) (Scheme 4.13).[35a] The catalytic cycle initiates with the generation 16-electron five-coordinate dichloride species *via* PPh_3 or CO dissociation from **4.21** and involves a Ru-H intermediate. Further, a series of control experiments and DFT studies pointed towards the involvement of metal-centred mechanism and *β*-hydride elimination step was found to be the RDS.[35a]

Later in 2021, Bera reported a Cp*Ir(III) complex bearing a pyridyl(benzamide)-functionalized NHC ligand (**4.26**) for the *β*-alkylation of secondary alcohols with primary alcohols operating *via* hydrogen borrowing pathway.[35b] The catalytic system exhibited a broad range of substrate scope under low catalyst loading (0.05mol%) and low base loading (10 mol%) in a very short span of time (Scheme 4.13).[35b] In the same year, Ghosh reported a picolyl-functionalized NHC based ruthenium complex (**4.26´**) for the catalytic cross-coupling of alcohols. They obtained moderate to good yields (*ca.* 63-89%) of the desired products in the presence of 1 mol% **4.26´**, 1 equivalent of base and toluene at 110 °C after 3h (Scheme 4.13).[35b] The catalytic protocol was also extended for the tandem one-pot synthesis of flavan derivatives and plant-derived bio-active natural products.[35b]

In the context of *3d*-metal based *β*-alkylation of alcohols, majorly reports have been described with Cr,[36] Mn,[27, 28] Fe,[30] Co,[29] Ni,[31] and Cu.[32] Although, the base-metals catalyzed reaction have lower activity as compared to their noble-metal counterparts, but their easy availability and high abundance makes them highly desirable candidate and such replacement would result in conservation of our rare element resources.

The first report on chromium catalyzed *β*-alkylation of secondary alcohols with primary alcohols came in 2022, wherein Kumar utilized simple base metal salt $CrCl_3.6H_2O$ and its corresponding NNN-pincer complex **4.24** for this catalytic reaction (Scheme 4.14).[36] This protocol afforded high yields of the *β*-alkylated product **4.13** under both conventional and microwave conditions. At 0.005 mol% loading of **4.24** and 5 mol% of NaO^tBu at 140 °C, 90% yield (180000 TON in 1.5 h at 12000 TOs/h) and 84% yield (16800 TON in 3 h at 5600 TOs/h) of **4.13** was obtained under microwave heating and conventional heating respectively.[36] In the case of $CrCl_3.6H_2O$ under similar conditions, lower yields of **4.13** were obtained under both microwave (*ca.* 76%) as well as conventional heating (*ca.* 79%).

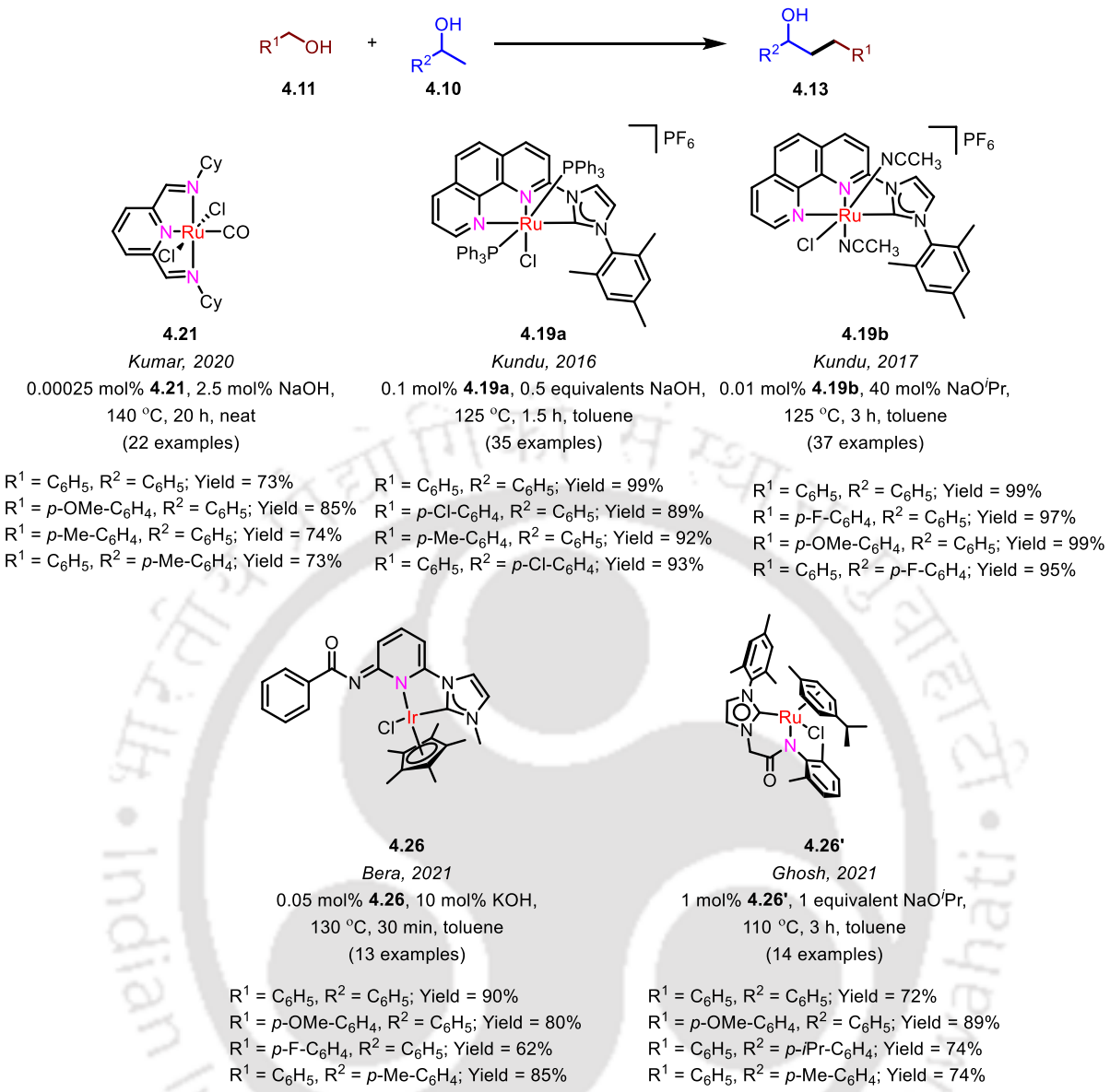

Scheme 4.13. *β*-alkylation of secondary alcohols with primary alcohols using homogeneous complexes based on noble metals ruthenium and iridium.[21, 23, 35]

Kumar and co-workers recently reported that easily accessible $CoCl_2$ (0.01 mol %) is capable of catalyzing *β*-alkylation of alcohols affording high yields of **4.13** (up to 87%) and unprecedented turnovers (ca. 8700) in the presence of only 2.5 mol % of NaO^{t}Bu (Scheme 4.15).[37] They observed that on higher loadings of cobaltous chloride (1 mol%), instant formation of nano-particles were noticed which were well characterized by SEM and TEM analysis. Later, similar studies were performed with NNN pincer-cobalt complexes **4.23** of the type ^{R2}NNN (R = ^{t}Bu, Cy, ^{i}Pr, Ph, *p*-F-C$_6$H$_4$) (Scheme 4.15).[38] While cobaltous chloride at a 0.0025 mol % loading and 2.5 mol % of NaO^{t}Bu at 140 °C resulted in 66% yield of **4.13** (26400 TON at 1100 TOF h^{-1}) in the *β*-alkylation of 1-phenyl ethanol with benzyl alcohol, its corres-

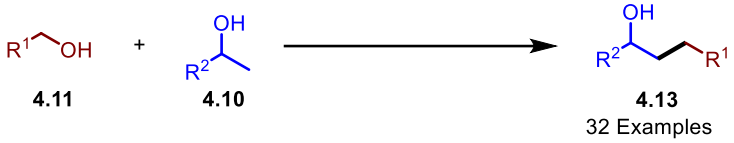

Reaction condition: Conventional
4.24 or $CrCl_3.6H_2O$ (0.005 mol%), NaO^{t}Bu (5 mol%), 140 °C, 3 h, air

Up to 16800 TON with **4.24** and up to 15800 TON with $CrCl_3.6H_2O$

Reaction condition: Microwave
4.24 or $CrCl_3.6H_2O$ (0.005 mol%), NaO^{t}Bu (5 mol%), 140 °C, 1.5 h, 75 W

Up to 18000 TON with **4.24** and up to 15200 TON with $CrCl_3.6H_2O$

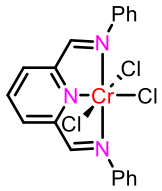

4.24

$R^1 = C_6H_5$, $R^2 = C_6H_5$; Yield = 90%
$R^1 = C_6H_5$, $R^2 = p$-Cl-C_6H_4; Yield = 91%
$R^1 = p$-OMe-C_6H_4; $R^2 = C_6H_5$; Yield = 84%
$R^1 = p$-Me-C_6H_4; $R^2 = C_6H_5$; Yield = 83%

Scheme 4.14. The first report on chromium catalyzed *β*-alkylation of alcohols reported by Kumar and co-workers.[36]

-ponding pincer complex (^{i}Pr2NNN)$CoCl_2$ (0.0025 mol %) was highly efficient (*ca.* 1.3-fold *vs* $CoCl_2$) and afforded 85% yield of **4.13** (*ca.* 34000 TON at 1417 TOF h^{-1}) under similar conditions (Scheme 4.15).[38]

Reaction condition: Conventional
4.23 or $CoCl_2$ (0.0025 mol%), NaO^{t}Bu (5 mol%), 140 °C, 24 h, air

85% yield of **4.13** (up to 34000 TON) with **4.23**
66% yield of **4.13** (up to 26400 TON) with $CoCl_2$

Reaction condition: Microwave
4.23 or $CoCl_2$ (0.0025 mol%), NaO^{t}Bu (5 mol%), 140 °C, 2 h, 75 W

83% yield of **4.13** (up to 33200 TON) with **4.23**
61% yield of **4.13** (up to 24400 TON) with $CoCl_2$

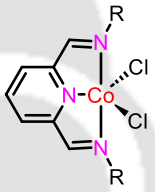

4.23a; R = ^{t}Bu
4.23b; R = Cy
4.23c; R = ^{i}Pr
4.23d; R = Ph
4.23e; R = *p*-F-C_6H_4

$R^1 = C_6H_5$, $R^2 = C_6H_5$; Yield = 85%
$R^1 = C_6H_5$, $R^2 = p$-Br-C_6H_4; Yield = 80%
$R^1 = p$-OMe-C_6H_4; $R^2 = C_6H_5$; Yield = 83%
$R^1 = p$-Me-C_6H_4; $R^2 = C_6H_5$; Yield = 81%

Scheme 4.15. *β*-alkylation of secondary alcohols with primary alcohols employing cobaltous chloride and pincer-cobalt(II) complexes.[38]

Later in 2023, the same group reported a series of Mn(I) complexes (**4.25**) based on *bis*(imino)-pyridine ligands of the type ^{R2}NNN (R = Cy, ^{i}Pr, Ph, *p*-FC_6H_4) (Scheme 4.16).[39] The complexes existed as NN bidentate-Mn(I) *tris* carbonyl species in solid state while in solution phase, a gradual loss of a CO molecule was observed resulting in tridentate-Mn(I) *bis* carbonyl

species which eventually disproportionates to an NNN pincer-Mn(II) dibromide and an NNN pincer-Mn(0) complex.[39]

The pincer-Mn(I) complexes were then investigated for the catalytic *β*-alkylation of secondary alcohols by primary alcohols (35 substrates) at 0.05 mol% catalyst loading in presence of 2.5 mol% of NaO^{t}Bu under both conventional (air, 140 °C, 12h) and microwave heating (75 W, 2h) (Scheme 4.16). Among the complexes investigated, **4.25d** gave maximum yield of 92% (1840 TON) under conventional heating and yield of 85% (1700 TON) was obtained under microwave conditions.[39]

In the context of iron-based complexes mediated alkylation of alcohols, the first report came from Sun in 2012, where he employed commercially available and inexpensive ferrocenecarboxaldehyde (**4.18**) for the catalytic *β*-alkylation of secondary alcohols with primary alcohols.[30] In this protocol, 97% yield of *β*-alkylated product with 97% selectivity was achieved when 5 mol% of ferrocenecarboxaldehyde was reacted with benzyl alcohol and 1-phenyl ethanol in presence of 20 mol% NaOH, in *p*-xylene, at 130 °C for 12 h (Scheme 4.17).[30]

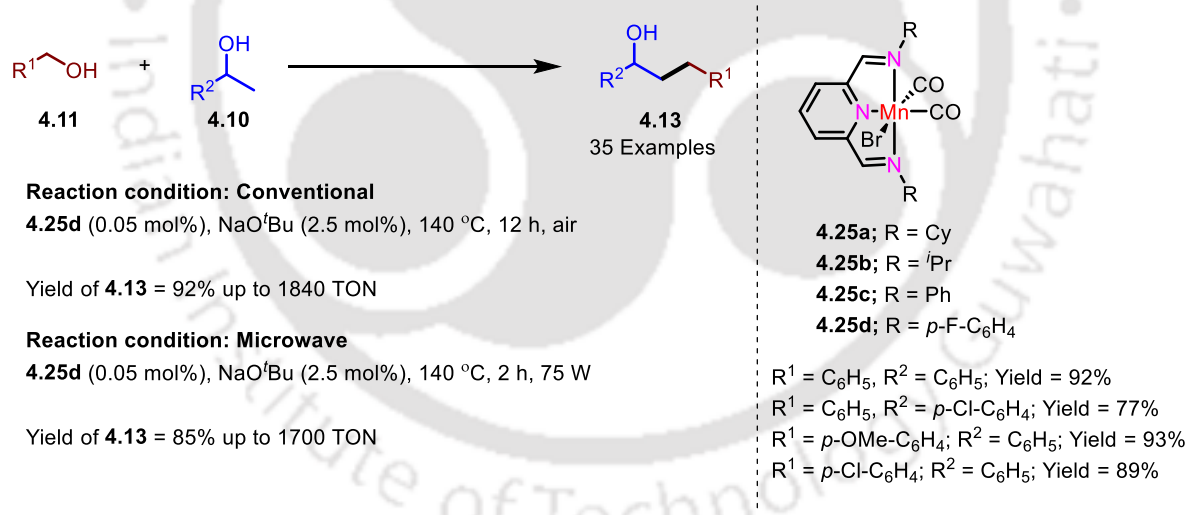

Scheme 4.16. Pincer-Mn(I) catalyzed *β*-alkylation of secondary alcohol with primary alcohols.[39]

In the context of alkylation of alcohols utilizing homogeneous nickel complexes, the first report came in 2019 from Lang and co-workers, where they exhibited the utility of hexanickel cluster embedded with a 4,6-dimethylpyrimidine-2-thion ligand (**4.27**) in mediating the C–C bond formation *via* hydrogen borrowing methodology.[31] The Ni(II) catalyst (**4.27**) displayed good activity towards synthesis of *α*-alkylated ketones, *α,β*-unsaturated ketones, and quinolines

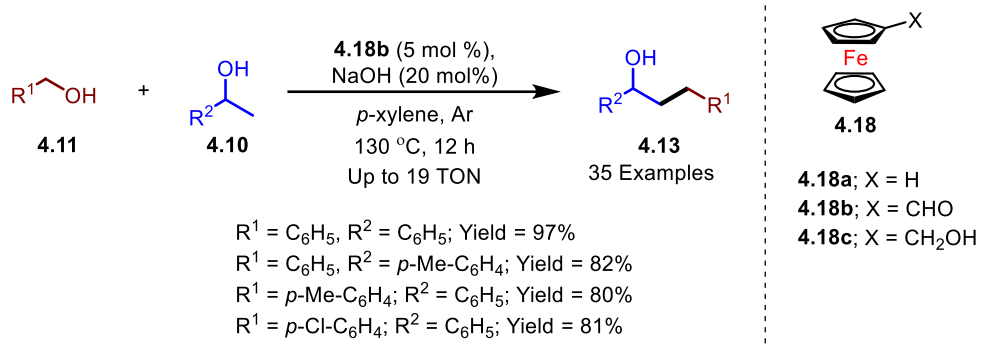

Scheme 4.17. *β*-alkylation of secondary alcohols with primary alcohols using ferrocenecarboxaldehyde described by Sun in 2012.[30]

under slightly different optimized conditions. Performing the reaction at higher temperatures and under sealed conditions afforded complete hydrogenation of *α,β*-unsaturated ketones and resulted in corresponding alcohols (**4.13**) (Scheme 4.18).[31]

Later in 2021, Balaraman demonstrated the *β*-alkylation of alcohols employing $NiBr_2$/TMEDA (1:1) system along with 1 equivalent of KOH at 130 °C in the presence of *n*-octane as solvent (Scheme 4.19).[40] A broad range of substrates including aromatic, cyclic, acyclic and, aliphatic alcohols were tolerated by $NiBr_2$/TMEDA and the scope was further extended towards the double alkylation of cyclopentanol with various alcohols (Scheme 4.19). The initial mechanistic studies and isotopic labelling experiments pointed towards the operation of hydrogen borrowing strategy in the C–C coupling reaction, with the formation of water as a by-product.[40]

Apart from transition-metal catalyzed alkylation of secondary alcohols with primary alcohols, there have been few reports employing metal-free conditions where the *β*-alkylated alcohol is obtained in the presence of high base loading (up to 100 mol%) (Scheme 4.20).[2, 3, 41, 42] But, this process leads to the generation of enormous amounts of waste leading to poor atom economy and selectivity.[3] The first report was published by Crabtree in 2010, where he used metal hydroxides (1 equivalent KOH or NaOH) for the alkylation of several 1-phenylethanol derivatives with primary alcohols under air.[2] They observed complete conversion of the starting materials to *β*-alkylated alcohol and *α*-alkylated ketone (up to 99%) but with low selectivity towards the *β*-alkylated product (*ca.* 78% yield). Recently, Gunanathan and Wendt also utilized KOH (up to 25 mol%) for the base-mediated alkylation of alcohols in the presence of toluene at 135 °C and 120 °C respectively (Scheme 4.20).[42, 43] Gunanathan observed the involvement of radical intermediates in the catalytic cycle, which was proved using radical scavengers and

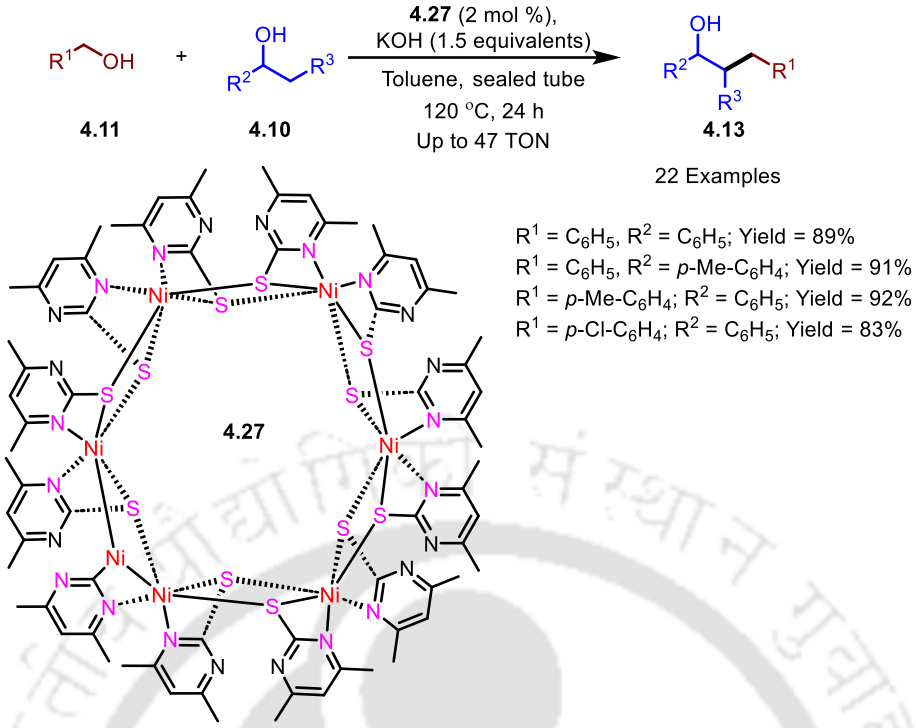

Scheme 4.18. Nickel(II) catalyzed cross coupling of secondary alcohol with primary alcohol reported by Lang.[31]

EPR studies.

4.2 Objectives

In chapter II and III, a series of NNN pincer-ruthenium complexes (Figure 3.11) were demonstrated towards the aqueous reforming of (m)ethanol resulting in high yields of corresponding acids and hydrogen. Notably, dehydrogenation is a key step here.[1] Therefore, our aim in current chapter is to move away from precious metals and test the ability of earth abundant base metal such as nickel towards the transformation of alcohols where dehydrogenation is a key step. Formation of C-C bonds using alcohols as alkylating agents involves dehydrogenation as a pivotal step and is a very convenient reaction to probe. On the basis of these facts, the current chapter attempts to address the following questions,

- In comparison to corresponding noble metals, will NNN pincer-nickel(II) complexes show good activity towards the alkylation of alcohols, that involve a key dehydrogenation step?
- Is it possible to achieve *β*–alkylation of alcohols at low base loadings in the pincer-nickel catalyzed reactions?

- Will it be possible to obtain a detailed kinetic and mechanistic understanding of the process?
- Can these pincer-nickel complexes tolerate vast substrate scope and afford good yields of the desired product?

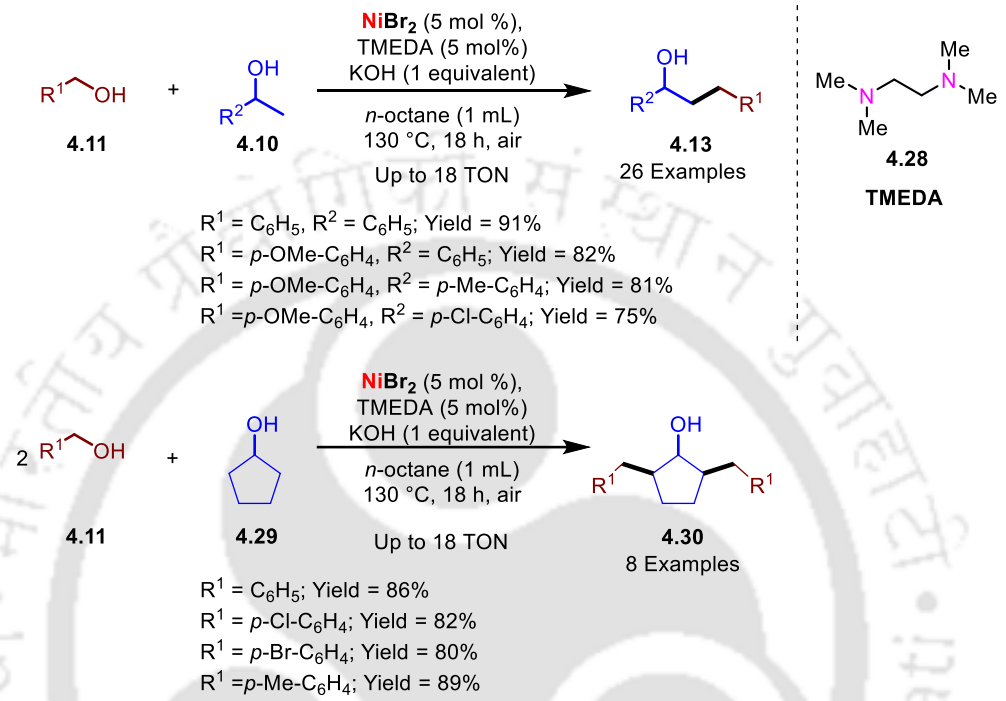

Scheme 4.19. *β*-alkylation of secondary alcohols with primary alcohols catalyzed by a $NiBr_2$/TMEDA (1:1) system reported by Balaraman and co-workers.[40]

4.3 Results and Discussion

4.3.1 Synthesis and characterization of pincer-nickel complexes based on *bis*(imino)pyridine ligands.

The NNN pincer ligands[44, 45] and their corresponding Ni complexes[46] were synthesized according to our recently reported protocol (Scheme 4.21). Treatment of anhydrous $NiCl_2$(DME) (DME = dimethoxyethane) with (^{R2}NNN) ligand in acetonitrile at room temperature for 20 h, followed by washing with diethyl ether, afforded the corresponding pincer-Ni(II) complexes (**4.32a-e**) in good yields (Scheme 4.21). While NMR analysis was not possible for these paramagnetic complexes, the magnetic susceptibility measurements of these complexes provided evidence for their octahedral structure and paramagnetic nature (**4.32a**, $\mu_{eff} = 3.20\ \mu_B$; **4.32b**, $\mu_{eff} = 3.28\ \mu_B$; **4.32c**, $\mu_{eff} = 3.21\ \mu_B$; **4.32d**, $\mu_{eff} = 3.01\ \mu_B$; **4.32e**, $\mu_{eff} = 4.24\ \mu_B$) due to the presence of 2 unpaired electrons ($S = 1$).[47-49]

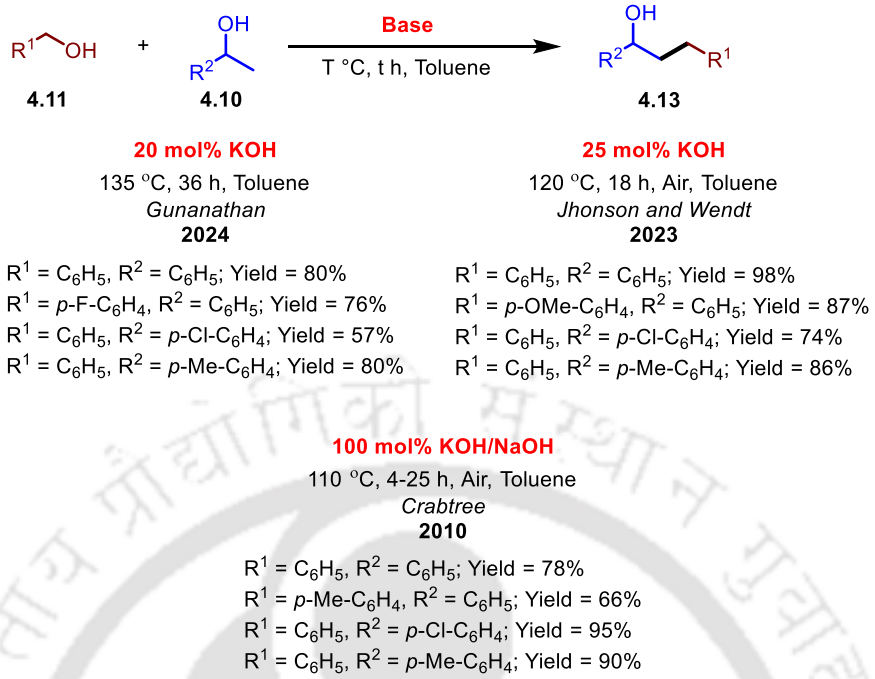

Scheme 4.20. Base mediated *β*-alkylation of secondary alcohols with primary alcohols reported independently by Crabtree, Wendt and, Gunanathan.[3, 41, 42]

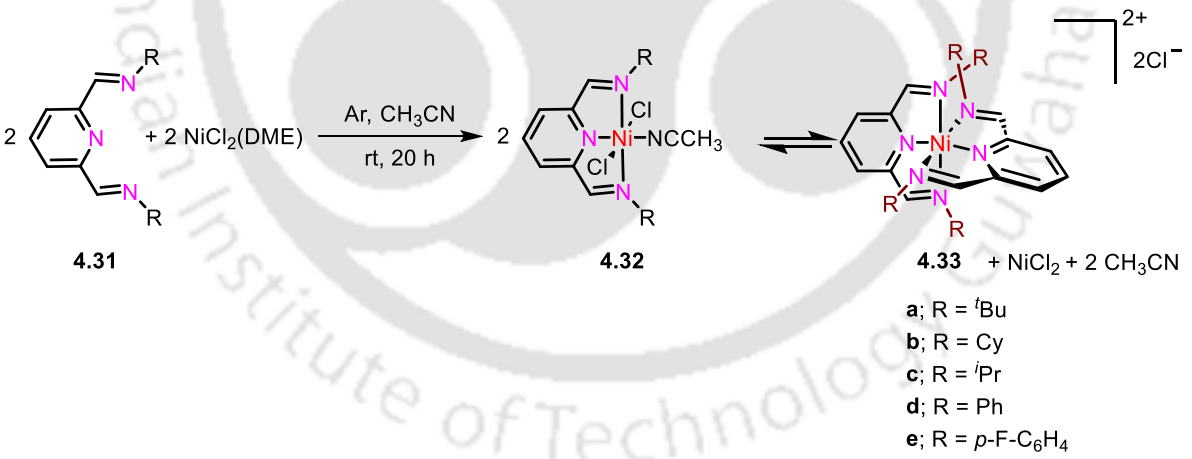

Scheme 4.21. A general pathway to the synthesis of (^{R2}NNN)NiCl$_2$(CH$_3$CN) (**4.32a-e**).

The EPR signals of the octahedral complexes **4.32a-e** were broad and hard to detect (even at very low temperatures, Figures S3.107-S3.110, Appendix III) which is typical of an octahedral d^8 Ni(II) species.[50-52]

The single-crystal X-ray analysis of **4.32c′** (obtained by the substitution of acetonitrile in **4.32c** by a water molecule)[46] showed Ni is in an octahedral environment having the pincer ligand

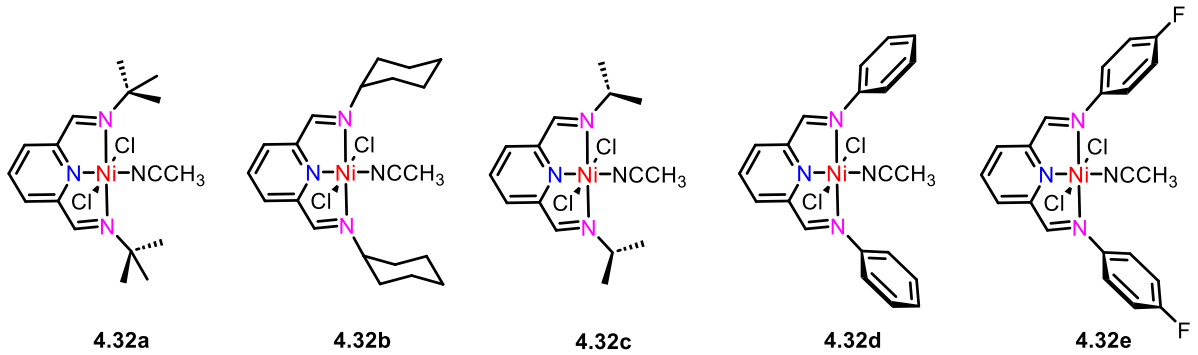

Figure 4.11. Pincer-nickel(II) complexes employed in current study.

bound in a meridional fashion with the two chlorides *trans* to each other (Figure 4.12). Surprisingly, crystallization of **4.32e** *via* slow evaporation from methanol led to the isolation of a dicationic complex **4.33e** (presumably formed due to its equilibration with **4.32e** in the mother liquor (Scheme 4.21)) where the Ni is in an octahedral environment with two pincer ligands attached to it in a meridional geometry (Scheme 4.21). While the complex **4.32c′** crystallized in the C2/c space group, the dicationic complex **4.33e** crystallized in the triclinic $P\bar{1}$ space group (Figure 4.12). The Ni–N(pyridyl) bond distance was slightly longer in the case of neutral complex **4.32c′** (**4.32c′**, 2.008(6) Å; **4.33e**, 1.983(3) Å) (Table 4.10). On the other hand, the Ni–N(imine) bond length was similar in both the complexes (**4.32c′**, 2.171(5) Å; **4.33e**, 2.172(3) Å) (Table 4.10). The (pyridyl)N–Ni–N(imine) bond angles in both the complexes were comparable (**4.32c′**: 77.60(5)°; **4.33e**: 77.73(12)°). A detailed comparison of the crystallographic parameters of **4.32′** and **4.33e** is provided in Table 4.10.

Table 4.10. Selected crystallographic bond distances (Å) and bond angles (°) of complexes **4.33e** and **4.32c′**.

4.33e		**4.32c′**	
Ni-N (Å) (Pyridine)	1.983(3)	Ni-N (Å) (Pyridine)	2.008(6)
Ni –N (imine) (Å)	2.172(3)	Ni –N (imine) (Å)	2.171(5)
(Imine)N-Ni-N(Imine) (°)	154.13(10)	(Imine)N-Ni-N(Imine) (°)	153.4(2)
		Ni-Cl (Å)	2.4167(14)
(Pyridine)N-Ni-N(Imine) (°)	77.73(12)	Ni-OH_2 (Å)	2.049(7)
		N=C-Ni-Cl (°)	86.49
		<Ar-N-Ni-N=C (°)	77.60(5)
		<Cl-Ni-OH_2 (°)	88.03(5)

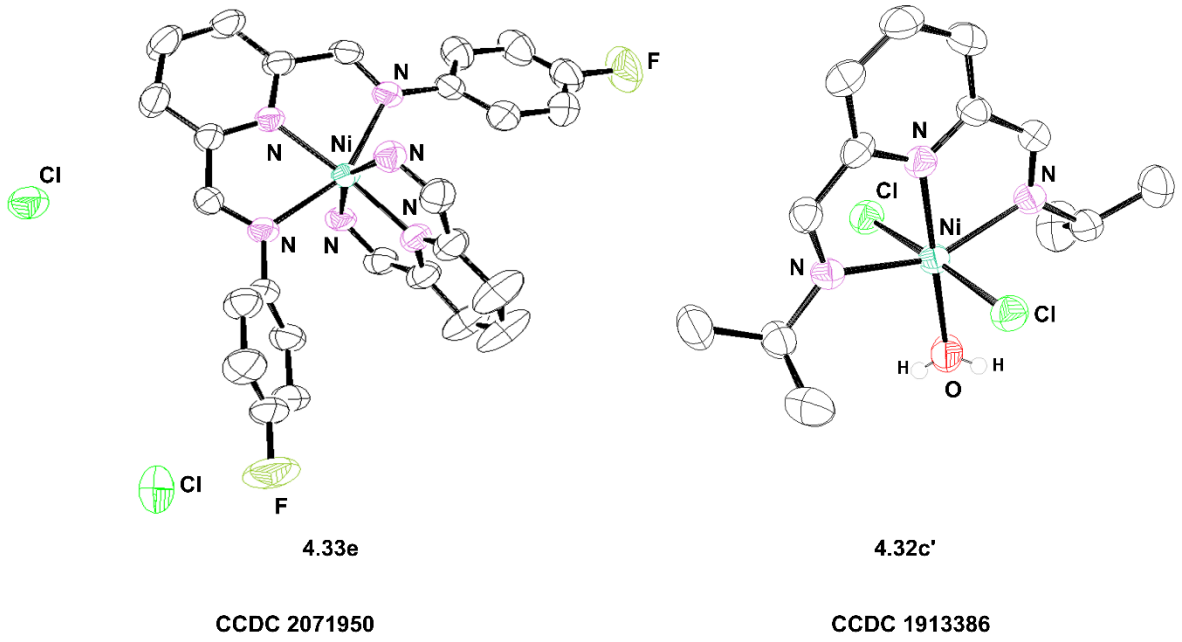

Figure 4.12. Crystal structures of **4.33e** and **4.32c´** with ORTEP drawn at 50% probability. All the hydrogen atoms and the aromatic groups on two N atoms of one of the pincer fragment in **4.33e** are omitted for the sake of clarity.

Interesting observations were made from the HRMS analysis that provided evidence for the presence of fragments originating from both **4.32** and **4.33** (Figures S3.69, S3.74, S3.78, S3.82 and, S3.86, Appendix III). For instance, the HRMS analysis of **4.32a** showed peaks at m/z values 274.1783 and 338.1178 that correspond to [**4.32a** – 2Cl]$^{2+}$ and [**4.32a** – CH_3CN − Cl]$^{+}$, respectively. Similar observations were made in the HRMS analysis of the other considered complexes (Figures S3.69, S3.74, S3.78, S3.82 and, S3.86, Appendix III). Single-crystal X-ray analysis and HRMS studies thus clearly indicate that, in solution, the complex **4.32** exists in equilibrium with **4.33** (Scheme 4.21), the extent of which is likely to be different for various complexes based on the nature of the R group (R = ^{i}Pr, ^{t}Bu, Cy, Ph, and *p*-F-C_6H_4). The pincer-Ni complexes (**4.32a-e**)/ (**4.33a-e**) demonstrated very good thermal stability as indicated by the TGA analysis (Figure S3.65-S3.68, Appendix III) and they were stable up to 250-300 °C. The mass loss could be correlated to loss of fragments either from **4.32** or from **4.33** (Figure S3.65-S3.68, Appendix III).

4.3.2 Investigations on the pincer-nickel catalyzed *β*–alkylation of 1-phenyl ethanol with benzyl alcohol.

To arrive at the optimal conditions, the catalytic *β*-alkylation reactions were initiated in the

presence of **4.32a-e** along with a variety of bases using 1-phenyl ethanol and benzyl alcohol as a model secondary and primary alcohol, respectively, at 140 °C (Table 4.11). At a loading of 0.01 mol % of **4.32d**, the reaction of **4.10** with **4.11** did not proceed when 5 mol % of either Na_2CO_3 or K_2CO_3 was used (entries 1 and 2, Table 4.11). Poor yields of *β*-alkylated product **4.13** were obtained when the **4.32d** (0.01 mol %) catalyzed reaction was performed independently with KO^{t}Bu (5 mol %) and KOH (5 mol %) (entries 3 and 4, Table 4.11). On the other hand, use of 5 mol % of NaOH provided moderate yields (68%) of **4.13** in the **4.32d** (0.01 mol %) catalyzed reaction (entry 5, Table 4.11). The yields of **4.13** dropped steadily upon lowering the NaOH loading (entries 6 and 7, Table 4.11). Employing Na (5 mol %) to generate the base *in-situ* (prior to addition of **4.32d**) resulted in yields that are comparable to that obtained with the use of NaOH (5 mol %) (entry 5 *vs* entry 8, Table 4.11). The yield of **4.13** improved (75%) with the use of NaO^{t}Bu (5 mol %) in the **4.32d** (0.01 mol %) catalyzed *β*-alkylation of **4.10** with **4.11** (entry 9, Table 4.11).

Similar to the observations made during the use of NaOH, lowering the amounts of NaO^{t}Bu led to reduced yields (entries 10 and 11, Table 4.11). Lowering the loading of **4.32d** to 0.005 mol % while maintaining NaO^{t}Bu at 5 mol % resulted in about 82% of **4.13** and 11% of **4.12** that amounts to a total of 18600 TON (**4.12** + **4.13**) (entry 12, Table 4.11). Repeating the same at a lower temperature (120 °C) or with a different base (5 mol % NaOH) resulted in a decrease in productivity of **4.13** (entries 13 and 15, Table 4.11). The *β*-alkylation of **4.10** with **4.11** did not proceed either in the absence of a base (entry 14, Table 4.11) or in the absence of a catalyst.[35] Under the optimized conditions comprising 0.005 mol % of Ni catalyst in the presence of NaO^{t}Bu (5 mol %) at 140 °C, the total turnovers (**4.12** + **4.13**) obtained were clearly lower with the other considered catalysts (entries 16–21, Table 4.11) in comparison with **4.32d** (entry 12, Table 4.11).

The practical utility of this reaction was confirmed by carrying out the **4.32d** (0.005 mol %) catalyzed *β*-alkylation of 1 g of **4.10** with 0.895 g of **4.11** in the presence of 5 mol % of NaO^{t}Bu at 140 °C to obtain 1.301 g of **4.13** in 74% isolated yield and 85% selectivity. The synthetic utility of the optimized catalytic system (entry 12, Table 4.11) was further investigated for the catalytic *β*-alkylation of several 1-phenyl ethanol derivatives with a variety of benzyl alcohols (Table 4.12 and Table 4.13).

In most cases, good tolerance was observed for the electron-withdrawing (–Cl, –F) and electron-donating (–Me, –OMe) groups at the *para* and *meta* positions of the phenyl ring in

Table 4.11. Solvent-free *β*-alkylation of 1-phenyl ethanol with benzyl alcohol under varying conditions.

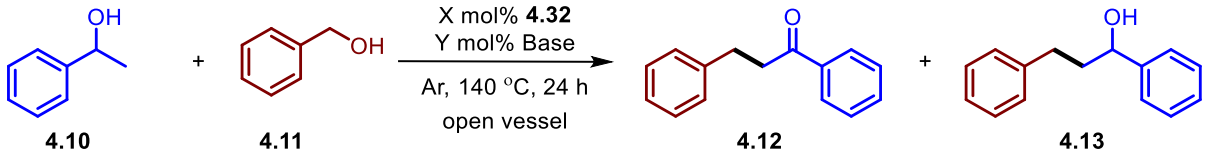

Entry	Base (Y mol%)	Catalyst (X mol %)	% Yield[a] [TON]		Selectivity of **4.13**[b]
			4.12	**4.13**	
1	Na_2CO_3 (5)	**4.32d** (0.01)	0 [0]	0 [0]	0
2	K_2CO_3 (5)	**4.32d** (0.01)	1 [100]	0 [0]	0
3	KO^{t}Bu (5)	**4.32d** (0.01)	2 [100]	23 [2300]	92
4	KOH (5)	**4.32d** (0.01)	3 [300]	31 [3100]	91
5	NaOH (5)	**4.32d** (0.01)	2 [200]	68 [6800]	97
6	NaOH (2.5)	**4.32d** (0.01)	2 [200]	37 [3700]	95
7	NaOH (1.25)	**4.32d** (0.01)	2 [200]	15 [1500]	88
8	Na (5)	**4.32d** (0.01)	9 [900]	62 [6200]	87
9	NaO^{t}Bu (5)	**4.32d** (0.01)	14 [1400]	75 [7500]	84
10	NaO^{t}Bu (2.5)	**4.32d** (0.01)	3 [300]	47 [4700]	94
11	NaO^{t}Bu (1.25)	**4.32d** (0.01)	7 [700]	18 [1800]	72
12[c]	NaO^{t}Bu (5)	**4.32d** (0.005)	10±1 [2200]	82±1 [16400]	89
13[d]	NaO^{t}Bu (5)	**4.32d** (0.005)	2 [400]	51 [10200]	96
14	--	**4.32d** (0.005)	0 [0]	0 [0]	0
15	NaOH (5)	**4.32d** (0.005)	23 [4600]	71 [14200]	75
16[c]	NaO^{t}Bu (5)	**4.32c** (0.005)	12±3 [2400]	78±1 [15600]	87
17[c]	NaO^{t}Bu (5)	**4.32a** (0.005)	9±1 [1800]	80±2 [16000]	90
18[c]	NaO^{t}Bu (5)	**4.32b** (0.005)	11±0 [2200]	76±3 [15200]	87
19[c]	NaO^{t}Bu (5)	**4.32e** (0.005)	13±1 [2600]	77±2 [15400]	86
20	NaO^{t}Bu (5)	$NiCl_2$ (0.005)	2 [400]	50 [10000]	96
21	NaO^{t}Bu (5)	$NiCl_2$(DME) (0.005)	3 [600]	77 [15400]	96
22[c]	NaO^{t}Bu (5)	**4.33e** (0.005)	16±1 [3200]	72±2 [14400]	82
23	K_3PO_4	**4.32d** (0.005)	1 [200]	3 [600]	75

[a]Reaction conditions: 4.14 mmol of **4.10**, 4.14 mmol of **4.11**, X mol% of **4.32** and Y mol% of base at 140 °C. [a]Yield was determined from ^{1}H NMR using toluene as a standard. [b]Selectivity of **4.13** = (Yield of **4.13**/Total yield of **4.12** and **4.13)** *100. [c]Yield reported as an average of two runs. [d]Reaction was performed at 120 °C.

primary alcohols, affording good yields of the desired products (**4.13a-g**, Table 4.12) with high selectivity (up to 98%, Table 4.12). A decrease in product yield (**4.13h-l**, Table 4.12) barring **4.13l** was observed when heteroaromatic primary alcohols were used as alkylating agents presumably due to inhibition of Ni by the heteroatoms. The inhibition affect appears to be more pronounced in the case of **4.13h** that is capable of forming a chelate with the Ni center. The formation of **4.13l** in good yields points to the poor inhibition of the Ni(II) by the relatively soft S. Aromatic primary alcohols consisting of naphthyl and anthracyl groups could be used as alkylating agents with moderate yields (**4.13m-n,** Table 4.12). Lower yields were observed upon use of primary aliphatic alcohols (**4.13o**, **4.13p**, and **4.13q**, Table 4.12).

A general trend of good yields was observed across various 1-phenylethanol substrates using benzyl alcohol as alkylating agent in the **4.32d** (0.005 mol %) catalyzed *β*-alkylation at 140 °C (Table 4.13). However, in particular, the presence of electron-withdrawing groups in the *meta* position (–Cl and CF_3 in **4.13y** and **4.13zd**, respectively, Table 4.13) and in the *para* position (–F, $–OCF_3$, and NO_2 in **4.13u**, **4.13ze**, and **4.13zf**, respectively, Table 4.13) leads to lower yields of products. A lower yield was also obtained for the *β*-alkylation of an aliphatic secondary alcohol (**4.13zg**, Table 4.13).

Mechanistic studies (*vide infra*) have indicated that the aldol condensation of benzaldehyde **4.11′** with acetophenone **4.10′** is the rate-determining step (RDS). Apparently, electron-withdrawing groups on **4.10** are likely to have a detrimental effect on the overall yield of the reaction. Accordingly, very poor yields of **4.13u** were obtained as a result of the highly electronegative fluoro group in the *para* position that withdraws electrons by an inductive effect. The compound **4.13v** that had a less electronegative chloro group was obtained in better yields.

The higher yields of **4.13v** in comparison with **4.13y** can be traced to the fact that the inductive effect of the chloro group is more pronounced at the *meta* position as compared to the *para* position considering the fact that the inductive effect of a substituent is directly proportional to the distance.[53, 54] However, upon replacement of chloro with a poorer electron-withdrawing and less electronegative bromo substituent in **4.13w** and **4.13x**, the inductive effect is hardly noticeable. Not surprisingly, the yields of the corresponding *para*- and *meta*-substituted bromo derivatives **4.13w** and **4.13x** are comparable. The $-CF_3$ group demonstrates an electron-withdrawing nature only by an inductive effect which is more significant in the *meta* position in comparison to the *para* position. Rightly, the yield of **4.13zd** was poorer than that of **4.13zc.**

Table 4.12. **4.32d** catalyzed solvent-free *β*-alkylation of 1-phenyl ethanol with a variety of benzyl acohols.

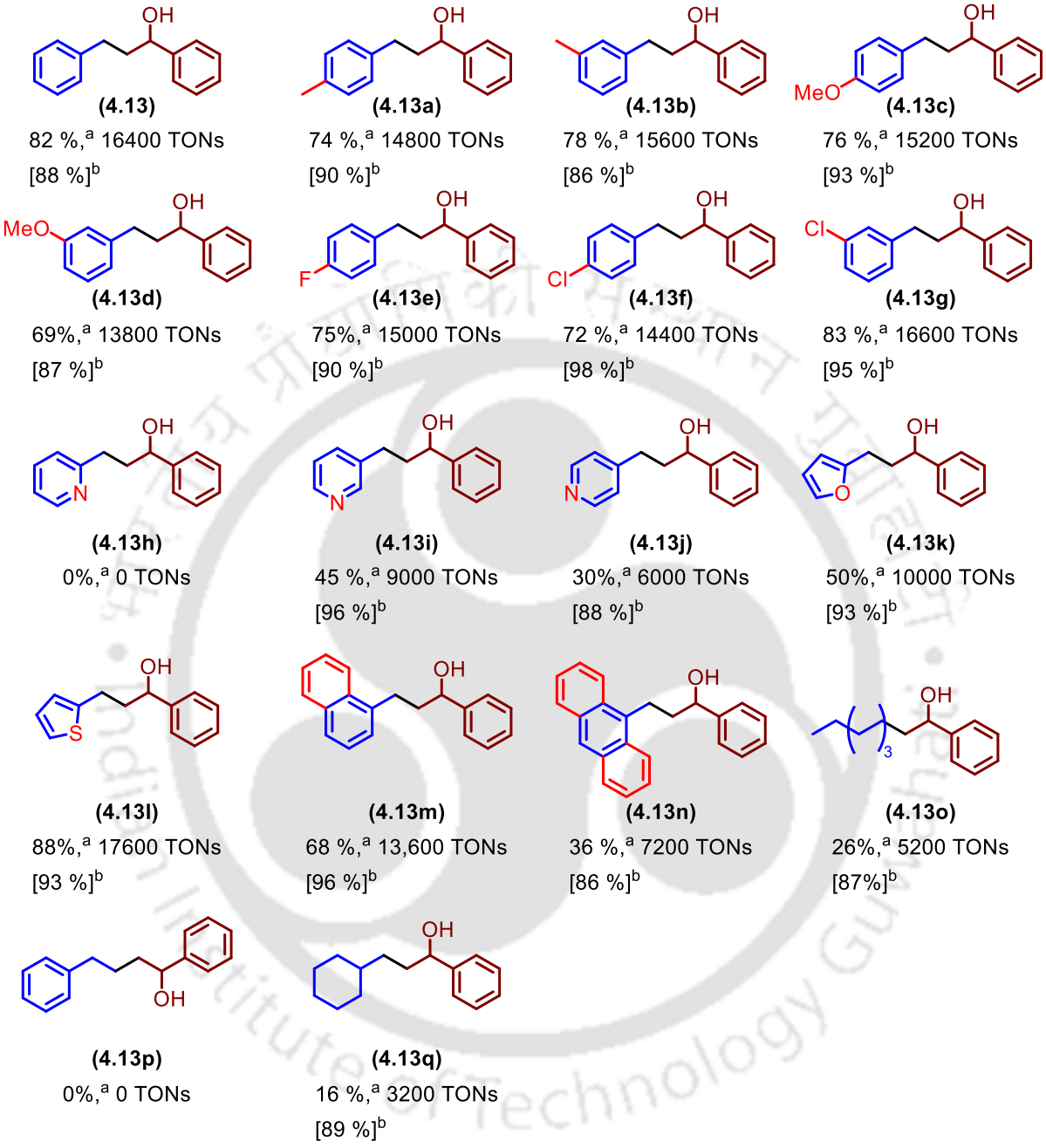

Reaction conditions: 4.14 mmol of **4.10**, 4.14 mmol of **4.11**, 5 mol% of NaO^{t}Bu (0.04 g, 0.416 mmol) and 0.005 mol% of **4.32d** (0.0002 g, 0.44 μmol) at 140 °C. [a]Yield was determined from ^{1}H NMR using toluene as a standard. [b]Selectivity of **4.13** is mentioned in parenthesis **(**(Yield of **4.13**/ Total yield (**4.12** + **4.13**) *100).

However, in the case of **4.13zf**, the nitro group exhibits a very strong electron-withdrawing character due to the involvement of both inductive and resonance activities that result in a complete mitigation of reactivity.

Table 4.13. **4.32d** catalyzed solvent-free *β*-alkylation of 1-phenyl ethanol derivatives with benzyl acohol.

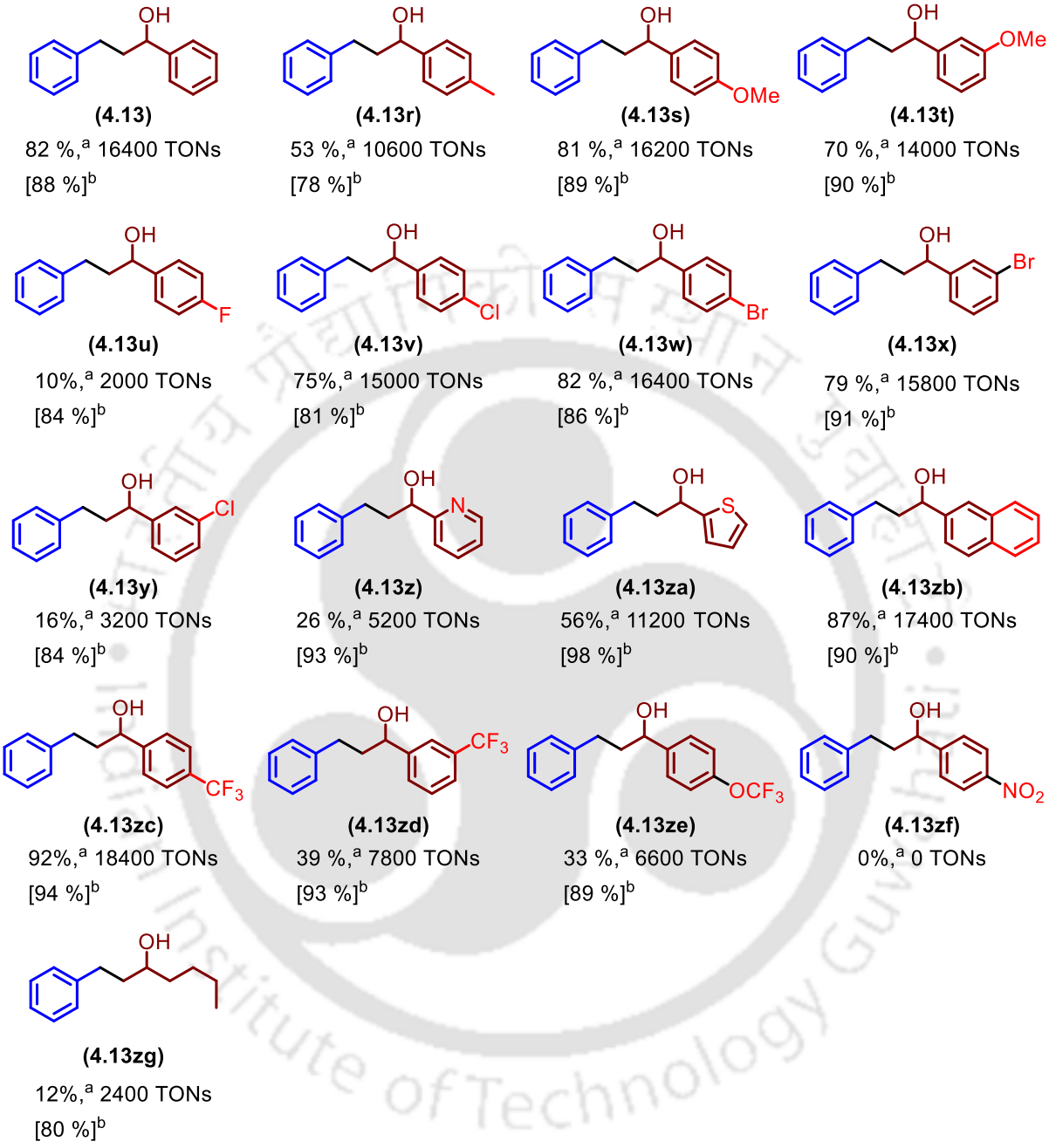

Reaction conditions: 4.14 mmol of **4.10**, 4.14 mmol of **4.11**, 5 mol% of base (0.04 g, 0.416 mmol) and 0.005 mol% of **4.32d** (0.0002 g, 0.44 μmol) at 140 °C. [a]Yield was determined from ^{1}H NMR using toluene as a standard. [b]Selectivity of **4.13** is mentioned in parenthesis **((**Yield of **4.13**/ Total yield (**4.12** + **4.13**) *100).

4.3.3 Control experiments and mechanistic insights

The hydrogen evolution was demonstrated in the **4.32c** catalyzed dehydrogenation of **4.11** with an associated formation of benzaldehyde **4.11′** and trace amounts of benzyl benzoate (equation

1, Scheme 4.22).[46] Similarly, one could anticipate formation of **4.10′** and hydrogen in the **4.32**

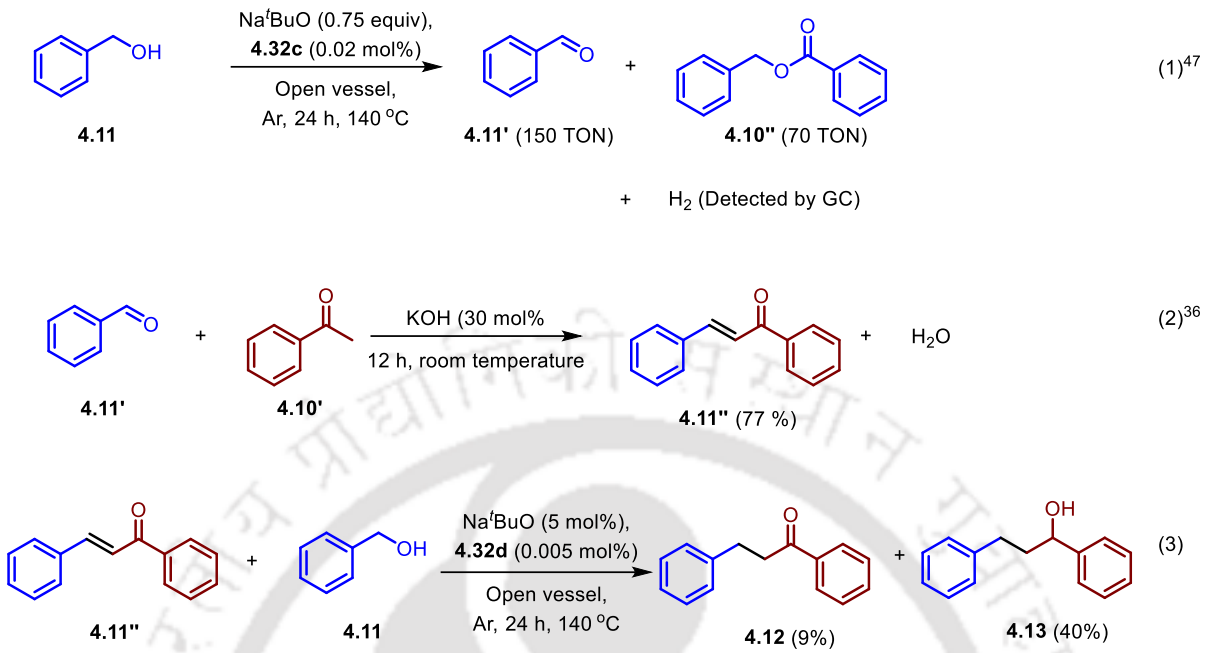

Scheme 4.22. Control experiments.

catalyzed dehydrogenation of **4.10**. The reaction of **4.10′** and **4.11′** in the presence of catalytic amounts of base yields the *α,β*- unsaturated ketone **4.11″** (equation 2, Scheme 4.22).[35a] Furthermore, **4.11″** has been detected in the reaction mixture by HRMS experiments (Figures S3.101, S3.104, and S3.105, Appendix III). Transfer hydrogenation of **4.11″** with **4.11** results in the formation of a mixture of **4.12** (9% isolated yield with respect to **4.11″**) and 4.13 (40% isolated yield with respect to **4.11″**) (equation 3, Scheme 4.22). The above observations in addition to the fact that both **4.12** and **4.13** are isolated in minor and major amounts, respectively (Table 4.11), form the basis of the proposed mechanism (Scheme 4.23) for the **4.32** catalyzed *β*- alkylation of **4.10** with **4.11** under open-vessel conditions.

Treatment of the NNN pincer-Ni complex with NaO^{t}Bu in the presence of **4.11**/**4.10** results in the formation of **4.35**/**4.34** by the dissociation of either CH_3CN from **4.32** or the ligand **4.31** from **4.33** along with the formation of NaCl (Scheme 4.23).[46] The *β*-hydride elimination from **4.35**/**4.34**, followed by extrusion of **4.11′**/**4.10′**, results in the formation of a pincer Ni-H species **4.36** similar to that reported by us earlier (Scheme 4.23).[46] The active species **4.35**/**4.34** is regenerated by the alcoholysis of **4.36** with **4.11**/**4.10** along with the liberation of H_2. In the presence of NaO^{t}Bu, the aldol reaction of **4.11′** with **4.10′** results in the formation of *α,β*-unsaturated ketone **4.11″**.

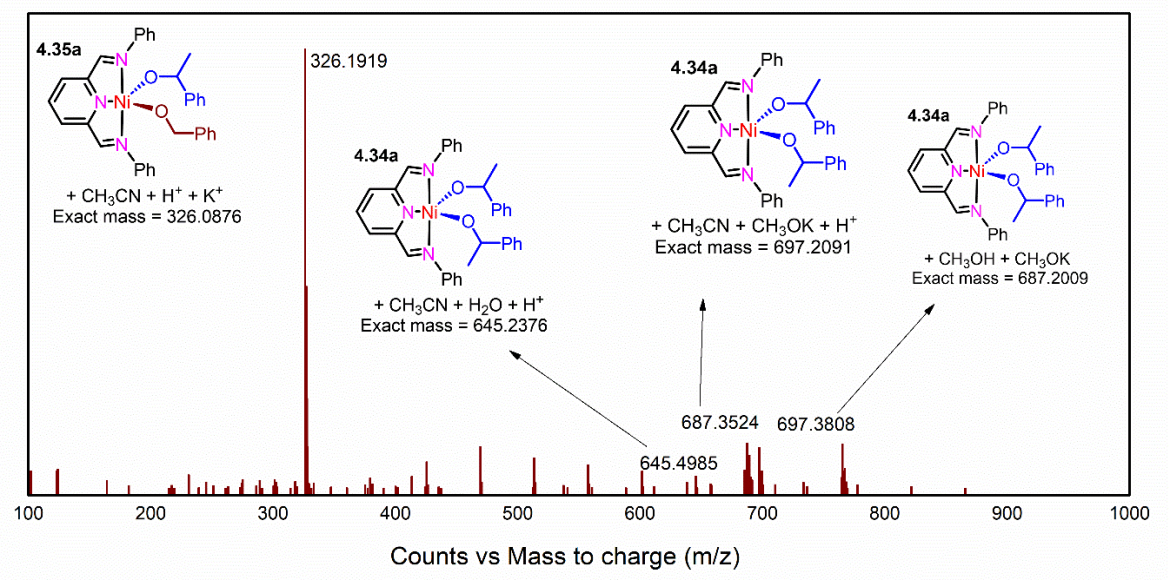

Figure 4.13. HRMS analysis of the reaction mixture containing **4.10** and **4.11** in the presence of 0.5 mol% **4.32d** (0.02 g, 0.044 mmol) and Na^{t}BuO (0.04 g, 0.416 mmol) at t = 0 h at room temperature.

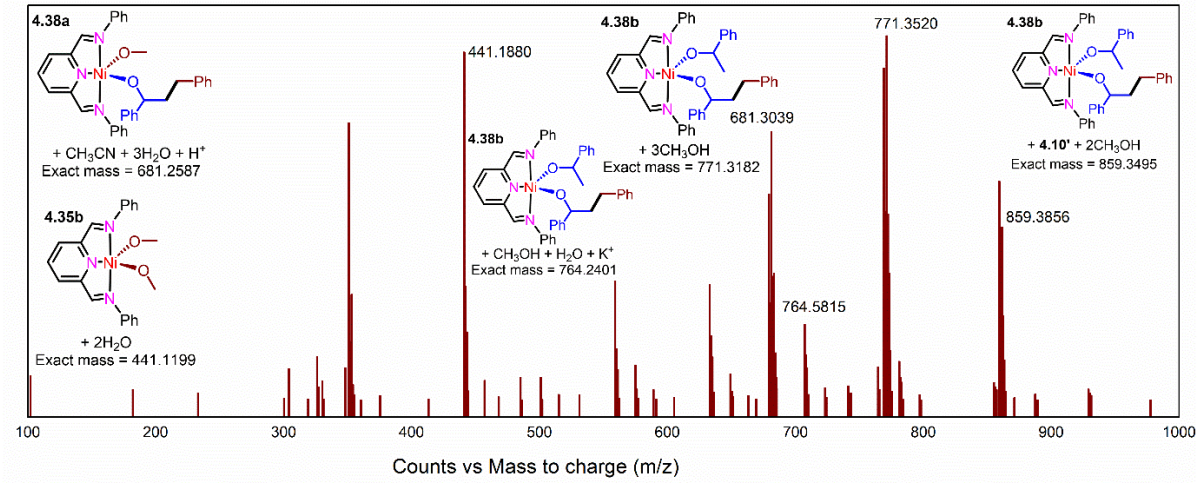

Figure 4.14. HRMS analysis of the reaction mixture containing **4.10** and **4.11** in the presence of 0.5 mol% **4.32d** (0.02 g, 0.044 mmol) and Na^{t}BuO (0.04 g, 0.416 mmol) at t = 2 h at 140 °C.

Insertion[35] of the C−C double bond in **4.11″** into the Ni−H bond of **4.36** results in the formation of intermediate **4.37** (Scheme 4.23). The carbonyl compound **4.12** is obtained from **4.37** either by the hydrogenolysis with H_2 or by the alcoholysis with **4.11**/**4.10** while regenerating **4.36**/**4.35**/**4.34**. A similar insertion, followed by a hydrogenolysis/alcoholysis pathway involving **4.36**→ **4.38**→ **4.36**/**4.35**/**4.34**, can account for the transformation of **4.12** to **4.13** (Scheme 4.23). We have previously shown that both hydrogenolysis and alcoholysis contribute

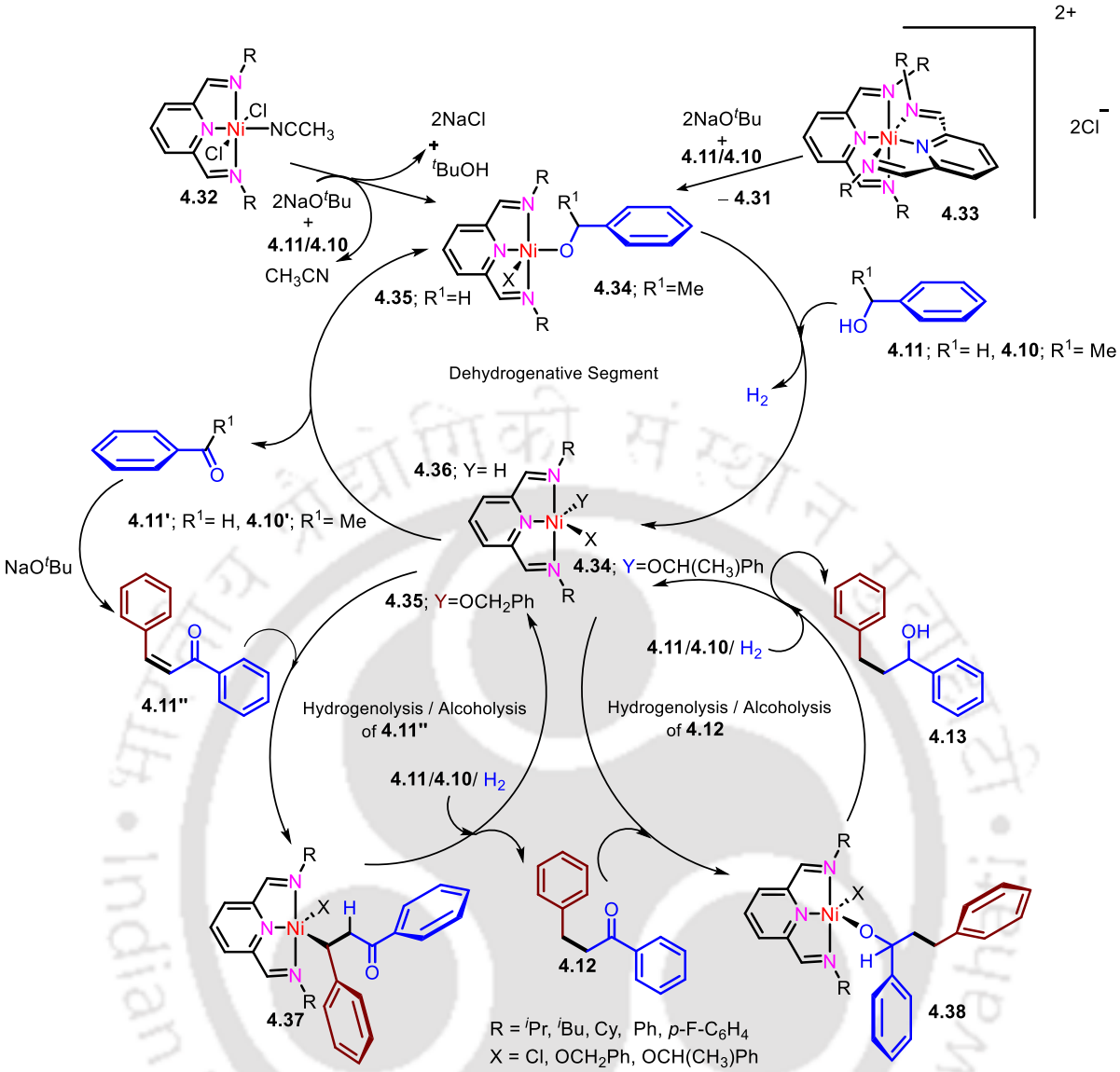

Scheme 4.23. Plausible mechanism involved in the **4.32**/**4.33** catalyzed *β*-alkylation of **4.10** with **4.11**.

to the **4.32c** catalyzed *N*-alkylation reactions under open-vessel conditions.[46] DFT studies indicate that the latter is the more favorable path in comparison to the former.[46] Despite the low-steady state concentration of hydrogen in the reaction mixture, the highly pressurized conditions in closed vessel systems would ensure hydrogenolysis not only leading to the product but also to the starting material alcohol which typically results in lower reactivity. On the other hand, the alcoholysis step would be the major contributor under open-vessel conditions owing to equilibrium driven reasons. Not surprisingly, in the case of *N*-alkylation of benzyl alcohol,[46] open-vessel condition gave higher overall yield (*ca.* 60%) in comparison to closed vessel (*ca.* 43%). Therefore, in the present work open-vessel conditions

were employed and the fact that **4.13** is obtained as a major product in our current studies further fortifies the involvement of alcoholysis as the major contributor to the observed reactivity (Scheme 4.23).

Valuable information on the intermediates proposed in Scheme 4.23 was obtained from the HRMS(ESI) analysis performed by periodic sampling of the reaction between **4.11** and **4.10** in the presence of 0.5 mol % of **4.32d** and 5 mol % of NaO^{t}Bu. The HRMS analysis of the reaction mixture at t = 0 (Figure 4.13) contained several adducts of **4.11**/**4.10** with pincer-Ni species such as [**4.35a** + CH_3CN + K + H]$^{2+}$, [**4.34a** + CH_3CN + H_2O + H]$^+$, [**4.34a** + CH_3OH + CH_3OK]$^+$, and [**4.34a** + CH_3CN + CH_3OK + H]$^+$ corresponding to peaks at m/z 326.1919, 645.4985, 687.3524, and 697.3808, respectively. The HRMS profile at t = 2 h (Figure 4.14) provided key evidence to the intermediates proposed in Scheme 4.23 and demonstrated peaks at m/z 681.3039, 764.5815, 771.3520, and 859.3856 that correspond to [**4.38a** + CH_3CN + $3H_2O$ + H]$^+$, [**4.38b** + CH_3OH + H_2O + K]$^+$, [**4.38b** + $3CH_3OH$]$^+$, and [**4.38b** + **4.10′** + $2CH_3OH$]$^+$, respectively. The profile of HRMS analysis at t = 4, 8, 16, and 24 h (Figures S3.101−S3.106, Appendix III) were similar to that observed at t = 2 h, and some of them contained an additional peak at m/z = 209.0986 corresponding to [**4.11′** + H]$^+$ (Figures S3.101, S3.104, and S3.105, Appendix III).

Kinetic studies were carried out for the **4.32d** catalyzed reaction of **4.11** with **4.10** in the presence of 5 mol % of NaO^{t}Bu at 140 °C (Figure 4.15). Notably, upon use of 0.005 mol % of **4.32d**, a very high initial rate (TOF = 3200 h^{-1}) was observed (Figure S3.111a, Appendix III). Using the initial rate method, it was observed that the plot of initial rate *vs* [**4.32d**] was a straight line that ran parallel to the x-axis, implying a zero-order dependence of rate on catalyst concentration (Figure 4.15). On the other hand, the corresponding plots of initial rate *vs* concentrations of base, **4.11**, and **4.10** were all linear and nearly passing through the origin. This indicates that the reaction has a first-order dependence of rate on the concentrations of base and primary and secondary alcohols.

This can be explained only if one invokes the possibility of a fast dehydrogenation (**4.11**/**4.10** → **4.11′**/**4.10′** + H_2) and hydrogenolysis (**4.11″** and **4.12** with H_2)/alcoholysis (**4.11″** and **4.12** with **4.11**/**4.10**) steps. Apparently, the base mediated coupling of benzaldehyde **4.11′** and acetophenone **4.10′** that gives *α,β*-unsaturated ketone **4.11″** is the rate-determining step. Not surprisingly, **4.11″** (Figures S3.101, S3.104, and S3.105, Appendix III) and its Ni-adducts **4.37a** and **4.37b** (Figures S3.101− S3.106, Appendix III) are detected in HRMS analysis.

4.4 Conclusion

We have accomplished the synthesis of a series of NNN pincer-nickel complexes of the type (^{R2}NNN)NiCl(CH$_3$CN) (R = ^{i}Pr, ^{t}Bu, Cy, Ph, and *p*-F-C$_6$H$_4$) based on *bis*(imino)-pyridine ligands. Single-crystal, HRMS, and TGA analyses reveal that these complexes exist as equilibrium mixtures of neutral and dicationic pincer-nickel complexes containing one and two pincer ligands, respectively. Among the five pincer-Ni complexes that have been screened for the catalytic *β*-alkylation in the presence of 5 mol% of NaO^{t}Bu at 140 °C, (^{Ph2}NNN)NiCl$_2$(CH$_3$CN) (0.005 mol %) was the most efficient catalyst, giving up to 92% yield

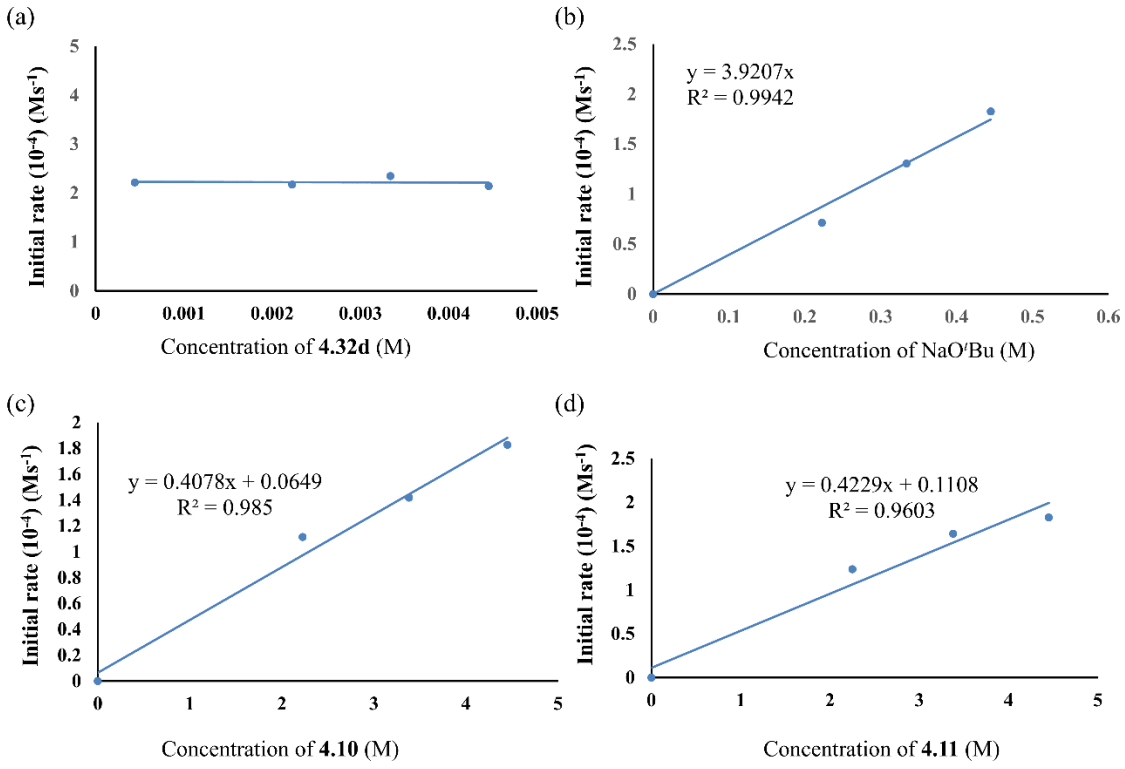

Figure 4.15. Variation of initial rate of formation of **4.13** with concentration of (a) **4.32d**, (b) NaO^{t}Bu, (c) **4.10** and, (d) **4.11**.

(*ca.* 18400 TON) for a combination of benzyl alcohol and 1-(4-(trifluoro-methyl)phenyl)ethane-1-ol. Kinetic studies on the (^{Ph2}NNN)NiCl$_2$(CH$_3$CN) catalyzed *β*-alkylation of 1-phenyl ethanol with benzyl alcohol revealed a first-order dependence of rate on the concentration of base, first-order dependence on both the alcohols, and zero-order dependence on catalyst concentration. This is indicative of a base-mediated aldol condensation as the rate-determining step. HRMS analysis proved to be a useful tool in the identification of several intermediates that are involved in the catalytic cycle.

4.5 Experimental section

4.5.1 General procedure and materials

All manipulations were carried out under an argon atmosphere in a glovebox or by using a standard double manifold. The nickel precursor, $NiCl_2$(DME), was purchased from Sigma-Aldrich. Benzyl alcohol, acetonitrile, and hexane were purchased from MERCK and were dried according to a literature procedure prior to experiment.[55] Other chemicals were purchased from MERCK or Sigma-Aldrich and used as such. All catalytic reactions were carried out under an argon atmosphere using dried glassware. The ligands (**4.31a-e**)[44, 45] and complex **4.32c**[46] were prepared according to literature procedures.

^{1}H, ^{2}H, ^{13}C{H} and ^{31}P were recorded on a Bruker ASCEND 600 operating at 600 MHz for ^{1}H, 150 MHz for ^{13}C{H} and 564 MHz for ^{31}P or on a Bruker AVANCE 400 operating at 400 MHz for ^{1}H, 100 MHz for ^{13}C{H}, 376 MHz for ^{31}P or on a Bruker AVANCE 500 operating at 500 MHz for ^{1}H, 125 MHz for ^{13}C{H}, 470 MHz for ^{31}P. HRMS measurements were performed using an Agilent Accurate-Mass Q-TOF ESI–MS 6520. X-ray crystallographic data were acquired on a Bruker D8 Venture single-crystal X-ray diffractometer using graphite monochromated Mo Kα radiation. The data refinement and cell reductions were carried out by the Bruker SAINT program.[56] Structures were further solved and refined by the full matrix least- squares method using SHELXS-14.[57] A JES-FA200 ESR spectrometer was use to record the X-band EPR spectra. Thermogravimetric analyses were performed using a thermal analyzer (SDTQ600) with a simultaneous DTA/TGA system, under nitrogen with a heating rate of 10 °C min^{-1}. Solid-state magnetic susceptibilities of the complexes at room temperature were recorded using a Sherwood Scientific magnetic balance MSB-1.

4.5.2 Synthesis of (1*E*,1′*E*)-1,1′-(Pyridine-2,6-diyl)*bis*(*N*-(4-fluorophenyl)methanimine) (4.31e)

The ligand **4.31e** was prepared according to the procedure reported in literature.[44, 45] The reaction of pyridine-2,6- dicarbaldehyde (0.1 g, 0.529 mmol) with 4-fluoroaniline (0.117 g, 1.06 mmol) in anhydrous dichloromethane containing molecular sieves (4 Å) was stirred for 12 h at 40 °C, followed by filtration and removal of solvent, affording the ligand **4.31e** as light-yellow powder (0.102 g) in 60% yield. ^{1}H NMR (400 MHz, $CDCl_3$): δ 8.66 (s, 2H), 8.27 (d, J = 7.8 Hz, 2H), 7.94 (t, J = 7.8 Hz, 1H), 7.35−7.29 (m, 4H), 7.12 (t, J = 8.6 Hz, 4H). ^{13}C{H} NMR (101 MHz, $CDCl_3$): δ 163.25, 160.81, 159.85, 154.71, 146.90, 137.52, 123.40, 122.98,

122.90, 116.34, 116.12. ^{19}F NMR (377 MHz, $CDCl_3$): δ −115.59. HRMS (ESI): *m/z* calculated for [**4.31e** + $4H_2O$]$^+$: 393.1500, found 393.1826.

4.5.3 General procedure for the synthesis of (^{R2}NNN)$NiCl_2(CH_3CN)$ complexes (4.32a-e).

The complex **4.32a** was prepared by the reaction of corresponding ligands **4.31a** (0.037 g, 0.154 mmol) with $NiCl_2$(DME) (0.034 g, 0.15 mmol), using anhydrous acetonitrile as the solvent and stirred for 20 h at room temperature. The solvent was evaporated under reduced pressure, and mustard solid (**4.32a**) was washed with diethyl ether (3 × 3 mL). The residue was dried under a vacuum and 3a isolated as mustard solid with 61% yield (0.039 g). A similar procedure was followed for the synthesis of **4.32b, 4.32d and 4.32e**.

(^{tBu2}NNN)$NiCl_2(CH_3CN)$ (4.32a). (0.037 g) 61% yield. HRMS (ESI): *m/z* calculated for [**4.33a** − 2Cl]$^{2+}$: 274.1569, found 274.1783; *m/z* calculated for [**4.32a** − Cl − CH_3CN]$^+$: 338.0934, found 338.1178; *m/z* calculated for [(**4.32a** − 2Cl − CH_3CN) + HCOO]$^+$: 348.1222, found 348.1521; *m/z* calculated for [**4.33a** + H]$^+$: 619.2593, found 619.4700; *m/z* calculated for [**4.33a** + H + $2H_2O$ + CH_3OH + CH_3CN]$^+$: 728.3332, found 728.5434. Magnetic susceptibility μ_{eff} = 3.20 μ_B.

(^{Cy2}NNN)$NiCl_2(CH_3CN)$ (4.32b). (0.057 g) 47% yield. Light green solid. HRMS (ESI): *m/z* calculated for [**4.33b** − 2Cl]$^{2+}$: 326.1882, found 326.1894; *m/z* calculated for [**4.32b** − Cl − CH_3CN]$^+$: 390.1247, found 390.1240; *m/z* calculated for [**4.33b** − Cl]$^+$: 687.3452, found 687.3447. Magnetic susceptibility μ_{eff} = 3.28 μ_B.

(^{Ph2}NNN)$NiCl_2(CH_3CN)$ (4.32d). (0.041 g) 89% yield. Light orange solid. HRMS (ESI): *m/z* calculated for [**4.33d** − 2Cl]$^{2+}$: 314.0943, found 314.0944; *m/z* calculated for [**4.32d** − Cl − CH_3CN]$^+$: 378.0808, found 378.0276; *m/z* calculated for [**4.33d** − Cl]$^+$: 663.1574, found 663.1526. Magnetic susceptibility μ_{eff} = 3.01 μ_B.

($^{(p\text{-F-Ph})2}$NNN)$NiCl_2(CH_3CN)$ (4.32e). (0.041 g) 89% yield. Orange solid. Crystals suitable for X-ray analysis were obtained by slow evaporation of a solution containing **4.32e** (10 mg) in 1 mL of methanol under non-inert conditions. HRMS (ESI): *m/z* calculated for [**4.33e** − 2Cl]$^{2+}$: 350.0755, found 350.0788; *m/z* calculated for [**4.32e** − Cl − CH_3CN]$^+$: 414.0120, found 414.0128; *m/z* calculated for [**4.33e** − Cl]$^+$: 735.1179, found 735.1196. Magnetic susceptibility μ_{eff} = 4.24 μ_B.

4.5.4 General procedure for the pincer-nickel catalyzed *β*–alkylation of alcohols

In a 10 mL two-neck round-bottom flask was added NaO^{t}Bu (0.04 g, 0.416 mmol) inside the glovebox. This was followed by addition of 0.005 mol % of **4.32d** (0.0002 g, 0.44 μmol) (from a stock solution in either benzyl alcohol or 1-phenyl ethanol) under an argon atmosphere. Subsequently, the reaction mixture as made up with the required amounts of benzyl alcohol (**4.11**) and 1-phenyl ethanol (**4.10**). Ultimately, the reaction mixture contained 0.430 mL of **4.11** (4.14 mmol) and 0.500 mL of **4.10** (4.14 mmol). The mixture was heated at 140 °C for 24 h and was then cooled down to room temperature. An aliquot (10 mg) was withdrawn from the reaction mixture, and the yield was determined by ^{1}H NMR using $CDCl_3$ as solvent and toluene as a standard (10 μL added in the NMR tube). The rest of the reaction mixture was quenched with water, followed by extraction of the organic fraction with dichloro- methane. The organic phase was separated and was dried over anhydrous Na_2SO_4. The solvent was removed from the organic fraction under reduced pressure. Silica gel column chromatography using 0−5% ethyl acetate in hexane as eluent gave the product **4.13** in a pure form.

1,3-Diphenylpropan-1-ol (**4.13**): ^{1}H NMR (600 MHz, $CDCl_3$): δ 7.39 – 7.36 (m, 4H, Ar), 7.32 – 7.29 (m, 3H, Ar), 7.22 – 7.20 (m, 3H, Ar), 4.69 (m, J = 6.0 Hz, 1H, C*H*OH), 2.79 – 2.74 (m, 1H, CH_2), 2.71 – 2.66 (m, 1H, CH_2), 2.18 – 2.12 (m, 1H, CH_2), 2.07 – 2.02 (m, 1H, CH_2). ^{13}C{H} NMR (151 MHz, $CDCl_3$): δ 144.65, 141.88, 128.63, 128.55, 128.50, 127.75, 126.04, 125.96 (Ar), 73.97(*C*HOH), 40.55, 32.15 (*C*H_2). HRMS (ESI): m/z calculated for $[M + Na]^+$: 235.1099, found 235.0846.

1-Phenyl-3-(p-tolyl)propan-1-ol **(4.13a):** ^{1}H NMR (400 MHz, $CDCl_3$): δ 7.44 – 7.38 (m, 4H, Ar), 7.34 (ddd, J = 8.6, 3.7, 2.1 Hz, 1H, Ar), 7.15 (brs, 4H, Ar), 4.72 (ddd, J = 8.1, 5.3, 3.1 Hz, 1H, C*H*OH), 2.80 – 2.64 (m, 2H, CH_2), 2.39 (s, 3H, CH_3), 2.22 – 2.02 (m, 3H, CH_2). ^{13}C{H} NMR (151 MHz, $CDCl_3$): δ 144.72, 138.76, 135.42, 129.20, 128.63, 128.43, 127.74, 126.06 (Ar), 74.02 (*C*HOH), 40.68, 31.72 (*C*H_2), 21.12 (*C*H_3).

1-Phenyl-3-(m-tolyl)propan-1-ol **(4.13b):** ^{1}H NMR (400 MHz, $CDCl_3$) δ 7.25 (d, J = 4.3 Hz, 4H, Ar), 7.21 – 7.16 (m, 1H, Ar), 7.11 – 7.06 (m, 1H, Ar), 6.93 – 6.89 (m, 4H, Ar), 4.58 (ddd, J = 7.9, 5.3, 2.3 Hz, 1H, C*H*OH), 2.67 – 2.48 (m, 2H, CH_2), 2.23 (s, 3H, CH_3), 2.08 – 1.92 (m, 2H, CH_2), 1.91 (brs, J = 3.0 Hz, 1H, O*H*). ^{13}C{H} NMR (126 MHz, $CDCl_3$): δ 144.71, 141.82, 137.98, 129.34, 128.56, 128.37, 127.66, 126.67, 126.03, 125.53 (Ar), 73.99 (*C*HOH), 40.57, 32.06 (*C*H_2), 21.46 (*C*H_3).

3-(4-Methoxyphenyl)-1-phenylpropan-1-ol (**4.13c**): ^{1}H NMR (400 MHz, $CDCl_3$): δ 7.43 – 7.35 (m, 5H, Ar), 7.20 – 7.18 (m, 2H, Ar), 6.93 – 6.91 (m, 2H, Ar), 4.70 (t, J = 4.0 Hz, 1H, C*H*OH), 3.83 (s, 3H, OCH_3), 2.80 – 2.65 (m, 2H, CH_2), 2.19 – 2.04 (m, 2H, CH_2). ^{13}C{H} NMR (151 MHz, $CDCl_3$): δ 157.87, 144.73, 133.91, 129.44, 128.62, 127.72, 126.05, 113.91 (Ar), 73.94 (*C*HOH), 55.37 (OCH_3), 40.80, 31.24 (*C*H_2). HRMS (ESI): m/z calculated for $[M + Na]^+$: 265.1204, found 265.1055.

3-(3-Methoxyphenyl)-1-phenylpropan-1-ol **(4.13d):** ^{1}H NMR (400 MHz, $CDCl_3$): δ 7.36 (d, J = 4.3 Hz, 4H, Ar), 7.32 – 7.25 (m, 1H, Ar), 7.20 (td, J = 7.4, 1.7 Hz, 1H, Ar), 6.80 (d, J = 7.6 Hz, 1H, Ar), 6.74 (d, J = 7.0 Hz, 2H, Ar), 4.70 (ddd, J = 8.1, 5.3, 2.8 Hz, 1H, C*H*OH), 3.79 (s, 3H, OCH_3), 2.79 – 2.61 (m, 2H, CH_2), 2.20 – 1.98 (m, 2H, CH_2), 1.93 (brs, J = 3.2 Hz, 1H, O*H*). ^{13}C{H} NMR (101 MHz, $CDCl_3$): δ 159.83, 144.70, 143.57, 129.47, 128.65, 127.77, 126.05, 120.99, 114.35, 111.35 (Ar), 74.00 (*C*HOH), 55.27 (OCH_3), 40.47, 32.24 (*C*H_2). HRMS (ESI): m/z calculated for $[M + H]^+$: 265.1204, found 265.1198.

3-(4-fluorophenyl)-1-phenylpropan-1-ol **(4.13e)***:* ^{1}H NMR (600 MHz, $CDCl_3$): δ 7.37 – 7.34 (m, 4H, Ar), 7.30 – 7.28 (m, 1H, Ar), 7.15 – 7.13 (m, 2H, Ar), 6.96 (t, J = 6 Hz, 2H, Ar), 4.67 (brs, 1H, C*H*OH), 2.75 – 2.70 (m, 1H, CH_2), 2.67 – 2.60 (m, 1H, CH_2), 2.14 – 2.08 (m, 1H, CH_2), 2.02 – 1.97 (m, 1H, CH_2), 1.87 (brs, 1H, O*H*). ^{13}C{H} NMR (151 MHz, $CDCl_3$): δ 162.21, 144.61, 137.48, 129.91, 129.86, 128.71, 127.88, 126.03, 115.31, 115.17 (Ar), 73.92 (*C*HOH), 40.72, 31.37 (*C*H_2). ^{19}F NMR (377 MHz, $CDCl_3$): δ -117.65.

3-(4-Chlorophenyl)-1-phenylpropan-1-ol (**4.13f**): ^{1}H NMR (600 MHz, $CDCl_3$): δ 7.29 – 7.25 (m, 4H, Ar), 7.23 – 7.20 (m, 1H, Ar), 7.18 – 7.16 (m, 2H, Ar), 7.04 (d, J = 6.0 Hz, 2H, Ar), 4.58 (t, J = 6.0 Hz, 1H, C*H*OH), 2.66 – 2.61 (m, 1H, CH_2), 2.59 – 2.54(m, 1H, CH_2), 2.05 – 1.99 (m, 1H, CH_2), 1.94 – 1.88 (m, 1H, CH_2), 1.85 – 1.82 (m, 1H, CH_2). ^{13}C{H} NMR (151 MHz, $CDCl_3$): δ 144.52, 140.34, 131.68, 129.92, 128.71, 128.59, 127.89, 126.01 (Ar), 73.84 (*C*HOH), 40.44, 31.51 (*C*H_2). HRMS (ESI): m/z calculated for $[M + Na]^+$: 285.0448, found 285.1295.

3-(3-Chlorophenyl)-1-phenylpropan-1-ol (**4.13g**): ^{1}H NMR (400 MHz, $CDCl_3$): δ 7.30 – 7.17 (m, 5H, Ar), 7.14 – 7.07 (m, 3H, Ar), 6.99 (d, J = 4.0 Hz, 1H, Ar), 4.61 – 4.57 (m, 1H, C*H*OH), 2.69 – 2.53 (m, 2H, CH_2), 2.08 – 1.83 (m, 3H, CH_2). ^{13}C{H} NMR (151 MHz, $CDCl_3$): δ 144.49, 143.99, 134.25, 129.76, 128.73, 127.92, 126.79, 126.20, 126.01 (Ar), 73.85 (*C*HOH), 40.32, 31.86 (*C*H_2).

1-Phenyl-3-(pyridin-3-yl)propan-1-ol **(4.13i)**: ^{1}H NMR (600 MHz, $CDCl_3$): δ 8.43 – 8.37 (m, 2H, Ar), 7.51 –7.50 (m, 1H, Ar), 7.35 – 7.34 (m, 4H, Ar), 7.29 – 7.28 (m, 1H, Ar), 7.20 – 7.18 (m, 1H, Ar), 4.68 – 4.66 (m, 1H, C*H*OH), 2.77 – 2.65 (m, 2H, CH_2), 2.15 – 2.08 (m, 1H, CH_2), 2.02 – 1.98 (m, 1H, CH_2), 1.71 (s, 1H, O*H*). ^{13}C{H} NMR (151 MHz, $CDCl_3$): δ 149.91, 147.30, 144.60, 137.34, 136.14, 128.70, 127.84, 125.99, 123.50 (Ar), 73.50 (*C*HOH), 40.21, 29.29 (*C*H_2).

1-Phenyl-3-(pyridin-4-yl)propan-1-ol **(4.13j)**: ^{1}H NMR (500 MHz, $CDCl_3$): δ 8.32 – 8.30 (m, 2H, Ar), 7.27 – 7.26 (m, 4H, Ar), 7.21 – 7.19 (m, 1H, Ar), 7.02 – 7.01 (m, 2H, Ar), 4.61 – 4.58 (m, 1H, C*H*OH), 2.70 – 2.64 (m, 1H, CH_2), 2.62 – 2.56 (m, 1H, CH_2), 2.07 – 2.00 (m, 1H, CH_2), 1.97 – 1.90 (m, 1H, CH_2). ^{13}C{H} NMR (151 MHz, $CDCl_3$): δ 151.16, 149.70, 144.43, 128.75, 127.95, 125.97, 124.08 (Ar), 73.65 (*C*HOH), 39.38, 31.5 (*C*H_2). HRMS (ESI): m/z calculated for $[M + H]^+$: 214.1232, found 214.1273.

3-(Furan-2-yl)-1-phenylpropan-1-ol **(4.13k)**: ^{1}H NMR (500 MHz, $CDCl_3$): δ 7.35 (d, 4H, Ar), 7.31 – 7.28 (m, 2H, Ar), 6.28 (brs, 1H, Ar), 6.06 – 6.01 (s, 1H, Ar), 4.73 – 4.70 (m, 1H, C*H*OH), 2.79 – 2.68 (m, 2H, CH_2), 2.17 – 2.03 (m, 2H, CH_2), 1.93 (brs, 1H, O*H*). ^{13}C{H} NMR (151 MHz, $CDCl_3$): δ 155.66, 144.46, 141.10, 128.68, 128.65, 127.83, 126.02, 110.27, 105.17 (Ar), 73.84 (*C*HOH), 37.30, 24.54 (*C*H_2).

1-Phenyl-3-(thiophen-2-yl)propan-1-ol **(4.13l)**: ^{1}H NMR (500 MHz, $CDCl_3$): δ 7.27 – 7.19 (m, 5H, Ar), 7.02 – 7.01 (m, 1H, Ar), 6.83 – 6.82 (m, 1H, Ar), 6.71 (s, 1H, Ar), 4.61 (s, 1H, C*H*OH), 2.88 – 2.77 (m, 2H, CH_2), 2.11 – 1.94 (m, 2H, CH_2). ^{13}C{H} NMR (126 MHz, $CDCl_3$): δ 144.73, 144.46, 128.66, 127.81, 126.87, 126.00, 124.43, 123.20 (Ar), 73.60 (*C*HOH), 40.78, 26.32 (*C*H_2).

3-(Naphthalen-1-yl)-1-phenylpropan-1-ol **(4.13m)**: ^{1}H NMR (600 MHz, $CDCl_3$): δ 7.98 (d, J = 6.0 Hz, 1H, Ar), 7.85 – 7.81 (m, 1H, Ar), 7.71 (d, J = 12.0 Hz, 1H, Ar), 7.49 – 7.45 (m, 2H, Ar), 7.40 – 7.34 (m, 5H, Ar), 7.31 – 7.28 (m, 1H, Ar), 4.81 – 4.80 (m, 1H, C*H*OH), 3.28 – 3.23 (m, 1H, CH_2), 3.14 – 3.09 (m, 1H, CH_2), 2.29 – 2.23(m, 1H, CH_2), 2.19 – 2.14 (m, 1H, CH_2), 1.93 (brs, J = 3.1 Hz, 1H). ^{13}C{H} NMR (151 MHz, $CDCl_3$): δ 144.65, 138.13, 134.04, 131.96, 128.90, 128.69, 127.84, 126.82, 126.09, 125.93, 125.68, 125.59, 123.91 (Ar), 74.34 (*C*HOH), 39.97, 29.26 (*C*H_2).

3-(Anthracen-9-yl)-1-phenylpropan-1-ol **(4.13n):** ^{1}H NMR (600 MHz, $CDCl_3$): δ 8.33 (s, 1H, Ar), 8.18 (d, J = 8.6 Hz, 2H, Ar), 7.99 (d, J = 8.1 Hz, 2H, Ar), 7.46 (dt, J = 16.6, 7.0 Hz, 6H, Ar), 7.39 (t, J = 7.5 Hz, 2H, Ar), 7.32 (t, J = 7.3 Hz, 1H, Ar), 4.94 (p, J = 3.7 Hz, 1H, C*H*OH), 3.78 (ddd, J = 13.4, 11.2, 5.0 Hz, 1H, CH_2), 3.65 (ddd, J = 13.8, 10.9, 6.0 Hz, 1H, CH_2), 2.34 – 2.26 (m, 1H, CH_2), 2.22 (ddd, J = 13.9, 10.6, 5.4 Hz, 1H, CH_2), 2.05 (brs, 1H, O*H*). ^{13}C{H} NMR (151 MHz, $CDCl_3$) δ 144.60, 134.47, 131.76, 129.72, 129.33, 128.73, 127.92, 126.10, 125.92, 125.66, 124.96, 124.46 (Ar), 74.57 (*C*HOH), 40.18, 24.12 (*C*H_2).

3-Phenyl-1-(p-tolyl)propan-1-ol (**4.13r**): ^{1}H NMR (500 MHz, $CDCl_3$): δ 7.18 – 7.15 (t, J = 7.5 Hz, 2H, Ar), 7.12 – 7.10 (m, 2H, Ar), 7.08 – 7.03 (m, 5H, Ar), 4.50 (t, J = 5.0 Hz, 1H, C*H*OH), 2.64 – 2.58 (m, 1H, CH_2), 2.56 – 2.50 (m, 1H, CH_2), 2.23 (s, 3H, CH_3), 2.03 – 1.96 (m, 2H, CH_2), 1.92 – 1.85 (m, 1H, CH_2). ^{13}C{H} NMR (151 MHz, $CDCl_3$): δ 141.94, 131.65, 137.33, 129.24, 128.53, 128.44, 126.00, 125.88 (Ar), 73.73 (*C*HOH), 40.41, 32.15 (*C*H_2), 21.21 (*C*H_3). HRMS (ESI): m/z calculated for $[M + Na]^+$: 249.1255, found 249.1276.

1-(4-Methoxyphenyl)-3-phenylpropan-1-ol (**4.13s**): ^{1}H NMR (600 MHz, $CDCl_3$): δ 7.28 (d, J = 5.0 Hz, 3H, Ar), 7.19 (d, J = 7.1 Hz, 3H, Ar), 6.89 (d, J = 8.6 Hz, 2H, Ar), 4.64 (brs, 1H, C*H*OH), 3.81 (s, 3H, OCH_3), 2.68 (d, J = 79.0 Hz, 2H, CH_2), 2.17 – 1.98 (m, 2H, CH_2). ^{13}C{H} NMR (101 MHz, $CDCl_3$): δ 159.28, 141.98, 128.57, 128.51, 127.35, 125.97, 114.05 (Ar), 73.65 (*C*HOH), 55.44 (O*C*H_3), 32.27 (*C*H_2). HRMS (ESI): m/z calculated for $[M + Na]^+$: 265.1204, found 265.1384.

1-(3-Methoxyphenyl)-3-phenylpropan-1-ol (**4.13t**): ^{1}H NMR (500 MHz, $CDCl_3$): δ 7.16 (q, J = 7.9 Hz, 3H, Ar), 7.09 (d, J = 7.7 Hz, 3H, Ar), 6.82 (d, J = 7.0 Hz, 2H, Ar), 6.72 (d, J = 8.4 Hz, 1H, Ar), 4.59 – 4.54 (m, 1H, C*H*OH), 3.70 (s, 3H, OCH_3), 2.69 – 2.53 (m, 2H, CH_2), 2.06 – 1.89 (m, 2H, CH_2), 1.85 (brs, 1H, O*H*). ^{13}C C*H*OH {H} NMR (126 MHz, $CDCl_3$): δ 159.95, 146.45, 141.90, 129.66, 128.57, 128.51, 125.98, 118.37, 113.22, 111.56 (Ar), 73.94 (*C*HOH), 55.36 (O*C*H_3), 40.52, 32.16 (*C*H_2).

1-(4-Bromophenyl)-3-phenylpropan-1-ol **(4.13w):** ^{1}H NMR (600 MHz, $CDCl_3$) δ 7.49 – 7.46 (m, 2H, Ar), 7.29 (t, J = 7.5 Hz, 2H, Ar), 7.24 – 7.17 (m, 5H, Ar), 4.65 (ddd, J = 8.2, 5.1, 3.0 Hz, 1H, C*H*OH), 2.77 – 2.63 (m, 2H, CH_2), 2.13 – 1.96 (m, 2H, CH_2), 1.95 (brs, J = 3.4 Hz, 1H, O*H*). ^{13}C{H} NMR (151 MHz, $CDCl_3$): δ 143.62, 141.56, 131.70, 128.58, 128.54, 127.78, 126.09, 121.46 (Ar), 73.28 (*C*HOH), 40.57, 32.01 (*C*H_2).

1-(3-Bromophenyl)-3-phenylpropan-1-ol (**4.13x**): ^{1}H NMR (500 MHz, $CDCl_3$): δ 7.42 (brs, 1H, Ar), 7.33 –7.31 (d, J = 10.0 Hz, 1H, Ar), 7.22 – 7.16 (m, 3H, Ar), 7.14 – 7.09 (m, 4H, Ar), 4.55 (brs, 1H, C*H*OH), 2.69 – 2.59 (m, 2H, CH_2), 2.04 – 1.88 (m, 3H, CH_2). ^{13}C{H} NMR (126 MHz, $CDCl_3$): δ 147.10, 141.57, 130.76, 130.21, 129.17, 128.59, 128.55, 126.11, 124.64, 122.77 (Ar), 73.25 (*C*HOH), 40.60, 32.03 (*C*H_2).

3-Phenyl-1-(thiophen-2-yl)propan-1-ol **(4.13za):** ^{1}H NMR (400 MHz, $CDCl_3$) δ 7.27 – 7.20 (m, 3H, Ar), 7.16 (d, J = 7.5 Hz, 3H, Ar), 6.97 – 6.90 (m, 2H, Ar), 4.88 (t, J = 6.7 Hz, 1H, C*H*OH), 2.79 – 2.63 (m, 2H, CH_2), 2.25 – 2.05 (m, 2H, CH_2), 1.95 (s, 1H, O*H*). ^{13}C{H} NMR (101 MHz, $CDCl_3$): δ 148.67, 141.60, 128.63, 128.59, 126.82, 126.11, 124.83, 124.06 (Ar), 69.69 (*C*HOH), 40.86, 32.16 (*C*H_2).

1-(Naphthalen-2-yl)-3-phenylpropan-1-ol (**4.13zb**): ^{1}H NMR (500 MHz, $CDCl_3$): δ 7.71 – 7.68 (m, 3H, Ar), 7.62 (brs, 1H, Ar), 7.37 – 7.32 (m, 3H, Ar), 7.18 – 7.15 (m, 2H, Ar), 7.09 – 7.07 (m, 3H, Ar), 4.68 (brs, 1H, C*H*OH), 2.67 – 2.60 (m, 1H, CH_2), 2.58 – 2.53 (m, 1H, CH_2), 2.12 – 2.06 (m, 1H, CH_2), 2.01 – 1.94 (m, 1H, CH_2). ^{13}C{H} NMR (151 MHz, $CDCl_3$): δ 141.93, 141.82, 133.31, 133.06, 128.56, 128.51, 128.48, 128.03, 127.80, 126.29, 125.98, 124.79, 124.14 (Ar), 74.03 (*C*HOH), 40.38, 32.12 (*C*H_2). HRMS (ESI): m/z calculated for $[M + Na]^+$: 285.1255, found 285.1200.

3-Phenyl-1-(4-(trifluoromethyl)phenyl)propan-1-ol (**4.13zc**): ^{1}H NMR (600 MHz, $CDCl_3$): δ 7.63 (d, J = 8.0 Hz, 2H, Ar), 7.49 (d, J = 8.0 Hz, 2H, Ar), 7.32 (t, J = 7.5 Hz, 2H, Ar), 7.22 (d, J = 7.8 Hz, 3H, Ar), 4.78 (b rs, J = 3.7 Hz, 1H, C*H*OH), 2.83 – 2.70 (m, 2H, *C*H_2), 2.17 – 2.03 (m, 2H, *C*H_2), 2.03 (brs, J = 3.4 Hz, 1H, O*H*). ^{13}C{H} NMR (151 MHz, $CDCl_3$): δ 148.61, 141.42, 129.83 (q, J = 32.4 Hz, *C*F_3), 128.62, 128.54, 126.27, 126.17, 125.57 (q, J = 3.7 Hz), 125.14, 123.34 (Ar), 73.27 (*C*HOH), 40.69, 31.96 (*C*H_2). ^{19}F NMR (377 MHz, $CDCl_3$) δ -62.45.

3-Phenyl-1-(3-(trifluoromethyl)phenyl)propan-1-ol (**4.13zd**): ^{1}H NMR (500 MHz, $CDCl_3$): δ 7.55 (s, 1H, Ar), 7.47 – 7.45 (m, 2H, Ar), 7.40 – 7.37 (m, 1H, Ar), 7.23 – 7.18 (m, 2H, Ar), 7.13 – 7.11 (m, 3H, Ar), 4.70 – 4.67 (m, 1H, C*H*OH), 2.73 – 2.60 (m, 2H, CH_2), 2.06 – 1.91 (m, 3H, CH_2). ^{13}C{H} NMR (126 MHz, $CDCl_3$): δ 145.77, 141.48, 129.38, 129.09, 128.65, 128.57, 126.20 (Ar), 124.53 (q, J = 3.8 Hz, *C*F_3), 122.86 (q, J = 3.7 Hz, Ar), 73.38 (*C*HOH), 40.76, 32.08 (*C*H_2). ^{19}F NMR (471 MHz, $CDCl_3$): δ -62.60.

3-phenyl-1-(4-(trifluoromethoxy)phenyl)propan-1-ol (**4.13ze**): ^{1}H NMR (500 MHz, $CDCl_3$): δ 7.30 – 7.29 (m, 2H, Ar), 7.22 – 7.18 (m, 2H, Ar), 7.12 – 7.11 (m, 5H, Ar), 4.63 (s, 1H, C*H*OH), 2.71 – 2.57 (m, 2H, CH_2), 2.07 – 2.00 (m, 1H, CH_2), 1.97 – 1.90 (m, 1H, CH_2), 1.86 (s, 1H, O*H*). ^{13}C{H} NMR (126 MHz, $CDCl_3$): δ 148.70, 143.42, 141.59, 128.61 (*C*F_3), 128.55, 127.44, 126.14, 121.13 (Ar), 73.23 (*C*HOH), 40.71, 32.09 (*C*H_2). ^{19}F NMR (471 MHz, $CDCl_3$): δ -57.88.

Supporting information containing NMR spectra, HRMS analysis, SCXRD data, EPR analysis, Kinetics data and, TGA analysis of the complexes for chapter IV is available as appendix III and can be found at:

https://drive.google.com/file/d/1ppAVRIRsJuQ7DK_-J4LtayNnSOUh6GvV/view?usp=sharing

4.6 References

1. Brahmachari, G. Design for carbon–carbon bond forming reactions under ambient conditions. *RSC Adv.* **2016,** *6*, 64676-64725.
2. Allen, L. J.; Crabtree, R. H. Green alcohol couplings without transition metal catalysts: base-mediated β-alkylation of alcohols in aerobic conditions. *Green Chem.* **2010,** *12*, 1362-1364.
3. Xu, Q.; Chen, J.; Liu, Q. Aldehyde-Catalyzed Transition Metal-Free Dehydrative β-Alkylation of Methyl Carbinols with Alcohols. *Adv. Synth. Catal.* **2013,** *355*, 697-704.
4. Xu, Q.; Chen, J.; Tian, H.; Yuan, X.; Li, S.; Zhou, C.; Liu, J. Catalyst-Free Dehydrative α-Alkylation of Ketones with Alcohols: Green and Selective Autocatalyzed Synthesis of Alcohols and Ketones. *Angew. Chem., Int. Ed.* **2014,** *53*, 225-229.
5. Wang, Q.; Wu, K.; Yu, Z. Ruthenium (III)-catalyzed β-alkylation of secondary alcohols with primary alcohols. *Organometallics* **2016,** *35*, 1251-1256.
6. Reed-Berendt, B. G.; Latham, D. E.; Dambatta, M. B.; Morrill, L. C. Borrowing Hydrogen for Organic Synthesis. *ACS Cent. Sci.* **2021,** *7*, 570-585.
7. Mullick, S.; Ghosh, A.; Banerjee, D. Recent advances in cross-coupling of alcohols via borrowing hydrogen catalysis. *Chem. Commun.* **2024,** *60*, 4002-4014.
8. Ruiz-Botella, S.; Peris, E. Unveiling the Importance of π-Stacking in Borrowing-Hydrogen Processes Catalysed by Iridium Complexes with Pyrene Tags. *Chem. Eur. J.* **2015,** *21*, 15263-15271.
9. Jiménez, M. V.; Fernández-Tornos, J.; Modrego, F. J.; Pérez-Torrente, J. J.; Oro, L. A. Oxidation and β-Alkylation of Alcohols Catalysed by Iridium(I) Complexes with Functionalised N-Heterocyclic Carbene Ligands. *Chem. Eur. J.* **2015,** *21*, 17877-17889.
10. Xu, C.; Goh, L. Y.; Pullarkat, S. A. Efficient Iridium-Thioether-Dithiolate Catalyst for β-Alkylation of Alcohols and Selective Imine Formation via N-Alkylation Reactions. *Organometallics* **2011,** *30*, 6499-6502.
11. Segarra, C.; Mas-Marzá, E.; Mata, J. A.; Peris, E. Shvo's Catalyst and [IrCp*Cl2(amidine)] Effectively Catalyze the Formation of Tertiary Amines from the Reaction of Primary Alcohols and Ammonium Salts. *Adv. Synth. Catal.* **2011,** *353*, 2078-2084.
12. Gong, X.; Zhang, H.; Li, X. Iridium phosphine abnormal N-heterocyclic carbene complexes in catalytic hydrogen transfer reactions. *Tetrahedron Lett.* **2011,** *52*, 5596-5600.

13. Gnanamgari, D.; Sauer, E. L. O.; Schley, N. D.; Butler, C.; Incarvito, C. D.; Crabtree, R. H. Iridium and Ruthenium Complexes with Chelating N-Heterocyclic Carbenes: Efficient Catalysts for Transfer Hydrogenation, β-Alkylation of Alcohols, and N-Alkylation of Amines. *Organometallics* **2009,** *28*, 321-325.
14. da Costa, A. P.; Sanaú, M.; Peris, E.; Royo, B. Easy preparation of Cp*-functionalized N-heterocyclic carbenes and their coordination to rhodium and iridium. *Dalton Trans.* **2009**, 6960-6966.
15. Pontes da Costa, A.; Viciano, M.; Sanaú, M.; Merino, S.; Tejeda, J.; Peris, E.; Royo, B. First Cp*-Functionalized N-Heterocyclic Carbene and Its Coordination to Iridium. Study of the Catalytic Properties. *Organometallics* **2008,** *27*, 1305-1309.
16. Gnanamgari, D.; Leung, C. H.; Schley, N. D.; Hilton, S. T.; Crabtree, R. H. Alcohol cross-coupling reactions catalyzed by Ru and Ir terpyridine complexes. *Org. Biomol. Chem.* **2008,** *6*, 4442-4445.
17. Fujita, K.-i.; Asai, C.; Yamaguchi, T.; Hanasaka, F.; Yamaguchi, R. Direct β-Alkylation of Secondary Alcohols with Primary Alcohols Catalyzed by a Cp*Ir Complex. *Org. Lett.* **2005,** *7*, 4017-4019.
18. Satyanarayana, P.; Reddy, G. M.; Maheswaran, H.; Kantam, M. L. Tris(acetylacetonato)rhodium(III)-Catalyzed α-Alkylation of Ketones, β-Alkylation of Secondary Alcohols and Alkylation of Amines with Primary Alcohols. *Adv. Synth. Catal.* **2013,** *355*, 1859-1867.
19. Cho, C. S.; Kim, B. T.; Kim, H.-S.; Kim, T.-J.; Shim, S. C. Ruthenium-catalyzed one-pot β-alkylation of secondary alcohols with primary alcohols. *Organometallics* **2003,** *22*, 3608-3610.
20. Prades, A.; Viciano, M.; Sanaú, M.; Peris, E. Preparation of a series of "Ru (p-cymene)" complexes with different N-heterocyclic carbene ligands for the catalytic β-alkylation of secondary alcohols and dimerization of phenylacetylene. *Organometallics* **2008,** *27*, 4254-4259.
21. Chakrabarti, K.; Paul, B.; Maji, M.; Roy, B. C.; Shee, S.; Kundu, S. Bifunctional Ru (ii) complex catalysed carbon–carbon bond formation: an eco-friendly hydrogen borrowing strategy. *Org. Biomol. Chem.* **2016,** *14*, 10988-10997.
22. Roy, B. C.; Chakrabarti, K.; Shee, S.; Paul, S.; Kundu, S. Bifunctional RuII-Complex-Catalysed Tandem C− C Bond Formation: Efficient and Atom Economical Strategy for the Utilisation of Alcohols as Alkylating Agents. *Chem. Eur. J.* **2016,** *22*, 18147-18155.
23. Shee, S.; Paul, B.; Panja, D.; Roy, B. C.; Chakrabarti, K.; Ganguli, K.; Das, A.; Das, G. K.; Kundu, S. Tandem Cross Coupling Reaction of Alcohols for Sustainable Synthesis of β-Alkylated Secondary Alcohols and Flavan Derivatives. *Adv. Synth. Catal.* **2017,** *359*, 3888-3893.
24. Roy, B. C.; Debnath, S.; Chakrabarti, K.; Paul, B.; Maji, M.; Kundu, S. ortho-Amino group functionalized 2, 2′-bipyridine based Ru (ii) complex catalysed alkylation of secondary alcohols, nitriles and amines using alcohols. *Org. Chem. Front.* **2018,** *5*, 1008-1018.
25. Zhang, C.; Zhao, J.-P.; Hu, B.; Shi, J.; Chen, D. Ruthenium-Catalyzed β-Alkylation of Secondary Alcohols and α-Alkylation of Ketones via Borrowing Hydrogen: Dramatic Influence of the Pendant N-Heterocycle. *Organometallics* **2019,** *38*, 654-664.
26. Kose, O.; Saito, S. Cross-coupling reaction of alcohols for carbon–carbon bond formation using pincer-type NHC/palladium catalysts. *Org. Biomol. Chem.* **2010,** *8*, 896-900.
27. Liu, T.; Wang, L.; Wu, K.; Yu, Z. Manganese-Catalyzed β-Alkylation of Secondary Alcohols with Primary Alcohols under Phosphine-Free Conditions. *ACS Catal.* **2018,** *8*, 7201-7207.
28. El-Sepelgy, O.; Matador, E.; Brzozowska, A.; Rueping, M. C-Alkylation of Secondary Alcohols by Primary Alcohols through Manganese-Catalyzed Double Hydrogen Autotransfer. *ChemSusChem* **2019,** *12*, 3099-3102.
29. Freitag, F.; Irrgang, T.; Kempe, R. Cobalt-Catalyzed Alkylation of Secondary Alcohols with Primary Alcohols via Borrowing Hydrogen/Hydrogen Autotransfer. *Chem. Eur. J.* **2017,** *23*, 12110-12113.
30. Yang, J.; Liu, X.; Meng, D. L.; Chen, H. Y.; Zong, Z. H.; Feng, T. T.; Sun, K. Efficient Iron-Catalyzed Direct β-Alkylation of Secondary Alcohols with Primary Alcohols. *Adv. Synth. Catal.* **2012,** *354*, 328.
31. Zhang, M.-J.; Li, H.-X.; Young, D. J.; Li, H.-Y.; Lang, J.-P. Reaction condition controlled nickel(ii)-catalyzed C–C cross-coupling of alcohols. *Org. Biomol. Chem.* **2019,** *17*, 3567-3574.

32. Liao, S.; Yu, K.; Li, Q.; Tian, H.; Zhang, Z.; Yu, X.; Xu, Q. Copper-catalyzed C-alkylation of secondary alcohols and methyl ketones with alcohols employing the aerobic relay race methodology. *Org. Biomol. Chem.* **2012,** *10*, 2973-2978.
33. Irrgang, T.; Kempe, R. 3d-Metal Catalyzed N- and C-Alkylation Reactions via Borrowing Hydrogen or Hydrogen Autotransfer. *Chem. Rev.* **2019,** *119*, 2524-2549.
34. Cho, C. S.; Kim, B. T.; Kim, H.-S.; Kim, T.-J.; Shim, S. C. Ruthenium-Catalyzed One-Pot β-Alkylation of Secondary Alcohols with Primary Alcohols. *Organometallics* **2003,** *22*, 3608-3610.
35. (a) Das, K.; Yasmin, E.; Das, B.; Srivastava, H. K.; Kumar, A. Phosphine-free pincer-ruthenium catalyzed biofuel production: high rates, yields and turnovers of solventless alcohol alkylation. *Catal. Sci. Technol.* **2020,** *10*, 8347-8358. (b) Kaur, M.; Reshi, N. U. D.; Patra, K.; Bhattacherya, A.; Kunnikuruvan, S.; Bera, J. K. A Proton-Responsive Pyridyl(benzamide)-Functionalized NHC Ligand on Ir Complex for Alkylation of Ketone and Secondary Alcohols. *Chem. - Eur. J.* **2021,** *27*, 10737-10748. (c) Prakasham, A.; Ta, S.; Dey, S.; Ghosh, P. One pot tandem dual C-C and C-O bond reductions in the β-alkylation of secondary alcohols with primary alcohols by ruthenium complexes of amido and picolyl functionalized N-heterocyclic carbenes. *Dalton Trans.***2021**, *50*, 15640-15654
36. Narjinari, H.; Tanwar, N.; Kathuria, L.; Jasra, R. V.; Kumar, A. Guerbet-Type β-alkylation of Secondary Alcohols Catalyzed by Chromium Chloride and its Corresponding NNN Pincer Complex. *Catal. Sci. Technol.* **2022**.
37. Nandi, P. G.; Kumar, P.; Kumar, A. Ligand-free Guerbet-type reactions in air catalyzed by in situ formed complexes of base metal salt cobaltous chloride. *Catal. Sci. Technol.* **2022,** *12*, 1100-1108.
38. Nandi, P. G.; Thombare, P.; Prathapa, S. J.; Kumar, A. Pincer-Cobalt-Catalyzed Guerbet-Type β-Alkylation of Alcohols in Air under Microwave Conditions. *Organometallics* **2022,** *41*, 3387-3398.
39. Bisarya, A.; Jasra, R. V.; Kumar, A. NNN Pincer-Manganese-Catalyzed Guerbet-Type β-Alkylation of Alcohols under Microwave Irradiation. *Organometallics* **2023,** *42*, 1818-1831.
40. Babu, R.; Subaramanian, M.; Midya, S. P.; Balaraman, E. Nickel-Catalyzed Guerbet Type Reaction: C-Alkylation of Secondary Alcohols via Double (de)Hydrogenation. *Org. Lett.* **2021,** *23*, 3320-3325.
41. Allen, L. J.; Crabtree, R. H. Green alcohol couplings without transition metal catalysts: base-mediated β-alkylation of alcohols in aerobic conditions. *Green Chem.* **2010,** *12*, 1362-1364.
42. Nayak, A. S.; Jaiswal, S.; Sahu, M. K.; Gunanathan, C. KOH-catalyzed cross-coupling of primary and secondary alcohols: evidence for radical pathways. *J. Chem. Sci.* **2024,** *136*, 5.
43. Garg, N. K.; Tan, M.; Johnson, M. T.; Wendt, O. F. Highly Efficient Base Catalyzed N-alkylation of Amines with Alcohols and β-Alkylation of Secondary Alcohols with Primary Alcohols. *ChemCatChem* **2023,** *15*, e202300741.
44. Das, K.; Dutta, M.; Das, B.; Srivastava, H. K.; Kumar, A. Efficient Pincer-Ruthenium Catalysts for Kharasch Addition of Carbon Tetrachloride to Styrene. *Adv. Synth Catal.* **2019,** *361*, 2965-2980.
45. Wong, W.-Y.; Lee, S.-F.; Chan, H.-S.; Mak, T. C. W.; Wong, C.-H.; Huang, L.-S.; Stoddart, J. F.; Cham-Fai Leung, K., Recognition between V- and dumbbell-shaped molecules. *RSC Adv.* **2013,** *3*, 26382-26390.
46. Arora, V.; Dutta, M.; Das, K.; Das, B.; Srivastava, H. K.; Kumar, A. Solvent-Free N-Alkylation and Dehydrogenative Coupling Catalyzed by a Highly Active Pincer-Nickel Complex. *Organometallics* **2020**.
47. Huheey, J. E.; Keiter, E. A.; Keiter, R. L.; Medhi, O. K., *Inorganic chemistry: principles of structure and reactivity*. Pearson Education India **2006**.
48. Packová, A.; Miklovič, J.; Titiš, J.; Koman, M.; Boča, R., Positive zero-field splitting in a hexacoordinate nickel(II) complex. *Inorg. Chem. Commun.* **2013,** *32*, 9-11.
49. Sengupta, D.; Bhattacharjee, R.; Pramanick, R.; Rath, S. P.; Saha Chowdhury, N.; Datta, A.; Goswami, S., Exclusively Ligand-Mediated Catalytic Dehydrogenation of Alcohols. *Inorg. Chem.* **2016,** *55*, 9602-9610.
50. Parish, R. V. *NMR, NQR, EPR, and Mössbauer spectroscopy in inorganic chemistry*; Ellis Horwood Ltd., 1990.
51. Drago, R. S. *Physical Methods for Chemists*; Saunders College Pub, 1992.

52. Hausinger, R. P., *Biochemistry of nickel*; Biochemistry of the elements, Vol. *12*; Springer Science & Business Media, 2013.
53. Jackson, R. A. *Mechanisms in organic reactions*. Royal Society of Chemistry 2004; Vol. *23*, pp 45-71.
54. Wade, L. G., *Organic chemistry*. Pearson Education India, 2008.
55. (a) Armarego, W. L. F.; Chai, C. Purification of Inorganic and Metal-Organic Chemicals. In *Purification of Laboratory Chemicals*, 7th ed.; Armarego, W. L. F., Chai, C., Eds.; Butterworth-Heinemann: Boston, 2013; Chapter 5, pp 555−661. (b) Armarego, W. L. F.; Chai, C. Purification of Organic Chemicals. In *Purification of Laboratory Chemicals*, 7th ed.; Armarego, W. L. F., Chai, C., Eds.; Butterworth-Heinemann: Boston, 2013; Chapter 4, pp 103−554.
56. *APEX, SAINT and SADABS*; Bruker AXS Inc.: Madison, WI, USA, **2013**.
57. Sheldrick, G. M. Crystal structure refinement with SHELXL. *Acta Crystallogr., Sect. C: Struct. Chem.* 2015, *71*, 3-8.

Summary and Outlook

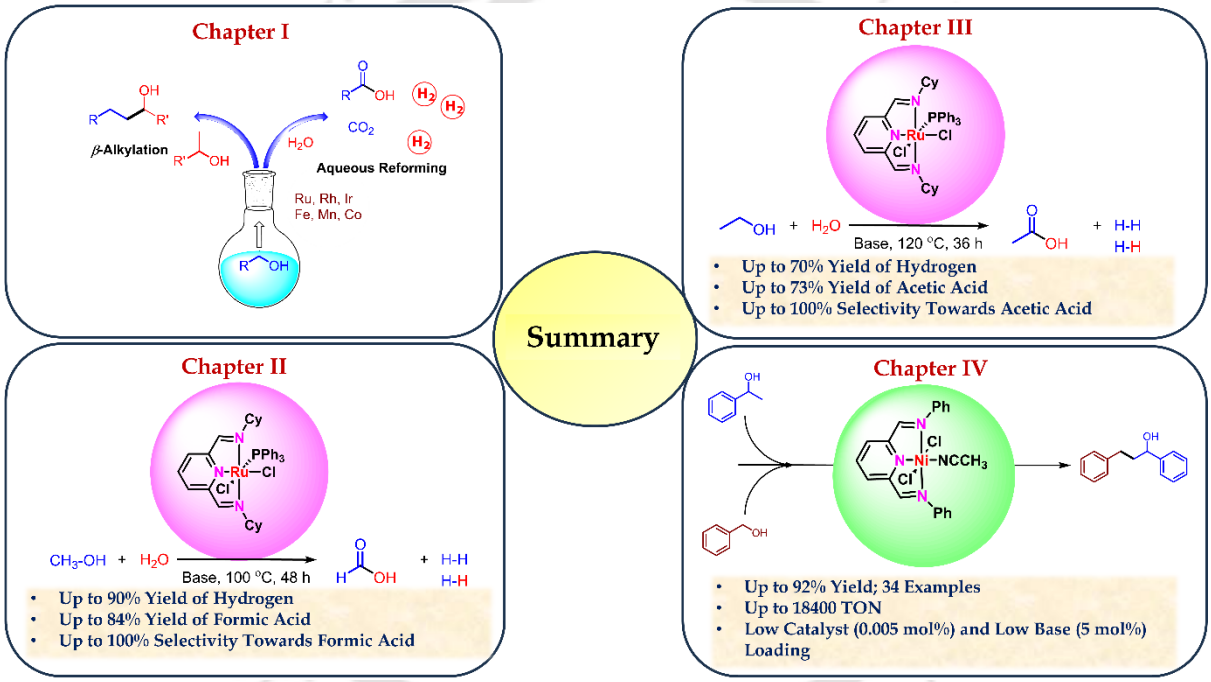

Chapter I outlines the use of organometallic complexes in catalysis. Among the vast array of transition-metal complexes that have been documented in the literature, pincer-metal complexes have proven to be highly effective and serve a crucial role in organic transformations. Among the various reactions, catalytic transformation to alcohols to various value-added products using pincer-metal systems has been well documented. The chapter concludes with a consideration of the current thesis's scope.

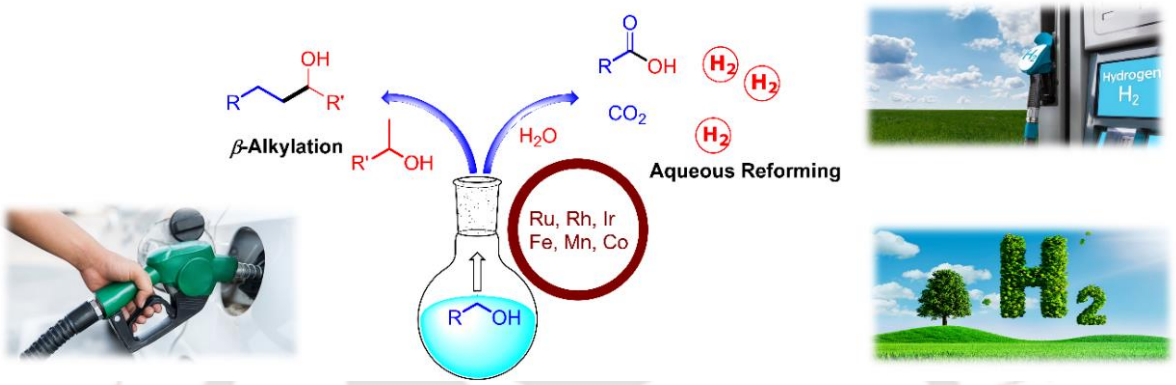

Figure 1. Catalytic transformation of alcohols to produce hydrogen and value-added chemicals using pincer-metal complexes.

Chapter II deals with the synthesis of novel *bis*(imino)pyridine based pincer-ruthenium complexes having ^{R2}NNN ligand (R = ^{t}Bu, ^{i}Pr, Cy and Ph). All of these complexes along with their phosphine and carbonyl based counterparts were employed towards catalytic methanol reforming for generation of hydrogen. Methanol, due to its high hydrogen content (12.6% H_2) and ease of handling is the most preferred alcohol for the hydrogen storage systems. The complex (^{Cy2}NNN)$RuCl_2(PPh_3)$ was found to be the most efficient among the considered complexes. For a mixture of methanol and water in a 2:1 ratio, (^{Cy2}NNN)$RuCl_2(PPh_3)$ (0.2 mol %) resulted in a yield of 81% each of H_2 and formic acid at 100% selectivity in the presence of KO^{t}Bu (1.5 equivalents with respect to water) at 100 °C. In contrast with the previous reports, where complete dehydrogenation of methanol to carbon dioxide (a greenhouse gas) has been observed, the present catalyst system selectively generates formic acid and hydrogen. The increment in the concentration of methanol (3:1 methanol/water mixture) resulted in good yields (84%) of hydrogen with 82% formic acid at 95% selectivity at a 0.8 mol% catalyst loading. The deuterium-labelling studies were indicative of an average KIE of 1.96 that points towards the involvement of methanol C−H bond activation in the mechanism but not as a part of the RDS, while the O-H bond activation is the RDS and contributes majorly to the observed

average k_H/k_D value of 1.96 These studies are in accordance with the DFT studies that compute that either for the cycle leading to formic acid and 2 moles of hydrogen or for the cycle that results in carbon dioxide and 3 moles of hydrogen, the release of first hydrogen molecule is the RDS. The current protocol has also been successfully extended towards to the generation of D_2 and its incorporation in various unsaturated compounds.

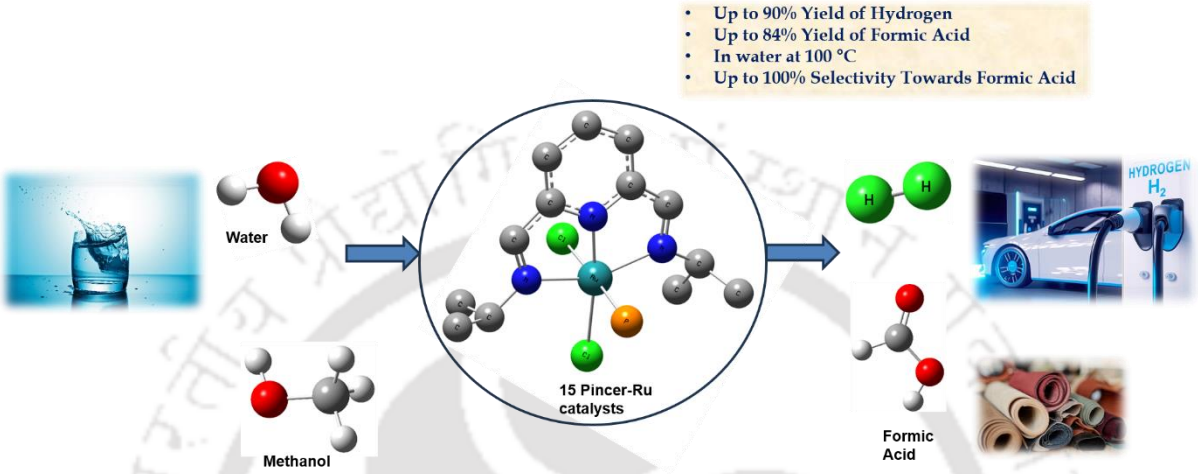

Figure 2. Pincer-ruthenium catalyzed reforming of methanol in water to generate H_2 and formic acid with high selectivity.

In line with the above chapter, **Chapter III** is based on the aqueous reforming of ethanol to valuable acetic acid and hydrogen. After methanol, bioethanol has emerged as a promising LOHC due to its high hydrogen output (13% H_2) and easy availability. The pincer-ruthenium complexes based on *bis*(imino)pyridine and 2,6-*bis*(benzimidazole-2-yl) pyridine ligands have been studied for the reforming of ethanol to produce hydrogen and acetic acid. Among the complexes screened, the best yield was obtained with 0.2 mol% of (^{Cy2}NNN)$RuCl_2(PPh_3)$, which afforded up to 70% of H_2 and 73% of acetic acid from a 2:1 mixture of ethanol and water in the presence of 1.5 equivalents KO^{t}Bu. The kinetic isotope effect studies point towards the involvement of C–H activation in the aqueous ethanol reforming reaction with an average KIE of 5.23. The first order dependence of rate on the concentration of both pincer-ruthenium catalyst and ethanol was observed from kinetic studies, which also confirms the homogeneous nature of the reaction. The release of PPh_3 and generation of (^{Cy2}NNN)RuCl(H) species (detected as phosphine adduct) which plays a pivotal role in the catalytic cycle has been observed by HRMS and NMR studies. DFT studies are accordance with the control experiments which shows that the σ-bond metathesis step resulting in the release of the first molecule of H_2 is the rate–determining step (RDS).

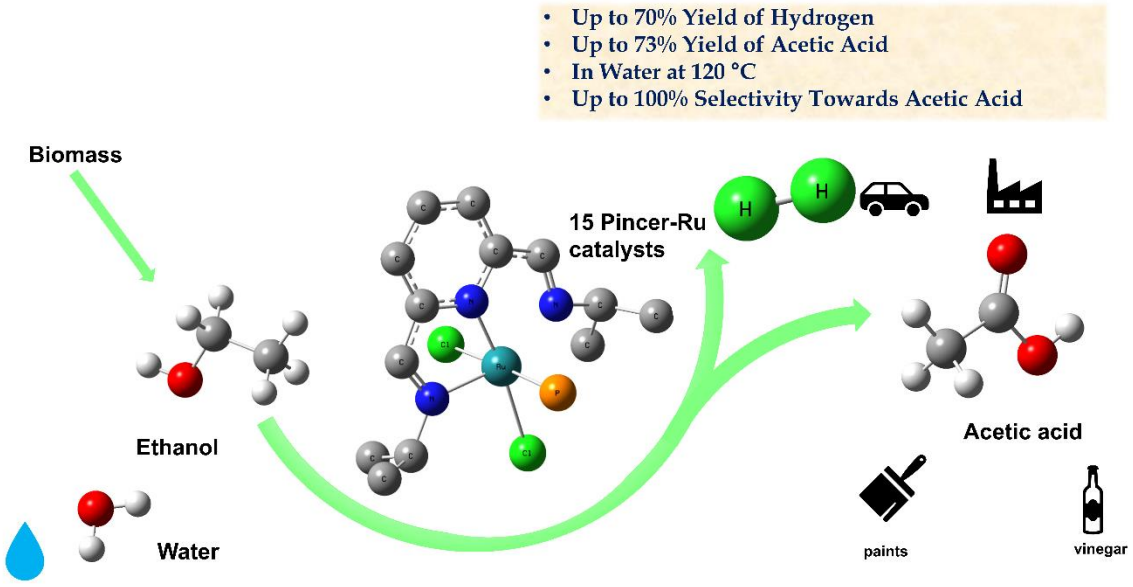

Figure 3. Pincer-ruthenium catalyzed aqueous reforming of ethanol for the selective production of H_2 and CH_3COOH.

Chapter IV discusses the synthesis of NNN pincer-Ni(II) complexes based on *bis*(imino)pyridine ligands ($(^{R2}NNN)NiCl_2(CH_3CN)$; R = ^{i}Pr, ^{t}Bu, Cy, Ph and *p*-F-C_6H_4), which are well characterized using HRMS, thermogravimetric analysis, magnetic susceptibility measurements and SCXRD studies. In solution, these complexes are found to exist in equilibrium mixtures containing one and two pincer ligands, respectively. These complexes have been further tested towards the Guerbet type *β*–alkylation of benzyl alcohol with 1-phenyl ethanol at 140 °C under very low catalyst (0.005 mol%) and base loading (5 mol%). Notably, the highest TON (up to 16400) was achieved with $(^{Ph2}NNN)NiCl_2(CH_3CN)$ 5 mol% NaO^{t}Bu under 0.005 mol% catalyst loading at140 °C after 24 h. The catalytic system tolerated a broad spectrum of substrates having electron-withdrawing and electron-donating groups. For the reaction of benzyl alcohol with 1-(4-trifluoromethyl)phenyl)ethane-1-ol, very high TONs (up to 18400) were observed in the presence of 0.005 mol% of $(^{Ph2}NNN)NiCl_2(CH_3CN)$ and 5 mol% NaO^{t}Bu at 140 °C after 24 h. The overall reaction exhibits zero-order kinetics in terms of catalyst concentration and first-order kinetics with respect to base and substrate concentrations. The control experiments and HRMS studies support the proposed mechanism, which shows the involvement of hydrogenolysis/alcoholysis pathway.

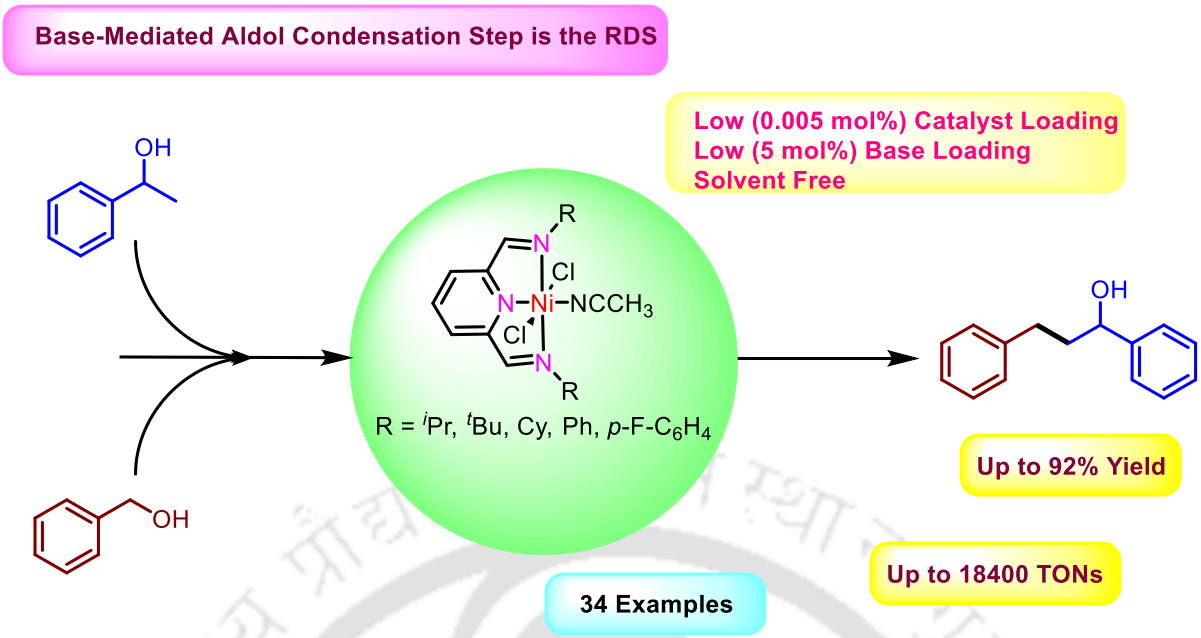

Figure 4. Pincer-nickel catalyzed *β*-alkylation of secondary alcohols with primary alcohols.

The current thesis has demonstrated synthetic protocols for a series of pincer-ruthenium and pincer-nickel complexes. These complexes have successfully accomplished the transformation of alcohols to clean burning hydrogen and industrially valuable chemicals. These results offer great promise from an industrial point of view as alcohols are abundant and an important feedstock in the context of synthetic organic chemistry. The reactivity exhibited by the considered complexes reflects their versatility in catalyzing various other related important organic transformations.

Among numerous intriguing opportunities, this thesis could pave the way for new avenues in activation of small molecules such as carbon dioxide (considering its presence in the reforming cycle) using pincer-metal systems. Apart from the various catalytic reactions discussed in the thesis, following challenges still remain unaddressed that could be taken up during future studies,

- Can one design catalytic systems based on *bis*(imino)pyridine pincer-ruthenium complexes and heterogenize them on inert solid supports?
- Can these immobilized pincer-metal complexes bring about generation of hydrogen from other abundantly available LOHCs which have been less explored?
- Is it possible to achieve reforming of various alcohols using pincer-metal complexes derived from *3d*-metals?

Ph.D Student

Department of Chemistry

Indian Institute of Technology, Guwahati

Guwahati – 781039, Assam, India

E-mail: vinay18@iitg.ac.in
vinay.arora1993@outlook.com

Mobile: +91-9729012662, 8399023947
Date of Birth: 06.08.1993

Sex: Male
Nationality: Indian
Language: English, Hindi
Address: D-248, Lohit Hostel, IIT Guwahati, Guwahati-781039, Assam, India.
Google Scholar ID: https://scholar.google.com/citations?hl=en&user=VzgD00EAAAAJ
ORCID: 0000-0003-0356-4680

Academic Record

Doctor of Philosophy (PhD) in Chemistry from Indian Institute of Technology, Guwahati (2018-2025), Assam, India under the supervision of Dr. Akshai Kumar A.S.

Thesis title: "*Catalytic Transformation of Alcohols for the Production of Hydrogen, Fuels and Specialty Chemicals Using Pincer-Ruthenium and Pincer-Nickel Complexes"*

MSc Chemistry in Inorganic Specialization from Kurukshetra University, Kurukshetra, Haryana, India (2014-2016).

BSc (H) Chemistry from Ramjas College, Delhi University, Delhi, India (2011-2014).

Research Interest

- Organometallics chemistry
- In depth mechanistic study of new or reported systems using computational studies
- Heterogeneous catalysis
- Inorganic synthesis

Patent and Publications

List of Publications:

- **Arora, V**.; Dutta, M.; Das, K.; Das, B.; Srivastava, H. K.; Kumar. A**.** *Organometallics*, **2020**, *39*, 2162-2176.
- **Arora, V.;** Narjinari, H.; Nandi, P. G.; Kumar. A**.** *Dalton Trans.*, **2021**, *50*, 3394–3428.
- **Arora, V**.;Narjinari, H.; Kumar. A**.** *Organometallics*, **2021**, *40*, 2870-2880
- Islam, K.; **Arora, V.**; Vikas,; Nag, B.; Kumar. A**.** *ChemCatChem*, **2022**, e202200440.
- **Arora, V**.; Yasmin, E.; Tanwar, N.; Hathwar, V.; Wagh, T.; Dhole, S.; Kumar, A. *ACS Catal.* **2023**, *13*, 3605-3617.
- **Arora, V**.; Dhole, S.; Kumar, A. *Catal. Sci. Technol.* **2023**, *13*, 6699-6711.
- Bisarya, A.; Karim, S.; Narjinari, H.; Banerjee, A.; **Arora, V**.; Dhole, S.; Dutta, A.; Kumar, A. *Chem. Commun.* **2024**, *60*, 4148-4169.

List of Book Chapters:

- Narjinari, H.; Bisarya, A.; **Arora, V**.; Nandi, P. G. Das, K.; Kumar, A. In: Sundararaju, B. (eds) Dehydrogenation Reactions with 3d Metals. *Topics in Organometallic Chemistry*, **2023**, vol 73. pp 93–127, Springer.
- Nandi, P. G.; **Arora, V.**; Yasmin, E.; Kumar, A. Book chapter, Elsevier (2021), pp 69-122 Pincer-group(8) and pincer-group (9) metal complexes for catalytic alkane dehydrogenation reactions. Title of the Book: Pincer-Metal Complexes: Applications in Catalytic Dehydrogenation Chemistry (Editor: Dr. Akshai Kumar).

List of Indian Patents:

- Kumar, A.; Yasmin, E.; **Arora, V.**; Dhole, S.; Wagh, T.; IN Patent Application; 202231027887, May 14, 2022. GROUP(VIII) CATALYSTS FOR PRODUCTION OF GREEN HYDROGEN FROM ETHANOL AND ITS MECHANISM THEREOF.
- Kumar, A.; Yasmin, E.; **Arora, V.**; Dhole, S.; Wagh, T.; IN Patent Application; 202231020801, April 6, 2022. GROUP(VIII) CATALYSTS FOR PRODUCTION OF GREEN HYDROGEN FROM METHANOL AND ITS MECHANISM THEREOF.

List of US Patents:

- Kumar, A.; Yasmin, E.; **Arora, V.**; Dhole, S.; Wagh, T.; PCT Patent Application; PCT/IB2023/054707, May 05, **2023**. GROUP(VIII) CATALYSTS FOR PRODUCTION OF GREEN HYDROGEN FROM ETHANOL AND ITS MECHANISM THEREOF.
- Kumar, A.; Yasmin, E.; **Arora, V.**; Dhole, S.; Wagh, T.; PCT Patent Application; PCT/IB2023/051407, February 16, **2023.** GROUP(VIII) CATALYSTS FOR PRODUCTION OF GREEN HYDROGEN AND FORMIC ACID FROM METHANOL AND ITS MECHANISM THEREOF.

Conferences Attended

- **Arora, V.**; Kumar, A. Poster presentation during 30th International Conference on Organometallic Chemistry, ICOMC, Agra, India, July **2024**. "Pincer-Ruthenium Catalyzed Aqueous Phase (M)ethanol Reforming for the Selective Production of Specialty Chemicals and Hydrogen".
- **Arora, V.**; Yasmin, E.; Tanwar, N.; Hathwar, V.R.; Wagh, T.; Dhole , S.; Kumar, A. Poster presentation during 3rd International Conference on Main-group Molecules to Materials MMM III, IIT Hyderabad, University of Hyderabad, Telangana, December **2023**. "Pincer-Ruthenium Catalyzed Selective Production of Carboxylic Acid and Hydrogen from Aqueous Phase (M)ethanol Reforming".
- **Arora, V.;** Narjinari, H.; Kumar, A. Poster presentation during Modern Trends in Inorganic Chemistry MTIC-XIX, Banaras Hindu University,Varanasi. December **2022**. "Pincer-Nickel Catalyzed Selective Guerbet-Type Reactions under Solvent-Free Conditions".
- **Arora, V.;** Kumar, A. Oral presentation during ACS National Meeting & Exposition, ACS Fall 2022, Aug 21-25, **2022**. "Pincer-Nickel Catalyzed N-Alkylation of Amines and Selective Guerbet-Type Reactions under Solvent-Free Conditions".
- **Arora, V**.; Narjinari, H.; Kumar, A. Poster presentation during 28th CRSI National Symposium in Chemistry, IIT Guwahati. March **2022**. "Pincer-Nickel Catalyzed Selective Guerbet-Type Reactions under Solvent-Free Conditions".

- **Arora, V**.; Narjinari, H.; Kumar, A. Poster presentation during 2021#Catalysis Science & Technology 10th anniversary symposium **2021**, Nov 2021."Pincer-Nickel Catalyzed Selective Guerbet-Type Reactions under Solvent-Free Conditions".
- **Arora, V.;** Dutta, M.; Das, K.; Das, B.; Srivastava, H. K.; Kumar, A. Poster presentation during **2021** #RSC Poster Twitter Conference, March 2021. "Highly Efficient Pincer-Nickel Complex for Solvent-Free Catalytic N-Alkylation and Catalytic Dehydrogenative Coupling Reactions".
- **Arora, V**.; Dutta, M.; Das, K.; Das, B.; Srivastava, H. K.; Kumar, A.Poster presentation during 26th CRSI National Symposium in Chemistry, VIT, Vellore. February **2020**."Pincer-Nickel Catalyzed N-Alkylation and Catalytic Dehydrogenative Coupling Reaction"